ADVANCED MASTERS IN STRUCTURAL ANALYSIS
OF MONUMENTS AND HISTORICAL CONSTRUCTIONS

Master's Thesis

Leidy Elvira Bejarano Urrego

Methodology for Seismic Assessment applied to the Case Study of Tower Anziani in Padua (Italy).

This Masters Course has been funded with support from the European Commission. This publication reflects the views only of the author, and the Commission cannot be held responsible for any use which may be made of the information contained therein.

Italy I 2014

DECLARATION

Name: Leidy Elvira Bejarano Urrego

Email: lebejaranou@gmail.com

Title of the Msc Dissertation: Methodology for Seismic Assessment applied to the Case Study of Tower Anziani in Padua (Italy)

Supervisor(s): Phd. Francesca da Porto, Phd. Giulia Bettiol

Year: 2014

I hereby declare that all information in this document has been obtained and presented in accordance with academic rules and ethical conduct. I also declare that, as required by these rules and conduct, I have fully cited and referenced all material and results that are not original to this work.

I hereby declare that the MSc Consortium responsible for the Advanced Masters in Structural Analysis of Monuments and Historical Constructions is allowed to store and make available electronically the present MSc Dissertation.

University: University of Padua

Date: July 23th, 2014

Signature:

_____

This page is left blank on purpose.

A mis padres Nelly y Adán quienes, a donde quiera que vaya, siempre están ahí para apoyarme y motivarme. Por confiar en mí, incluso en los momentos difíciles cuando las cosas salen mal. Por educarme y hacerme ser quien soy. Por darme la mano siempre que lo necesito.

Para ambos, siempre mi amor y gratitud.

To my parents Nelly and Adán who, wherever I go, are always there to support me and motivate me; for trusting on me, even during hard times when things go wrong; for making me be who I am and giving me always a helping hand when I need it.

To you both, forever my heart and gratitude.

This page is left blank on purpose.

ACKNOWLEDGEMENTS

I would like to thank all professors and staff involved in SAHC program coordination, especially Professor Paulo Lourenço from University of Minho, Professors Pere Roca and Luca Pelà from Technical University of Catalonia in Barcelona, Professor Petr Kabele from Czech Technical University in Prague and Professor Claudio Modena from University of Padua, who have given me the opportunity of carrying out this master's program, something that I deeply desired. Also, I thank European Commission for giving me the scholarship.

I want to thank all professors who gave me classes at CTU in Prague, from whom I learnt innumerable things which I commit to put into practice responsibly on preservation of cultural heritage.

I am very grateful to my supervisors Prof. Francesca da Porto and Prof. Giulia Bettiol from University of Padua, who supported me throughout this work and without the help of whom this thesis would not have been possible. Additionally, I would like to thank Elvis Cescatti for important guidance and advice about in-situ tests and analysis of results, all lab members for assistance in performing the tests and Letizia Carducci and Lucia Mosca for their help on processing test data.

I want to express my sincere gratitude to my boyfriend and colleague León for his advices about this work and persistent support, as well as for his patience and love during my absence.

My very special thanks go to my classmates from Prague and Padua, with who I shared unforgettable moments not only studying hard but also also having fun. I would like to thank, as well, my friend Sebastian for helping me since I arrived in Padua and assistance in the issues regarding to the Italian language.

Last but not least I want to thank my family, especially my parents, my sisters and my brother, whose constant encourage and support all the time was paramount for the completion of this thesis.

Thank you all.

This page is left blank on purpose.

ABSTRACT

METHODOLOGY FOR SEISMIC ASSESSMENT APPLIED TO THE CASE STUDY OF TOWER ANZIANI IN PADUA

This work was aimed to assess the seismic vulnerability of the Tower Anziani (Torre degli Anziani), a Romanesque masonry tower with great cultural value in Padua since 13th C.

The work includes basically three stages: 1.Inspection, 2.Seismic analysis and 3.Safety verifications and decision of intervention.

1. Inspection lets understand broadly the behavior of the structure, it involves historic and geometrical survey, visual inspection and non-destructive and minor destructive testing.

Historic survey was essential to define the historic and present function of the tower, main structural elements (structural typology), main phases from historical perspective including alterations and restorations, geometrical drawings, previous testing campaigns and materials used. By means of visual inspection, it was possible to identify the main damage patterns, material deterioration state and verification of geometry. NDT and MDT were useful to assess features and quality of materials and tension state of iron tie rods.

2. The main objective was to implement a methodology for seismic assessment where the Tower Anziani could be analyzed locally and globally using information obtained in the inspection and testing campaigns.

Local assessment was carried out by means of Kinematic Limit Analysis as it has been observed that following earthquakes several masonry structures develop local collapse mechanisms such as overturning of some elements in-plane or out of plane due to poor wall clamping. The chosen collapse mechanisms arose from the careful observation of this kind of structures after earthquakes and the current state of the tower.

Global assessment was performed considering the entire tower composed by several structural elements well connected each other. For this approach, Dynamic Modal Analysis by means of FEM was chosen following recommendations from literature about accurate seismic analysis on this kind of historical constructions. The model was calibrated by means of the known natural frequencies of vibration obtained in previous tests. Additionally, a global Linear Static Analysis, taking into account different load actions such as self-weight, snow and wind, was performed.

3. Once the results for each methodology were obtained, safety verifications were made following standards for evaluation of cultural heritage and the Italian code. According to the verification, intervention works were proposed.

This methodology proved to be and effective tool for analyzing masonry towers. For this case, Tower Anziani resulted to be more vulnerable to local collapse mechanisms than to global ways of collapse.

This page is left blank on purpose.

SOMMARIO

METODO DI VALUTAZIONE DELLA VULNERABILITA' SISMICA APPLICATA AL CASO STUDIO DELLA TORRE DEGLI ANZIANI A PADOVA

L'obiettivo del presente lavoro è la valutazione della vulnerabilità sismica della Torre degli Anziani, un complesso in muratura risalente al 1285 di grande valore culturale per la città di Padova. Il lavoro è stato suddiviso in tre fasi: 1.Ispezione, 2.Analisi sismica, 3.Verifica di sicurezza e definizione interventi.

1. La fase preliminare di conoscenza ha permesso di interpretare il comportamento della struttura più prossimo alla realtà. Ciò include l'analisi storico, il rilevo geometrico, l'ispezione visiva e le prove in sito - sono state svolte sia prove non distruttive (NDT) che prove debolmente distruttive (MDT) -.

La ricerca storica è stata essenziale per definire le funzioni originarie e attuali della torre e le trasformazioni che si sono susseguite nel corso dei secoli. Ha permesso inoltre di identificare i principali elementi strutturali (verticali e orizzontali), la geometria, le campagne di indagini pregresse e la tipologia e le caratteristiche dei materiali utilizzati. Mediante ispezione visiva è stato possibile identificare i principali danni presenti nella struttura (rilievo del quadro fessurativo e del danno) e la verifica della geometria. Sono state svolte delle indagini in sito di tipo NDT e MDT che sono risultate essenziali per valutare le caratteristiche e la qualità dei materiali, e lo stato di tensione dei tiranti.

2. L'obiettivo principale è stato quello di implementare una metodologia di valutazione della vulnerabilità sismica della torre analizzandola sia a livello locale che a livello globale utilizzando le informazioni ottenute dalla fase conoscitiva.

La valutazione locale è stata effettuata mediante un'analisi cinematica. E' stato infatti osservato che dopo un terremoto diverse strutture in muratura sviluppano meccanismi di collasso locali, come l'attivazione del meccanismo di ribaltamento fuori del piano o meccanismi nel piano. Spesso ciò è strettamente legato alla scarsa connessione tra le pareti. I meccanismi sono stati scelti in base all'osservazione dettagliata del comportamento di questo tipo di strutture a seguito di eventi sismici e allo stato attuale di conservazione della torre oggetto di studio.

La valutazione globale è stata effettuata considerando la torre nel suo complesso. Per questo approccio è stata scelta l'analisi dinamica modale mediante la creazione di un modello ad elementi finiti (FEM). Il modello è stato calibrato considerando le frequenze naturali di vibrazione ottenute da indagini pregresse. E' stata inoltre svolta un'analisi statica lineare.

3. Dai risultati ottenuti dal modello sono state svolte le verifiche di sicurezza seguendo le prescrizioni contenute nella normativa italiana (Norme Tecniche 2008) e le Linee Guida per i Beni Culturali. Sono quindi state valutate le proposte di intervento.

La metodologia qui utilizzata si è dimostrata un'efficace strumento per l'analisi delle torri in muratura. In particolare, per il caso della Torre degli Anziani è emerso che la vulnerabilità maggiore si ha nei confronti dei meccanismi di collasso locali rispetto al comportamento globale della struttura.

This page is left blank on purpose.

RESUMEN

METODOLOGÍA DE EVALUACIÓN SÍSMICA APLICADA AL CASO ESTUDIO DE LA TORRE ANZIANI EN PADUA

Este trabajo tuvo como objetivo evaluar la vulnerabilidad sísmica de la Torre Anziani (Torre degli Anziani), una torre de mampostería de estilo Románico con un gran valor cultural en Padua desde el siglo13. El trabajo incluye básicamente tres etapas: 1.Inspection, 2.Análisis sísmico 3. Verificaciones de seguridad y decisión de intervención.

1. La inspección permite entender el comportamiento de la estructura. Esta incluye el estudio histórico y geométrico, inspección visual y pruebas no destructivas (NDT) y de daño leve (MDT).

El estudio histórico fue esencial para definir la función histórica y actual de la torre, principales elementos estructurales (tipología estructural), principales fases desde una perspectiva histórica, (incluyendo modificaciones y restauraciones), esquemas geométricos, campañas de pruebas anteriores y materiales usados. Por medio de la inspección visual, fue posible identificar los principales patrones de daño y deterioro y verificación de la geometría. NDT y MDT fueron esenciales para evaluar las características y calidad de los materiales y el estado de tensión de los tirantes.

2. El objetivo principal fue implementar una metodología de evaluación sísmica, donde la Torre Anziani pudiera ser analizada a nivel local y global utilizando la información obtenida previamente.

La evaluación local se llevó a cabo por medio de un Análisis Límite cinemático ya que se ha observado que después de un terremoto varias estructuras de mampostería desarrollan mecanismos de colapso locales, tales como giro (vuelco) de algunos elementos en el plano o fuera del plano, debido a la mala conexión entre las paredes. Los mecanismos elegidos surgieron de la observación detallada de este tipo de estructuras después de terremotos y el estado actual de la torre.

Evaluación global se llevó a cabo teniendo en cuenta toda la torre, compuesta por varios elementos estructurales bien conectados entre sí. Para este enfoque, se eligió un Análisis Dinámico Modal empleando FEM (método de elementos finitos) siguiendo recomendaciones de la literatura sobre análisis sísmicos adecuados para este tipo de construcciones históricas. El modelo fue calibrado usando las frecuencias naturales de vibración obtenidas en las pruebas. Además, se llevó a cabo un análisis global estático lineal, teniendo en cuenta las diferentes acciones de carga como el peso propio, la nieve y el viento.

3. Una vez obtenidos los resultados de cada metodología, se realizaron verificaciones de seguridad siguiendo los estándares para la evaluación del patrimonio cultural y el código italiano. De acuerdo con la verificación, se propusieron las obras de intervención.

Esta metodología demostró ser una herramienta eficaz para analizar las torres de mampostería. En el caso particular de la Torre Anziani, esta resultó ser más vulnerable ante los mecanismos de colapso locales que a las formas de colapso global.

TABLE OF CONTENT

This page is left blank on purpose.

1 INTRODUCTION

Tower Anziani is a Romanesque civil tower built in the medieval age. It is located in the city center of Padua and belongs to the Palazzo Comunale (Communal Palace), a large complex composed by several palaces connected each other but built in different periods.

Towers and bell towers, usually affected by earthquakes, constitute an important set of cultural heritage in Italy; additionally, Tower Anziani represents an important icon of the city so it needs to be investigated in order to carry out required interventions aimed to its preservation. On the other hand, since Italy is a country with important seismic hazard, seismic assessment is paramount.

The tower has been subjected to many structural modifications though time; it has passed from Romanesque style, to Gothic-Romanesque and finally again Romanesque. In the past, it got a maximum height of 65 meters, nowadays 45 meters, and it presents slightly tilt to the east. The current main structural elements are two masonry cross vaults, four masonry barrel vaults and solid walls made also of brick masonry connected each other with iron tie rods.

Factors that could be involved in the seismic vulnerability of the tower are the slenderness of walls, clamping between walls, interaction with adjacent structures which could provide a horizontal constraint, presence of slender elements at top, thrust of vaults and tilt. The goal is to consider all of these factors in the structural analysis and find out their effect on the dynamic behavior of the tower when it is subjected to earthquake.

Usually, masonry structures subjected to earthquakes behave properly as long as their structural components are well clamped each other, but this condition is not satisfied in the most of cases; in contrast, it has been observed that following earthquakes several masonry structures develop local collapse mechanisms. That is why, this work will present a methodology of seismic analysis applied to the case the Tower Anziani, taking into account both global analysis, considering the structural elements perfectly connected, and local analysis, considering some structural elements working independently.

This page is left blank on purpose.

2 THE TOWER ANZIANI (*Torre degli Anziani*)

2.1 Location and description

Torre Anziani is a Romanesque civil tower built in the medieval age; it is located in the downtown of Padua in Italy (see Figure 1) next to Piazza della Frutta square. The tower belongs to the Palazzo Comunale (Communal Palace) a large complex composed by several palaces connected each other but built in different periods.

The tower has great cultural value for the city of Padova due to its important role through its history. It used to be called “Torre Vechia” (Old Tower), “Torre Alta” (High Tower), “Torre d'Ognissanti” (Tower of All Saints) because its bells were played in several patronal feasts, and also “Torre Bianca” (white tower) due to its white lime plaster which does not remain nowadays.

Figure 1. Left: Location of Province of Padua in Italy. Right: View of Tower Anziani and Palazzo della Ragione from Piazza della Frutta

The Comunale Palace, also called Moroni Palace, is mainly composed by five imposing buildings, *Palazzo della Ragione*, *Palazzo del Consiglio*, *Palazzo degli Anziani* and Tower Anziani, *Palazzo del Podesta* and *L'ala Moretti-Scarpari.* These buildings are connected each other as it is seen in Figure 2. The tower Anzini connects *Palazzo del Consiglio* to *Palazzo degli Anziani* overlooking Piazza della Frutta. Some characteristics of the buildings belonging to the Communal Palace are shown in Table 1.

Table 1. Buildings belonging to Communal Palace

Building	Style	Construction period	Initial use	Current use
Palazzo della Ragione	Romanesque	1218-1306	Court	Events and public exhibitions
Palazzo del Consiglio	Romanesque-Gothic	13th century (rebuilt several times)	Palace of Chancellery	Municipal Administration
Palazzo degli Anziani	Romanesque-Gothic	13th century	Palace of Chancellery	Municipal Administration
Torre Anziani	Romanesque	13th century	Bell tower	Icon of the city
Palazzo del Podesta	Renaissance from Veneto	Entirely restored in 16th century by Andrea Moroni (originally 13th cent.)	Palace of Podesta (chief magistrate)	Municipal Administration
L'ala Moretti-Scarpari	Renaissance from Veneto	20th century Between the two World Wars	Municipal Administration	Municipal Administration

Figure 2. Tower Anziani in Communal Palace Complex

2.2 Historical survey

Historical survey is essential to understand the current state of the building and allows doing a correct interpretation of the structural and non-structural elements. The main events regarding to the tower Anziani in historical perspective are presented in the time line of Table 2.

Table 2. Historic survey of Torre Anziani [1] [5] [13]

Date	Event	Description
1174-1215	Origin	The original tower was built after a great fire in Padova in1174 and it was sold to the city from Tiso Camposampiero VI in 1215
1285	Construction of *Palazzo del Consiglio* and *Palazzo degli Anziani*	It was flanked, first to the west by *Palazzo del Consiglio* and then to the east by *Palazzo degli Anziani* from which it took the name
1294	**Raising of tower and try to straighten**	The tower was raised perhaps to its current height (45 meters) trying to straighten the structure because it was already leaning toward the east, due to a failure of the foundation (subsidence). The tower was commonly called the White Tower because of its lime white plastered.
1294	Placing of one bell	As soon as the fortress of the city was demolished in 1293, the conqueror Padovani placed one bell which was played in several occasions.
1348-1490-1503	Earthquakes that affected Padova	There is not much information about the damage of the tower Anziani after these earthquakes, but it is known that following the earthquake of January 25, 1348, the Tower Rossa, located between *Palazzo del Consiglio* and *Palazzo del Podesta,* collapsed.
14^{th}-15^{th} Centuries	Installation of Gothic spire at top	This spire was rebuilt several times and removed definitely in 1610.
1610	**Addition of octagonal lantern, dome and statue (gothic style)**	At top, a balustrade was placed made of marble and also a gothic style dome with an octagonal lantern surmounted by a large and rough wooden statue of Justice covered with lead (Figure 3).

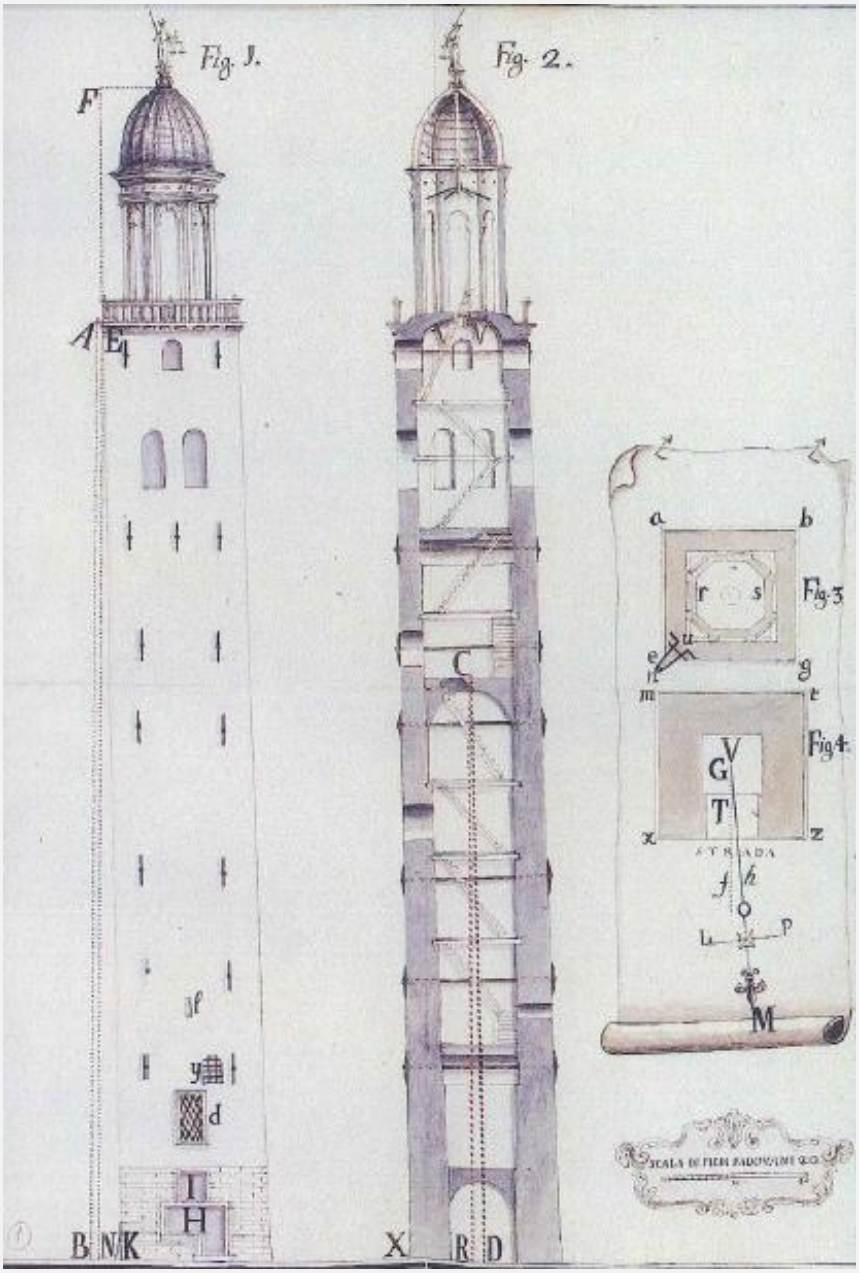

Figure 3. Northern view of Tower Anziani with its octagonal lantern in 1746 (also showing inclination) [1]

February 1695	Earthquake of Asolo	The tower had already important damage and deterioration through time but just after the earthquake in 1695 when the cracks were aggravated, the alarm was raised to call attention to the dangerous condition of the tower, then gentlemen deputies of the city began to care about it.

June 1695	Execution of report describing the damages by Francesco Tentori	The expert Francesco Tentori reported a crack on the wall and inclination of the tower to the East.
January 1696	Inspection by the architect Antonio Gaspari.	He reported obvious and considerable damage to the exterior brick and decided to check the foundation. He noted that the greatest damage was not caused by the earthquake, but by the sewage coming from the offices of the judges and the caretaker's house, with consequent infiltration along the walls to the east which had caused the large damage of the wall. He reported a leaning of the tower (deviation of the top from the perpendicular line) around 1.01 m (2 piede and 11 oncie). *Note: 1 piede= 12 once, 1 once=0.02893 m)*
1696	Intervention proposed by the architect Gaspari and the expert Ciotto	They considered necessary to build a **stone buttress** on the unsafe side (east), of approximately 23 m until the tilted side as it is seen in Figure 4. The buttress was supported on a base made of wood tied with stone and brick. Nowadays the buttress rises 18 meters above the street, the rest is underground.
1727	1st Inspection by the physical and mathematical Giovanni Poleni and the archeologist Lorenzo Orsato	After fall of some balustrade fragments from the north side to the street, Giovanni Poleni and Lorenzo Orsato performed minor repairs and measured again the leaning using a more accurate plummet with a heavy stone (Figure 3). The measured deviation was **0.81** m (28 once), corresponding to the distance NK in Figure 3.

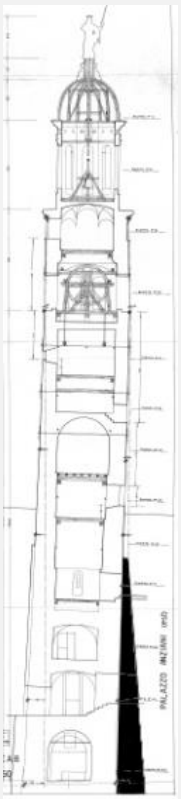

Figure 4. Buttress on eastern wall

1741-1746	Repair of the bell box ("Castello" of the bell) and fall of part of balustrade	In 1741 the bell box was restored, while the upper balustrade continued falling down. In 1746, 26 columns belonging to balustrade had already fallen and one of them had broken the roof of a dwelling.
1746	2nd evaluation of the tower by Giovanni Poleni	He pointed two mean damages: 1. Considerable crack in the lower part of northern façade of the tower. For this reason, a strong iron chain was used to connect the walls but after some years it became corroded and did not operate anymore. 2. Deviation from perpendicular line of **0.84 m** (29+1/3 once), which meant 3 cm more than 19 years before (this deviation is represented as the distance NK in Figure 3). Despite this increasing on the deviation from the perpendicular line, he concluded that there was not considerable danger and proposed to make an evaluation of the state of the tower once each 5 years.
1749-1750	Recasting of the big bell and placing of a second smaller bell	The big bell got broken due to excessive use and a new one lighter was placed but 12 years later it broke again and it had to be recast, that year a new decree was issued to limit the occasions when the bell would have to be played. Another smaller bell was mounted inside the lantern.
1753	3rd evaluation by Giovanni Poleni	He carried out new tests but they drew reassuring conclusions, generally the same already reported by previous surveys.
1772-1778	Minor repair works were performed	In 1777, after just some minor repair works, the Lords deputies of the city asked to Capitanio Vicepodestà Pietro Manin for urgent repair of the top of the tower and also for the external layer of the walls which was deteriorated due to weather effects and water infiltration. In 1778, the Capitanio and the Vicepodestà Domenico sent another letter to the Senate asking for a deep evaluation and restoration.

1779	***Removal of all balustrade columns** ***Prohibition of ringing the bells**	While an evaluation and restoration were expected, the balustrade was removed completely and the bells stop ringing.
1789	Renovation of stairs and bell box	A restoration was agreed in 1789, however, it was limited to renew the stairs and the bell box ("castello"of the bell).
1834	**Inspection and restoration of lantern and statue on top**	The interior of the statue was completely decayed and the frame of the lantern was deteriorated by weather action. The timber was renovated.
1834	Announcement about the need of cutting off the tower	Both Austrian and the Italian authorities proposed to cut off the Tower Anziani in order to definitively secure the area and put end to an age-old problem, but a large part of the citizenship was opposed to such decision. The debate continued throughout the nineteenth century and the beginning of the next century. Many towers nearby and buildings had been demolished at that time but it seems that this tower had a special meaning as an icon of the city; after many debates, finally, the tower was not cut off since it was respected as a glorious sign from ancient times.
1938	**Demolition of the17th century lantern and reopening of battlements from 13th century**	Restoration of the tower was performed by the Architect Forlati Ferdinand. Given the serious state of the octagonal lantern, he demolished the lantern, dome and statue, and reopened the battlements. The upper bell was removed as well. The height of the tower became, once the lantern was removed, from 56.7 to 45.6 meters. 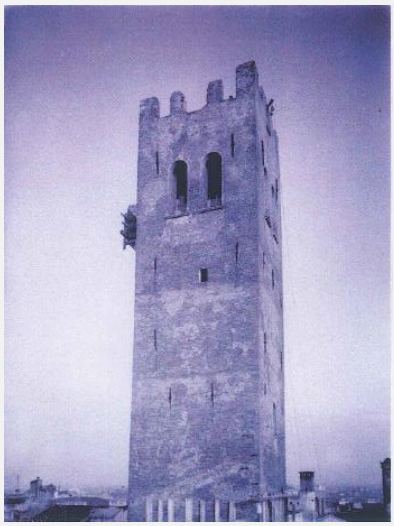 Figure 5. Tower after removal of lantern. 1938 [5]

1939-1940	**Strengthening of walls using cement injection and removal of white lime plaster** Implementation of new iron rods to connect the walls (perhaps also as a safety measure in the war)	Since the masonry was highly deteriorated, the walls were consolidated using cement injection (also carried out by Forlati). They bind up the lantern with sturdy wooden frames and built a high scaffolding and protection works. At the end of 150 tons of cement was injected in 2500 m^3 of masonry walls.	 Figure 6. Tower with scaffolding in consolidation works. 1938[13]
1939-1940	The masonry from battlements (at top) was replaced and a new roof with wooden truss was set up.	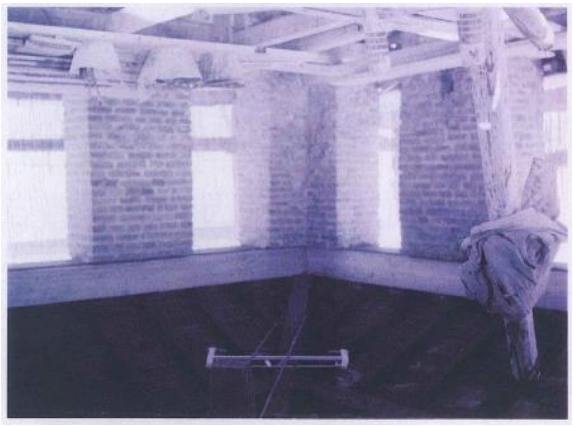 Figure 7. Battlement and roof in 1939 [13]	
1940	A shop located in the ground floor, on Via Oberdan street, was closed. The windows that connected the tower with the two neighboring buildings were closed as well.	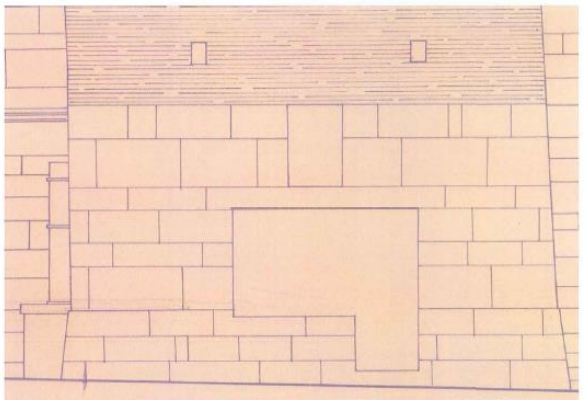 Figure 8. Shop located in ground floor (northern view) [5]	

1943	Bombing and fire nearby. There is not much information about damage or repair works after the event.	
2003-2005	Inspection and diagnosis of tower	An extensive inspection was carried out including: -Photographic survey. Ref [5] -Tests: Ground Penetration Radar, Dynamic characterization, Petrographic characterization of brick and mortar and coring. The results of these tests are shown in the Chapter 4. Ref [2] [3] [4] - Numerical simulation of dynamic and static analysis which concluded that the tower is safe and there was not recent abnormal movement. Ref[9][5]

In summary, the original tower was ceded to the city in 1215, it was raised in 1294 and arranged to set up a bell. During 17th century a gothic lantern was built at top which was demolished in 1938. From 1938 to 1940, the tower had an extensive restoration work including consolidation of walls and construction of a new roof. In 2005, new tests and analysis were carried out concluding the safety of the tower. Nowadays, the tower is subjected to new analysis to reconfirm its safety and it is not accessible to visitors. The following figure shows the view of the Tower Anziani, with its gothic lantern, in 1922 and the current state in 2014. Figure 10 shows a time-line of the tower presenting the most important events through time.

Figure 9. View of tower from Piazza della Frutta. Left: In 1922 [14]. Right: In 2014

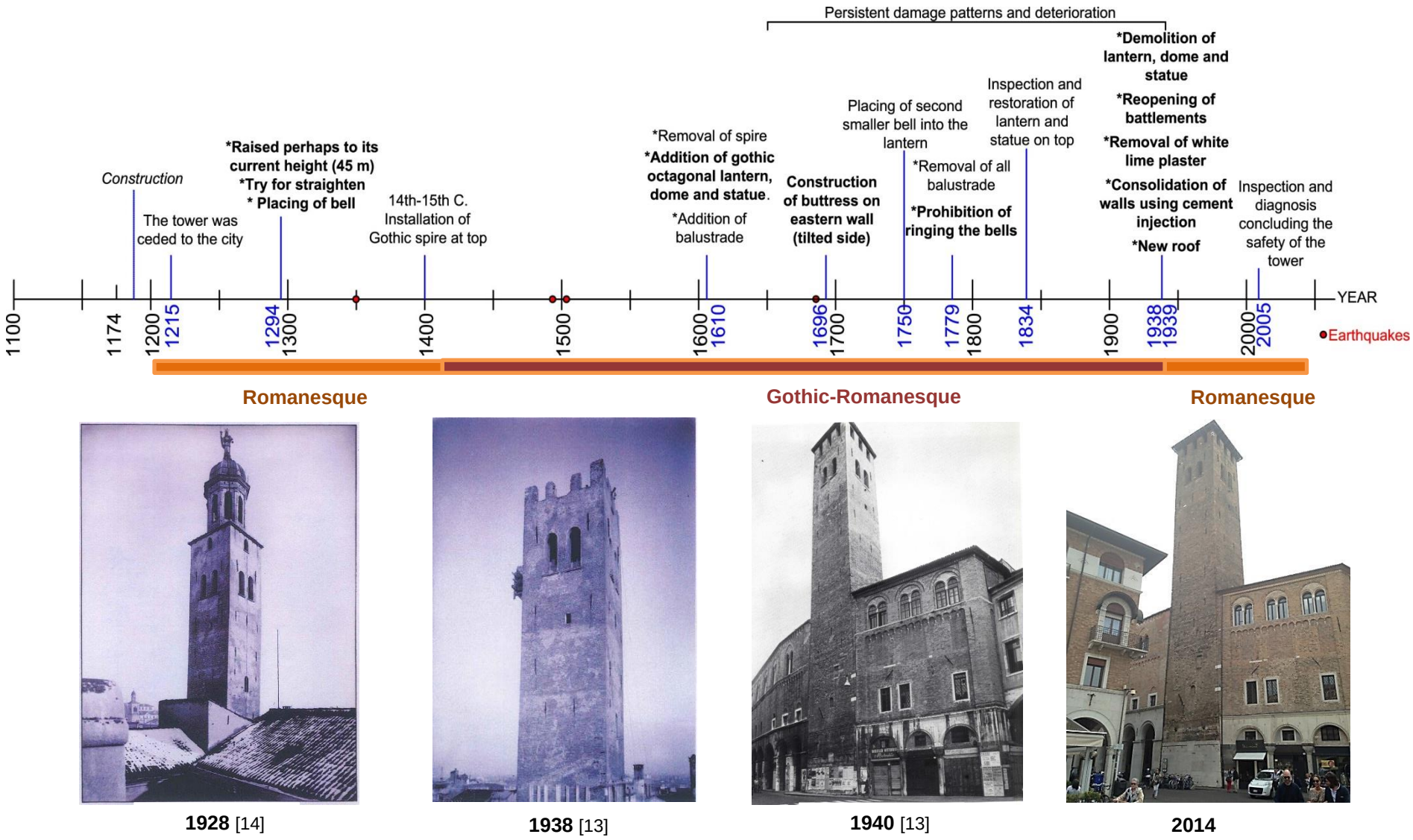

1928 [14]

1938 [13]

1940 [13]

2014

Figure 10. Time line of Tower Anziani.

2.3 Description and structural arrangement

Nowadays the tower rises a height of 47.2 meters including the roof, the walls are made mainly of brick masonry from 13th century, except the battlement (at top) which was rebuilt with the same material in 1939. As it was mentioned in the historical survey, the tower presents a slight leaning to the east which might have occurred short time after the construction, de deviation from the vertical line is 1.1 m or 1.8 degrees (Figure 11). In fact, the upper part of the tower (from 35 m to the top) which comprises the belfry with lancet windows and the battlement is straight; it confirms that the tower axis was corrected before being finished.

The buttress, built in 1696 on the eastern side, rises above the street level about 18 m (Figure 11); it has a thickness of 2.25 m at the base and 0.47 m at the upper part.

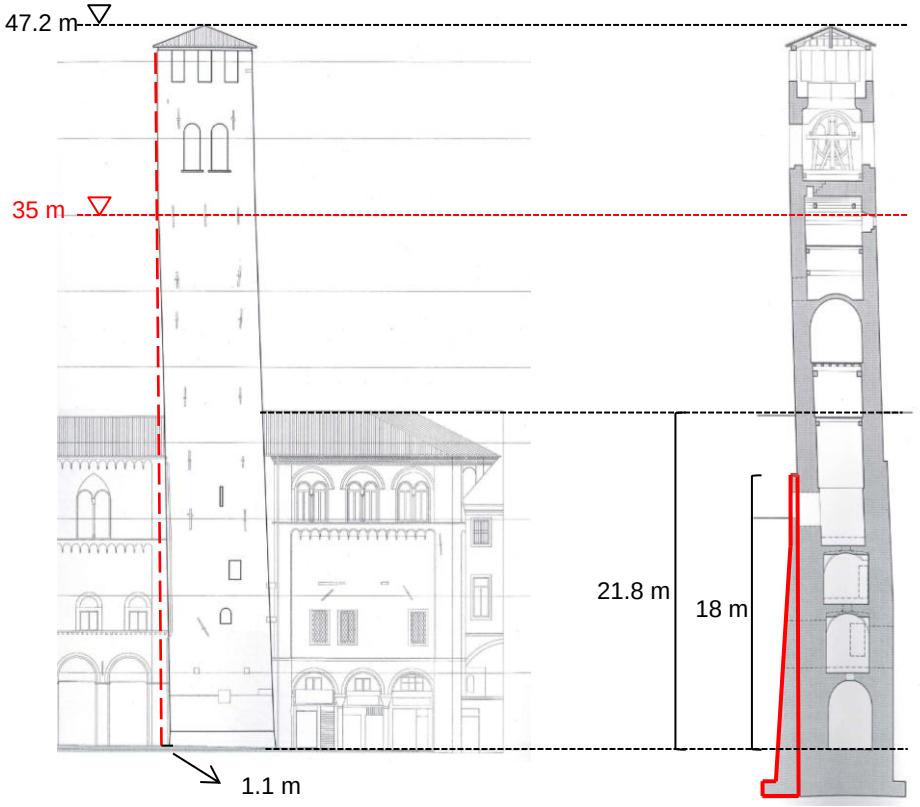

Figure 11. Northern façade and cross section showing leaning and buttress [15]

The plant is approximately square with a side of about 7.2 m at the base (excluding the buttress) and 6.6 m at top level. The tower is composed by 11 levels where the thickness of the walls decreases with the height, having a thickness around 1.88 m at the base (excluding buttress) and 0.57 m at top. Figure 12 and Figure 13 show the main structural components of the tower including 3 barrel vaults, 2 cross vaults, 2 wooden platforms and roof.

Access is allowed only at eastern wall, in level 4 at an altitude of 15.10 m from the ground. The levels 1, 2 and 3 are masonry vaulted rooms composed by one barrel vault and two cross vaults respectively, these rooms have no openings except a square hole at middle-top to access using a ladder.

It seems that there was another wooden platform at an altitude of 21.70 m (between level 5 and 6) but it does not exist anymore (Figure 12). The exact location of all wooden platforms and vaults is shown in Table 3.

Table 3. Location of vaults and wooden platforms

Structural element	Level	Altitude from ground (m)
Vault 1 (Barrel)	1	4.82
Vault 2 (Cross)	2	9.34
Vault 3 (Cross)	3	13.24
Wooden platform 1	6	25.31
Vault 4 (Barrel)	7	29.46
Wooden platform 2	8	32.9
Vault 5 (Barrel)	9	36.85

The belfry (from 36.85 m to 42.25 m) has 8 vaulted windows (lancet type), two in each wall, of about 1.1 m wide and 3.05 m high; the walls at this level are 98 cm thick and have light reinforcement in the contour of the windows. Above the belfry, there is a battlement wall (from 42.49 m to 45.6 m) composed by 3 crenels in each wall of about 0.85 m wide and 2.0 m high; the thickness of the wall at this level is 57 cm.

The roof is four-pitch roof made by brick and clay tiles and supported by a wooden truss.

The most of windows have been sealed in all facades, except for the eight large vaulted windows in the belfry, one vaulted window on the eastern façade (to 30 m from ground) and a small rectangular window on the western wall (to 35 m from ground). All the current openings of the tower are shown in Table 4.

Table 4. Current openings in the tower

Openings	Location	Altitude from ground (m)	Area-each (m^2)	Quantity
Entrance	Eastern wall	15,1	1,68	1
Vaulted window	Eastern wall	30	1,43	1
Rectangular window	Western wall	35	0,35	1
Vaulted windows	All walls	37,9	2,98	8
Crenels (battlement)	All walls	43,6	1,80	9

On the other hand, the tower is reinforced with several wrought iron ties, some of them installed since the construction and some set up in 20th century in war time (detailed description is presented in section 3.2).

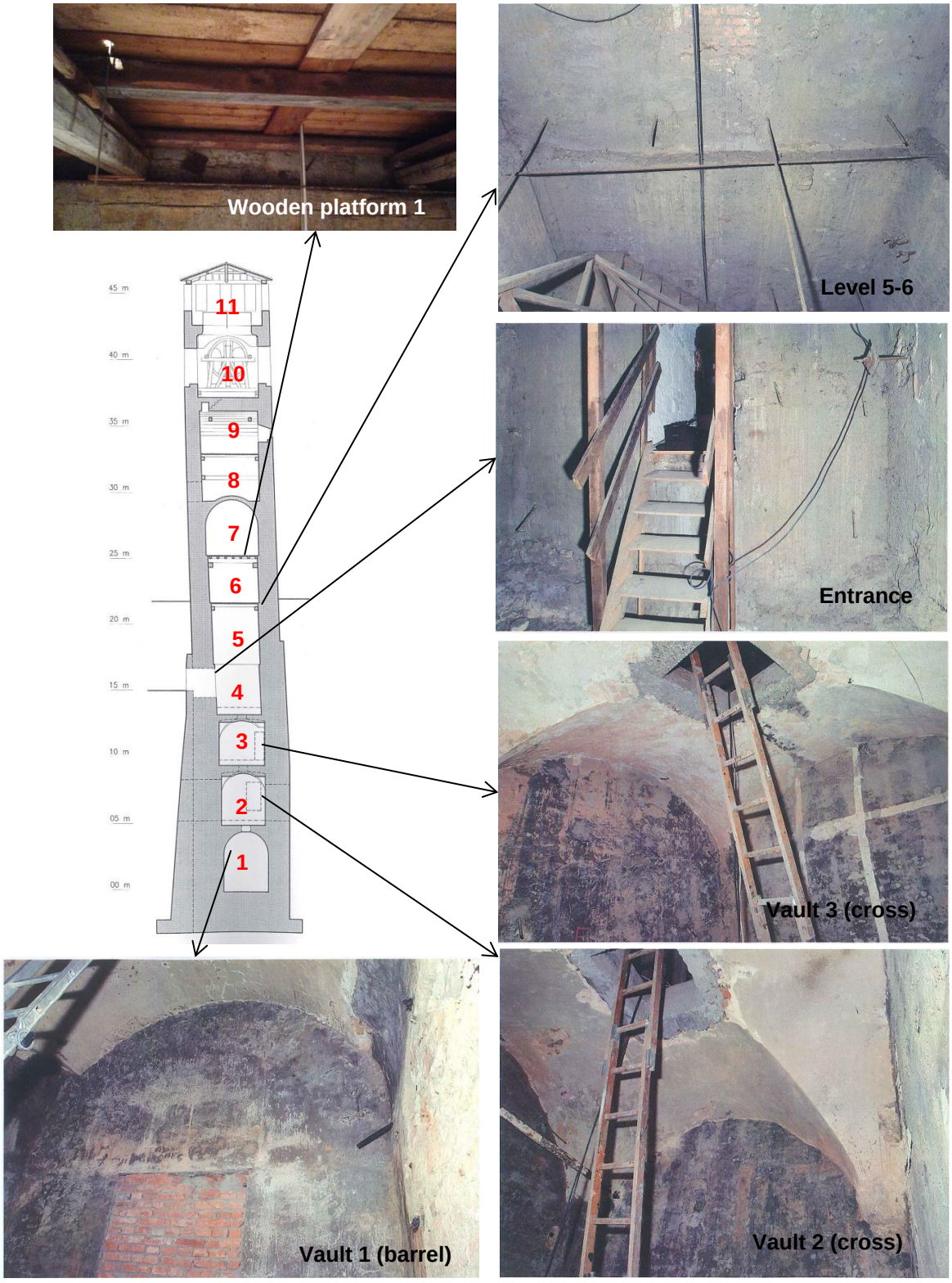

Figure 12. Structure elements from base to 25 m high (north view cross section). [Images Ref.[15],[5]]

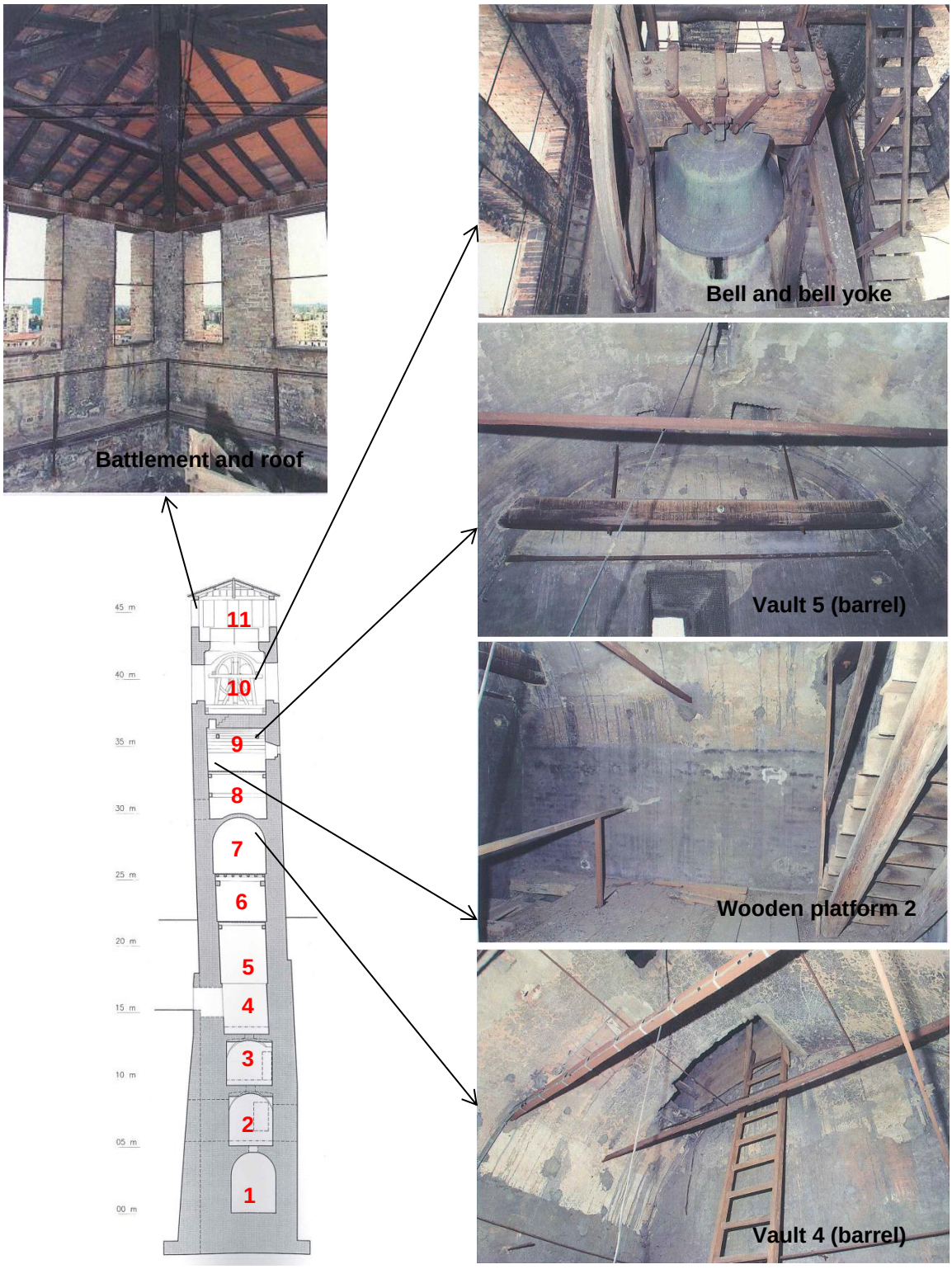

Figure 13. Structure elements from 25 m to the top (north view cross section). [Images Ref.[15],[5]])

2.3.1 Bell and bell yoke

The bell is wider than high; its diameter is 175 cm and height 150 cm excluding support. There is not much information about where it was brought from but it is well known that it stopped being played in 1779. The dimensions and arrangement of the bell is shown in Figure 14. The bell is mounted on a wooden yoke which transfers the weight though four beams to the northern and southern walls. The weight has been estimated in 3600 kg for the bell and 800 kg for the yoke.

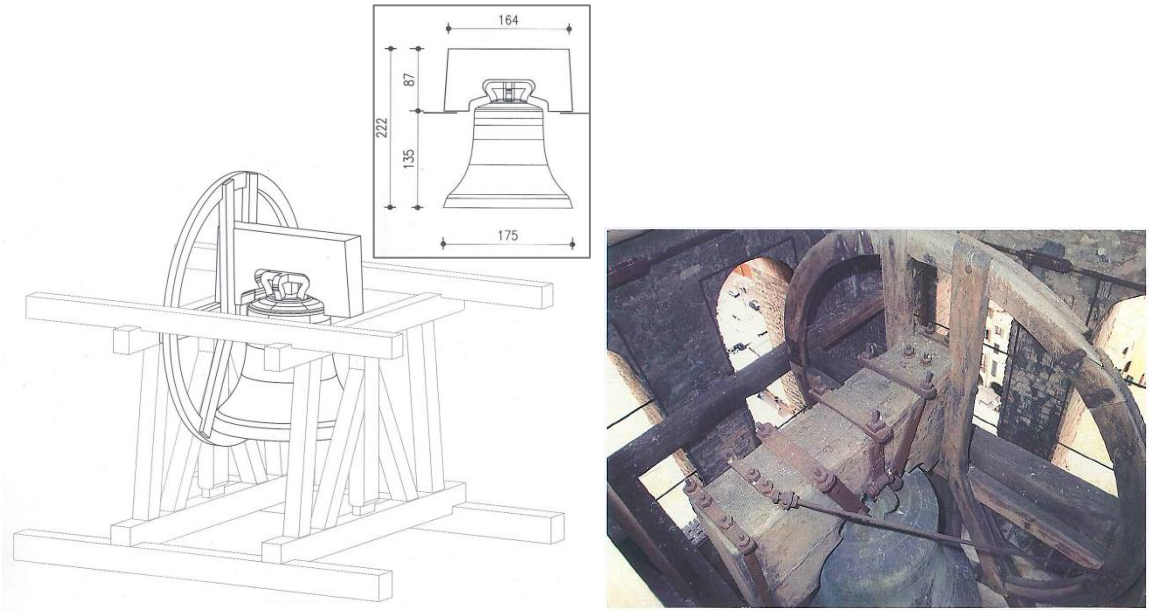

Figure 14. Dimensions and arrangement of bell [15]

2.4 Soil characterization and foundation

In 1998, an extensive soil exploration was carried out as part of a restoration project of the Palazzo della Ragione (Figure 2). This geotechnical work included soil characterization, standard penetration test results (SPT) with a maximum depth of 30 m, static penetrometer test with a maximum depth of 30.7 m and laboratory tests on undisturbed samples. This information is available in Ref. [21].

Figure 15 shows the location of boreholes for soil exploration; two of them were performed in 1998. The closest one to the Tower Anziani is the borehole SFR.

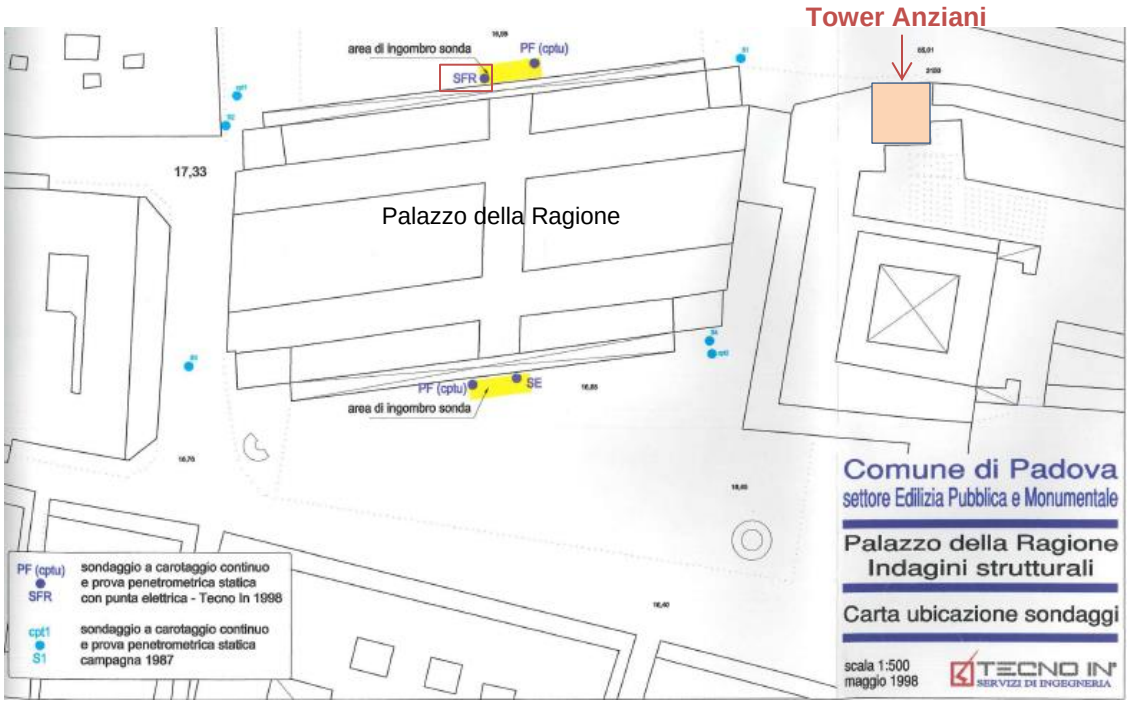

Figure 15. Location of boreholes for soil exploration near Tower Aanziani [21]

From the geological point of view, recent alluvial sediments were found, placed on no homogenous marine deposits with large thicknesses, testified by the presence of a marine environment subjected to subsidence more or less active.

The exploration of the soil from the borehole SFR shows a profile composed meanly by granular soil presenting silty sand and fine and coarse sand. Figure 16 shows the stratigraphic profile from this borehole showing the type of soil and the results of cone penetration test and standard penetration test (SPT).

Table 5 presents the lithological description of the terrain and soil for each layer.

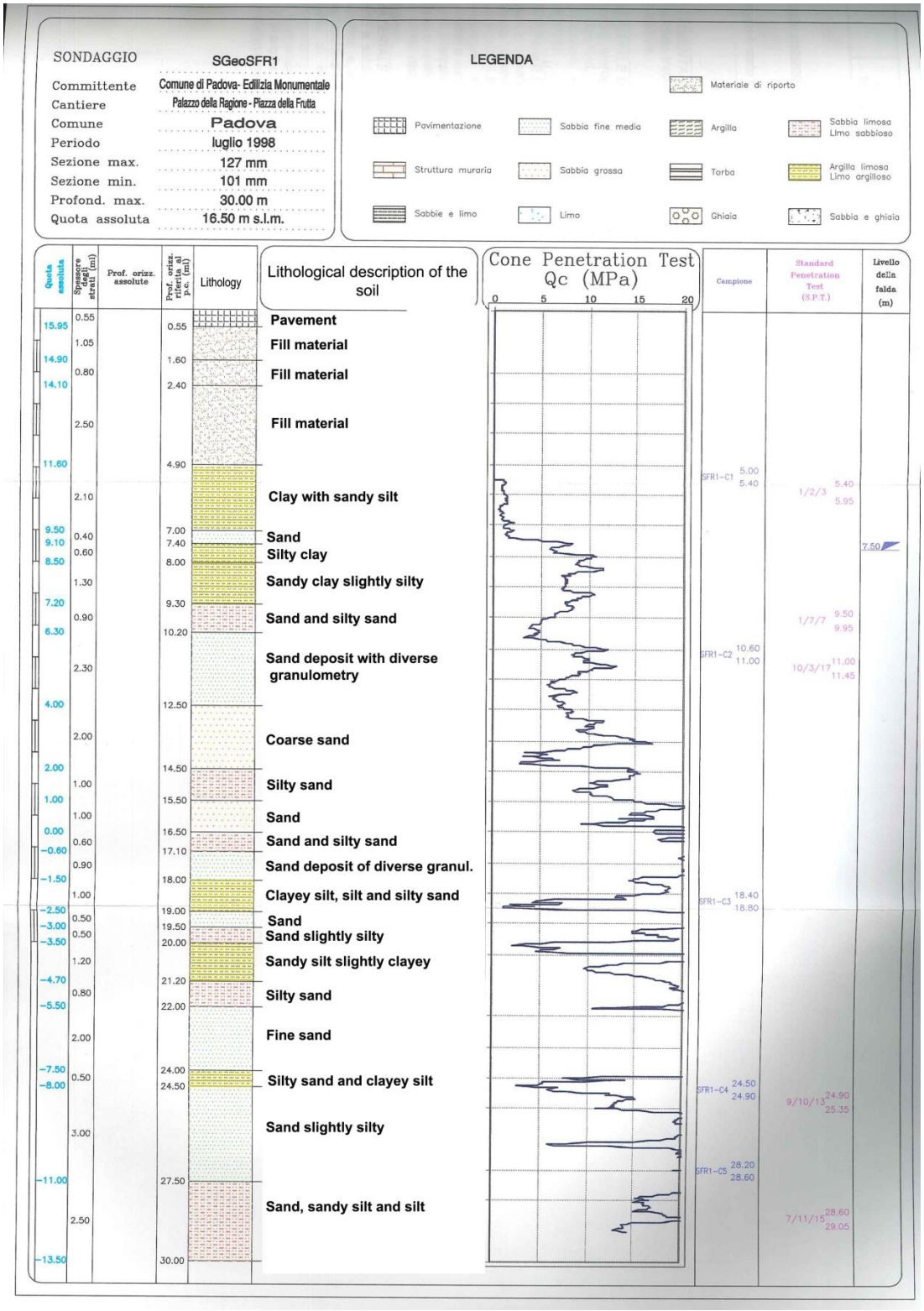

Figure 16. Stratigraphic profile of the soil including test results from borehole SFR [21]

Table 5. Lithological description of the terrain and soil from borehole SFR. [21]

Depth (m)	Material	Description
0.00-0.55	Pavement	It is made of cement reinforced with metallic net.
0.55-1.60	Fill material	Heterogeneous material composed principally by fragments of brick, mortar, polygenic clasts immersed in a light sandy matrix.
1.60-2.40	Fill material	Silt and silty sand color brownish-gray with numerous polygenic clasts, abundant fragments of brick (of large dimension, some completely altered and reduced to dust) and core of mortar. The layer presents abundant carbonaceous materials and old biological alterations (plant nodules and bioturbation).
2.40-4.90	Fill material	Sandy and clayey silt with presence of organic and carbon materials. The layer presents also large fragments of brick and plant nodules (1-3 cm).
4.90 - 7.00	Clay with sandy silt	Clay with sandy silt intercalated with brownish silt. Also, cores of yellowish sandstone clasts, generally altered, were found. The layer presents abundant carbonaceous materials and diatoms. Polygenic clasts are dispersed within the layer, presenting predominantly sandstone and a few fragments of pottery and bricks. In the lower part, there is a layer of around 20cm thick composed essentially by silt, clay and sand slightly laminated with abundant plant remains. **5.40-5.95 Standard Penetration Test: N_{SPT}=5**
7.00- 7.40	Sand	Poorly graded brownish sand but densified, with yellowish streaks containing a minimum percentage of silt.
7.40-8.00	Silty clay	Silty clay of color grey with greenish veins including predominantly lithic sandstone. The layer presents abundant carbonaceous materials and few plant remains. Consistency is clearly plastic.
8.00 -9.30	Sandy clay slightly silty	Sandy clay slightly silty intercalated with thin layers of silty sand color brownish in different shades. Some areas present reddish color due to oxidation phenomena. The consistency of the layer varies from plastic to hard.
9.30- 10.20	Sand and silty sand	Alternated layers of sand and sandy silt with hazelnut and hazelnut-brown color, from slightly stratified to stratified. From depth of 9.60 m to the base of the layer, abundant plant remains and carbonaceous materials are presented. **9.50-9.95 Standard Penetration Test: N_{SPT}=14**

10.20- 12.50	Sand deposit with diverse granulometry	Alternation of fine and rarely coarse sand with layers of variable thickness. Presence of silt, and oxidation phenomenon which gives a reddish coloration. **11.00-11.45 Standard Penetration Test: N_{SPT}=20**
12.50- 14.50	Coarse sand	Coarse sand poorly graded of brown color with intercalations of thin layers of medium and fine sand. At different depths, there are intercalations of thin layers of silty sand. The layer is moderately stiff.
14.50-15.50	Silty sand	Silty sand with intercalated layers of brownish sand. The layer is moderately stiff.
15.50-16.50	Sand	Coarse sand with silty areas brown color with intercalated layers of gravely sand. The layer is moderately stiff to stiff.
6.50-17.10	Sand and silty sand	Intercalations of thin sand layers of brown color and silty sand of dark brown color. There are also are layers of coarse sand ocher color. At the lower part, there is a level constituted by coarse sand ocher color with a thickness of about 20 cm. Evident obvious oxidation phenomena, which gives reddish color. The layer is stiff.
17.10 -18.00	Sand deposit of diverse granulometry	Alternation of medium and coarse sands including polygenic pebbles rounded and flattened. In some levels, a brownish silty fraction is presented. Some intercalations are composed by coarse sand layers poorly graded. The layer is stiff.
18.00- 19.00	Alternation of clayey silt, silt and silty sand	Layers of clayey silt of light brown color, silt of brown color, and yellowish silty sand. The strata present carbonaceous materials and plant remains. The consistency is moderately hard.
19.00- 19.50	Sand	Brownish sand with presence of clayey silt. The consistency of the strata varies as a function of granulometry but generally it is high.
19.50- 20.00	Sand slightly silty	Fine brownish sand slightly silty. The layer is moderately stiff.
20.00-21.20	Sandy silt slightly clayey	Sandy silt slightly clayey of brown color with intercalations of sand.

		At the base of the strata, there is a level of medium sand monogranular with thickness of about 20 cm. The consistency of the strata varies as a function of granulometry but generally it is high.
21.20- 22.00	Silty sand	Silty sand of brown color, with intercalations of sandy and silty layers. The layer is stratified (centimeters) to slightly stratified (millimeters). The layer is moderately stiff. At the base of the strata, there is a level of fine brownish sand poorly consistent and gray plastic silt.
22.00-24.00	Fine sand	Fine sand intercalated with layers of sand slightly silty, of color brown and brown-gray respectively. The layer is high stiff.
24.00- 24.50	Alternation of silty sand and clayey silt	It presents layers of silty sand of brownish color and clayey silt of grayish color with intercalations of coarse sand of yellowish color. The consistency of the layer varies as a function of particle size; in general the silty sand is moderately consistent, while the clayey silt is plastic.
24.50-27.50	Sand slightly silty	Brownish sand slightly silty, with intercalations of silt and clayey silt levels. The layer is moderately stratified. Oxidation phenomenon is presented. The layer is generally stiff. **24.90 – 25.35 Standard Penetration Test: N_{SPT}=23**
27.50-30.00	Sand, sandy silt and silt	Alternation of brownish sand, sandy silt of light brown color and grayish brownish silt, stratified. The consistency of the layer varies as a function of particle size but it is generally medium to high. **28.60 – 29.05 Standard Penetration Test: N_{SPT}=26**

Five standard penetration test (SPT) were carried out in the borehole SFR to provide an indication of the relative density of soil (consistency). Table 6 shows a correlation (given by Terzagui and Peck) between the N_{SPT} and consistency and uniaxial compression resistance of soil:

Table 6. Consistency and uniaxial compression resistance as a function of N_{SPT}. Ref [22]

Consistency	N_{SPT}	Uniaxial compression resistance q_o (kg/cm^2)
Very soft	<2	<0.25
Soft	2-4	0.25-0.50
Medium	4-8	0.50-1.0
Stiff	8-15	1.0-2.0
Very stiff	15-30	2.0-4.0
Hard	>30	>4.0

The location, results and evaluation of the SPT performed in-situ are shown in Table 7. Following criteria of Table 6, it is seen that the consistency of the soil increases through the depth from consistency medium to very stiff.

Table 7. Consistency of the soil

Depth (m)	Length of taken core (cm)	N_{SPT}	Consistency	Uniaxial compression resistance q_o (kg/cm^2)
5.4-5.95	41	5	Medium	0.50-1.0
9.50 - 9.95	23	14	Stiff	1.0-2.0
11.00-11.45	42	20	Very stiff	2.0-4.0
24.90 – 25.35	42	23	Very stiff	2.0-4.0
28.60 – 29.05	30	26	Very stiff	2.0-4.0

Regarding to the foundation, it is known that the base of the tower is built of stone, presumably limestone, with a depth of 4,20 m from ground level [5].

In November of 2004, three cores were extracted, one from the foundation and two from the perimeter walls. Coring on foundation was performed to a depth of 250 cm in the vertical direction, while the cores from perimeter walls were extracted from an average depth of 130 cm. Figure 17 shows the images of cores extracted from perimeter walls.

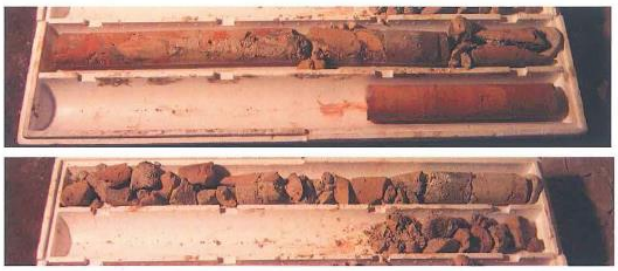

Figure 17. Cores extracted from perimeter walls [5]

This page is left blank on purpose.

3 INSPECTION AND INVESTIGATION

3.1 Visual Inspection and Investigation

The visual inspection of the accessible levels of the tower was carried out in two different days; the first one was on April 8th 2014 in order to inspect the exterior and level 4 (entrance) of the tower and the second day was on May 2nd 2014 in order to check the interior from the level 4 to the top including inspection and location of wrought iron ties.

It was conducted using some basic tools, such as:

•*Camera:* photographic survey was done using two cameras and a plan to mark the exact position from which the pictures were taken.

•*Laser meter and measuring tape:* used basically for checking and comparing the real measurements respecting to the ones provided in the plans.

The main objectives of the visual inspection were:

1. Identification of damage including location and interpretation (also iron ties).

2. Identification of structural and non-structural elements

3. Checking geometry measurements in order to evaluate the precision of the plans.

3.1.1 Geometrical survey

Nowadays, the tower raises a height of 45.6 meters (47.2 m including the roof). As it was described in section 2.3, the tower is composed by 11 levels, 5 vaults and 2 wooden platforms.

The internal separation of walls varies from 3.45 m at the base to 4.75 m in the belfry and 5.50 m at top (battlement). The thickness of walls varies as well, through the height having around 188 cm at the base (excluding buttress), 178 cm at entrance level, 98 cm in the belfry and 57 cm at battlement.

The plant and elevation plans elaborated in 2005 (Ref. [15]) are presented in APPENDIX 1. According to the correlation, there is high accuracy between the measured distance values in-situ and the ones taken from the drawings, it was supported by a photogrammetric analysis scaling the photos adequately.

Figure 18 shows the elevation view of the Tower Anziani with few modifications regarding to the ones elaborated in 2005, for example without the wooden platform that divided level 5 and 6.

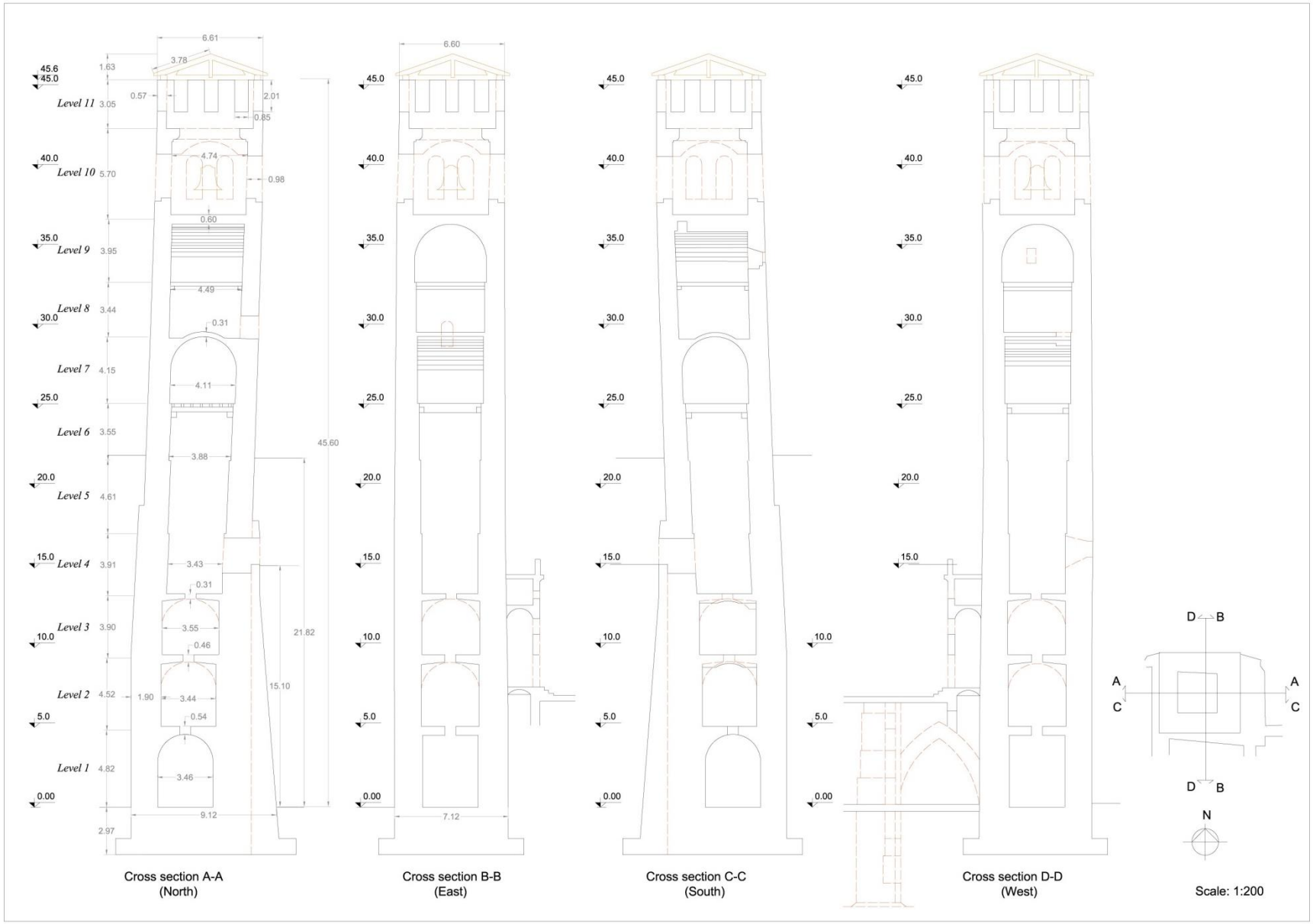

Figure 18. Elevation views of Tower Anziani

3.1.2 Visual inspection from outside

Figure 19 shows the current view of the tower from outside. The building has no special decorations except a wall of 5 meters high above the ground, in the north façade next to Piazza della Frutta, made of white stone-blocks, built perhaps for protection since it is facing the street.

In general, the outer surface of the masonry shows signs of deterioration due to air pollution. Some places present a slight black crust.

Several anchor plates of the original iron ties are visible on each side and seem to be corroded. Some extremes of iron ties, put in 20th century in war time, are also visible (detailed description of ties is presented in section 3.2).

The most of openings have been sealed in almost all the walls, except for the eight large vaulted windows in the belfry, one vaulted window on the eastern façade (to 30 m from ground) and a small rectangular window on the western wall (to 35 m from ground); the last two have a protection net.

Figure 20 shows the appearance of the masonry from outside and an external view of the southern wall which is enclosed by an adjacent structure from the base to the entrance level.

Figure 19. View of tower from outside. Right: North-West view. Left: South-East view

Figure 20. Left: Southern wall at 18 m from ground. Right: External view of southern wall at 13 m from ground

Figure 21, Figure 22, Figure 23 and Figure 24 shows some details of each wall from outside. The photographic survey of the exterior made in 2005 (Ref[15]) is presented in Appendix 2.

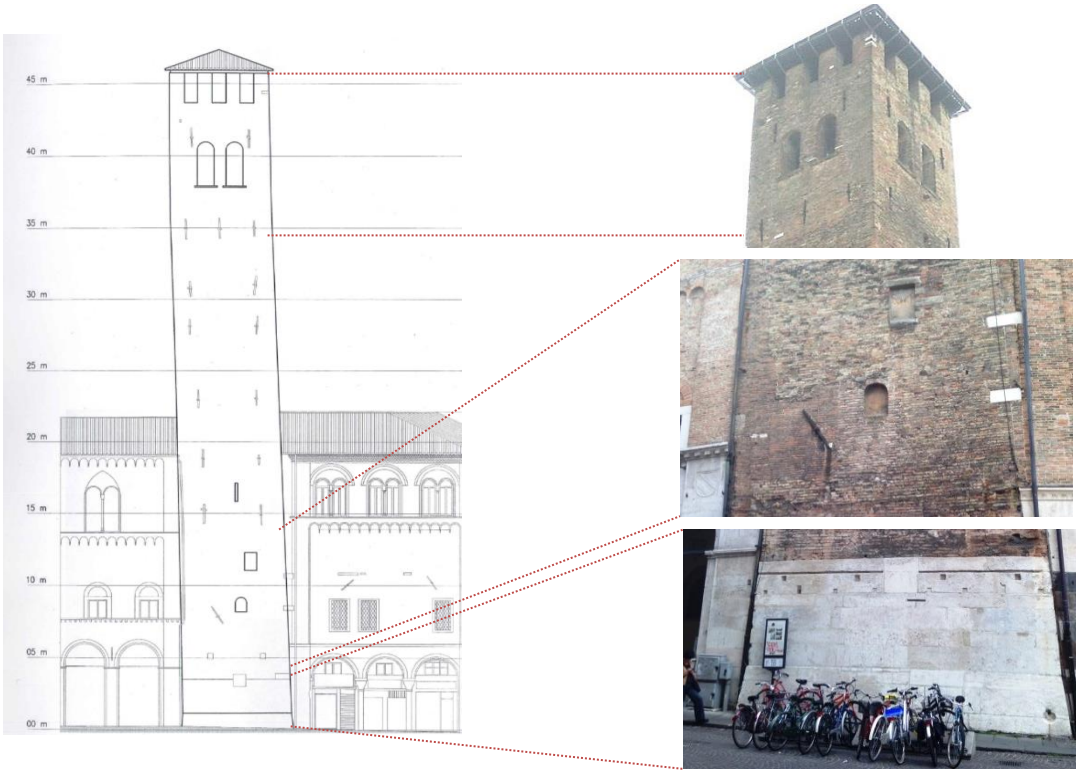

Figure 21. Photographic survey of northern wall from outside

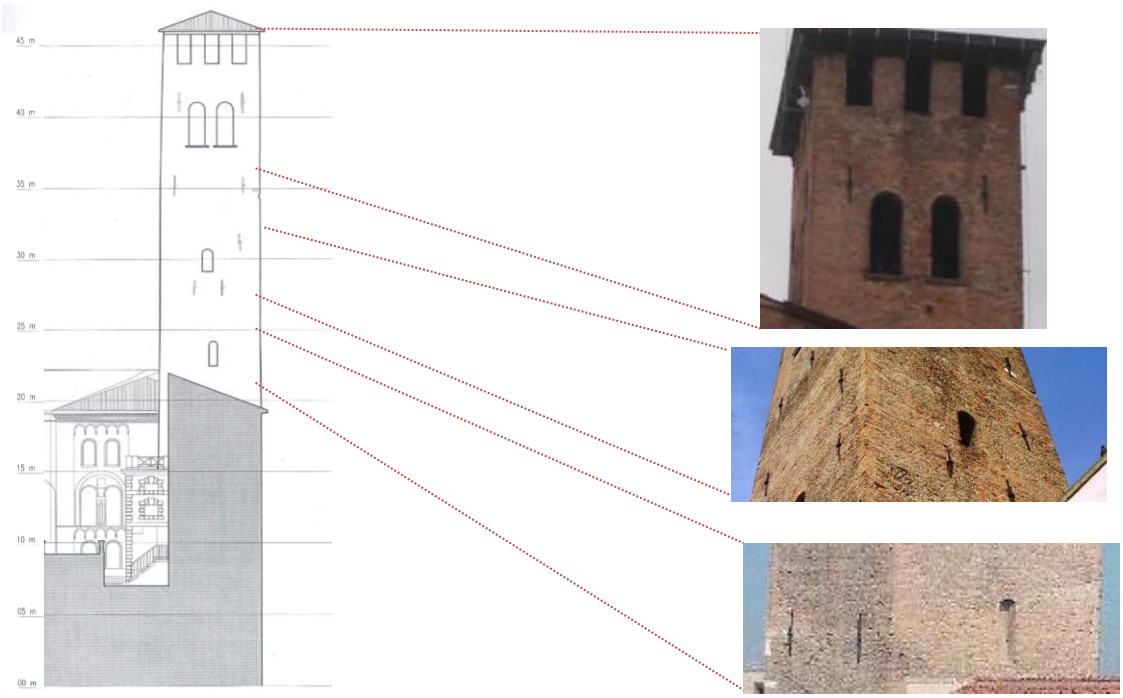

Figure 22. Photographic survey of eastern wall from outside

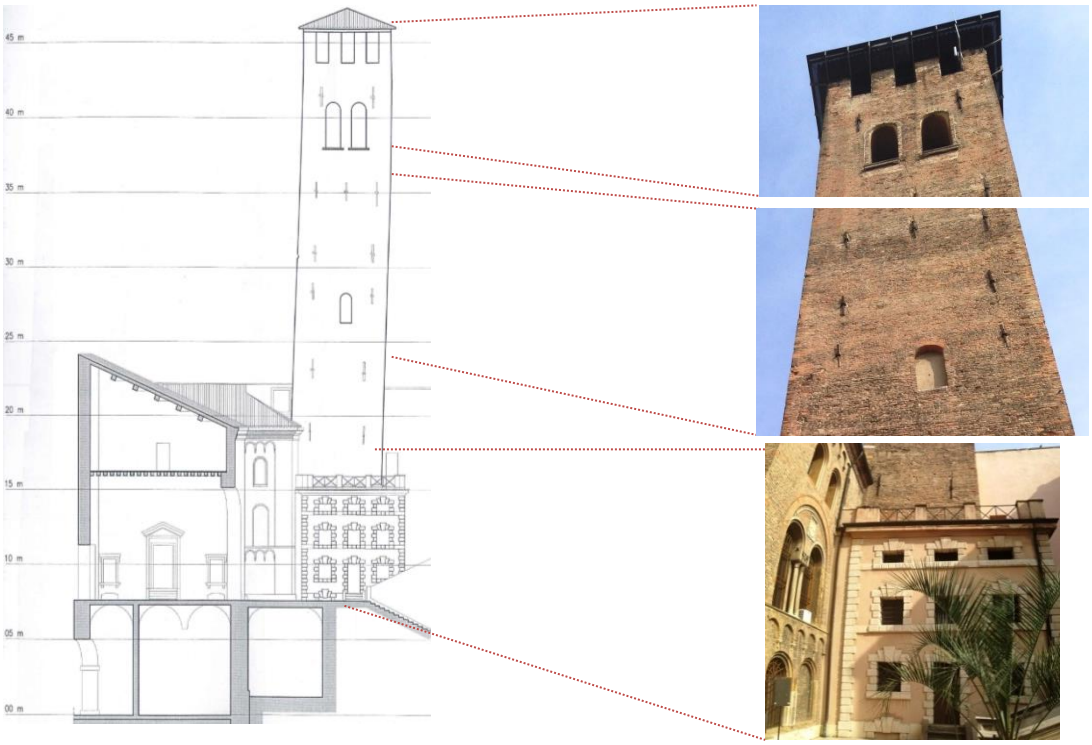

Figure 23. Photographic survey of southern wall from outside

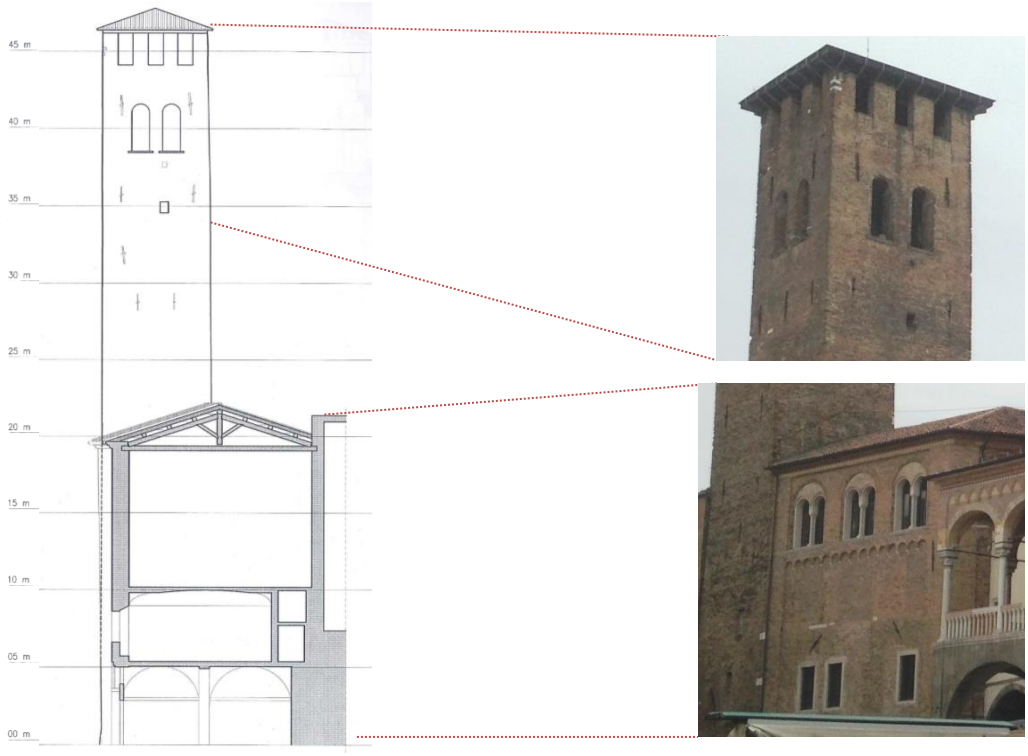

Figure 24. Photographic survey of western wall from outside

In general, there is no visible structural damage from outside. The masonry seems to be in good condition to the naked eye and no cracks were found.

3.1.3 Visual inspection and damage survey from inside

The inner surface of the masonry is almost entirely covered by a layer of cement mortar, which shows slightly degradation due to moisture. Several iron ties are visible in both directions; some of them were set up since the construction and some in 20th century in war time, some ties seem to be active and some passive (it is described in detail in section 3.2).

Figure 25. View of eastern wall from the entrance level

Table 8 shows a brief description of the visual inspection and main damages found in the interior of the tower.

Table 8. Visual inspection and damage survey from inside

The wooden stairs are poorly maintained and present dust deposits. Presumably, they do not fulfill the safety standards. 	Hole of about 20 cm wide in western wall and located to 22.9 m from the ground used to conduct cables. Through the hole it is possible to see that the wall is solid. 
The first wooden platform (+25.31 m) does not seem to fulfill the safety standards. It presents deposits of pigeon droppings and dust. 	Two holes on the vault 4 (+29.46 m), the first in the middle of 1x0.4 m and the second one of 2x0.8 m to access to the next level. 

Above the vault 4 (+29.46 m), there is biological colonization by pigeons and extensive deposits of droppings.

The timber of some beams and timber beams is subjected to biological decayed, probably due to fungi and environmental factors as moisture and humidity.

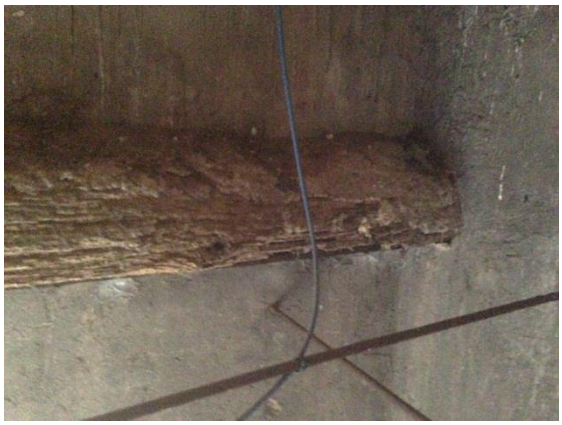

Also the second wooden platform (+32.9 m) does not seem to fulfill the safety standards. Some timber beams present decay and almost all the area is affected by deposits of pigeon droppings and biological colonization (nests and eggs).

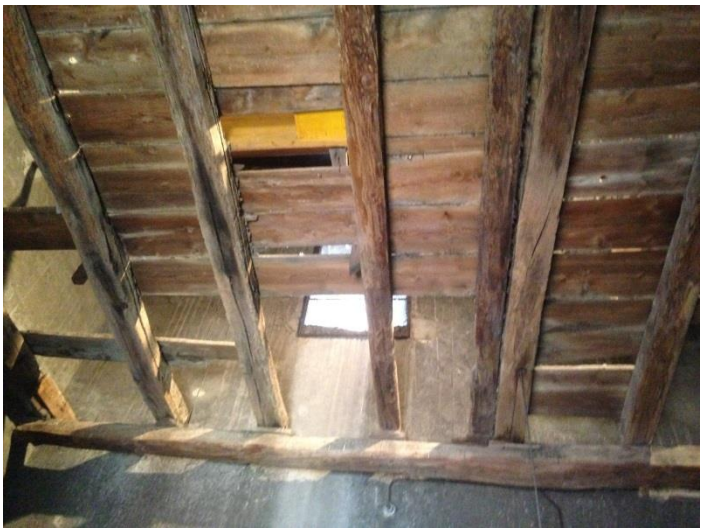

Two holes in the vault 5 (36.85 m from ground), the first (0.9x0.2 m) is located in the middle top and the second one (2.5x0.9 m) is located in the southern side to access to the belfry.

The whole belfry (+36.85 - +42.55 m) is subjected to biological colonization and extensive deposits of pigeon droppings. It includes stairs, vault and bell yoke.

Black crust and algae on masonry wall of battlement due to permanent direct exposition to the environment.

Brown staining on walls near the windows and under crenels due to iron oxides driven by water from the iron reinforcement.

In general, the most frequent deterioration patterns are deposits of pigeon droppings, decay of timber and black crust in the battlement, the deterioration patterns distribution is shown in Figure 26.

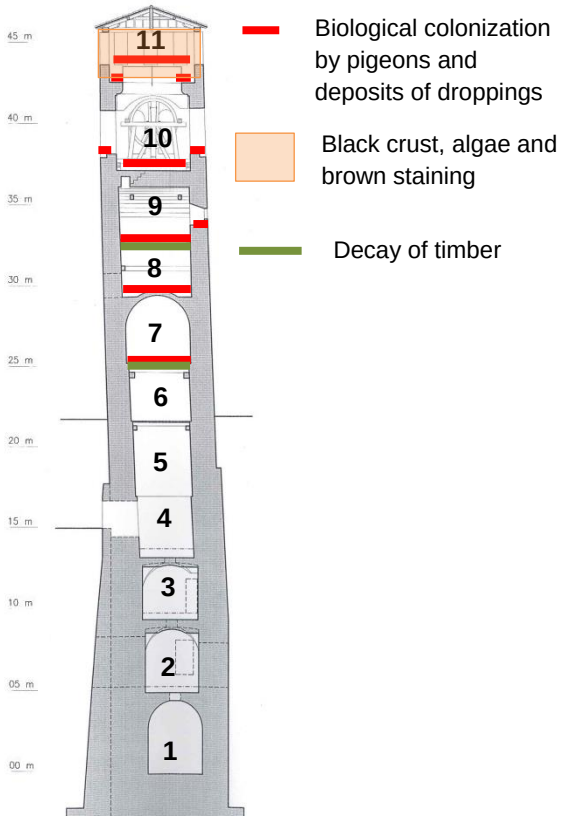

Figure 26. Distribution of deterioration in the tower (elevation cross section view from north)

3.1.4 Roof

As it is shown in Figure 27, the roof is brick four-pitch composed by bricks (tavelle) and clay tiles supported by a simple timber truss, the height is 1.63 m and the side is 6.6 m. The mean beams are about 30x30 cm and are probably made of larch wood, (larice), a conifer in the genus Larix and family Pinaceae, which is commonly used in Veneto region.

Figure 27. Roof arrangement

3.2 Inspection of wrought Iron ties

According to the visual inspection and investigation, in total there are 54 ties, 23 of them were installed since the construction in 13th C and 31 were set up in 20th C in war time. Ties arrangement is presented in Figure 29.

The original ties (13th C) can be identified easily from outside because of their anchor plates (Figure 28), the most of these ties have rectangular section but the cross area is not the same, it varies around 5.5 cm (height) x 2.5 cm (width). The anchor plates have an average height of 110 cm and side section of 10 cm.

Figure 28. View from outside of iron ties on southern wall

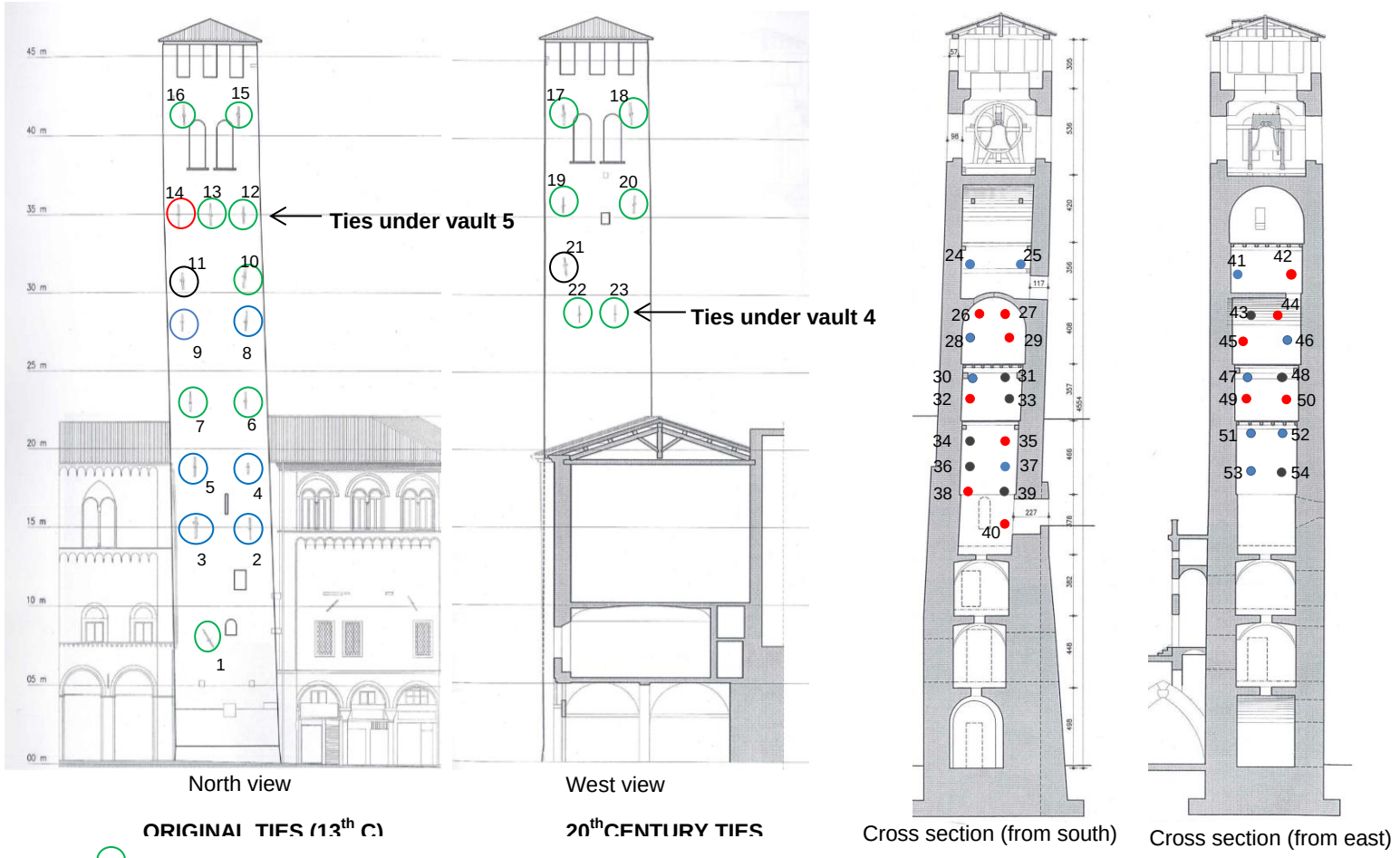

Figure 29. Distribution of ties in the tower

Two of the original ties (N11 and N21) are timber ties which extremes are supported on iron rods to fix the timber to the walls (Figure 30).

Figure 30. Timber tie N21 (13th C)

Figure 31 shows how both types of ties look like in the interior of the tower. The ties installed in 20th century have circular cross section with diameter between 1.6 and 2.0 cm, it is seen that many of them were cut off after the war. These ties were set up opening holes through the masonry walls and sealing them just with cement with no anchor plates.

By simple inspection by hand, it was noticed that many of those ties are passive (not subjected to tension), and some others perhaps are active, Figure 29 shows their distribution indicating the possible state.

Although these ties might work in a passive way, it is probable that they will not behave adequately in presence of an earthquake due to unsatisfactory transmission of stress to the wall because of lack of anchor plates.

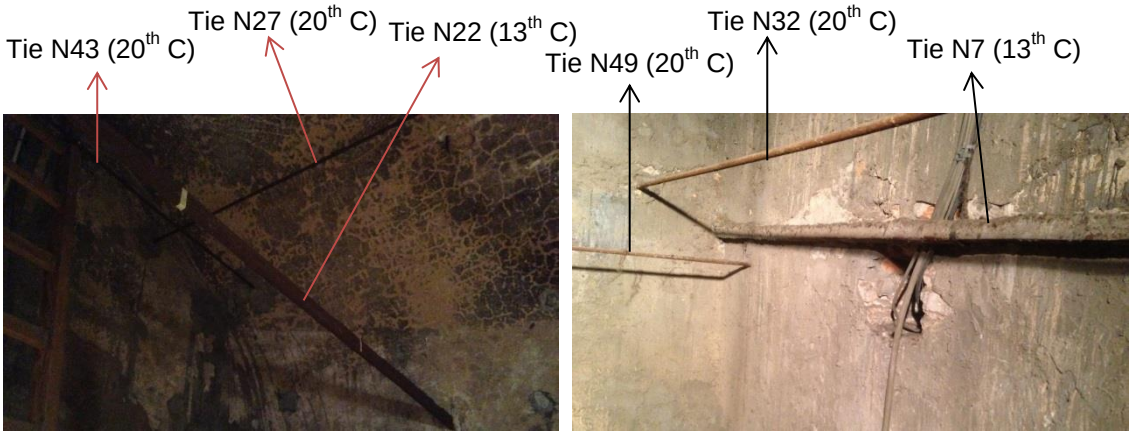

Figure 31. Arrangement of ties from 13th C and 20th C inside the tower

In general, all iron elements present corrosion due to prolonged exposure to corrosive agents for many years (humidity, rainfall, pollutants) which could have caused reduction of effective area and tension capacity.

It was found that the Tie N14 (Figure 32), located under the barrel vault 5, is broken at the middle connection, perhaps due to high level of corrosion, it can be a serious structural damage since the tie might be resisting the thrust generated by the vault.

In addition, the timber tie N11 is subjected to important biological decay, especially at the southern extreme, which surely could cause decreasing of mechanical properties of the material.

Figure 32. Tie N14, broken at the middle connection

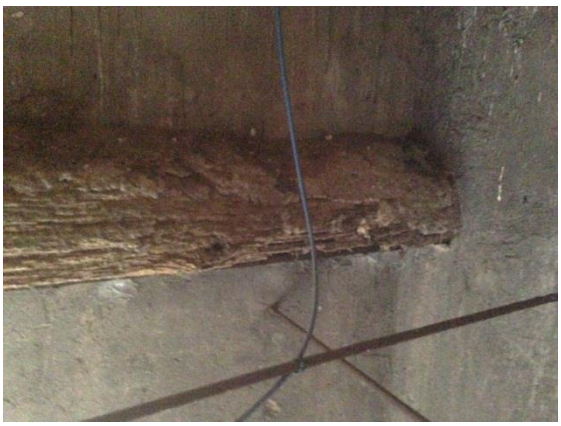

Figure 33. Biological decay of Timber Tie N11 (southern extreme)

4 MATERIALS AND STRUCTURE CHARACTERIZATION

Non Destructive Tests (NDT) and Minor destructive Tests (MDT) are adequate in-situ techniques to obtain qualitative or quantitative information about the materials properties with a minimum impact on the structure.

Table 9 shows the whole test campaign taken into account for the current study including some previous tests carried out in 2004 and 2005 and the current campaign performed on May 26th, 2014.

Table 9. Test campaign performed in Tower Anziani

	Test	Type of test	Date
Previous Tests	*Ground penetration radar (GPR)	NDT	September, 2004
	*Dynamic characterization of the structure under forced and environmental vibration	NDT	May, 2005
	*Petrographic study of brick and mortar	MDT	November, 2005
Current Test Campaign	*Endoscopy	MDT	May 26th, 2014
	*Sonic pulse velocity	NDT	May 26th, 2014
	*Drilling resistance and moisture content	MDT	May 26th, 2014
	*Dynamic characterization of iron ties to calculate tension state	NDT	May 26th, 2014

4.1 Previous tests

The Italian company “Metralab- Servizi per l’ngenieria” carried out several tests and surveys in the Tower Anziani in 2004 and 2005 which are described below.

4.1.1 Ground Penetration Radar (GPR)

The Ground Penetrating Radar is a non-destructive technique based on the propagation of electromagnetic waves or radiowaves through the ground or other dielectric media. Short pulses of electromagnetic waves are transmitted into the ground (in this case, the masonry) by means of a transmit, the signal is reflected and changed on interfaces of different materials, with different dielectric constant, and registered by an antenna receiver.

It is useful to detect voids, moisture, cracks, changes of material, localization of metal anchors, rebars, etc. It is also a practical tool to measure thickness of walls and recognize its typology (solid, three leaves, etc).

The GPR test was carried out on 21th September, 2004. The southern and western walls were evaluated in each floor. Figure 35 presents some obtained radar-scans showing the thickness of wall and details found.

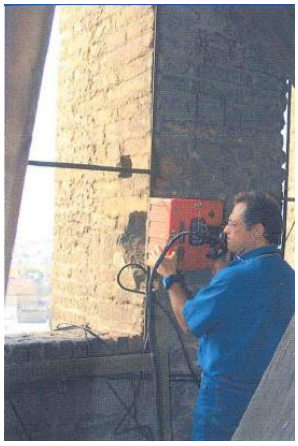

Figure 34. GPR test in belfry walls [2]

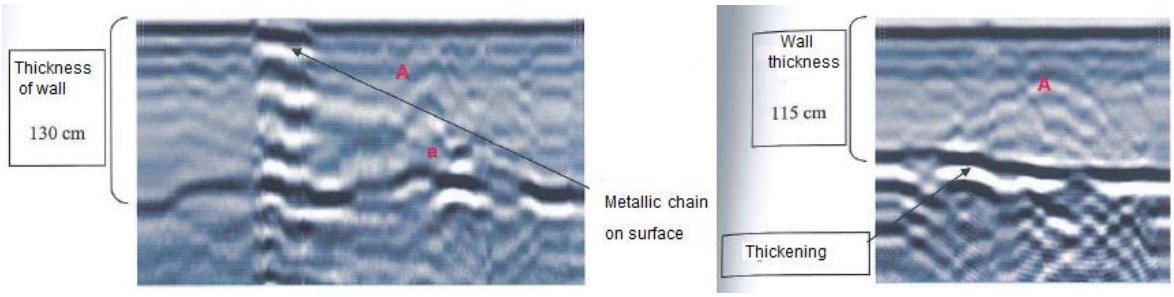

Figure 35. . Radar-scans. Left: western wall- 5th floor. Right: Southern wall-4th floor [2]

Table 10 shows the thickness of each wall tested with the GPR, it is clearly seen that the thickness of wall decreases with the height, starting from 180 cm at the third vaulted room (+13.24 m) and 98 cm in the belfry (+42.55 m). These results are quite approximated to the ones got in the geometrical survey.

On the other hand, it was found that all the masonry walls are solid presenting no leaves.

Table 10. Thickness of walls obtained using GPR [2]

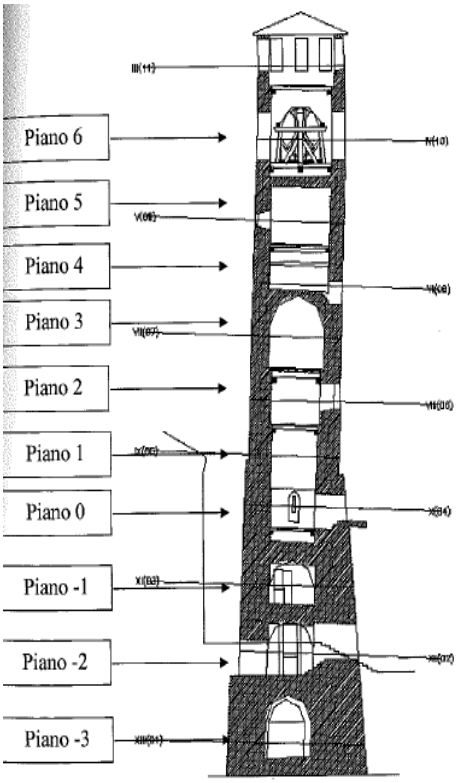

Floor	Wall	Thickness (cm)
6	Southern wall	98
6	Western wall	95
5	Southern wall	105
5	Western wall	130
4	Southern wall	115
4	Western wall	120
3	Southern wall	130
3	Western wall	135
2	Southern wall	145
2	Western wall	150
1	Southern wall	160
1	Western wall	165
0	Southern wall	175
0	Western wall	175
-1	Southern wall	180
-1	Western wall	180

4.1.2 Dynamic characterization

The dynamic study of the Tower Anziani was performed by means of piezoelectric accelerometers (linear electromechanical relation between mechanical and electrical state), which allow to detect the acceleration response of the structure and its frequency of vibration when it is subjected to excitation.

On May of 2005, the company “Metralab” performed this dynamic test on the tower Anziani to identify the dynamic characteristics of the structure such as natural frequencies and modes of vibration. Two different tests were carried out; the first one was an environmental testing, recording the acceleration under environmental vibration (May 19th, 2005) and the second one was a dynamic test recording the acceleration under excitation of the structure (May 26th, 2005).

The signal acquired by the accelerometers (sensors) was recorded and plotted using the multichannel analyzer LMS Pimento and its specific software, the workstation was located on the floor, at the entrance of the tower (to the south).

The sensors were attached to the wall either northern or southern depending on the test carried out; the acquired signal was recorded and plotted by the analyzer and its software. They were set up on several floors of the tower to record accelerations in longitudinal and transverse direction as it is seen in Figure 36, Table 11 and Table 13.

The impulsive force, emitted by the exciter, was applied on either northern or eastern wall from the 5th floor and it was recorded as well.

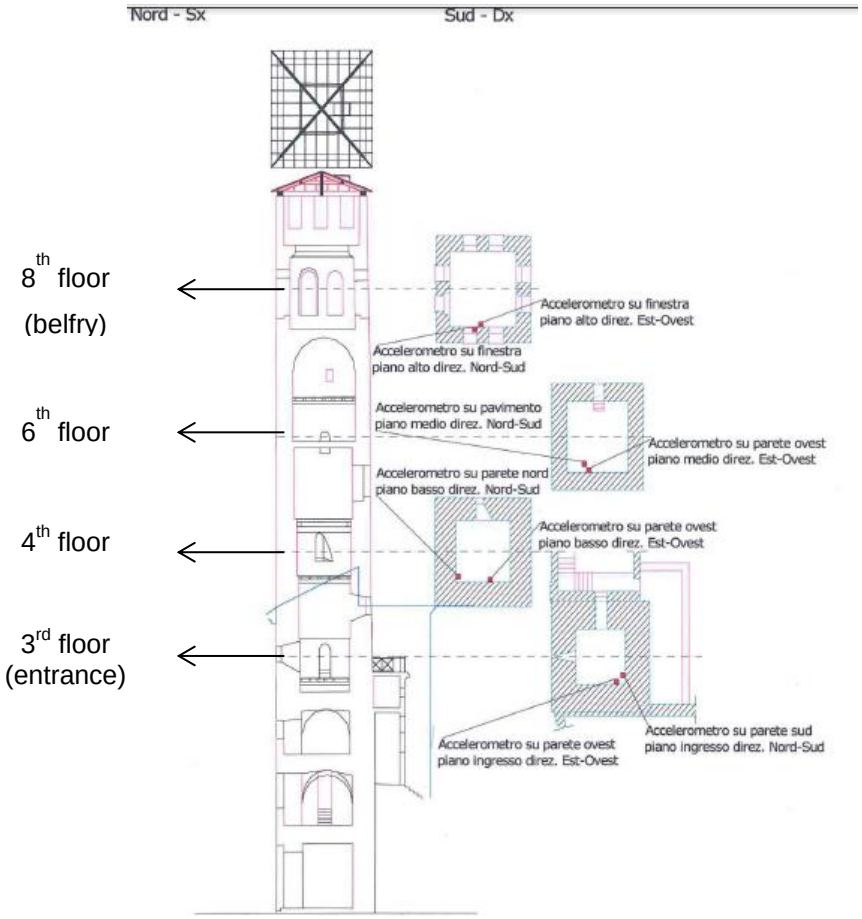

Figure 36. Distribution of accelerometers in the structure [3]

4.1.2.1 Dynamic characterization under environmental vibration

The dynamic test under environmental vibration was carried out on May 19th 2005. Four sensors were set up on 6th floor (top floor) and 4th floor (middle floor) measuring the response in direction east-west and north-south, the particular position of them is shown in the table below.

Table 11. Location of accelerometers for environmental test

N	Floor	Wall	Location	Direction of response
1	8th floor (belfry)	West	On lancet window	East-West
2	8th floor (belfry)	West	On lancet window	North-South
3	6nd floor	West	On wall	East-West
4	6nd floor	On the floor	On the floor	North-South

The results are shown in graphs divided into 3 types, each one is explained below:

1. Figure 37 shows the acceleration response in whole time domain (from 0 to 650 seconds)

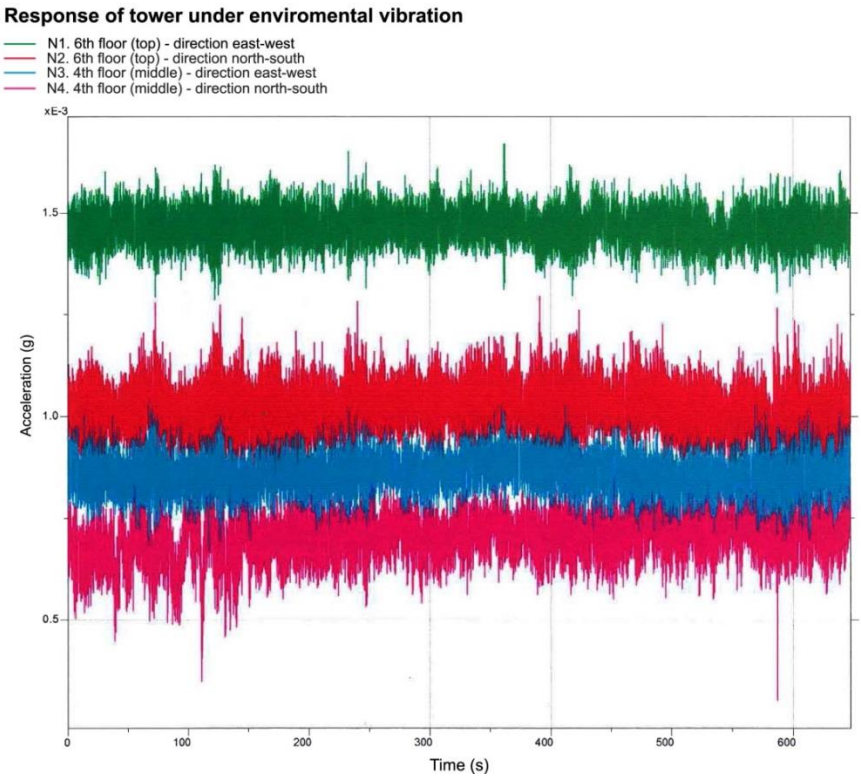

Figure 37. Acceleration response under environmental vibration (Time domain)[3]

2. Figure 38 shows a detailed response in an interval of 10 seconds, from 328 to 338 s. It is seen that the response is almost uniform through time.

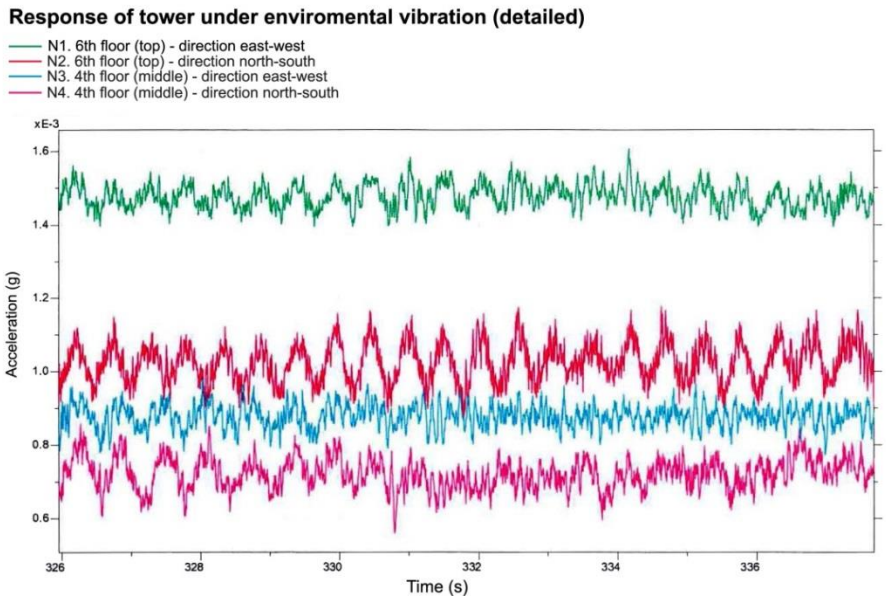

Figure 38. Detailed acceleration response under environmental vibration from 328 to 338 seconds [3]

3. Figure 39 shows the response of the structure in frequency domain for the first 160 seconds indicating some Eigen frequencies. The measured data in time domain was transformed to frequency domain using Fast Fourier Transform (FFT) algorithm calculated by the signal processing analyzer and its software package.

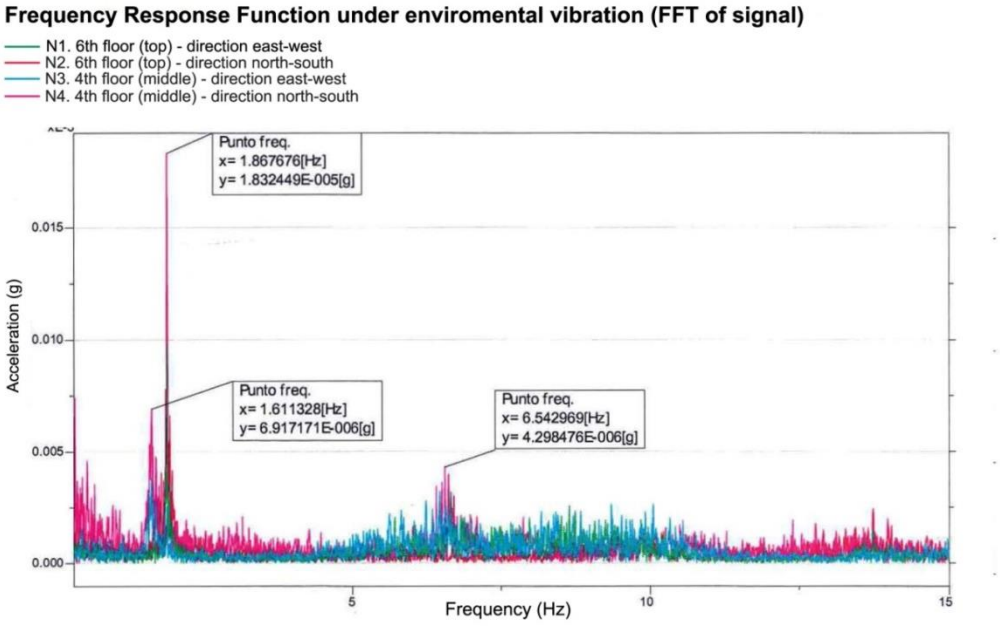

Figure 39.Response of the structure in frequency domain (first 160 s) [3]

Table 12 shows the first eigen frequency obtained under environmental vibration, it is seen that the frequency in direction east-west is slightly higher than direction north-south.

Table 12.First Eigen frequency under environmental vibration

Measuring direction	Location of sensors	Eigen frequency (Hz)
East-West	6th and 8th floor	1.87
North-South	6th and 8th floor	**1.61**

4.1.2.2 Dynamic characterization under forced vibration

The dynamic test under forced vibration was carried out on May 26th 2005. Eight sensors were set up but since the analyzer had just 6 channels for data acquisition, six tests were performed exciting either the northern or eastern wall and changing the channels of acquisition (location of sensors) as it is indicated on Table 14.

The particular positions of the 8 sensors are shown in the table below.

Table 13. Location of accelerometers for dynamic test under forced vibration

N	Floor	Position of Wall	Location	Direction of acquisition
1	8th floor (belfry)	West	On lancet window	East-West
2	8th floor (belfry)	West	On lancet window	North-South
3	6th floor	West	On wall	East-West
4	6h floor	On the floor	On the floor	North-South
5	4nd floor	West	On wall	East-West
6	4nd floor	North	On wall	North-South
7	3rd floor (entrance)	West	On wall	East-West
8	3rd floor (entrance)	South	On wall	North-South

The results for the test N2 (see Table 14) are shown in the graphs below; the graphs of the other tests results are attached in APPENDIX 3.

The graphs of results for the forced vibration test are divided into 4 types:

1. The graph in Figure 40 shows the acceleration response in time domain

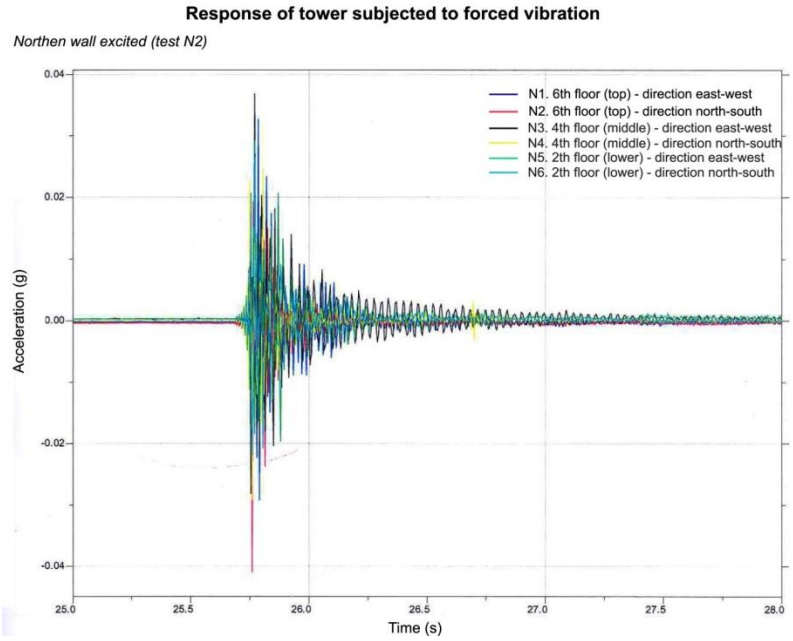

Figure 40. Acceleration response under forced vibration in time domain (Test N2) [3]

2. Figure 41 shows a detailed acceleration response in direction east –west in an interval of 0.3 seconds, from 25.7 to 26.0 s. It is seen that the maximum peak response is 0.035 g on the 6th floor. On the other hand, Figure 42 shows a detailed response in direction north-south in the same interval, the maximum peak for this case is 0.041 on the 6th floor as well.

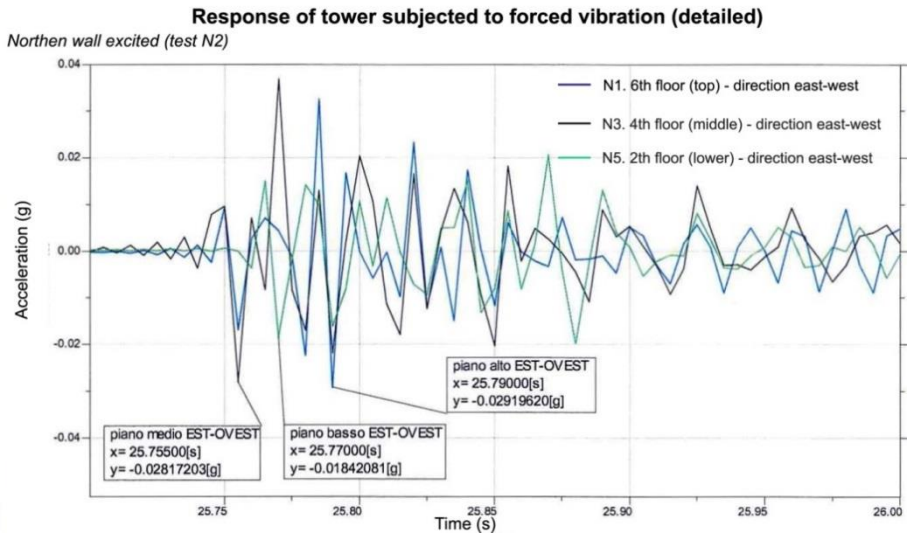

Figure 41. Detailed acceleration response in direction East-West from 25.7 to 26.0 seconds (Test N2) [3]

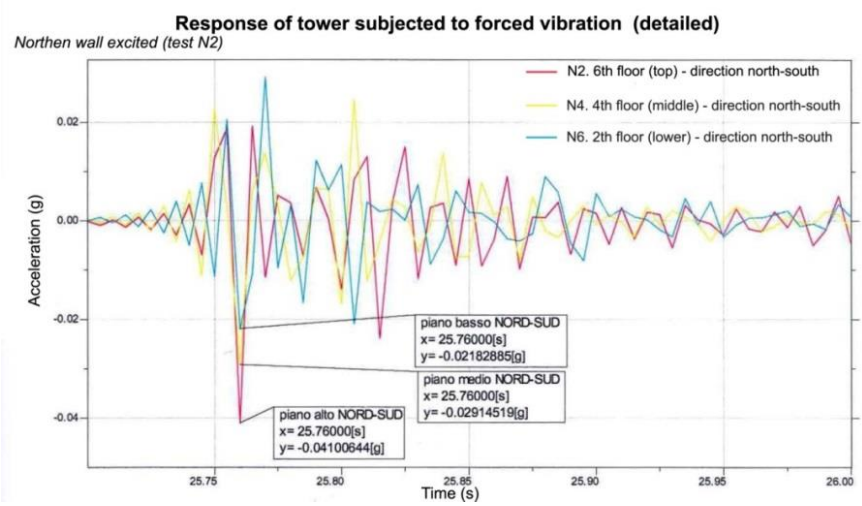

Figure 42. Detailed acceleration response in direction North-South from 25.7 to 26.0 seconds (Test N2) [3]

3. Figure 43 shows the impulse force applied to the structure, it is seen that the maximum force is 31.05 kN (in 25.74 s).

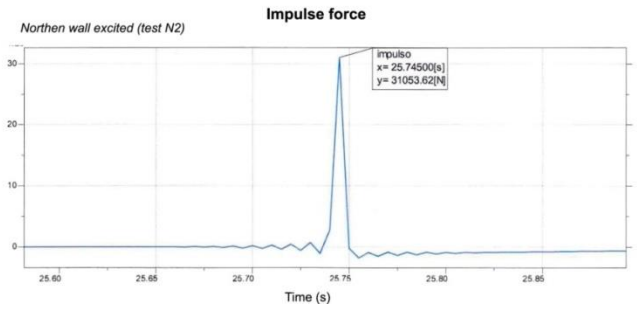

Figure 43. Impulse force applied to the structure (max 31.05 kN) [3]

4. Figure 44 shows the response of the structure in frequency domain indicating some natural frequencies. The measured data in time domain was transformed to frequency domain using Fast Fourier Transform (FFT) algorithm calculated by the signal processing analyzer and its software package.

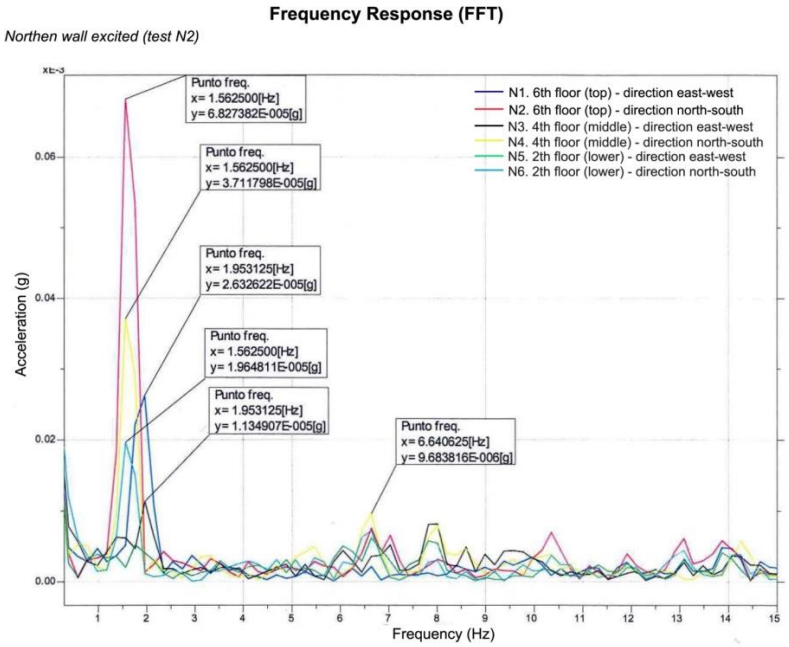

Figure 44. Response of the structure under forced vibration in frequency domain [3]

Table 14 shows the first natural frequency obtained under forced vibration, it is seen that the frequency in direction east-west is slightly higher than direction north-south as same as under environmental vibration.

Table 14.First natural frequency for each test under forced vibration

Test N	Excitation	Measuring dir.	Location of sensors	Natural frequency (Hz)
2	Northern wall	East-West	4nd, 6th and 8th floor	1.95
		North-South	4nd, 6th and 8th floor	**1.56**
3	Eastern wall	East-West	4nd, 6th and 8th floor	1.95
		North-South	4nd, 6th and 8th floor	**1.56**
4	Eastern wall	East-West	3, 4nd and 8th floor	1.95
		North-South	3, 4nd and 8h floor	**1.56**
5	Northern wall	East-West	3, 4nd and 8th floor	1.85-1.90
		North-South	3, 4nd and 8h floor	1.61
6	Northern wall	East-West	3, 4nd and 6th floor	1.90
		North-South	3, 4nd and 6th floor	1.61
7	Eastern wall	East-West	3, 4nd and 6th floor	1.85-1.95
		North-South	3, 4nd and 6th floor	1.66

In general, the results obtained under forced vibration are quite approximated (slightly higher) to the ones got under environmental vibration.

The average of natural frequencies for each measuring direction was obtained, the average of the first natural frequency corresponds to 1.59 Hz (period of 0.63 s) in direction north-south and the second natural frequency corresponds to 1.90 Hz (0.53 s) in direction east-west.

Table 15. Average of first and second natural frequencies obtained with all tests

N	Measuring direction	Natural frequency (Hz)	Natural period (s)
1st	North-South	**1.59**	0.63
2nd	East-West	**1.90**	0.53

These results of natural frequencies, obtained from the dynamic characterization test, are the only quantitative information available for the study of the behavior of the structure. These results will be indispensable not only for the calibration of the FEM model (section 8.3.1), but also to find an accurate modulus of elasticity for the masonry.

4.1.3 Petrographic study of brick and mortar

On November 2005, the company “Studi e Diagnostica per i Beni Culturali” carried out a mineralogical characterization and petrographic study of 2 samples of brick and mortar taken from the tower (Ref [4]). The study was aimed to define some mechanical parameters of the bricks and mortar with according to Italian code DM November 20, 1987. The results of the test are shown in Table 16.

Table 16. Characterization of two samples of mortar and brick [4]

	SAMPLE 1	SAMPLE 2
Material	Brick and bedding mortar	Mortar
Location	Eastern wall	Western wall
Characterization of mortar aggregate	3/4 parts of mixture is aggregate consisting of a sand particle size from coarse to very fine (1mm-62 μm)	3/4 parts of mixture is aggregate consisting of a sand particle size from coarse to very fine (1mm-62 μm)
Characterization of mortar binder	1/4 part is binder composed by mixture of hydraulic and air lime. The binder has numerous lumps (calcareous) from 1mm to 2.2cm.	1/4 part is binder composed by mixture of hydraulic and air lime. The binder has numerous lumps (calcareous) from 1mm to 1.3 cm.
Compressive strength of brick (compression test)	32.0 MPa	-

The mortar from sample 1 presented aggregate divided between quartz and silicate elements and carbonate elements (Figure 45), the matrix presented some porosity.

The mortar from sample 2 had quite similar characteristics to the first one; it was composed by carbonate - limestone, silicate type potassium feldspar and lithic metamorphic fragments (Figure 46).

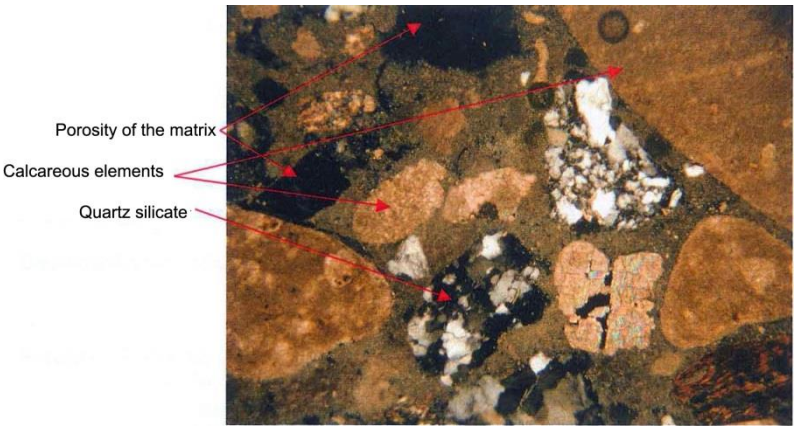

Figure 45. Mineral characterization of mortar (Sample 1) [4]

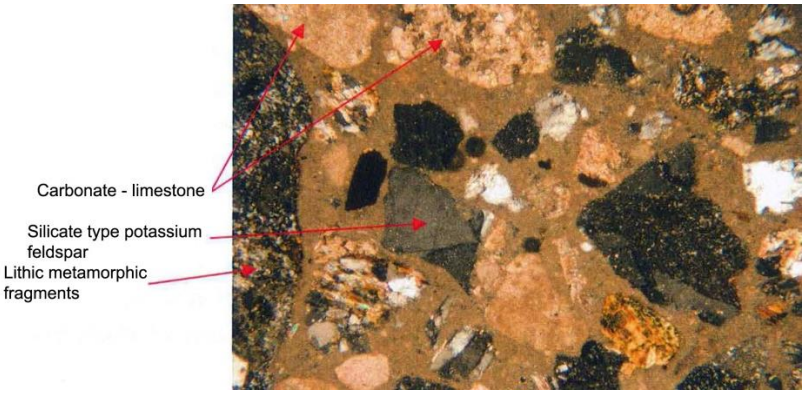

Figure 46. Mineral characterization of mortar (Sample 2) [4]

4.2 In-situ tests

The in-situ testing campaign was carried out on May 27th 2014 using equipment from University of Padua. The performed test were endoscopy on masonry walls, sonic pulse velocity test on masonry walls, drilling resistance and moisture content on timber ties and dynamic characterization of iron ties to determine the tension state; each test is described below.

4.2.1 Endoscopy

4.2.1.1 Overview

The endoscopy is used for visual inspection of inaccessible areas such as the interior of walls. It is a minor destructive technique consisting in introducing a borescope camera into a small drilled hole, made on the element, to inspect its morphology and recognize defects or imperfections. Figure 47 shows some photos of the performed tests.

Figure 47. Endoscopy tests. Left: Test N3. Right: Test N2

4.2.1.2 Implementation of test in Tower Anziani

For the current study, three tests were carried out to define the morphology and composition of the masonry walls, their location are shown in Figure 48 and geometrical characteristics are presented in the next table.

Table 17. Geometrical characteristics of endoscopy tests

Test N	Height from ground (m)	Wall	Thickness of wall (cm)	Diameter of bore (cm)	Bore depth (cm)
1	22.9	Eastern	236	2.5	120
2	14.29	Southern	172	2.5	105
3	14.29	Western	147	*10-20 (bore already existed)*	147

The test N3 was performed in an already existed hole of about 20 cm wide located to +22.9 m from the ground and used to conduct cables.

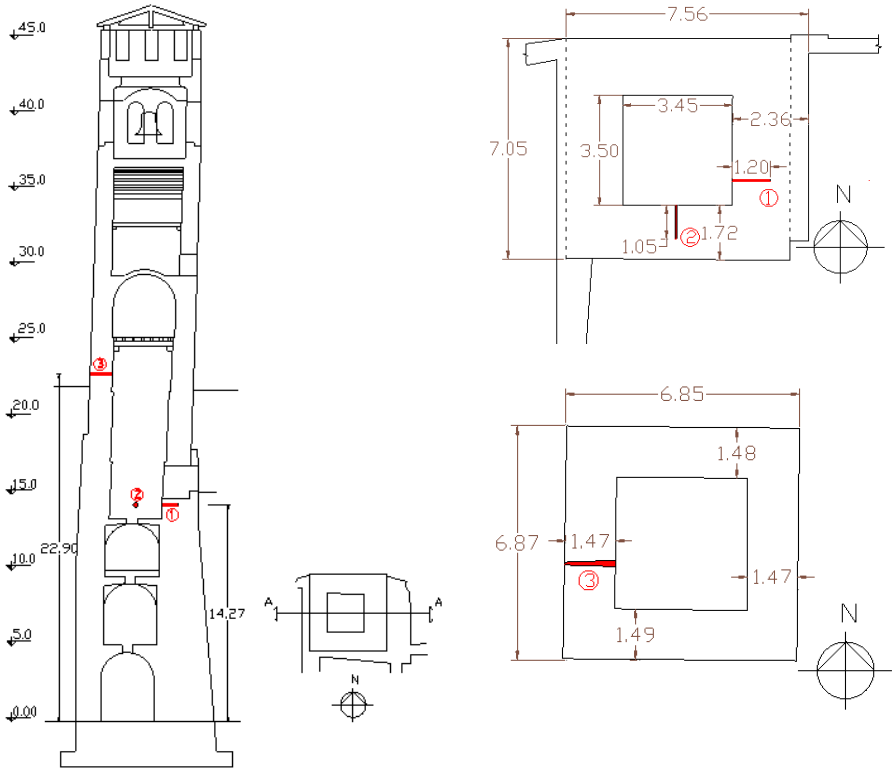

Figure 48. Location of endoscopy Tests. Left: Elevation view. Right: Plant view

Some outstanding images of the interior of the masonry wall, obtained in the tests, are shown in the next table:

Table 18. Images of interior of masonry wall

Test N1 – Eastern wall	Test N2 – Southern wall	Test N3 – Western wall
Depth: 95 cm	Depth: 91 cm	Depth: 127 cm
		

Depth: 15 cm	Depth: 51 cm	Depth: 37 cm
		

It was found that the walls are solid and most probably they are made of the same kind of brick masonry. However, the eastern wall (test 1) presented a smooth and homogenous surface, while the southern wall (test 2) presented a very rough surface showing some small voids and mortar lumps. The western wall (test 3) presented more irregularities and some areas are covered by cement mortar.

4.2.2 Sonic Pulse Velocity Test

4.2.2.1 Overview

The method is based on the generation of sonic impulses at a point of the structure; an elastic wave is generated by percussion or by an electrodynamics or pneumatic device (transmitter) and collected through a receiver which can be placed in various positions. The procedure consists in measuring the time that the wave takes to cover the distance between the transmitter and the receiver, this is affected by the quality and density of the material; then, knowing the thickness of the wall, the velocity wave is calculated.

The results of the test are mainly qualitative providing information about the quality of the masonry through the wall section and the presence of voids, discontinuities and damage patterns. The test is also useful to check the effectiveness of repairs of walls by grouting (Binda et al., 2009).

For the current case, the tests have been performed on two different walls using direct transmission procedure, what means that there was just one receiver located exactly at the opposite side of the transmitter (Figure 49). The transmitter used for this case was a hammer (percussion excitation) and the receiver was an accelerometer.

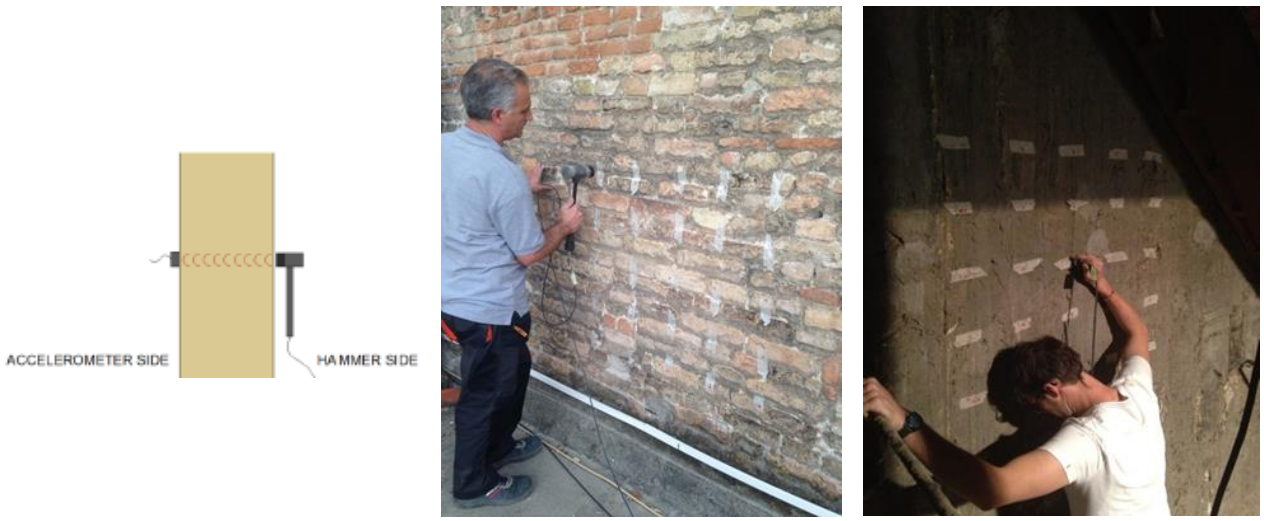

Figure 49. Sonic Pulse Velocity Test Mounting (direct transmission)

The impact hammer had a piezoelectric sensor incorporated to register the impulse force. Since, the input frequency and amplitude, corresponded to the impulse force, depend on the stiffness of the hammer tip; a hard tip was used to get low period and high amplitude. The mass of the hammer determines the energy content of the input stress wave (Ref.[20]).

The signal received in the opposite side of the wall was measured using an accelerometer, supported by hand.

The signals acquired by both, the hammer and the accelerometer, were recorded and plotted using an external analyzer and its specific software called *Soniche IRSnew*, configured with a scan rate of 100000 scans/s and 2048 required scans.

Figure 50 shows and example of both signals in time domain analyzed in *Soniche IRSnew* software, the signal of green color corresponds to the hammer signal, while the yellow one corresponds to the receiver. The time difference between the starting point of each signal represents the time of the wave to arrive and it is used to calculate the velocity wave.

Once the velocity was calculated for each point of the grid, the contour maps were made interpolating the data using the software SURFER 11.

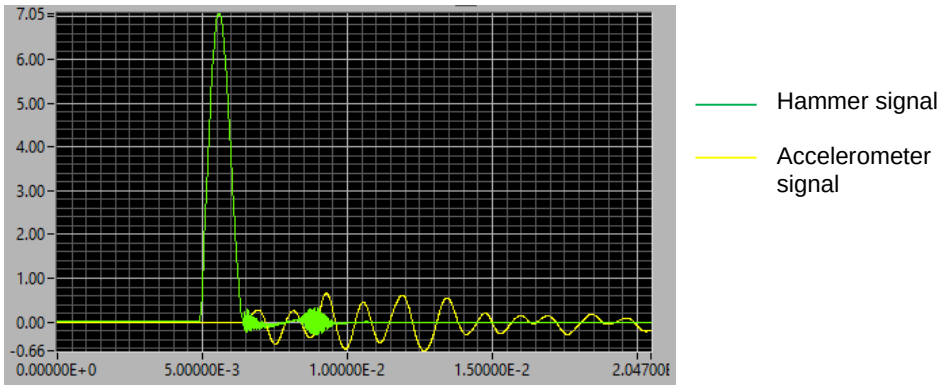

Figure 50. Signals acquired by both, hammer and accelerometer from *Soniche IRSnew* software

4.2.2.2 Implementation of test in Torre Anziani

Three people were required to perform the test, one for the hammer impact, a second one for positioning and supporting the accelerometer and a third one for controlling the data acquisition.

Figure 51 shows the location of both performed tests, on the eastern and southern masonry wall, at the entrance level (+15.1 m above ground level). The area of testing was 80 cm x 80 cm, using a grid of data acquisition of 5x5 points (5 rows and 5 columns) with a vertical and horizontal separation of 20 cm between points.

The eastern wall (Test 1) has a thickness of 2.34 m including the buttress, the exterior surface is covered by a rough white plaster layer and the interior side is covered by cement mortar (Figure 52).

The southern wall (Test 2) has a thickness of 1.72 m. From outside, the brick masonry looks irregular, having entire bricks in some areas and fragments in other areas; however, the distribution of the mortar is approximately regular having a thickness around 1.5 cm. The bricks show a slight decay due to environmental exposition through time. The interior side is covered by cement mortar (Figure 53).

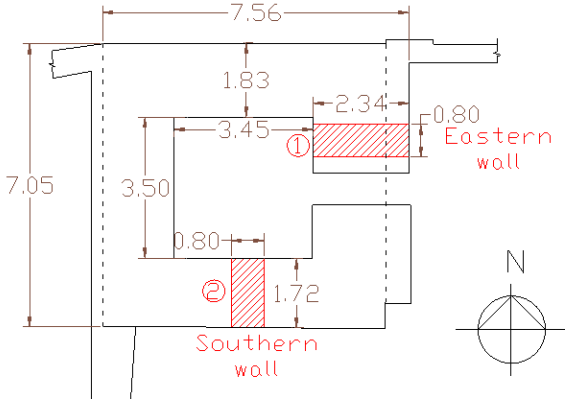

Figure 51. Location of Sonic Pulse Velocity Tests at entrance level (+15.1 m above ground level)

Exterior side of wall (transmitter side) Interior side of wall (receiver side)

Figure 52. Grid of data acquisition on eastern wall (Test 1)

Exterior side of wall (transmitter side) Interior side of wall (receiver side)

Figure 53. Grid of data acquisition on southern wall (Test 2)

4.2.2.3 Results

The test was made three times per each point and as soon as the data acquisition was finished, the time of arrival of sonic waves was determined using the mentioned software, then the velocity wave was evaluated taking into account the distance between the points of reception and transmission (thickness of wall).

The recorded time of wave arrival and average of time and velocity for both tests are reported in the following tables. The highlighted values were omitted because their signals perhaps were disturbed and the time of arrival resulted out of the trend.

Table 19. Data acquisition and wave velocity for Test 1 – Eastern wall

Point	Thickness	Time of wave arrival (s)			Average of time	Average Velocity
	(m)	ta	tb	tc	(s)	(m/s)
11	2.34	1.47E-03	1.38E-03	1.45E-03	1.46E-03	1600.2
12	2.34	1.49E-03	1.49E-03	1.52E-03	1.50E-03	1560.7
13	2.34	1.52E-03	1.58E-03	1.58E-03	1.56E-03	1497.8
14	2.34	1.57E-03	1.63E-03	1.60E-03	1.60E-03	1463.9
15	2.34	1.54E-03	1.45E-03	1.50E-03	1.50E-03	1559.8
21	2.34	1.56E-03	1.56E-03	1.63E-03	1.58E-03	1480.9
22	2.34	1.67E-03	1.75E-03	1.76E-03	1.73E-03	1354.0
23	2.34	1.89E-03	1.77E-03	1.77E-03	1.77E-03	1323.7
24	2.34	1.79E-03	1.86E-03	1.81E-03	1.82E-03	1285.1
25	2.34	1.68E-03	1.85E-03	1.84E-03	1.84E-03	1268.4
31	2.34	1.66E-03	1.50E-03	1.61E-03	1.63E-03	1432.1
32	2.34	1.57E-03	1.63E-03	1.61E-03	1.60E-03	1459.1
33	2.34	1.64E-03	1.57E-03	1.62E-03	1.61E-03	1455.2
34	2.34	1.62E-03	1.65E-03	1.65E-03	1.64E-03	1428.5
35	2.34	1.64E-03	1.59E-03	1.66E-03	1.63E-03	1435.8
41	2.34	1.63E-03	1.66E-03	1.65E-03	1.65E-03	1418.3
42	2.34	1.66E-03	1.53E-03	1.60E-03	1.63E-03	1435.1
43	2.34	1.73E-03	1.69E-03	1.68E-03	1.70E-03	1375.1
44	2.34	1.72E-03	1.78E-03	1.74E-03	1.75E-03	1340.9
45	2.34	1.67E-03	1.70E-03	1.72E-03	1.70E-03	1378.2
51	2.34	1.44E-03	1.55E-03	1.54E-03	1.54E-03	1518.1
52	2.34	1.77E-03	1.69E-03	1.78E-03	1.74E-03	1341.1
53	2.34	1.68E-03	1.70E-03	1.76E-03	1.71E-03	1366.5
54	2.34	1.76E-03	1.78E-03	1.64E-03	1.77E-03	1319.8
55	2.34	1.61E-03	1.55E-03	1.57E-03	1.58E-03	1484.3

Value omitted

Table 20. Data acquisition and wave velocity for Test 2 – Southern wall

Point	Thickness (m)	Time of wave arrival (s) ta	tb	tc	Average of time (s)	Velocity (m/s)
11	1.72	1.26E-03	1.26E-03	1.23E-03	1.25E-03	1373.9
12	1.72	1.26E-03	1.26E-03	1.28E-03	1.27E-03	1356.3
13	1.72	1.26E-03	1.25E-03	1.28E-03	1.26E-03	1364.9
14	1.72	1.25E-03	1.27E-03	1.28E-03	1.27E-03	1357.1
15	1.72	1.10E-03	1.03E-03	1.14E-03	1.12E-03	1535.0
21	1.72	1.26E-03	1.30E-03	1.28E-03	1.28E-03	1342.1
22	1.72	1.56E-03	1.46E-03	1.66E-03	1.56E-03	1103.2
23	1.72	1.17E-03	1.21E-03	1.34E-03	1.24E-03	1387.0
24	1.72	1.17E-03	1.19E-03	1.20E-03	1.19E-03	1447.8
25	1.72	1.15E-03	1.15E-03	1.11E-03	1.14E-03	1512.6
31	1.72	1.48E-03	1.51E-03	1.45E-03	1.48E-03	1159.1
32	1.72	1.43E-03	1.40E-03	1.40E-03	1.41E-03	1219.1
33	1.72	1.56E-03	1.57E-03	1.59E-03	1.57E-03	1096.6
34	1.72	1.38E-03	1.34E-03	1.37E-03	1.36E-03	1263.7
35	1.72	1.39E-03	1.39E-03	1.36E-03	1.38E-03	1247.1
41	1.72	1.37E-03	1.39E-03	1.38E-03	1.38E-03	1244.7
42	1.72	1.58E-03	1.57E-03	1.53E-03	1.56E-03	1101.4
43	1.72	1.49E-03	1.49E-03	-	1.49E-03	1153.4
44	1.72	1.39E-03	1.33E-03	1.31E-03	1.34E-03	1280.5
45	1.72	1.31E-03	1.25E-03	1.23E-03	1.26E-03	1363.5
51	1.72	1.68E-03	1.61E-03	1.59E-03	1.63E-03	1056.7
52	1.72	1.62E-03	1.58E-03	1.64E-03	1.61E-03	1066.5
53	1.72	1.34E-03	1.39E-03	1.42E-03	1.38E-03	1243.7
54	1.72	1.35E-03	1.26E-03	1.28E-03	1.30E-03	1326.6
55	1.72	1.59E-03	1.64E-03	1.56E-03	1.60E-03	1077.8

Value omitted

The results of wave velocities for both tests were summarized in Figure 54 and Figure 55. The graphs at the left show the histogram and the figures at the right show contour maps of velocity waves.

Table 21 shows the maximum, minimum and average velocity for both walls.

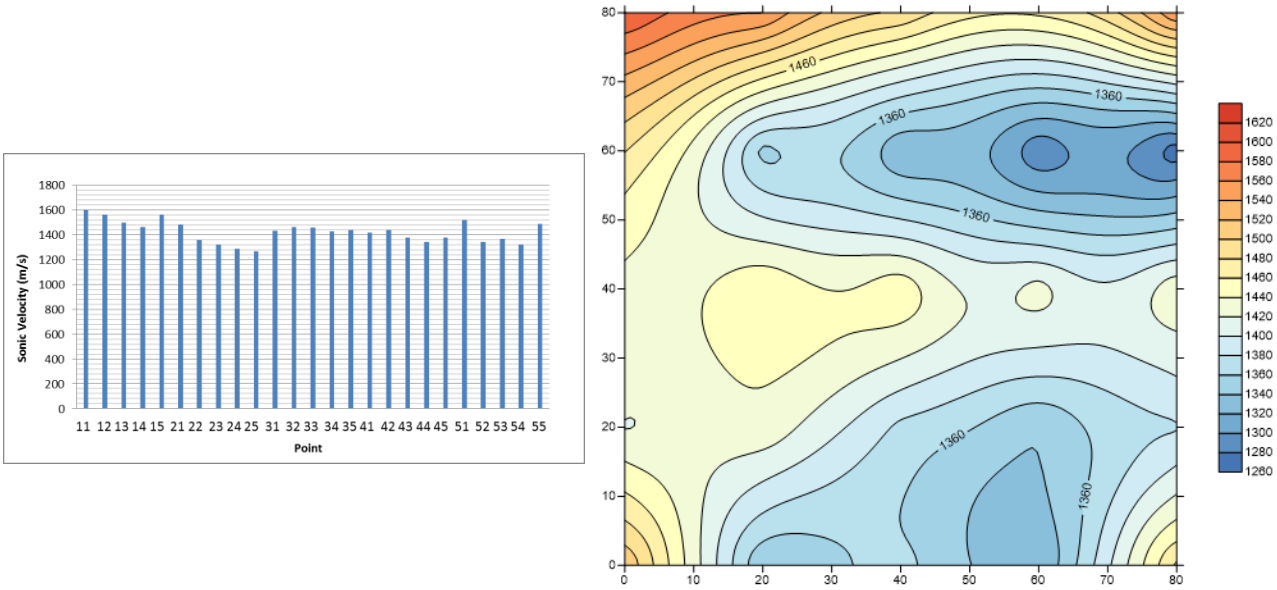

Figure 54. Average velocity plots for Test 1-Eastern wall. Left: Histogram. Right: Contour map

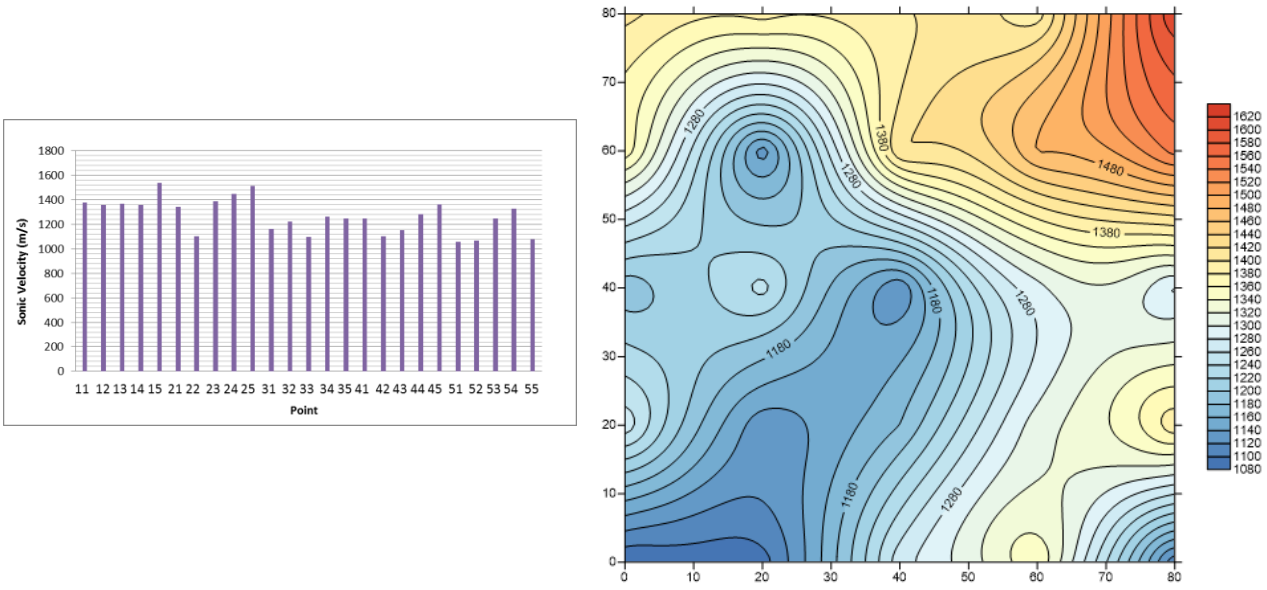

Figure 55. Average velocity plots for Test 2-Southern wall. Left: Histogram. Right: Contour map

Table 21. General results of Pulse Sonic Velocity Tests

Test	Wall	Max velocity (m/s)	Min velocity (m/s)	Average velocity (m/s)	CV (%)
1	Eastern	1600.22	1268.36	1423.29	6.2
2	Southern	1535.03	1056.73	1267.22	11.01

The average of velocity wave for test 1 was 1423.3 m/s and for the test 2 it was 1267.2 m/s corresponding to brick masonry of good quality (velocities higher than 1000 m/s may indicate good quality).

The analysis of data for Test 1 at eastern wall reveals a quite homogenous area, presenting no significant velocity gradients (low coefficient of variation CV). The analysis of data for Test 2 (southern wall) shows some heterogeneity within the surveyed area having velocity gradients at the upper part, with a minimum value of 1056.7 m/s and maximum of 1535.03 m/s.

It is important to notice that the observations obtained from Sonic Pulse Velocity Test are quite similar to those obtained with the Endoscopy, where the eastern wall presents a more homogenous material than southern wall.

In general, It was found that the walls are solid and most probably they are made of the same kind of brick masonry. The quality within the surveyed areas is good; presenting homogenous distribution of bricks and mortar, with neither voids nor discontinuities.

4.2.3 Drilling resistance and moisture content on timber ties

4.2.3.1 Overview

Microdrilling test provides qualitative information about the drilling resistance and quality of the wood throughout its cross section. The measured drilling resistance is based on the energy used to forward a needle through the wood and it depends on the density and quality of the timber.

Microdrilling with a long and thin drill is a useful tool for describing the health profiles in massive wooden elements. This method offers information enabling to decide about a possibility of safeguarding original timber structures and to assess indirectly their load capacity. It allows for measurement of: cross section dimensions (where it is impossible to measure directly), residual cross section of decayed wood (hidden defects), distribution of annual rings, existence of natural defects, etc (Ref. [24]).

During the drilling, the penetration path and also de energy necessary for cutting the hole are recorded and displayed graphically as a function of drilling depth and resistance against drilling (Figure 56). From such a graph, it is easy to determine places with low or even zero resistance, indicating deteriorated zones and voids or cracks. The devices are sufficiently sensitive to measure differences between densities of annual rings, which are visible on the graphs as peaks (Ref. [24]).

To characterize the timber quality, the resistographic measure parameter RM is used which is defined as the area under the resistance graph divided by the length of drilling.

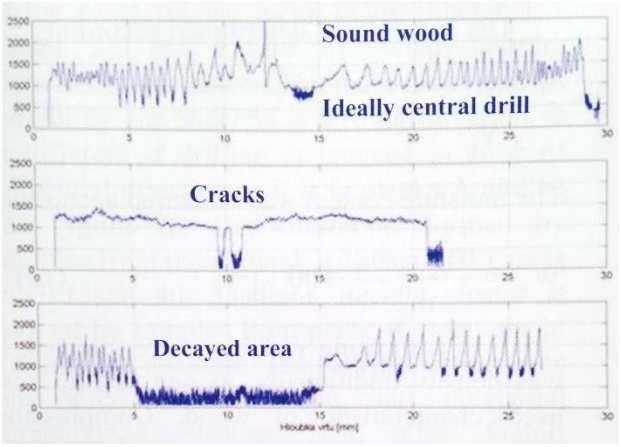

Figure 56. Typical resistance graphs with assessment. Ref.[24].

The tests were performed using a resistograph Resi PD-400 with a needle speed of 2500 r/min and a feed speed of 100 cm/min, the needle has a diameter of 2 mm and length of 40 cm that penetrates into the wooden structure at a constant speed, then the feed and drilling resistance is recorded.

The acquired data was processed in the equipment's software called *PD-Tools Pro* which generates the feed and drilling resistance profile, by which the quality of the wood can be assessed.

4.2.3.2 Implementation of test in Tower Anziani

The test was performed in 20 points distributed between the beams of both wooden platforms and both timber ties. However, it was found that the quality of the timber from wooden platforms was much better than the timber ties, since many of the tests failed due to impossibility of the needle to drill (that means very high resistance of the wood).

The most critical results were obtained in the timber ties. The test was carried on both timber ties located at 31 m above the ground level (Figure 29) between the barrel vault 4 and the wooden platform 2, they correspond to Tie N11 in direction north-south and Tie N21 in direction west-east.

Both timber ties had no constant cross section, the section of Tie N11 was around 20 cm high and 18 cm wide, and the section of Tie N21 was around 19 cm high and 20 cm wide. These timber ties are perhaps made of larch wood (larice) which is commonly used in Veneto region. Some tests were carried in horizontal direction and some in vertical direction.

Figure 57 shows both timber ties; according to visual inspection, timber tie N11 presented some longitudinal cracks and important biological decay, especially on the southern extreme. Timber tie N21 presented also some longitudinal cracks but seems to have better quality without important decay.

Figure 57. Left: Timber tie N21. Right: Timber tie N11 (southern extreme)

Figure 59 shows the location of test points on tie beams at the level +30.0 m. In total 5 tests were carried out, 2 points on Tie N21 and 3 on Tie N11:

Figure 58. Drilling test arrangement, made in horizontal direction (P3)

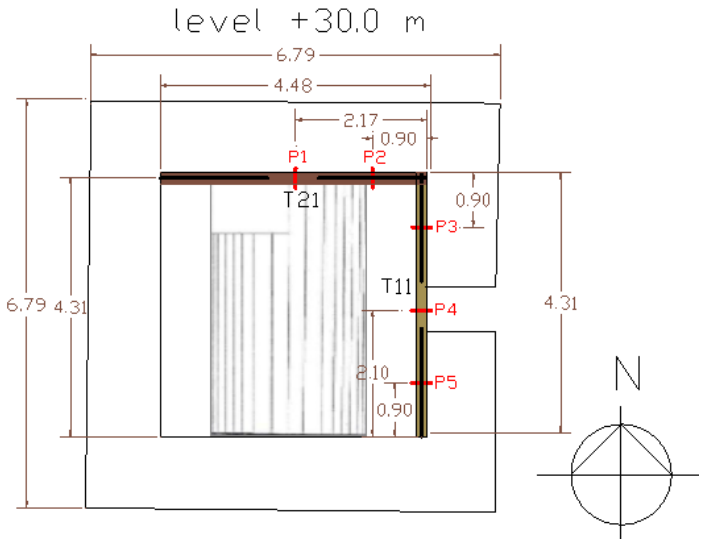

Figure 59. Location of tests points on timber ties (+30.0 m)

4.2.3.3 Moisture content

In addition to drilling test, the moisture content was measured in each point. It is a relevant parameter to evaluate the state of the timber since values higher than 18% represents high susceptibility to biological attack (such as fungi) and degradation of mechanical properties. The normal range of moisture content for timber elements located inside the structure is between 8 and 14%.

4.2.3.4 Results

As it is seen in Figure 59, five tests were carried out (P1, P2, P3, P4, P5), however test P1 failed due to the difficulty to penetrate the Timber tie N21 at this point. The following figures show the feed curve (blue) and drilling resistance curve (green) in terms of amplitude (%); it presents the drilling direction. The assessment is shown in different colors.

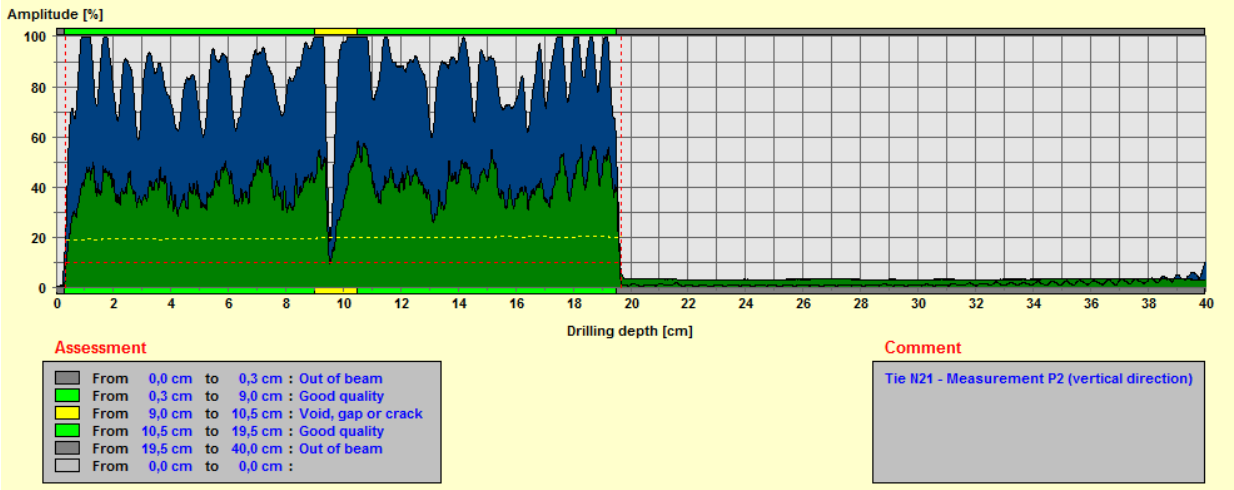

Figure 60. Feed and drilling curve for P2 (Timber tie N21)

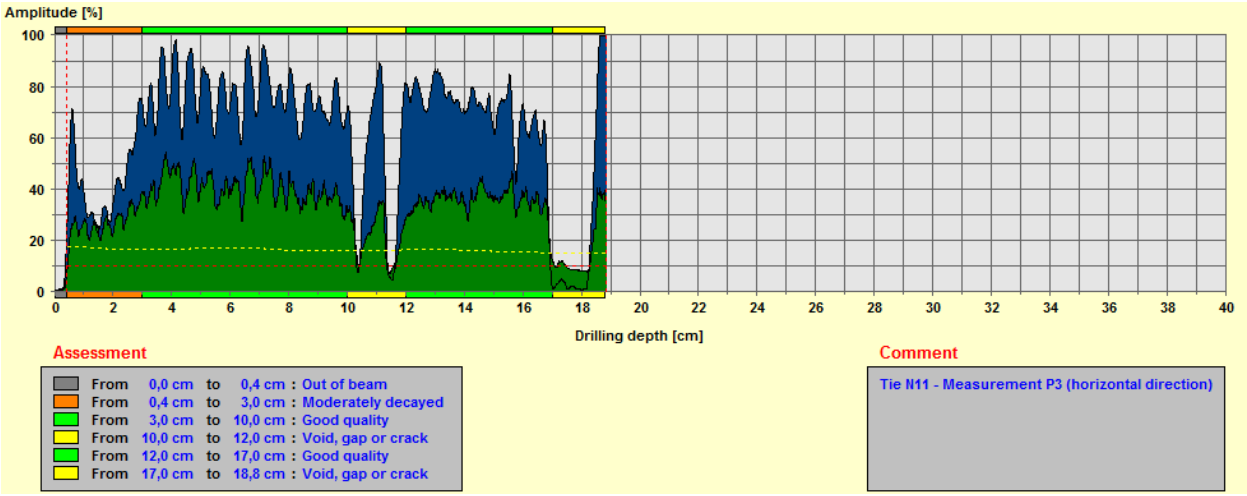

Figure 61. Feed and drilling curve for P3 (Timber tie N11)

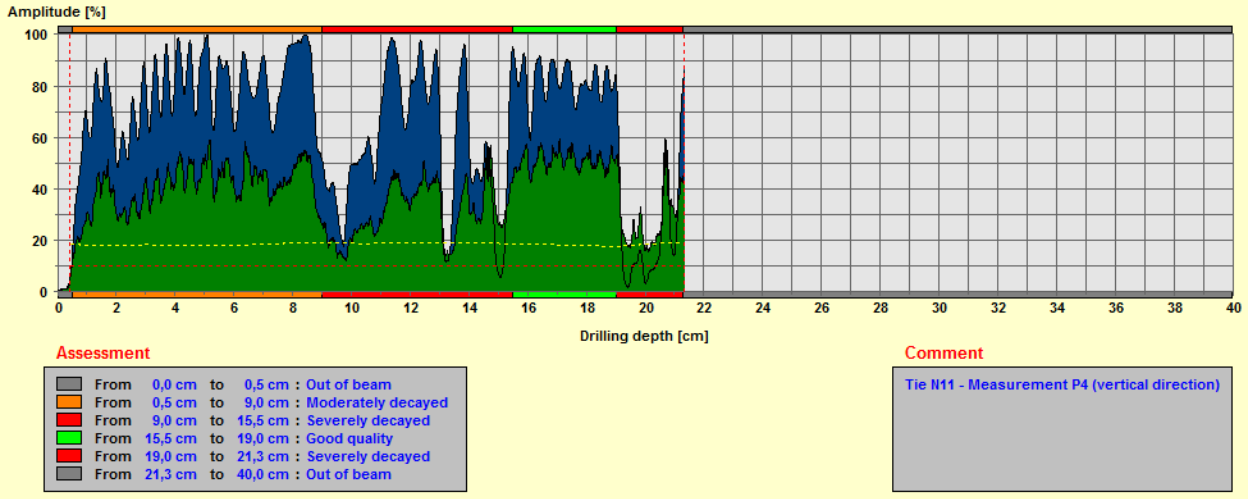

Figure 62. Feed and drilling curve for P4 (Timber tie N11)

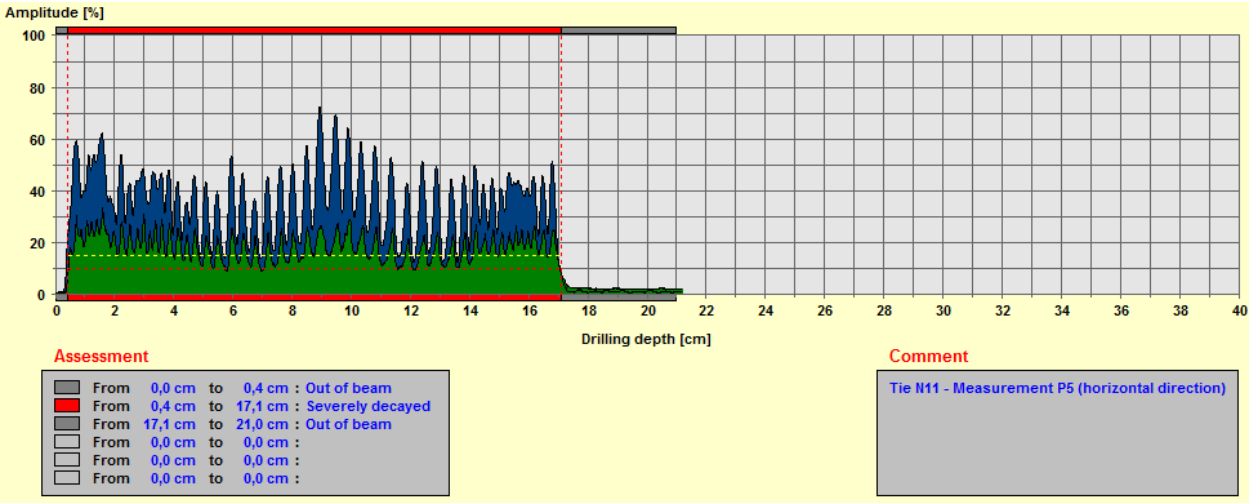

Figure 63. Feed and drilling curve for P5 (Timber tie N11)

The drilling curves of P3 and P4 from tie N11 show many gradients (heterogeneity) presenting areas with good quality, moderately decayed, severely decayed and voids. The drilling curve from test P5 (southern extreme of timber tie) presents much lower values through all the section which represents important decay in that zone as same as it was observed in visual inspection.

On the other hand, the quality of the timber from the test P2, made on timber tie N21, is better and more homogenous than the other timber tie.

The drilling curves for all tests are shown in Figure 64 and just for the timber tie N11 in horizontal direction in Figure 65.

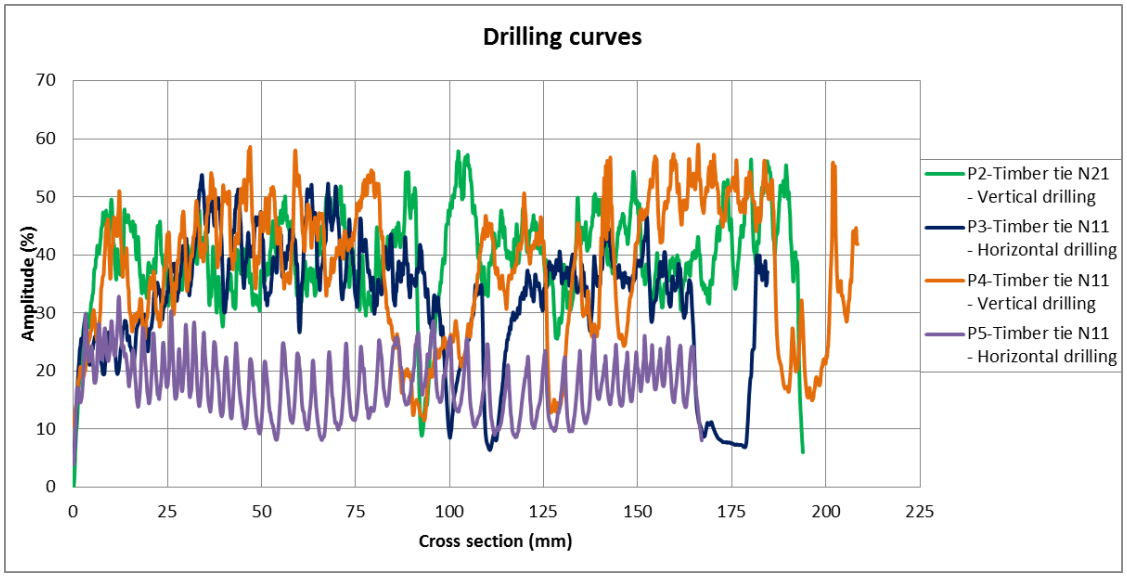

Figure 64. Drilling curves for all tests

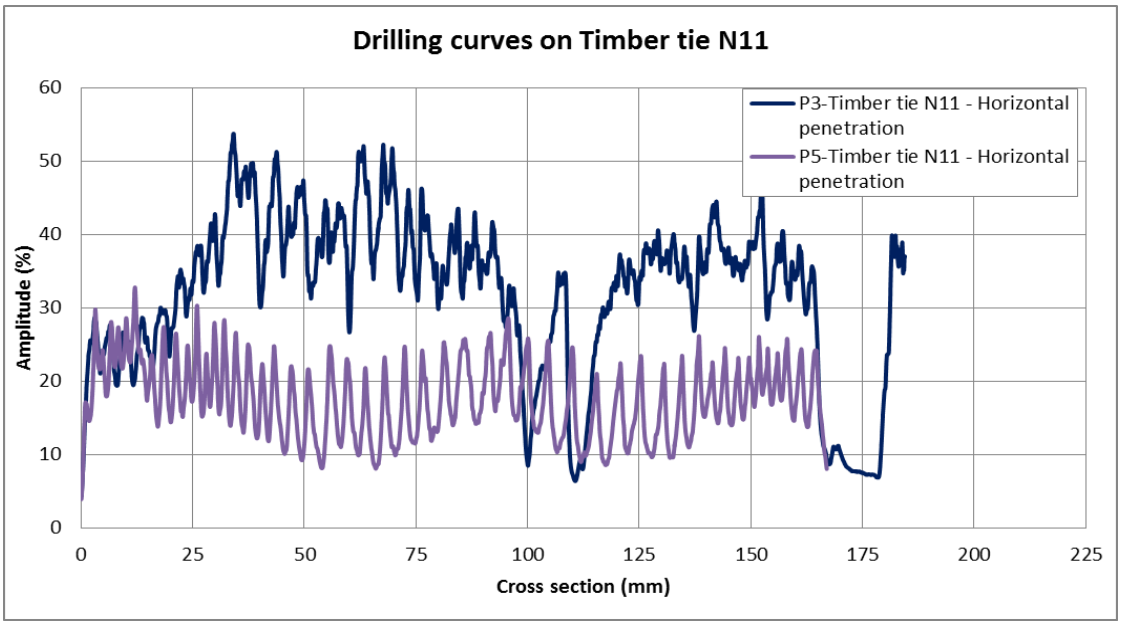

Figure 65. Drilling curves on Timber tie N11 - Horizontal direction

From Figure 64, it is seen that the drilling resistance in vertical direction tends to be higher than in horizontal direction, the high peaks represent cracks or voids. It is clear that the drilling resistance of P5 is much lower than the others.

Figure 65 shows two drilling curves for the timber tie N11 made in horizontal direction, since they belong to the same timber, it is clear that the area corresponding to the test P5 (southern side of the tie) is highly decayed.

The general resistographic measure parameter (RM) was calculated dividing the area under the drilling curve by the depth of penetration. The results are shown in Table 22, presenting also the average values of moisture content.

Table 22. Drilling resistance RM and MC

Point	Tie	Direction	Depth (mm)	Area under curve	Drilling resistance RM=Area/Depth (%)	Moisture Content MC (%)	Observation
P2	N21	Vertical	192	7705.04	40.1	17.2	Good quality, hard to drill
P3	N11	Horizontal	184	5920.21	32.2	19.0	Regular quality
P4	N11	Vertical	208	7834.52	37.7	16.8	Regular quality
P5	N11	Horizontal	168	2937.73	17.5	18.8	Poor quality - Very decayed

The moisture content is out of normal ranges (8-14%) for all cases which may cause biological attack.

In general, the timber from P2 (timber tie N21) has a good quality presenting the highest drilling resistance; the timber from P3 and P4 (timber tie N11) have regular quality presenting some discontinuities and density changes through the section; timber from P5 (southern extreme of timber tie N11) presents the lowest drilling resistance which represents very low quality of the material due to important decay.

The mechanical properties of timber tie N11 might be seriously affected due to high level of decay.

4.2.4 Dynamic characterization of iron ties to calculate tension state

4.2.4.1 Overview

Dynamic characterization on tie rods is required to evaluate the tension state by means of their natural frequencies. It is made by experimental modal analysis recording the response of the ties under either forced or environmental vibration using accelerometers conveniently attached to them.

Once the natural frequencies have been determined, the tension state of the ties can be estimated based on vibrating chord theory by means of the next equation:

$$\boldsymbol{f = \frac{n}{2\, l_o}\sqrt{\frac{T}{\mu}}} \qquad (1)$$

$$\boldsymbol{T = \frac{4\,\mu\, f_n^2\, l_o^2}{n^2}} \qquad (2)$$

Where T is the tension of the tie, f_n is the n^{th} natural frequency, l_o is the effective length and μ is the density of the material per unit length.

4.2.4.2 Implementation of test

The dynamic characterization was performed on 4 ties which are shown in Figure 66, tests T2 and T4 correspond to the ties N22 and N13 installed in 13th C, located under the vaults. Tests T1 and T3 correspond to the ties N29 and N32 set up in 20th century.

The test could not be performed on other ties from 20th C of other floors because they were set up very near the walls making very difficult the recording of the vibration response.

The experimental modal analysis was carried out using 3 piezoelectric accelerometers placed at the quarters of the tie length as it is seen in Figure 67 and Figure 68. The response was recorder by a data acquisition analyzer under environmental vibration and forced vibration generated by a hit by hand. The sampling frequency used was 200Hz for 80 seconds (1600 data).

The modes of vibration and natural frequencies were calculated using the software *NI Diadem 2010* and *Artemis_pro* which get the response in frequency domain from time domain by means of the Fast Fourier Transform.

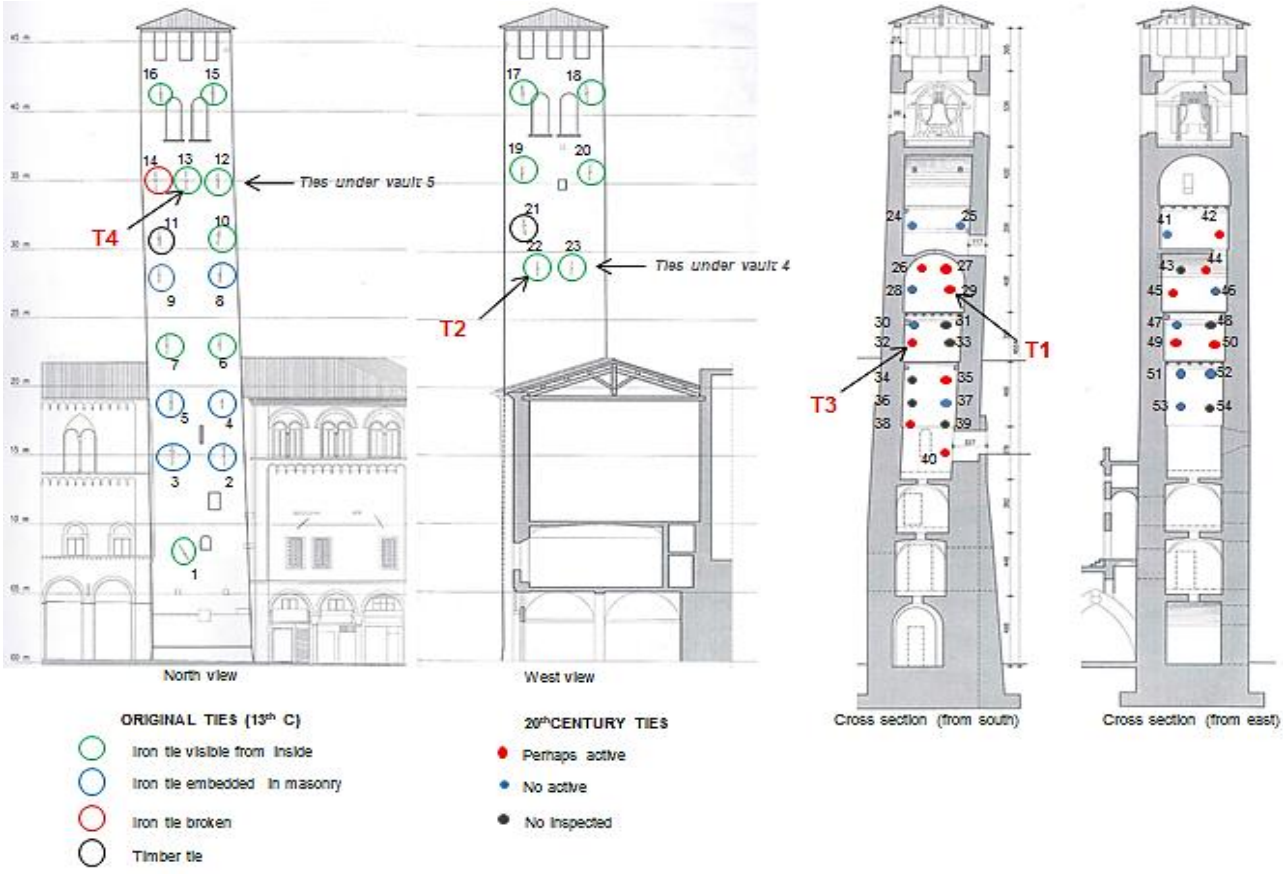

Figure 66. Location of tested ties (T1, T2, T3, T4)

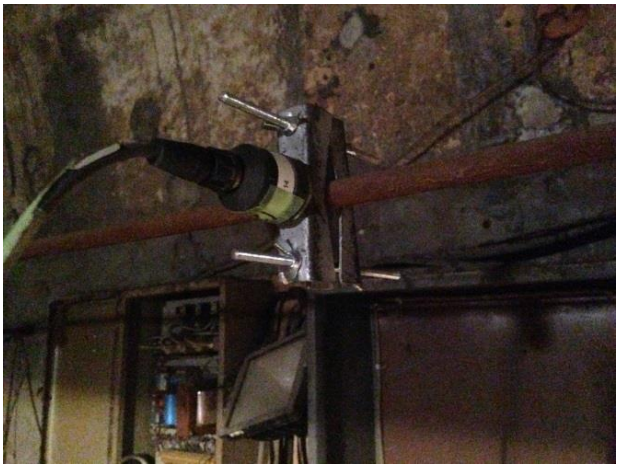

Figure 67. Mounting of accelerometer in tie - **T1**

Figure 68. Location of the 3 accelerometers in tie – **T2**

The test was done three times for both environmental and forced vibration to get an average of the resulted natural frequencies.

The following tables show the characteristics of each tested tie. The density of the material was taken from literature corresponding to wrought iron with a value of 7850 kg/m^3.

Considering the ties as fixed connected in the extremes, the effective length was calculated as the half of the total length.

Table 23. Characteristics of ties corresponded with tests T1 and T3

Test	Tie	Period	Circumference (cm)	Diameter (cm)	Area (cm2)	Length (m)	Effective length (m)	Density per unit length (kg/m)
T1	N29	**20th C**	5.2	1.66	2.15	4.19	2.10	1.69
T3	N32	**20th C**	6.0	1.90	2.83	3.87	1.93	2.22

Table 24. Characteristics of ties corresponded with tests T2 and T4

Test	Tie	Period	Height (cm)	Width (cm)	Area (cm2)	Length (m)	Effective length (m)	Density per unit length (kg/m)
T2	N22	**13th C**	6.1	1.53	9.35	3.84	1.92	7.34
T4	N13	**13th C**	5.23	2.83	14.83	4.21	2.11	11.64

Figure 69 shows the response in time domain under environmental vibration and forced vibration for test T1 –measurement 2. Figure 70 shows the FFT for both cases, it is seen that the natural frequencies are almost the same for environmental and forced vibration. The mode shapes are shown in Figure 71.

APPENDIX 4 shows the natural frequencies calculated for each measurement for each test and the corresponded average.

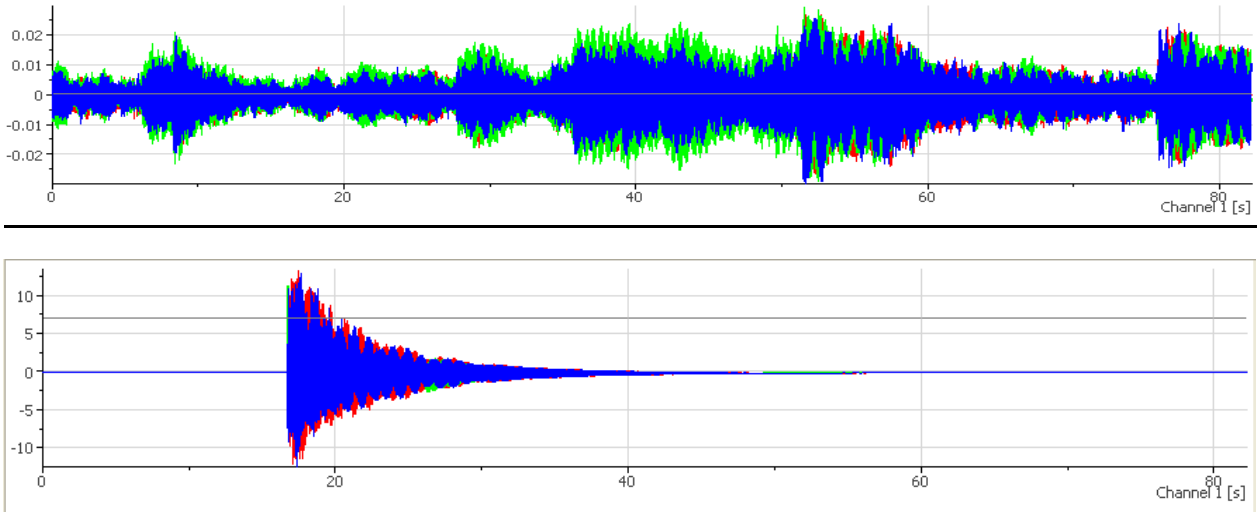

Figure 69. Response under environmental vibration (above) and forced vibration (below). T1-Measurement 2

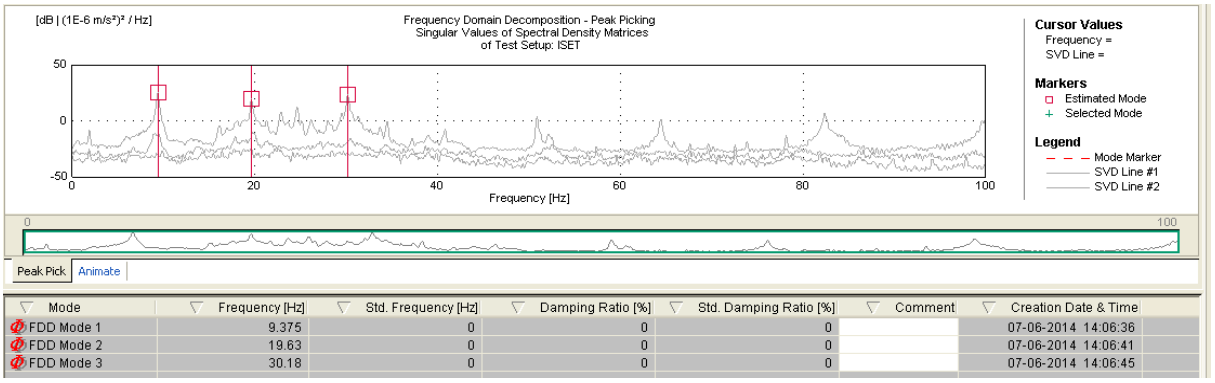

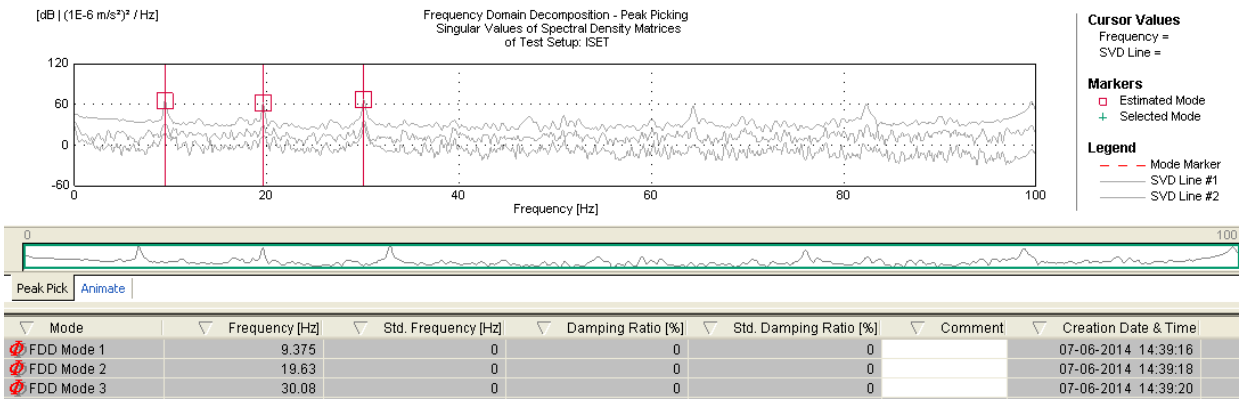

Figure 70. FFT of T1-Measurement 2. Environmental vibration (above). Forced vibration (below)

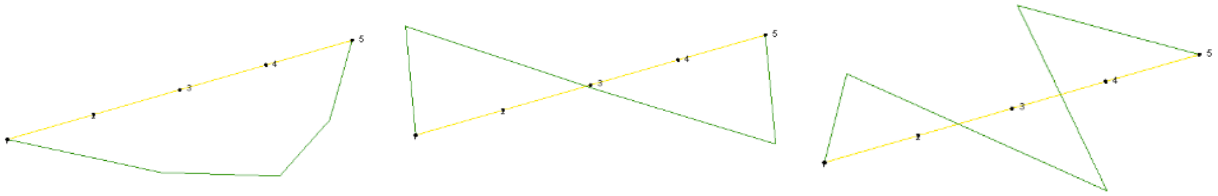

1st mode 2nd mode 3th mode

Figure 71. Mode shapes of vibration for ties

Table 25 and Table 34 show the three natural frequencies for each tie under environmental and forced vibration. Since the ties were restrained by the wall, they were considered as fixed and the effective length was assumed as the half of the total length. The density per unit length was calculated multiplying the density of the iron by the cross section area.

Table 25. Natural frequencies under environmental vibration

Environmental Vibration							
Test	**Tie**	**Period**	**f1 (Hz)**	**f2 (Hz)**	**f3 (Hz)**	**l (m)**	**μ (Kg/m)**
T1	N29	20th century	9.38	19.63	30.18	2.10	1.69
T2	N22	13th century	16.70	34.86	54.46	1.92	7.34
T3	N32	20th century	12.79	26.73	41.70	1.93	2.22
T4	N13	13th century	5.63	19.73	41.05	2.11	11.64

Table 26. Natural frequencies under forced vibration

Forced Vibration							
Test	**Tie**	**Period**	**f1 (Hz)**	**f2 (Hz)**	**f3 (Hz)**	**l (m)**	**μ (Kg/m)**
T1	N29	20th century	9.39	19.61	30.10	2.10	1.69
T2	N22	13th century	16.67	34.77	54.39	1.92	7.34
T3	N32	20th century	12.79	26.66	41.70	1.93	2.22
T4	N13	13th century	5.57	19.63	40.85	2.11	11.64

Table 27 and Table 28 show the tension level of the ties, calculated with each natural frequency and the respective average.

Table 27. Tension state of ties (environmental vibration)

Environmental Vibration							
Test	**Tie**	**Period**	**T_{f1} (KN)**	**T_{f2} (KN)**	**T_{f3} (KN)**	**Average (KN)**	**Stand. dev**
T1	N29	20th century	2.61	2.86	3.00	**2.82**	0.2
T2	N22	13th century	30.19	32.89	35.67	**32.92**	2.7
T3	N32	20th century	5.44	5.94	6.43	**5.93**	0.5
T4	*N13*	*13th century*	*6.55*	*20.12*	*38.70*	*21.79*	*16.1*

Table 28. Tension state of ties (forced vibration)

Forced Vibration							
Test	**Tie**	**Period**	**T_{f1} (KN)**	**T_{f2} (KN)**	**T_{f3} (KN)**	**Average (KN)**	**Stand. dev**
T1	N29	20th century	2.62	2.85	2.99	**2.82**	0.2
T2	N22	13th century	30.07	32.72	35.59	**32.79**	2.8
T3	N32	20th century	5.44	5.91	6.43	**5.92**	0.5
T4	*N13*	*13th century*	*6.41*	*19.91*	*38.32*	*21.55*	*16.0*

The results presented herein clearly evidence that the ties set up in 20th century are subjected to very low tension (almost inactive); in contrast, the original ties, installed in the construction of the tower, are subjected to important tension (32.79 KN-T2), however the deviation standard for T4 is quite high perhaps due to a failure in the test execution.

Although the ties from 20th C might work in a passive way, it is probable that they will not behave adequately in presence of an earthquake because of unsatisfactory transmission of stress to the wall due to absence of anchor plates.

Level of tension for each natural frequency in tests T1, T2 y T3 resulted to be very close each other (with very low standard deviation), what means that the assumption of the effective length equal to the half of the total length might be correct.

The tension state for tie N22 is **32.7 KN**, which will be taken into account for the kinematic analysis in section 7.6. Since the results of tie N13 are not reliable, these have been rejected and it is recommended to repeat the test in that tie.

This page is left blank on purpose.

5 ACTIONS ON THE STRUCTURE

5.1 Permanent loads

The permanent loads considered in this study are the self-weight of structural elements such as masonry walls, masonry vaults, wooden platforms and roof, and self-weight of non-structural elements such as the bell and bell yoke. In total the structure reaches a total of 28287 kN.

The loading description is described in the following sections.

5.1.1 Roof

As it was mentioned in section 3.1.4, the roof is brick four-pitch composed by bricks (tavelle) and clay tiles supported by a simple timber truss (Figure 72). The truss was considered to be made of larch wood (larice) which is commonly used in Veneto region.

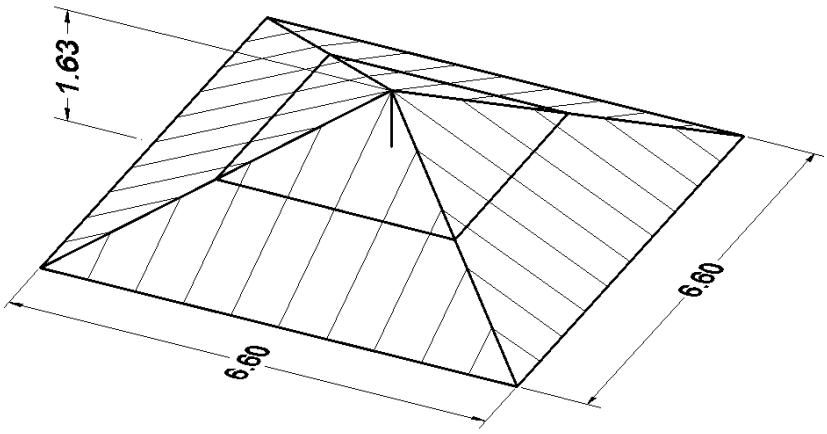

Figure 72. Timber truss arrangement

The characteristics of materials used are shown in Table 29.

Table 29. Characteristics of roof materials

Bricks (tavelle, 280x140x30mm)	kN/m^2	0,51
Clay tile (coppi)	kN/m^2	0,6
European larch timber	kN/m^3	5,64

Table 30 presents the self-weight of the timber truss and Table 31 shows the total self-weight of the roof which is 84.94 KN.

Table 30. Self-weight of timber truss

Wooden truss element	Area (mxm)	Length/pitch (m)	Quantity (pitches)	Volume (m^3)	Weight (KN)
Bottom chord	0,3x0,3	6,6	4	2,376	13,40
Top chord (diagonal)	0,2x0,2	4,94	4	0,7904	4,46
Braces (middle)	0,2x0,2	3,32	4	0,5312	3,00
King post	0,2x0,2	0,8	1	0,032	0,18
Wooden shelf to support bricks (9 elements in each pitch)	0,1x0,1	18,39	4	0,73568	4,15
				Total	**25,19** **KN**

Table 31. Total self-weight of roof

Brick layer	27.45	KN
Clay tile layer	32.30	KN
Wooden truss	25.19	KN
	84.94	**KN**
	1.58	KN/m^2

5.1.2 Wooden platforms

Both wooden platforms were considered to be made of the same wood that the roof truss (larch wood) and the geometry was based on the visual inspection and geometrical survey. The description of the elements and loading are shown in Table 32 and Table 33; the total self-weight for platform 1 is 13.73 KN and for platform 2 is 13.32 KN.

Table 32. Self-weight of wooden platform 1

Wooden element	Direction	Area (mxm)	Length (m)	Quantity	Volume (m^3)	Weight (KN)
Main beams	E-W	0,3x0,3	3,86	2	0,69	3,92
Secondary beams	N-S	0,2x0,2	3,87	4	0,62	3,49
Secondary beams	E-W	0,2x0,3	3,86	3	0,46	2,61
Platform		13,14		1	0,66	3,71
					Total	**13,73**

Table 33. Self-weight of wooden platform 2

Wooden element	Direction	Area (mxm)	Length (m)	Quantity	Volume (m^3)	Weight (KN)
Main beams	N-S	0,2x0,2	4,3	2	0,34	1,94
Secondary beams	E-W	0,18x0,18	4,49	8	1,16	6,56
Platform		17,06		1	0,85	4,81
					Total	**13,32**

It is important to notice that the load corresponded to platform 1 is transferred mainly to eastern and western walls, while the load of platform 2 is transferred to northern and southern walls. This fact will be considered in the Kinematic analysis in chapter 7 and FEM model in chapter 8.

5.1.3 Bell and bell yoke

As it was mentioned in section 2.3.1, the bell is mounted on a wooden yoke which distributes the weight by 4 beams to the northern and southern wall. The self-weight has been estimated in 3600 kg for the bell and 800 kg for the yoke; that is 35.32 KN and 7.85KN respectively.

5.1.4 Walls and vaults

For calculation of self-weight of brick masonry elements, the tower has been divided in 8 sections as it seen in Figure 73. The volumes were calculated using the available plant and elevation plans.

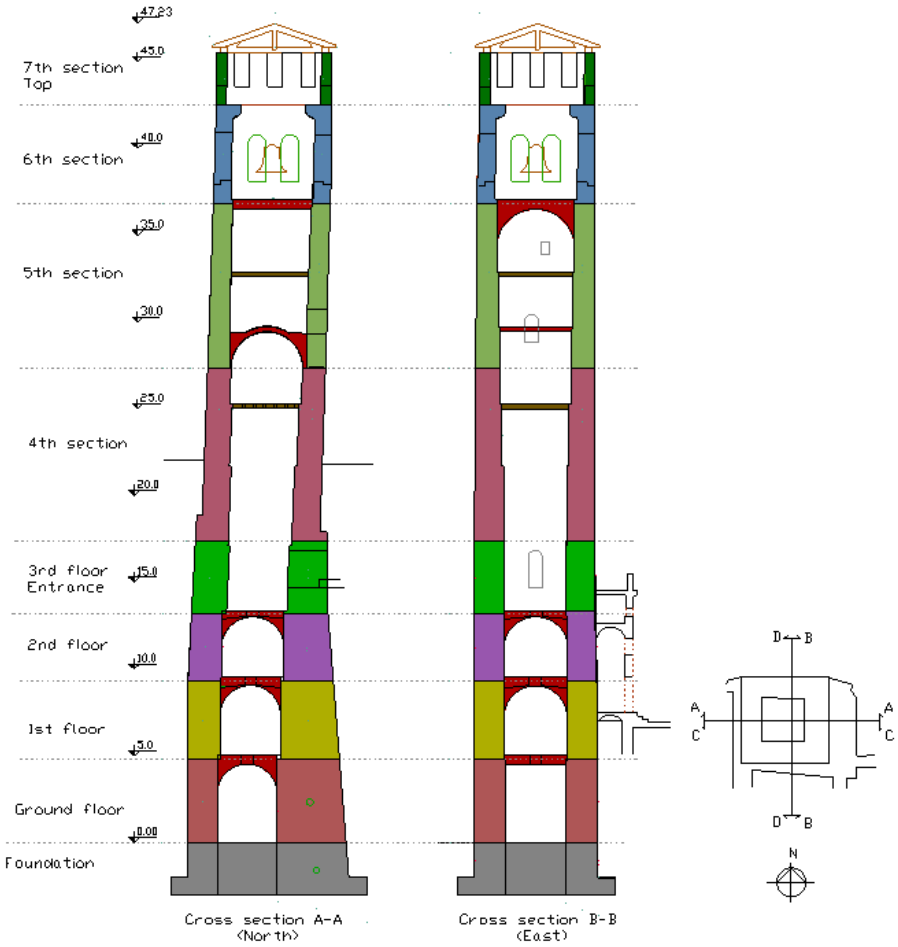

Figure 73. Division of tower for self-weight determination

Table 34 shows the values of all permanent loads including walls and vaults, wooden platforms, roof, bell and bell yoke, the total self-weight of the tower is 28287 kN.

The walls and vaults were considered to be made of the same type of brick masonry with specific weight of 18 KN/m^3 (section 6.3.2).

Table 34. Permanent load of the Tower Anziani

Section	Height (m)	From (m)	To (m)	Area (m^2)	Volume (m^3)	Self-weight (kN)
Ground floor	4.82	0	4.82	-	248.00	4464.0
Vault 1 (barrel)	-	-	-	-	*10.30*	185.4
1st floor	4.52	4.82	9.34	-	217.65	3917.7
Vault 2 (cross)				-	*7.41*	133.5
2nd floor	3.9	9.34	13.24	-	173.32	3119.8
Vault 3 (cross)	-	-	-	-	*6.52*	117.4
3rd floor (entrance)	4.14	13.24	17.38	-	165.44	2978.0
4th section	10.02	17.38	27.4	-	325.68	5862.2
Wooden platf.1	-	-	-	*13.14*	-	13.7
Vault 4 (barrel)	-	-	-	-	*11.00*	198.1
5th section	9.45	27.4	36.85	-	243.67	4386.1
Wooden platf.2	-	-	-	*17.06*		13.3
Vault 5 (barrel)	-	-	-	-	*21.38*	384.9
6th section	5.7	36.85	42.55	-	105.55	1899.8
7th section (top)	3.05	42.55	45.6	-	26.94	484.8
Roof	1.6	45.6	47.2	*53.83*	-	84.94
Bell	-	-	-	-	-	35.32
Bell yoke	-	-	-	-	-	7.85
						28286.7

5.2 Snow action

According to *§.3.4 NTC 08*, snow loads on roofs shall be determined as follows:

$$\boldsymbol{q_s = \mu_i * q_{sk} * C_E * C_t} \qquad (3)$$

Where:

q_s is the design snow load on the roof

$\boldsymbol{\mu_i}$ is the snow load shape coefficient

$q_{sk}$is the characteristic value of snow load on the ground for a return period of 50 years [kN/m^2]

C_E exposure coefficient

C_t thermal coefficient

The results are shown in the following table.

Table 35. Calculation of design snow load on the roof

Region	Padova	Zone II	
Meters above sea level		12	MAMSL
Characteristic value of snow load	q_{sk}	1	kN/m^2
Topography	Normal		
Exposure coefficient	C_E	1	
Thermal coefficient	C_t	1	
Slope of roof	α	20,49	
Snow load shape coefficient	μ_i	0,8	
Design value of snow load	**q_s**	**0,8**	**kN/m^2**

5.3 Wind action

The effect of the wind on the structure depends on the size, shape and dynamic properties of the structure. For this case, it was calculated according to *§.3.3 NTC 08*.

The wind pressure is calculated by means of the next expression:

$$\boldsymbol{p = q_b\, c_e\, c_p\, c_d} \qquad (4)$$

Where:

q_b is the kinetic pressure of reference

c_e is the exposure coefficient

c_p is the aerodynamic coefficient or shape coefficient depending on the geometry of the building and its orientation regarding to wind direction.

c_d is the dynamic coefficient which takes into account the effects associated with maximum local pressures and amplification effects due to structural vibrations. It can be conservatively assumed equal to 1 in buildings of regular shape, not exceeding 80 m in height and industrial buildings.

Kinetic pressure of reference is given by:

$$\boldsymbol{q_b = \frac{1}{2}\rho {v_b}^2} \qquad (5)$$

Where:

ρ is air density (1.25 kg/m^3)

v_b is the wind velocity of reference

The exposure coefficient (c_e) depends on the height (z) of the structure, the topography of the ground, and the exposure category of the site where the building is located. For heights not greater than z = 200 m, the exposure coefficient is given by the formula:

$$c_e(z) = k_f{}^2 c_t \ln(z/z_0)\,[7 + c_t \ln(z/z_0)] \quad for\ z \geq z_{min} \qquad (6)$$

$$c_e(z) = c_e(z_{min}) \quad for\ z < z_{min}$$

Where

c_t is the topography coefficient (NTC recommends ct=1).

The aerodynamic coefficient or shape coefficient (c_p) was determined according to *§. C3.3.10.1 CIRCOLARE 09.* For windward elements (i.e. directly affected by the wind) with tilt α> 60 , $c_{pe\text{-}w}$ = +0.8. For leeward elements (not directly affected by the wind), $c_{pe\text{-}l}$ = - 0.4 (see Figure 74).

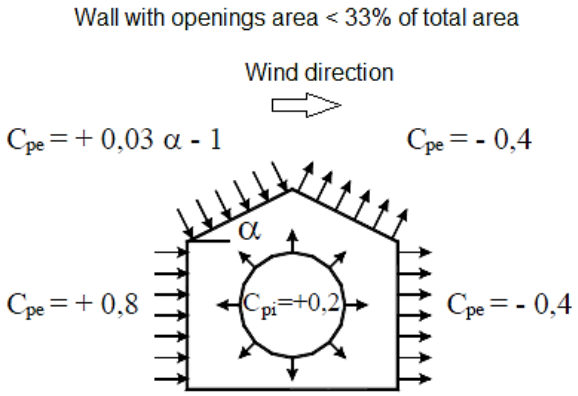

Figure 74. Shape coefficients for walls with openings area lower than 33% of total area [8]

The tangential action of the wind (parallel to wind direction) was calculated according to *§.3.3.5 NTC 08,* using the next equation:

$$p_f = q_b\, c_e\, c_f \qquad (7)$$

Where:

q_b is the kinetic pressure of reference

c_e is the exposure coefficient

c_f is the friction coefficient, according to *§.C3.3.11 CIRCOLARE 09* for rough surfaces such as concrete and masonry c_f can be considered as 0.02.

The parameters and results for the wind action are presented in Table 36.

Table 36. Calculation of wind action

Region	**Veneto**	**Zone I**	
Altitude of building above sea level	a_s	12	MAMSL
Altitude of reference	a_0	1000	m
Fundamental value of wind velocity	$v_{b,o}$	25	m/s
Wind velocity of reference(as<a0)	v_b	**25**	**m/s**
Air density	ρ	1,25	kg/m^3
Kinetic pressure of reference	q_b	**390,6**	**N/m^2**
Type of roughness of terrain	**A**: Urban areas in which at least 15% of the surface is covered by buildings whose average height exceeds 15m		
Zone (exposure category)		**IV**	
	k_r	0,22	
	z_0	0,3	m
	z_{min}	8	m
Height of building (above ground level)	z	46,9	m
Topography coefficient	c_t	1	
Exposure coefficient ($z>z_{min}$)	c_e	**2,95**	
Dynamic coefficient	c_d	1	
Parallel length to wind direction (northern or southern side)	d	6,82	m
Crosswind dimension (western or eastern side)	b	6,89	m
Aerodynamic coefficient for windward wall	c_{pe-w}	0,8	
Aerodynamic coefficient for leeward wall	c_{pe-l}	-0,4	
Friction coefficient	c_f	0,02	
Wind pressure - windward element (western wall)	p_w	**921,07**	**N/m^2**
Wind pressure - leeward element (eastern wall)	p_l	**-460,54**	**N/m^2**
Tangential action of the wind (northern and southern walls)	p_f	**23,03**	**N/m^2**

5.4 Seismic action

The seismic action evaluated for various limit states is defined starting from the "seismic hazard" of the construction site. The seismic hazard is defined in terms of the maximum expected horizontal ground

acceleration a_g and the ordinates (acceleration) of the elastic response spectrum $S_e(T)$ for a predetermined probability of exceedance P_{VR} during a reference period V_R.

Seismic actions were obtained following the section 3.2 of NTC (Ref. [6]) and by means of spreadsheet "Spettri-NTCver.1.0.3" provided by the National Institute of Geophysics and Volcanology of Italy – INGV (Istituto Nazionale di Geofisica e Vulcanologia).

The input and output data, of the spreadsheet "Spettri-NTCver.1.0.3", such as seismic hazard, type of building, soil properties, limit states and parameters of the design spectrum, are presented in the following sections.

5.4.1 Location of structure and seismic hazard

Figure 75 shows the seismic hazard map of the country expressed in terms of maximum acceleration of the soil with 10% probability of exceedance in 50 years, it is seen that the seismic hazard near Padua is low presenting ground peak acceleration between 0.05 and 0.1 g.

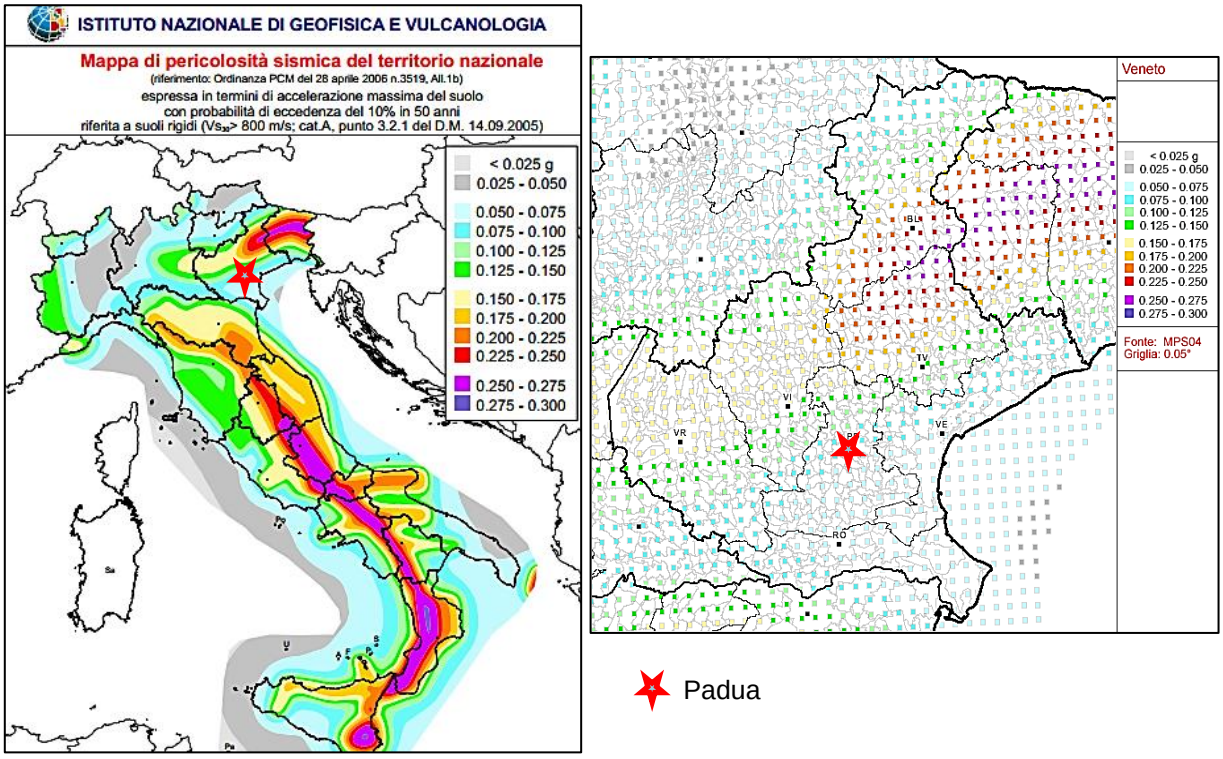

Figure 75. Seismic hazard map in terms of a_g. Right. Italy. Left: Region of Veneto [10]

Table 37 shows the geographical location of the tower and Figure 76 shows the seismic hazard input data for the spreadsheet “Spettri-NTCver.1.0.3”.

Table 37. Location of "Torre degli Anziani"

Region	Veneto
Province	Padova
Municipality	Padova
Latitude (geographical coordinate)	45°24'27.0"N
Longitude (geographical coordinate)	11°52'33.8"E

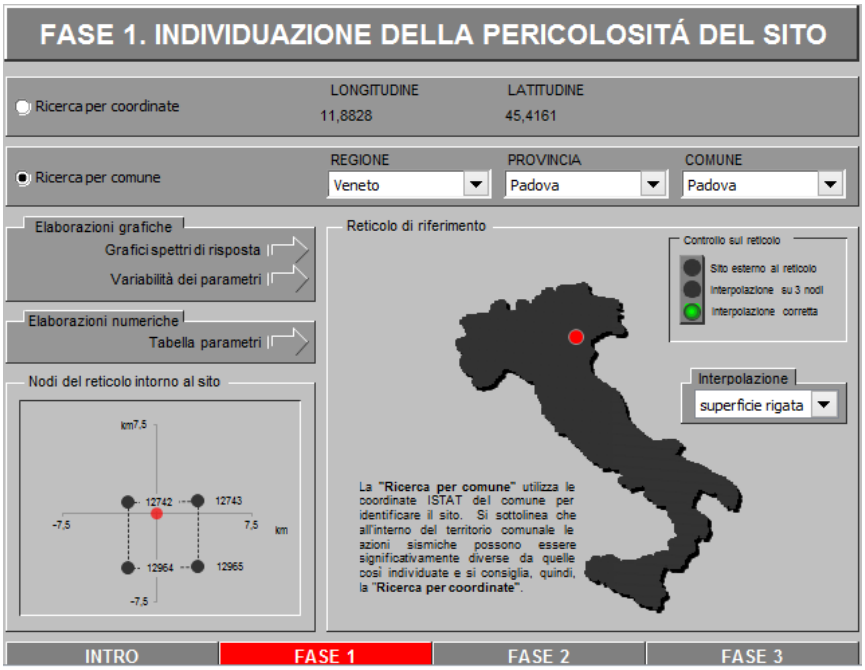

Figure 76. Seismic hazard input data of Spettri-NTCver.1.0.3. Phase 1

5.4.2 Nominal life, Class of use and Reference period

5.4.2.1 Nominal life of the building – V_N

The nominal life (V_N) is understood as the number of years in which the structure is subjected to routine maintenance and it must be usable for the purpose for which it is intended.

NTC-08 (Table 2.4.I - Ref. [6]) recommends the nominal life to be equal or higher than 50 for ordinary works, bridges, dams and infrastructure projects of limited size or normal importance. Since the Tower Anziani is a historical building with important cultural value but with possibility of intervention each determinate time, the nominal life has been assumed as 50 years.

5.4.2.2 Class of use

Regarding to the consequences of an interruption of operation or a possible collapse of a structure subjected to seismic activity, the NTC (Section 2.4.2 - Ref. [6]) presents 4 classes of use for buildings.

The tower has been classified as Class III (buildings whose use provides significant crowding. Industries with dangerous activities to the environment. Networks stations whose interruption results in emergency situations). Although the tower presents just occasional presence of people, its possible collapse would be quite dangerous for surrounding buildings.

The coefficient of use (C_u) for Class III is 1.5 (Section 2.4.3 - Ref. [6]).

5.4.2.3 Reference period - V_R

The seismic activity of each building is evaluated in relation to the reference period (V_R) which is obtained by multiplying the nominal life (V_N) by the coefficient of use (C_u):

$$\boldsymbol{V_R = V_N\, C_u = 50 * 1.5 = 75\, years} \qquad (8)$$

5.4.3 Limit states

§.3.2.1 NTC 08 presents four different limit states to be considered in seismic analysis:

A. Serviceability limit states

- **Operational Limit State (OLS):** following the earthquake, the construction as a whole, including structural elements, non-structural and equipment relevant to its function, does not suffer significant damage and disruption of use.

- **Damage Limit State (DLS):** following the earthquake, the construction as a whole, including structural elements, non-structural and equipment relevant to its function, takes damage that would not put users at risk and does not compromise significantly the capacity of resistance and stiffness against vertical and horizontal actions, remaining immediately usable after a possible short interruption.

B. Ultimate limit states

- **Ultimate Limit State (ULS):** following the earthquake, the building suffers cracks and collapse of non-structural components and installations, significant damage in structural components which is associated with a significant loss of stiffness against horizontal actions; the construction preserves part of the resistance and stiffness for vertical actions.

- **Collapse Limit State (CLS):** following the earthquake, the building suffered severe cracks and collapse of non-structural components and installations, very serious damage of structural components. The building still retains a margin of safety for vertical actions and small margin of safety against collapse due to horizontal actions.

The limit states considered for this study are damage limit state (DLS) and ultimate limit state (ULS), the last one is mandatory for existing buildings. These limit states will be explain in detail in section 6.5.

5.4.4 Probability of exceedance (P_{VR}) and Return period (T_R)

The probability of exceedance (P_{VR}) during the reference period (V_R), in each limit state considered, is presented in Table 3.2.I from NTC 08.

The return period (T_R) of the seismic action for each limit state has been calculated using the following expression:

$$\boldsymbol{T_R = \frac{V_R}{\ln(1 - P_{VR})}}$$

Table 38 shows the values of P_{VR} and T_R for each limit state.

Table 38. Probability of exceedance and Return period

LIMIT STATE		Probability of exceedance P_{VR} (%)	Return Period T_R (years)
Serviceability limit states	Operational Limit State (OLS)	81	45
	Damage Limit State (DLS)	**63**	**75**
Ultimate limit states	**Ultimate Limit State (ULS)**	**10**	**712**
	Collapse Limit State (CLS)	5	1462

For the seismic assessment of the tower, two limit states have been considered, Damage Limit State and Ultimate Limit State. Figure 77 shows the input data of Spettri-NTCver.1.0.3 regarding to probability of exceedance and return period. Figure 78 shows the response design spectrum for each limit state.

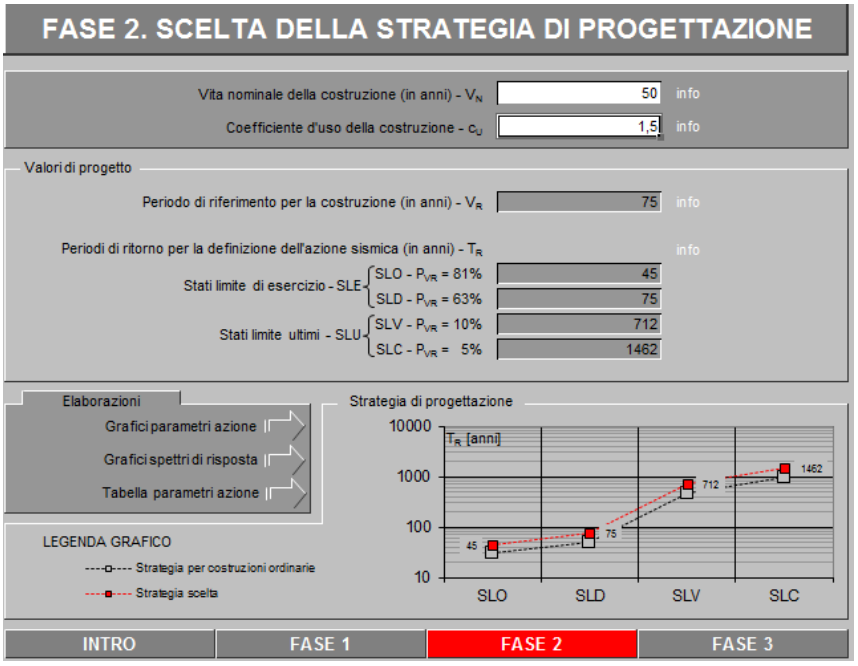

Figure 77. Probability of exceedance and return period input data of Spettri-NTCver.1.0.3. Phase 2.

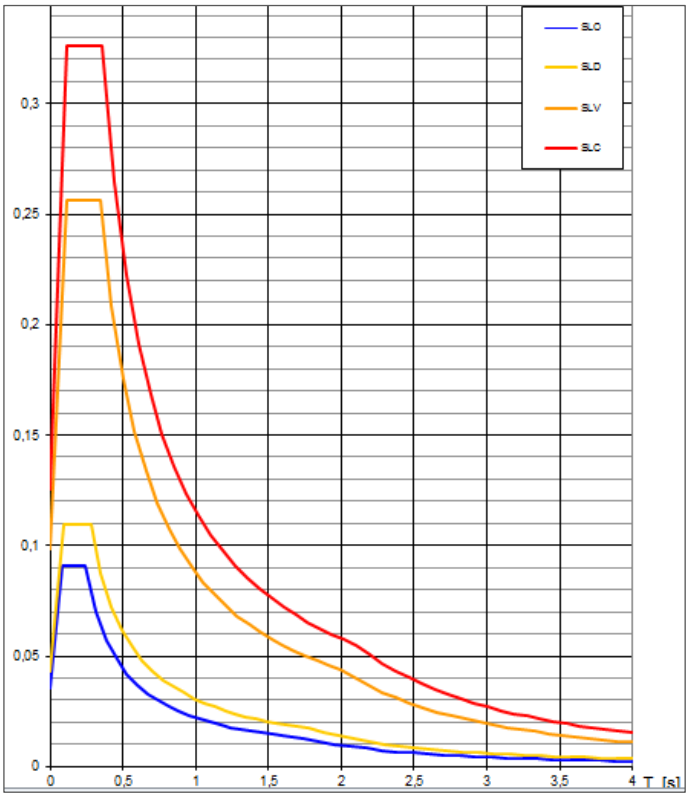

Figure 78. Response design spectrum for each limit state

5.4.5 Subsoil category and Topographic condition

According to the soil exploration carried out in 1998 near Tower Anziani (section 2.4) and the information presented in the report of November 2005 (Ref. [9]), the soil has been classified as category B since it is composed meanly by coarse-grained soil with consistency from medium to very stiff; the characteristics are presented in Table 39.

Table 39. Subsoil category and Topography condition

Subsoil category	**B**: corresponding to soft rock and deposits of coarse-grained soils or very consistent fine grain soils with depth greater than 30 meters and characterized by a gradual improvement of the mechanical properties with the depth. Shear wave velocity values $V_{s,30}$ between 360 m/s and 800 m/s.
Topographic condition	**T1:** corresponding to flat surfaces, hills and isolated peaks with an average slope lower than 15º

5.4.6 Evaluation of seismic action

According to NTC-08 (*§.3.23.3.1*), independently of the probability of exceedance (P_{VR}) in a reference period (V_R), the elastic response spectrum for the horizontal component is defined by the following expressions:

$$
\begin{aligned}
&0 \le T < T_B && S_e(T) = a_g \cdot S \cdot \eta \cdot F_o \cdot \left[\frac{T}{T_B} + \frac{1}{\eta \cdot F_o} \left(1 - \frac{T}{T_B} \right) \right] \\
&T_B \le T < T_C && S_e(T) = a_g \cdot S \cdot \eta \cdot F_o \\
&T_C \le T < T_D && S_e(T) = a_g \cdot S \cdot \eta \cdot F_o \cdot \left(\frac{T_C}{T} \right) \\
&T_D \le T && S_e(T) = a_g \cdot S \cdot \eta \cdot F_o \cdot \left(\frac{T_C T_D}{T^2} \right)
\end{aligned}
\qquad (9)
$$

Where:

$S_e(T)$ is the elastic response spectrum;

T is the vibration period of a linear single-degree-of-freedom system;

a_g is the peak ground acceleration of soil (design);

T_B is the lower limit of the period of the constant spectral acceleration branch:

$$T_B = \frac{T_C}{3} \qquad (10)$$

$\mathbf{T_c}$ is the upper limit of the period of the constant spectral acceleration branch, given by:

$$T_C = C_C \, T_C^* \qquad (11)$$

Where $\mathbf{T_c^*}$ is the value of $\mathbf{T_c}$ corresponding to the subsoil of category A and $\mathbf{C_c}$ is a coefficient in function of the subsoil category (*NTC-Table 3.2.V*).

$\mathbf{T_D}$ is the period corresponded to the beginning of the constant displacement range of the spectrum:

$$T_D = 4.0 \, \frac{a_g}{g} + 1.6 \qquad (12)$$

S is the soil factor that takes into account the category of subsoil and topographical conditions; it is given by the following relationship:

$$S = S_S \, S_T \qquad (13)$$

Where $\mathbf{S_S}$ is the coefficient of stratigraphic amplification (*NTC-Table 3.2.V*) and $\mathbf{S_T}$ is the coefficient of topographic amplification (*NTC-Table 3.2.VI*).

η is the damping correction with a reference value of η = 1 for ξ= 5%, for ξ≥5, η is determined using the next equation:

$$\eta = \sqrt{\frac{10}{5+\xi}} \geq 0.55 \qquad \xi \; expressed \; in \; \% \qquad (14)$$

$\mathbf{F_o}$ is the factor that quantifies the maximum spectral amplification, it has minimum value equal to 2.2.

Table 40 shows the parameters, previously explained, that define the Design Spectrum.

Table 40. Parameters for the Design Spectrum for DLS and ULS

Parameter	Unit	Damage Limit State (DLS)	Ultimate Limit State (ULS)
T_R	years	**75**	712
a_g	**(g)**	0,043	0,099
T_c^*	**(s)**	0,279	0,342
C_c		1,42	1,363
S_S		1,2	1,2
S_T		1	1
S		1,2	1,2
ξ	**(%)**	5	5
η		1	1
F_o		2,534	2,597
T_B	**(s)**	0,132	0,155
T_c	**(s)**	0,396	0,466
T_D	**(s)**	1,773	1,995

Figure 79 shows the soil parameters and seismic action input data of Spettri-NTCver.1.0.3 and Figure 80 shows the response design spectrum for Damage Limit State and Ultimate Limit State.

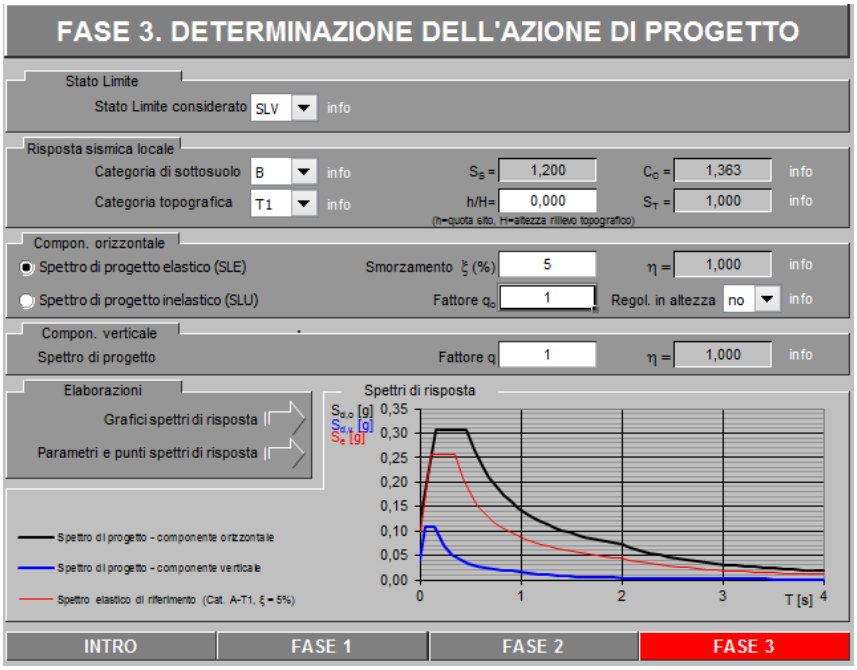

Figure 79. Soil parameters and seismic action input data of Spettri-NTCver.1.0.3. Phase 3.

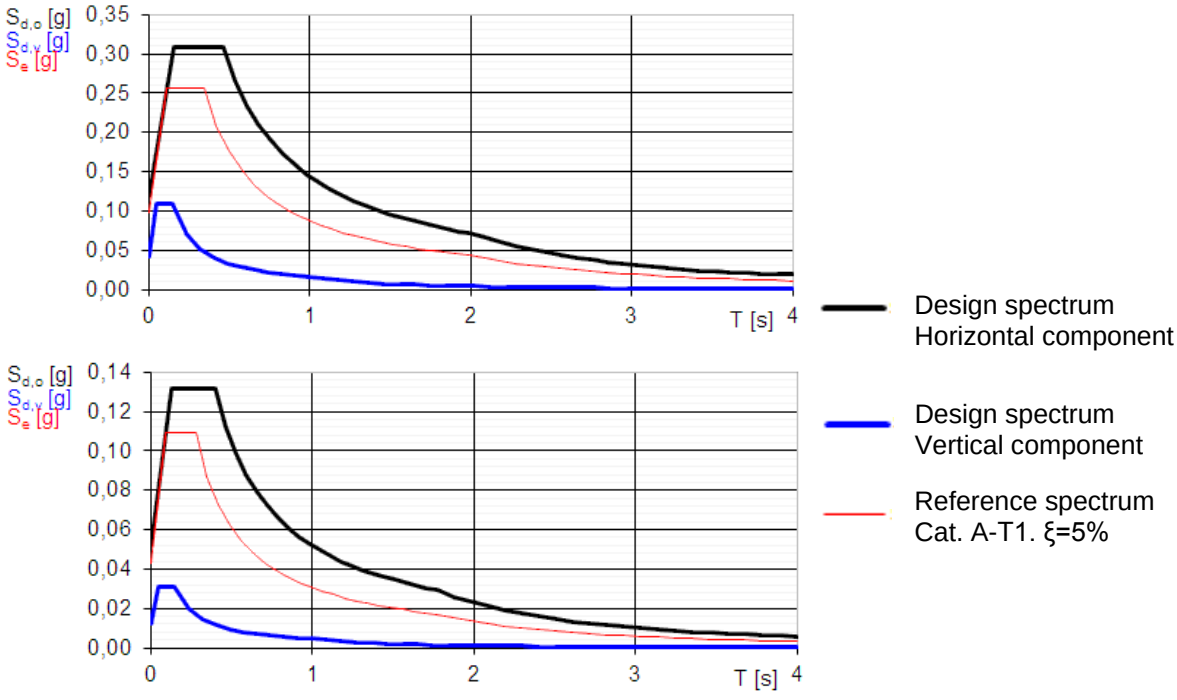

Figure 80. Response Design Spectrum. Above: ULS. Below: DLS

The previous spectrum might be divided by the value of the structure factor q which depends on the structural type, the degree of its hyperstaticity and design criteria adopted; it also takes into account the non-linearity of the material. It can be calculated using the following equation (*§.7.3.1 NTC 08*):

$$\boldsymbol{q = q_0 * K_R} \qquad (15)$$

Where:

$\boldsymbol{K_R}$ is the reduction factor that depends on the characteristics of regularity in height of the building, it is equal to 1 for regular buildings and 0.8 for non-regular constructions.

$\boldsymbol{q_0}$ is the maximum value of the structure factor that depends on the level of ductility. According to NTC (table 7.8.I), for structures made of unreinforced masonry, q_o can be calculated using the following expression:

$$\boldsymbol{q_0 = 2\,\alpha_u/\alpha_1} \qquad (16)$$

Where:

α_1 is the horizontal seismic force multiplier for which, keeping constant the other actions, the element (wall) reaches its ultimate strength (either shear or buckling).

α_u is 90% of the horizontal seismic force multiplier for which maintaining constant other actions, the building reaches its maximum resisting force.

For structures made of unreinforced masonry composed by two or more floors, *§.7.8.1.3 NTC*-08 recommends $\frac{\alpha_u}{\alpha_1} = 1.8$.

The structure factor value is presented in the following table.

Table 41. Structure factor

K_R	1
α_u/α_1	1.8
q	3.6

5.5 Load combinations

According to *§.2.5.3 NTC-08*, in case of civil and industrial constructions the verification of the limit states must be evaluated using several load combinations. For this study, the fundamental and seismic combinations have been used:

Fundamental combination: $\gamma_{G1}G_1 + \gamma_{G2}G_2 + \gamma_P P + \gamma_{Q1}Q_{k1} + \gamma_{Q2}\psi_{02}Q_{k2} + \gamma_{Q3}\psi_{03}Q_{k3} + \cdots$ (17)

Seismic combination: $G_1 + G_2 + P + E + \sum_j \psi_{2j} Q_{kj}$ (18)

Where:

G are the permanent loads: $\mathbf{G_1}$ is the self-weight of all the structural elements and $\mathbf{G_2}$ is the self-weight of all the non-structural elements

P are included pretension and pre-compression actions

Q are variable actions

E are seismic actions

γ_G are partial coefficients defined for permanent load considering favorable or unfavorable contribution.

γ_Q are partial coefficients defined for permanent load considering favorable or unfavorable contribution.

Ψ_{0j} are combination coefficients depending on the category of the variable action for fundamental combination

Ψ_{2j} are combination coefficients depending on the category of the variable action for seismic combination

Table 42 shows the coefficients values used for the load combinations. The description of the combinations considered during the analysis is included in the chapter 7 and 8.

Table 42. Coefficients for load combinations [NTC: Table 2.6.I and Table 2.5.I]

Load		γ_G		γ_Q	Ψ_0	Ψ_2
		Favorable	Unfavorable	Unfavorable		
Self-weight of structural elements	G_1	1.0	1.3	-	-	-
Self-weight of bell and bell yoke	G_2	0.0	1.5	-	-	-
Wind	Q_1	-	-	1.5	0.6	0
Snow	Q_2	-	-	1.5	0.5	0
Service	Q_3	-	-	1.5	0.7	0.3

This page is left blank on purpose.

6 SEISMIC ANALYSIS PROCEDURE

6.1 Type of seismic analysis in structures

Depending on the structural characteristic of the building, there are different approaches to assess the performance of the structure under an earthquake; the following approaches are some types of seismic analysis that can be achieved, showing the recommended ones for masonry structures.

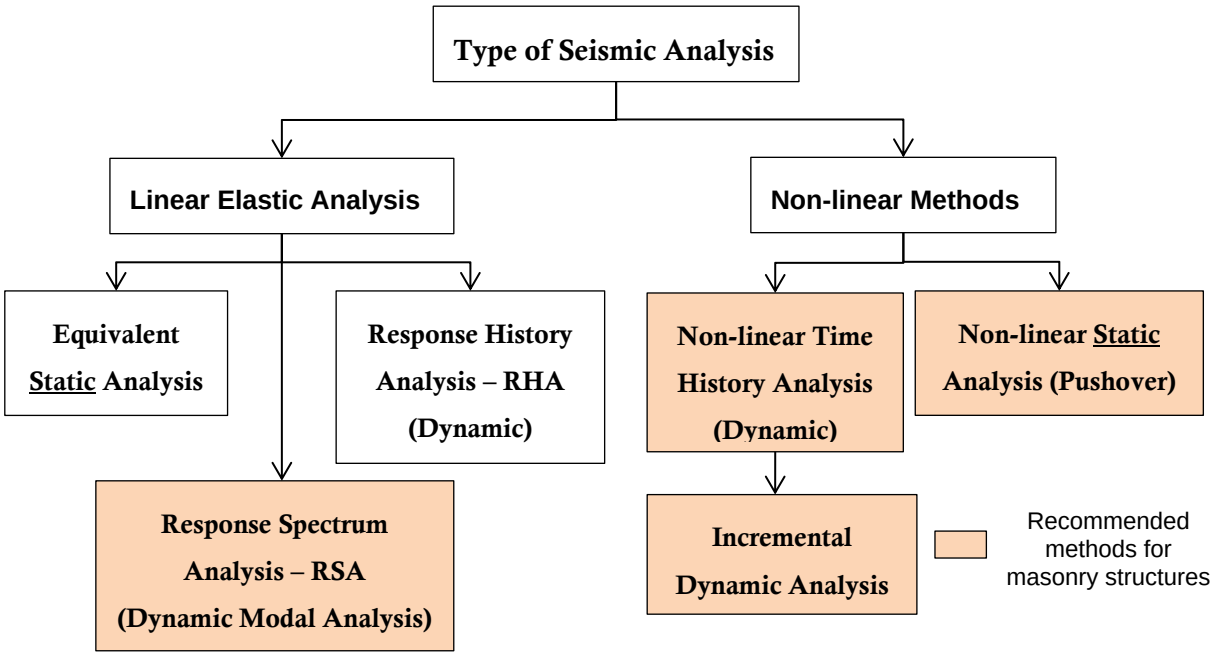

Figure 81. Types of seismic analysis

In addition to previous approaches, Kinematic Limit Analysis (linear and nor linear) can be used also to make a seismic assessment of the structure by means of a simplified method based on the evaluation of the horizontal acceleration that activates collapse mechanisms when the structure is modelled as an array of rigid blocks connected through joints.

Before choosing the adequate type of seismic analysis to perform, it is important to understand the behavior of towers, bell towers and in general tall and slender structures subjected to ground motion, which is depicted in the following section (section 6.2).

However the initial objective of this work was to adopt a methodology where the tower could be assessed in two different ways, on one hand in a global way considering the seismic safety of the entire tower where it is analyzed as a body composed by many structural elements perfectly connected each other; and on the hand, in a local way considering just some critical structural elements working independently.

The reason of covering those both approaches is that usually masonry structures subjected to earthquakes behave properly as long as their structural components are well clamped each other, but in historical constructions it does not occurred often, in contrast, it has been observed that following earthquakes several masonry structures develop local collapse mechanisms such as overturning of some elements in-plane or out of plane due to poor wall clamping. That is why, both global and local analysis approaches are essential in masonry structures.

Taking into account the previous issues, it was decided to assess the Tower Anziani using two approaches, the first one will be by means of Kinematic Limit Analysis, a simplified method used widely in Italy, in order to evaluate possible critical collapse mechanisms, and the second one will be Response Spectrum Analysis or also called Dynamic Modal Analysis by means of Finite Element Method in order to assess globally the structure. The reason of the choice of these types of analysis is explained in the following sections (sections 6.2 and 6.3).

6.2 Seismic behavior of towers, bell towers and tall and slender structures

Following the Guidelines for Evaluation and Mitigation of Seismic Risk to Cultural Heritage (Ref. [23]), seismic behavior of towers, bell towers and slender structures depends on many factors such as slenderness of the structure, clamping of walls, presence of adjacent lower structures which may create horizontal constraints and possible hinges for collapse mechanisms and the presence of slender architectural elements at top such as pinnacles, belfry, battlements, etc. In addition, for the case of vaulted rooms, the effect of the thrust influences in the behavior of the structure and it must be carefully evaluated (see Figure 82).

Vulnerability is influenced also by damage state of the structure caused for example by the vibrations induced by the ringing of bells and foundation problems; however the Tower Anziani does not present those problems (the bells stopped being played in 18^{th} C).

The presence of adjacent structures can seriously affect the behavior of the structure due to two reasons; the first is by limiting the effective slenderness and the second one is by creating localized stiffness and points where a concentration of forces is developed. Observation of damage after earthquakes has demonstrated that in fact this situation cause significant damage. For kinematic analysis, these junctions must be considered as possible hinges (rotation center) for collapse mechanisms.

In Tower Anziani, particularly, the belfry and battlement might be quite vulnerable elements due to the ample openings that are composed of slender load bearing pillars; their vulnerability is essentially due to their low vertical load capacity that limits the stability regarding to overturning.

Also the bell and bell yoke might be vulnerable elements since they behave as lumped elements at top; according to visual inspection of many towers after similar earthquakes, amplification of seismic motion is more critical when there are slender and lumped elements located in the upper part.

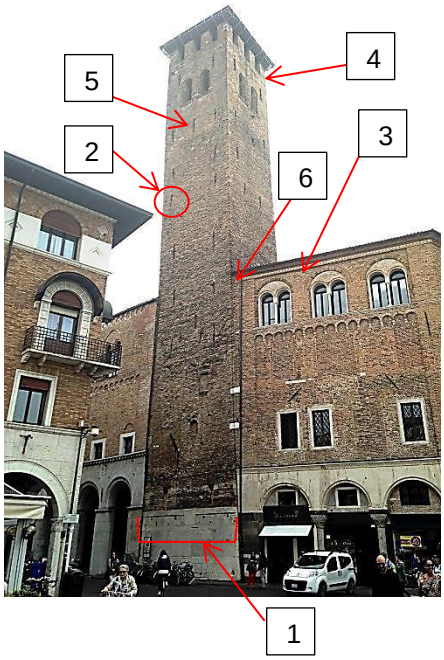

Vulnerability of the tower depends on:

1. Slenderness of the structure
2. Clamping of walls (tie rods)
3. Interaction with adjacent structures
4. Slender or lumped elements at top (belfry, battlement and bell)
5. Thrust of vaults
6. Tower's tilt
7. Ringing of bells
8. Foundation problems

Figure 82. Factors that may influence in the vulnerability of the tower

6.3 Why Dynamic Modal Analysis for Global Evaluation?

Dynamic Modal Analysis is performed by means of an elastic linear model which involves limited reliability in the evaluation of behavior in limited resistance conditions for historical masonry buildings, especially in the case of buildings with complex structures characterized by transformations (rehabilitation projects) and different construction phases.

The main vibratory mode in each direction may be useful for evaluating (which corresponds to the maximum value of the participation coefficient) and then determining a reliable distribution of forces to adopt in the linear static analysis. It is arguable, however, whether or not to consider the contribution of greater modes, which have little importance for structures characterized by nonlinear behavior of materials because of their modest values of lateral action (Ref. [23]).

Anyway, according to Guidelines for Evaluation and Mitigation of Seismic Risk to Cultural Heritage, based on several seismic analyses, Dynamic Modal Analysis can be used with great confidence in easily

modelled, flexible structures, for example, towers, bell towers and other structures which develop primarily along vertical lines, for which the contribution of superior modes may be important.

In addition, considering the minor geometric and constructive complexity of these kinds of structures (towers, bell towers, etc) compared to other often historic buildings such as religions buildings, villas, masonry bridges, triumphal arches, etc, and the fact that no structural cracks were found, most of the factors regarding to the vulnerability of the tower can be accurately studied using linear models since the redistribution of forces in such as isostatic structure is always conservative. This allows the use of dynamic analysis, in particular modal types, for understanding the aspects regarding to amplification of motion due to the factors described in section 6.2 (Ref. [23]).

On the other hand, the first and second natural period of vibration of the tower are known from the experimental modal test (section 4.1.2) which are essential information for calibrating the FEM model for Dynamic Modal Analysis. Since there is not extra information about mechanical properties of materials from tests, the calibration or verification of a model for other type of analysis, such as pushover analysis, would not be possible.

The verification is done by comparing both the calculated acting momentum with the ultimate moment of resistance and the calculated shear force with the shear resistance, assuming that the masonry is not resistant to traction. The verification should be performed according to the two main directions of inertia of the section at different heights, because of the impossibility of identification of critical sections in advance due to different thickness of masonry walls and weaknesses generated by openings.

A detailed explanation about Dynamic Modal Analysis, including the implementation in Tower Anziani by means of Finite Element Method and seismic verification, is presented in Chapter 8.

6.4 Why Kinematic Limit Analysis for Local Evaluation?

The relative clarity of the structural scheme and the behavior of these types of masonry structures, such towers and bell towers, and the observation of their local failure mechanisms after several earthquakes allow the creation and analysis of possible collapse mechanisms to evaluate some critical elements that might be poor clamped to the structural system and might work autonomously.

Traditional techniques which guarantee good clamping are: interlocking corners, reinforcement rings, tie-rods and well-connected diaphragms. Clamping techniques used in Tower Anziani are mainly the tie-rods and the vaults which work as diaphragms.

The following figures show some of the most common failure mechanisms after earthquakes on towers and masonry walls.

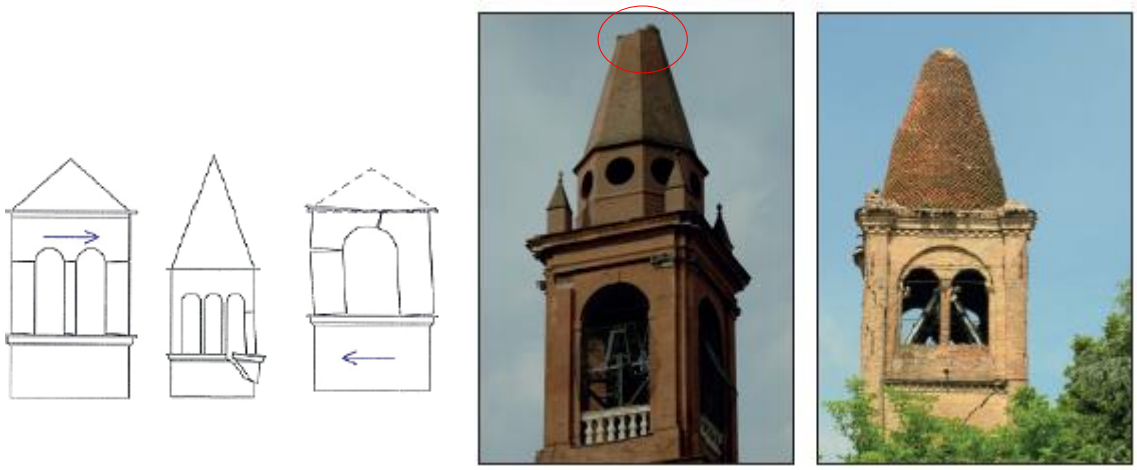

Figure 83. Collapse mechanisms involving belfry and top part of towers. Case of San Biagio Church (Ferrara) and Church of Santa Caterina d'Alessandria (Toscana). Ref. [27]

Figure 84. Collapse mechanism due to interaction with adjacent structures of lower height. Case of Sant'Egidio Abate Church (Abruzzo). Ref. [27]

Figure 85. Global collapse mechanism (overturning) due to high shear stress. Case of Church of S. Martino (Ferrara). Ref. [27]

Figure 86. Collapse mechanisms involving simple overturning (out of plane) of walls. Ref.[18]

An accurate and effective tool to evaluate macro elements and critical collapse mechanisms is by means of Kinematic Limit Analysis, whether linear or non-linear, by which the efficiency or need of tie rods and the effect of thrust of vaults can be considered.

This is a simplified method based on the evaluation of the horizontal acceleration that activate a collapse mechanism (a_o*) when the structure is modelled as an array of rigid blocks connected through joints. The verification for linear analysis is made comparing the acceleration that activates the collapse mechanism (a_o*) with a limit value in function of the peak ground acceleration of the site; in fact if a_o* is higher, there is no need to carry out seismic strengthening intervention to that element. For non-linear analysis, the ultimate displacement capacity (d_u*) is compared with the displacement demand of the earthquake from spectrum, in the same way, if d_u* is higher, there is no need of intervention.

In general, if the collapse mechanism is verified by linear analysis, there is no need of non-linear analysis.

A detailed explanation about Kinematic Limit Analysis, including the implementation in Tower Anziani and verification, is presented in Chapter 7.

6.5 Limits states for safety and protection of cultural heritage

The safety level and protection under earthquakes are determined mainly by two limit states, the ultimate limit state -SLU and the limit state of damage –SLD (EC8 and NTC 2008).

6.5.1 Ultimate limit states (ULS)

It is aimed to safeguard people from danger under a high intensity earthquake (high return period). SLU shall verify that the structure has the enough resistance and energy dissipation capacity (EC 8), the

foundation and support soil are able to resist the action effects under the response of the structure and that the non-structural elements do not represent risk. Also the sliding and overturning stability shall be checked.

Under the effect of a seismic event characterized by a probability of exceeding 10% in 50 years, the structure even when submitted to grave damage, maintains a residual resistance and lateral stiffness and the entire load capacity with reference to the vertical loads. The repair of the structure is likely not economically possible.

The safety verifications are made according to the model and the performed analysis in terms of strength using the following expression:

$$E_d \leq R_d$$

Where:

E_d: Demand: stress of the member using design values (deformation)

R_d: Strength design value of the element (deformation capacity)

All historical constructions must be verified for this ULS,

6.5.2 Limit state of damage (LSD)

It is aimed to limit economical and functional damage under more frequent low intensity earthquakes (lower return period).

It is basically a damage limitation state associated to degradations covering limitations of deformation (e.g. interstorey drift) in order to safeguard non-structural elements, equipment, etc. In case of structures for civil protection (e.g. hospitals, fire station), they must be checked to ensure enough resistance and stiffness.

Under the effect of a seismic event characterized by a probability of exceeding by 50% in 50 years, the entire building is not greatly damaged in a way that justifies the interruption of use, which means that the structural damage is limited and could be economically repaired.

The safety verifications are made according to the model and the performed analysis in terms of deformation. It is carried out only for some historical buildings at a global level, to guarantee functionality after the earthquake.

6.6 Level of knowledge of the structure and confidence factor

Following the investigation of the structure regarding to geometrical survey, material characterization, soil and foundation research and constructive surveys, the confidence factor (FC) can be determined. This factor grades the reliability of the structural analysis model and the evaluation of the seismic safety index.

According to Guidelines for evaluation and mitigation of seismic risk to cultural heritage (Ref. [23]), the confidence factor is used differently based on the following two types of seismic analysis:

*Models which consider the deformability and the resistance of the materials and structural elements: the confidence factor is applied to the properties of the materials, reducing both the plastic model as well as the resistance (applied in section 6.7 and section 8).

* Models which consider the balance limits of the various elements of the structure, taking into account the masonry materials as stiff and non-resistant to traction (the creation of kinematic models of rigid blocks, by means of the introduction of justifiable separations). For this case, regarding rigid blocks, in which the resistance of the materials is not taken into consideration, the confidence factor is applied directly to the structural capacity. It means by reducing the corresponding acceleration to the various limit states (applied in section 7.3 - step 4).

The interval of the confident factor is from 1 to 1.35. Table 43 shows the three levels of knowledge for existing buildings presented in *CIRCOLARE 2009 §C8A.1.A.4.*

Table 43. Level of knowledge of the structure. [*CIRCOLARE 2009 §C8A.1.A.4]*

Level of knowledge	Description	FC
LC1	- Limited inspections of ground and foundation, absence of geological data - Mechanical properties obtained from old data - Limited material and constructive details on site inspection	**1.35**
LC2	- Limited inspections on ground and foundations, presence of geological data - Limited on site testing to get mechanical properties of materials - Extended material and constructive details on site inspection	1.2
LC3	- Extended and comprehensive inspections on ground and foundation - Extended on site testing to get mechanical properties of materials - Comprehensive material and constructive details on site inspection	1

However, the previous criterion is very global and it does not include some aspects such as level of knowledge in geometric survey. The Guidelines for evaluation and mitigation of seismic risk to cultural heritage (Ref. [23]) proposes a more reliable methodology to determine the confidence factor FC for cultural heritage by means of the following equation, defining diverse partial confidence factors, Fck

(k=1,4), on the basis of the coefficients reported in Table 44, which are associated to four categories of research and the level of knowledge.

$$\boldsymbol{FC = 1 + \sum_{K=1}^{4} F_{Ck}} \quad (19)$$

Table 44. Partial confidence factors associated to category of research and level of knowledge (Ref. [23])

Geometric survey	Material and construction survey	Mechanical properties of materials	Terrain and foundation
The geometric survey has been completed F_{C1}=0.05	Limited survey of materials and constructive elements F_{C2}=0.12	Mechanical parameters deduced from available data F_{C3}=0.12	Limited survey of terrain and foundation, in absence of geological data or availability of information about the foundation F_{C4}=0.06
The geometric survey has been completed along with the graphic rendering of cracking and deformities F_{C1}=0	Extensive survey of materials and constructive elements F_{C2}=0.06	Limited research of mechanical parameters of materials F_{C3}=0.06	Geological data and information regarding to the foundation structures is available, limited research on terrain and foundation F_{C4}=0.03
	Exhaustive survey of materials and constructive elements F_{C2}=0	Extensive research of mechanical parameters of materials F_{C3}=0	Extensive or exhaustive research on the terrain and foundation F_{C4}=0

Since a complete inspection and geometric survey and soil characterization were carried out but there is no enough reliable information about materials, the confidence factor was determined as follows:

$$\boldsymbol{FC = 1 + (0 + 0.12 + 0.12 + 0.03) = 1.27}$$

According to the classification proposed by NTC (Table 43), for FC=1.27, the level of knowledge is between LC1 and LC2. To be on the safe side, the level of knowledge has been assumed as LC1.

6.7 Mechanical properties and specific weight of masonry

Since, there is no reliable information from tests about mechanical properties of the brick masonry of the Tower Anziani, this properties have been taken from literature following *NTC-2008* (Ref.[6]) and *Guidelines for evaluation and mitigation of seismic risk to cultural heritage* (Ref.[23]).

NTC (Circolare §.Table C8A.2.1) presents reference values of mechanical parameters (minimum and maximum) and specific weight for different types of masonry.

From the petrographic study of the material (section 4.1.3), it was found out that the masonry is composed by solid bricks and lime mortar, and from endoscopy and sonic pulse velocity test, it was proved that the walls are solid (with no leaves). Reference values of mechanical parameters for this type of masonry are showed in Table 45, where f_m is the characteristic compression strength, τ_0 is the characteristic shear strength, E is the modulus of elasticity, G is the shear modulus and γ is the specific weight.

Table 45. Reference values of mechanical parameters and specific weight for masonry made of solid brick and lime mortar. (Ref.[Circolare §.Table C8A.2.1])

f_m (MPa)		τ_o (MPa)		E (MPa)		G (MPa)		γ (KN/m^3)
Max.	Min.	Max.	Min.	Max.	Min.	Max.	Min.	18
4	2.4	0.092	0.06	1800	1200	600	400	

6.7.1 Modulus of elasticity - E

According to NTC (Circolare §. C8A.1.A.4), for level of knowledge LC1, the modulus of elasticity is the mean value of the values reported in Table 45. Therefore, the modulus of elasticity for the masonry can be assumed as:

$$\boldsymbol{E = \frac{(1800 + 1200)}{2} = 1500\ MPa}$$

It is important to take into account that this value of modulus of elasticity will be a starting value for the FEM model for Dynamic Modal Analysis; the real value can be obtained by means of a calibration of the model since the first and second frequencies are known (see section 8).

6.7.2 Specific weight - γ

The specific weight has been assumed considering the reference value for masonry made of solid brick and lime mortar from Table 45:

$$\boldsymbol{\gamma = 18\ kN/m^3}$$

6.7.3 Design compression strength - f_{dm}

According to NTC-2008 (Ref.[6]) and Guidelines for evaluation and mitigation of seismic risk to cultural heritage (Ref.[23]), the strength of materials must be reduced by the confidence factor FC and the safe coefficient γ_m:

$$\boldsymbol{f_{dm} = \frac{f_m}{FC * \gamma_m}} \qquad (20)$$

Where the confidence factor FC corresponds to 1.27 (section 6.6).

The Table 4.5.II from NTC-2008 presents the values of the safe coefficient $\gamma_{m,}$ for this case, it has been taken equal to 2.0.

f_m is the characteristic compression strength of the masonry. According to NTC (Circolare §C8A.1.A.4), for level of knowledge LC1, the characteristic compression strength is the minimum value of the values reported in Table 45.

Therefore, the design compression strength for the masonry is:

$$\boldsymbol{f_{dm}} = \frac{\mathbf{2.4}\ MPa}{\mathbf{1.27 * 2}} = \mathbf{0.94}\ \boldsymbol{MPa}$$

6.7.4 Design shear strength – τ_{od}

The design shear strength τ_{od} is determined as same as the procedure for obtaining the design compression strength:

$$\boldsymbol{\tau_{od}} = \frac{\boldsymbol{\tau_o}}{\boldsymbol{FC * \gamma_m}} \qquad (21)$$

τ_o is the characteristic shear strength of the masonry. According to NTC (Circolare §C8A.1.A.4), for level of knowledge LC1, the characteristic compression strength is the minimum value of the values reported in Table 45. Therefore, the design shear strength for the masonry is:

$$\boldsymbol{\tau_{od}} = \frac{\mathbf{0.06}\ MPa}{\mathbf{1.27 * 2}} = \mathbf{0.024}\ \boldsymbol{MPa}$$

This page is left blank on purpose.

7 KINEMATIC ANALYSIS

Kinematic Limit Analysis is a simplified method used widely in Italy in order to evaluate possible critical collapse mechanisms. The reason of the choice of this type of analysis is explained in section 6.4.

As it was explained in section 6.1, the initial objective of this work was to adopt a methodology where the tower could be assessed in two different ways, on one hand in a global way considering the seismic safety of the entire tower as a body composed by many structural elements perfectly connected each other; and on the hand, in a local way considering just some critical structural elements working independently.

Those critical elements such as facades may work autonomously due to poor clamping so their individual analysis is paramount. Traditional techniques which guarantee good clamping are interlocking corners, reinforcement rings, tie-rods and well-connected diaphragms, in the case of Tower Anziani, tie-rods and vaults which work as diaphragms are presented. An accurate and effective tool to evaluate macro elements and critical collapse mechanisms is by means of Kinematic Limit Analysis, whether linear or non-linear, by which the efficiency or need of tie rods and the effect of thrust of vaults can be considered.

7.1 Overview

Under seismic events, partial collapses usually happen in existing masonry buildings generally due to loss of equilibrium in elements; however, the verification of these mechanisms can be developed by means of limit equilibrium analysis, following the upper bound theorem which states that if a kinematically admissible mechanism can be found, for which the work developed by external forces is positive or zero, then the element will collapse.

This method is widely used on masonry structures which have no rigid floors and have poor connection between walls, in that way, the structure can be modelled as an array of rigid blocks connected through joints with no possible sliding and no tensile strength.

In general, limit analysis with kinematic approach is a simplified method that provides load capacity and failure mode in-plane and out-of-plane; however, it does not provide deformability information of the structure. The method evaluates the horizontal acceleration that activates the failure mechanisms, then, it is possible to evaluate the seismic capacity for each considered mechanism in terms of acceleration or displacement.

The method requires the analysis of local mechanisms considered meaningful for the building, which are selected according to the knowledge of the seismic behavior of similar structures, consideration of current damage such as crack, quality of walls connections, presence of ties and, in general, according to observation of the collapse modalities of analog buildings.

The verification for linear analysis is made comparing the acceleration that activates the collapse mechanism (a_o*) with a limit value in function of the peak ground acceleration of the site; in fact if a_o* is higher, there is no need to carry out seismic strengthening intervention to that element. For non-linear analysis, the ultimate displacement capacity (d_u*) is compared with the displacement demand of the earthquake from spectrum; if d_u* is higher, there is no need of intervention. If the collapse mechanism is verified by linear analysis, there is no need of non-linear analysis.

7.2 Assumed hypothesis

Basically, there are three hypotheses to apply to this method:

1. Masonry has no tension resistance

2. Masonry has infinite compression resistance

3. No slipping between blocks

4. Virtual work principle allows to calculate the factor that activates the mechanism

The procedure used, with focus on masonry structures, was based on the parameters and equations presented in the following references:

* Norme Technique per le Construzioni (NTC) 2008. (Ref.[6])

* Circolare del Ministero delle Infrastrutture e dei Trasporti n.617 del 2/2/09. (Ref.[8])

* Schede illustrative dei principali meccanismi di collasso locali negli edifice esistenti in muratura e dei modelli cinematici di analisi. (Ref.[17])

* SAHC Lectures. SA3. Seismic Behavoir and Structural Dynamics (Ref. [16])

7.3 Methodology

Once the mechanism is identified, the first objective is to find the load multiplier "α_0" that activates the mechanism; that is the ratio between the horizontal forces and vertical loads corresponding to weights of each element involves in the mechanism, it means that horizontal forces are proportional (α_0 times) to the carried vertical loads (Figure 87). The multiplier α_0 is evaluated through the application of Virtual Work Principle in terms of displacement, equalizing the total work performed by the external forces to zero.

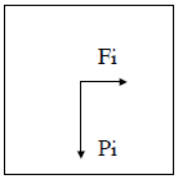

$$F_i = \alpha f\left(P_i\right)$$

Figure 87. Representation of multiplier α

In general, the methodology can be depicted in the following steps:

***Step 1:** Definition of mechanisms according to observation of collapse modalities of analog buildings and damage survey. Then, division of the system into rigid blocks following geometry, constructive characteristics and structural behavior.

***Step 2:** Application of external forces and blocks' self-weight in their barycenter. It includes permanent and imposed loads following the seismic combination presented in section 5.5:

$$\text{Seismic combination:} \qquad \boldsymbol{G_1 + G_2 + P + E + \sum_j \psi_{2j}\, Q_{kj}}$$

Table 46 and

Table 47 show the permanent and imposed loads taken into account in the analysis and the coefficient ψ_{2j} for imposed load. The actions on the structure are described in detail in section 5.

Table 46. Material characteristics and imposed loads

Material characteristics and Imposed loads		
Brick masonry	**18**	kN/m^3
Bricks (tavelle, 280x140x30mm)	0.51	kN/m^2
Clay tile (coppi)	0.6	kN/m^2
European larch timber	5.64	kN/m^3
Roof wooden truss	0.47	kN/m^2
Snow load	0.8	kN/m^2
Live load on floor (vaults and platt.)	1.5	kN/m^2

Table 47. Permanent and imposed loads per each element

Elements	**G-Dead load**		**Q-Live load (imposed load)**		**ψ_{2j} - (for Q)**
Brick masonry	20	kN/m^3	-	-	-
Vaults	20	kN/m^3	1,5	kN/m^2	0,3
Roof	84,94	KN	0,8	kN/m^2	0
Bell	35,32	KN	-	-	-
Bell yoke	7,85	KN	-	-	-
Wooden plattform1	13,73	KN	1,5	kN/m^2	0,3
Wooden plattform2	13,32	KN	1,5	kN/m^2	0,3

***Step 3**: Computation of α_o multiplier that activates the mechanism. It is obtained by applying the Virtual Work Principle (VWP) in terms of displacements equalizing the total work made by external forces to zero, following the limit analysis upper bound theorem which states that a kinematically admissible mechanism is found when the work developed by external or internal forces is positive or zero.

This equilibrium is satisfied when:

$$\boldsymbol{M_r = M_s} \qquad (22)$$

Where:

Ms is the stabilizing moment (due to self-weight loads)

Mr is the rotation moment (due to seismic forces, thrust forces, etc)

The equation of moment equilibrium or VWP might change according to the type of mechanism.

***Step 4**: Determination of spectral acceleration "$\mathbf{a_o^*}$" using the following equation:

$$\boldsymbol{a_o^* = \frac{\alpha_0 \sum(P_i + N_i)}{M^* \ FC} = \frac{\alpha_0 \ g}{e^* \ FC}} \qquad (23)$$

Each unknown component of this equation is explained below:

-$\mathbf{P_i}$ are the self-weight per each block

-$\mathbf{N_i}$ are the external vertical loads acting on the structure

-**g** is the acceleration of gravity

- $\boldsymbol{\alpha_o}$ is the multiplier that activates the mechanism

- FC is the confidence factor which takes into account the level of knowledge of the structure (explained in section 6.6)

-**M*** is the participation mass defined as:

$$\boldsymbol{M^* = \frac{\sum(P_i \delta_{x,P_i} + N_i \delta_{x,N_i})^2}{g \ \sum(P_i \delta_{x,P_i}^2 + N_i \delta_{x,N_i}^2)}} \qquad (24)$$

Where

$\delta_{x,i}$ is the virtual horizontal displacement of the barycenter for the i^{th} load (unit virtual displacement at top).

-**e*** is the mass fraction that participates in the kinematism, defined as:

$$\boldsymbol{e^* = \frac{g \ M^*}{\sum(P_i + N_i)}} \qquad (25)$$

Step 5**: ***Linear kinematic verification: according to SA3 – SAHC lectures (Ref. [16]), both ULS and DLS cases are verified if the spectral acceleration that activates the mechanism (a_o*) satisfies the following inequality:

$$a_0^* \geq \frac{a_g S}{q}\left(1 + 1.5\frac{Z}{H}\right) \qquad (26)$$

Where:

a_g is the peak ground acceleration of the soil (section 5.4.6)

S is the soil factor (section 5.4.6)

q is the structure factor, which for ULS has been taken as 2 and for DLS as 2.5 (Ref. [16])

H is the height of the whole structure measured from the foundation

Z is the distance from the foundation to the barycenter of the set of blocks involve in the kinematism.

Nonlinear kinematic analysis: The safety evaluation following either ULS (Ultimate Limit State) or DLS (Damage Limit State) is conducted using the curve capacity (simplified), in terms of acceleration "**a***" and spectral displacement "**d_o***" of an equivalent single degree of freedom system where the ultimate displacement capacity (**d_u***) is compared with the earthquake demand (**Δ_{Ts}**).

However, if the linear analysis is verified, nonlinear kinematic analysis is not required.

Step 6**: Determination of the spectral displacement **d_o, which is the average displacement of several points in which the loads Pi have been applied. In that way, knowing the displacement of a control point **d_k**, it is possible to define **d_o*** using virtual displacements **$\delta_{x,I}$** by means of the following equation:

$$d_o^* = d_{ko}\frac{\sum P_i \delta_{x,i}}{\delta_{x,k}\sum P_i} = d_{ko}\frac{\sum (N_i \delta_{x,Ni} + P_i \delta_{x,Pi})}{\delta_{x,k}\sum (P_i + N_i)} \qquad (27)$$

$\delta_{x,k}$ is the virtual horizontal displacement of the point **k** which is the global barycenter of the rigid blocks (barycenter of the generic block).

To get the displacement at this point (**d_{k0}**), to determine the finite rotation angle **θ** that annuls the stabilizing moment **M_S** is required. This equilibrium condition might be expressed as:

$$M_s = \sum P_i R_{P_i} cos(\beta_{P_i} + \theta) + \sum N_i R_{T_i} cos(\beta_{N_i} + \theta) + \sum T_i R_{T_i} sin(\beta_{T_i} + \theta) - \sum N_{hi} R_{T_i} sin(\beta_{N_{hi}} + \theta) = 0 \qquad (28)$$

T_i is a tension force applied to the structure to stabilize it by means of tie-rods. If the structure is not verified under self-weight and external forces, these tie-rods might be included.

As it is seen in Figure 88, R_i is the distance from the center of rotation to the point of application of each load, β_i is the angle between R_i and the horizontal level.

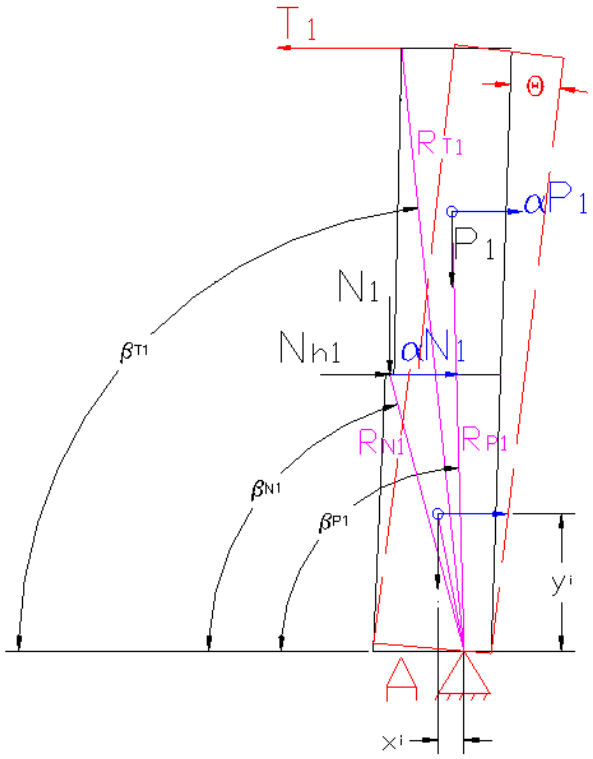

Figure 88. Representation of finite angle θ that activates mechanism. Ref. [18[16]

Once the angle θ is determined, displacement of a control point d_{ko} can be determined using the following expression:

$$\boldsymbol{d_{k0} = H_k \, sin\,(\theta)} \qquad (29)$$

***Step 7**: The simplified capacity curve can be obtained using the next expression:

$$\boldsymbol{a^* = a_0^*(1 - {d^*}/{d_0^*})} \qquad (30)$$

***Step 8**: Ultimate displacement capacity of an equivalent SDOF system:

$$\boldsymbol{d_u^* = 0.4\, d_0^*} \qquad (31)$$

***Step 9**: The demand displacement is evaluated on the spectrum corresponding to the secant period Ts defined as:

$$\boldsymbol{T_s = 2\pi \sqrt{\frac{d_s^*}{a_s^*}}} \qquad (32)$$

Where:

d^*_s is 0.4 times the ultimate displacement capacity of an equivalent SDOF system defined as:

$$d_s^* = 0.4\, d_u^* \qquad (33)$$

a^*_s is the corresponded spectral acceleration to **d^*_s**, defined as:

$$a_s^* = a_0^*\left(1 - {d_s^*}/{d_0^*}\right) \qquad (34)$$

***Step 10:** Displacement demand of the earthquake Δ_d (from spectrum)

The earthquake displacement demand is obtained from the spectrum (in displacement domain) defined with the following equations:

$$\begin{aligned} T_s < 1.5T_1 \qquad & \Delta_d(T_s) = a_g S \frac{T_s^2}{4\pi^2}\left(\frac{3(1+Z/H)}{1+(1-T_s/T_1)^2} - 0.5\right) \\ 1.5T_1 \le T_s < T_D \qquad & \Delta_d(T_s) = a_g S \frac{1.5T_1T_s}{4\pi^2}\left(1.9 + 2.4\frac{Z}{H}\right) \\ T_D \le T_s \qquad & \Delta_d(T_s) = a_g S \frac{1.5T_1T_D}{4\pi^2}\left(1.9 + 2.4\frac{Z}{H}\right) \end{aligned} \qquad (35)$$

T_D is the period corresponded to the beginning of the constant displacement range of the spectrum, it is defined as:

$$T_D = 4 * a_g + 1.6 \qquad (36)$$

T_1 is the first fundamental period of the structure which has been determined in the dynamic experimental test (section 4.1.2) and also approximately using an expression from NTC -2008. Table 48 shows both values for T_1, it is seen that the natural period obtained with the code is higher than the one obtained experimentally.

Table 48. First natural period of the Tower determined by means of test and standards

Dynamic Characterization Test	NTC-2008
First natural frequency = **1.59 Hz** **T_{1t} = 0.63 s**	$T_{1NTC} = C_1 H^{3/4} = 0.05\ (47.2)^{3/4} = 0.9\ s$

***Step 11: Nonlinear kinematic verification**

Once the previous values have been calculated, the capacity curve can be plotted as it is seen in Figure 89. The ultimate displacement capacity $\mathbf{d_u^*}$ is compared with the earthquake demand $\mathbf{\Delta_{Ts}}$ and it must satisfy:

$$\Delta_d \leq d_u^* \qquad (37)$$

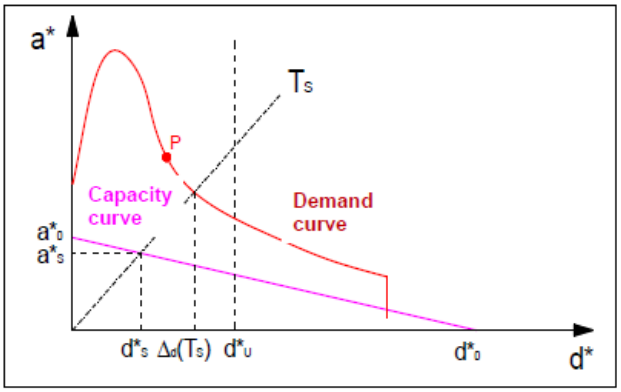

Figure 89. Simplified capacity curve. Ref. [16]

7.4 Mechanisms

Five kinematic mechanisms were considered taking into account the suggestion by "Schede Illustrative dei Principali Meccanismi di Collasso Locali Negli Edifici Esistenti in Muratura e dei Relativi Modelli Cinematici di Analisi" (Ref.[17]) and analyzing the possible failure mechanisms of the tower based on the inspection.

The considered mechanisms are divided in three types, the first type consists in the rotation of a wall out of its plane suggesting its impossibility of transmitting the seismic force; that means that the wall has to face an action which it is not able to resist and collapses. The second type consists in the global overturning of a structure part considering good connection between walls. The third type is the rotation in-plane of some pillars since they are vulnerable elements with low stiffness.
The mechanisms are (see Figure 90):

Mechanism 1: Simple out of plane wall failure of the leaned eastern wall

Mechanism 2: Simple out of plane wall failure of the southern wall

Mechanism 3: Simple out of plane wall failure of belfry and battlement

Mechanism 4: Global overturning of the tower above the level of adjacent buildings

Mechanism 5: Rigid rotation in-plane of belfry pillars

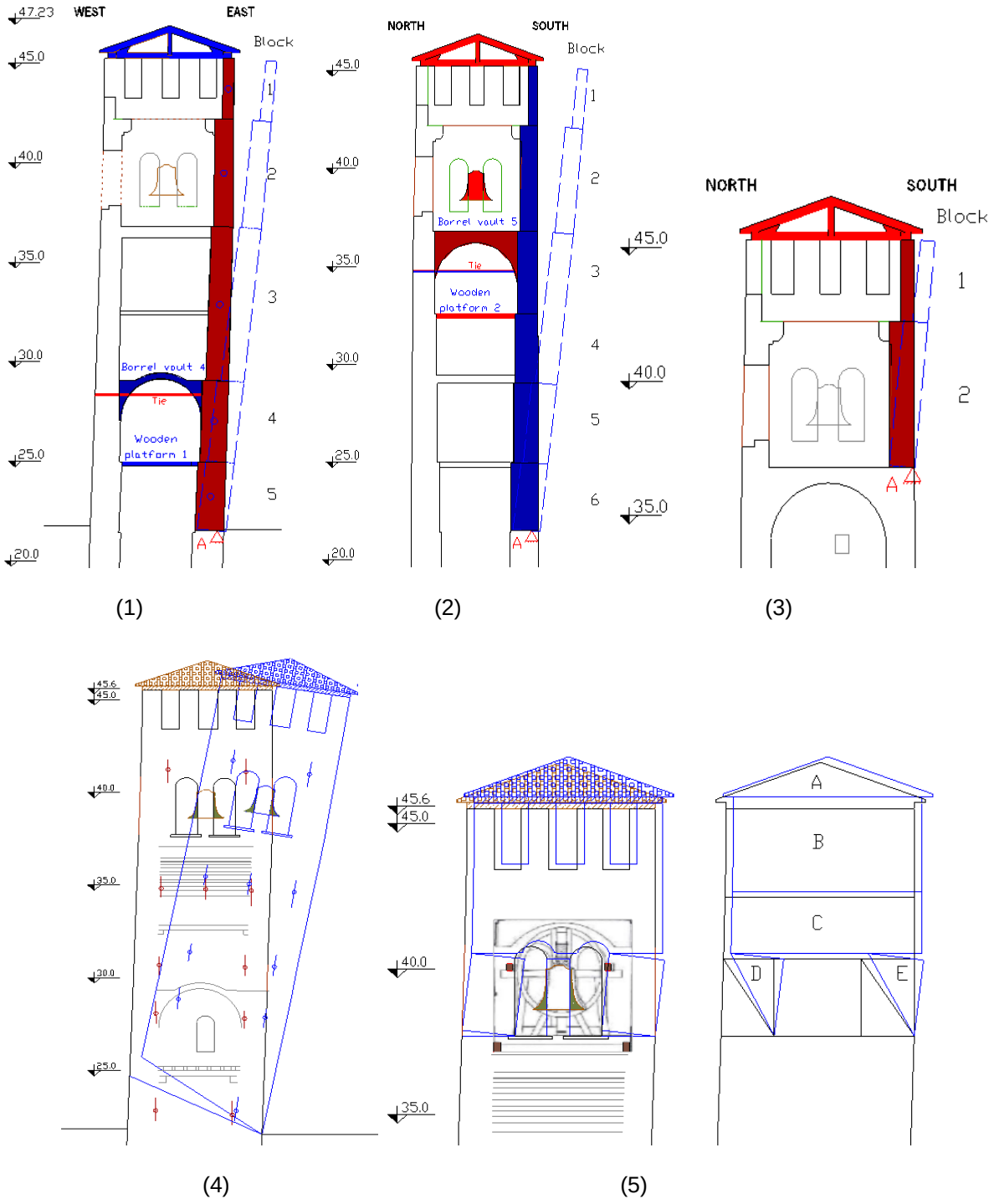

Figure 90. Kinematic mechanisms

7.5 Tension capacity of tie-rods

For the kinematic analysis, the effect of the iron tie rods will be taken into account. For safety reasons, the tie-rods have to maintain the state of stress below the yielding point to avoid any plastic behavior. For that, it is necessary to evaluate their tension capacity following three failure mechanisms (Ref.[18]) and choosing the minimum bearing capacity value:

1. Failure mechanism relative to the yielding strength of the tie rods (T1):

$$T1 = A * f_y \qquad (38)$$

Where:

A is the cross section area of the tie. Since the ties inspected in the tower have different cross section, a conservative cross area (lower than average) have been considered (254,47 mm^2).

f_y is the tensile strength of the tie material. Since the ties are made of wrought iron, the tensile strength has been taken from literature as f_y=180 MPa.

2. Failure mechanism relative to punching of the masonry around the anchor plates (T2):

$$T2 = f_v[2\,(b + t) + 2(a + t)]\,t \qquad (39)$$

Where:

a is the height of the anchor plate. According to geometrical survey, the anchor plates have an average height of 110 cm.

b is the width of the anchor plates. According to geometrical survey, the anchor plates have an average width of 10 cm

t is thickness of the wall on which the tie is set up

f_v is the design shear strength of the masonry which has been calculated in section 6.7.4 (0.024 MPa).

3. Failure mechanism relative to the resistance of the wall against the penetration of the anchor due to excess contact pressure (T3):

$$T3 = \sigma_c\, a\, b \qquad (40)$$

Where **σ_c** is the design compression strength of the brick masonry which has been calculated in section 6.7.3 (0.94 MPa).

Table 49 shows the parameters to calculate the bearing capacity of tie rods.

Table 49. Parameters to determine the tension capacity of iron tie rods

Diameter of bar	**D**	18	mm
Cross area	**A**	254,47	mm^2
Tensile strength of wrought iron	$\mathbf{f_y}$	180	MPa
Height of anchor plate	**a**	1,1	m
Width of anchor plate	**b**	0,1	m
Design shear strength of masonry	$\mathbf{f_v}$	0,024	MPa
Design compression strength of masonry	$\boldsymbol{\sigma_c}$	0.94	MPa

7.6 Mechanism 1 – Simple out of plane wall failure of the leaned eastern wall

7.6.1 Linear Kinematic Analysis

Since the tower is slightly leaned to the east (1.8 degrees) and considering poor connection between the walls, it is important to evaluate the behavior of the eastern wall as a macroelement subjected to an earthquake. The mechanism consists in the rotation of the upper part of the wall out of its plane from the level where it is constrained by the neighboring buildings. The mechanism takes into account the changes of geometry and thickness of wall, the inclination of the tower (change of barycenter), the openings such as vaulted windows and battlement (crenels), the effects of the roof (25% self-weight is applied at the top of this wall), the effect of the wooden platform 1 (50% of self-weight is considered, since this platform is supported on western and eastern wall) and the effect of both the vertical reaction and the thrust made by the barrel vault 4 (See Figure 91).

Due to the thrust generated by the vaults, it is assumed that at least the iron tie rods located in the vault-span are active, therefore, these ties have been considered from the beginning of the analysis. The objective is to determine if the system is verified just with the ties under the vaults; if it is not, the goal is to calculate the lowest number of ties necessary to make it verified.

The macroelement has been divided in 5 blocks whose geometry is presented in Table 50.

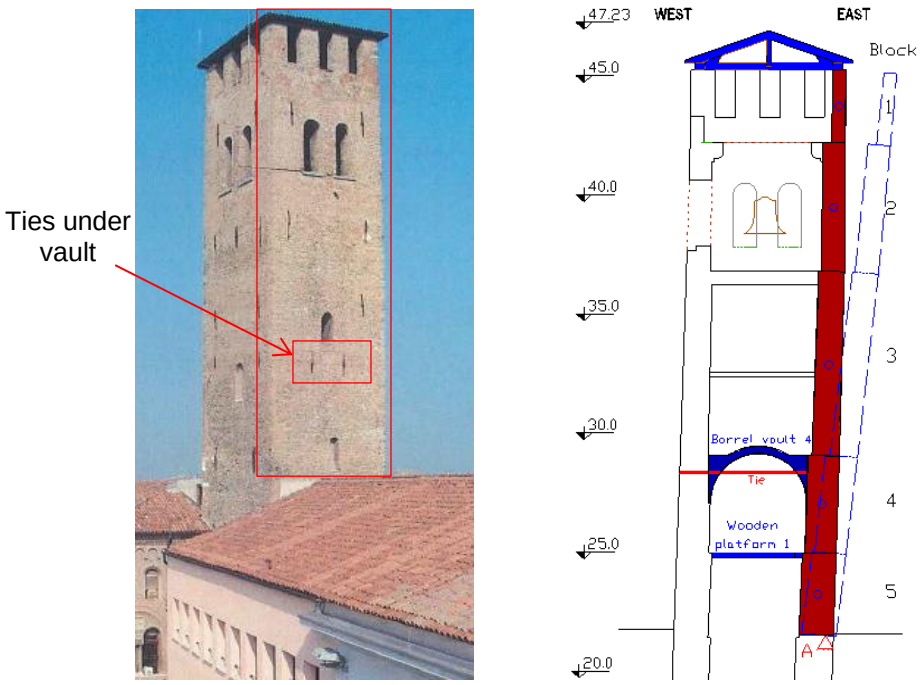

Figure 91. Left: View of eastern wall of tower. Right: Mechanism 1- Simple out of plane eastern wall failure

Table 50. Geometrical characteristics of blocks for mechanism 1

Block	b-Thickness (m)	Depth (m)	Cross Area (m^2)	V (m^3)
1 (battlement)	0,57	6,6	1,73	8,32
2 (with vaulted windows)	0,98	6,69	5,30	29,64
3 (with one window)	1,17	6,8	8,86	58,57
4	1,35	6,84	5,54	37,90
5	1,46	6,91	5,07	35,04

The thrust generated by the vault 4 must be taken into account, for that, the vault has been analyzed using the software “Arco” (Civil Engineering Free Software - Programmi Gratuiti per Ingegneria Civile sviluppati con la collaborazione degli student da Piero Gelfi) which is an analysis tool for masonry arches and vaults based on the “safe theorem” of the plastic analysis method.

In addition to the self-weight of the vault, the imposed load has been considered taking into account the seismic load combination (sections 5.5 and section 7.3). Since the service load is 1.5 kN/m^2 and the factor ψ_{2j} is 0.3, the imposed load for the vault is 0.45 KN/m^2. Figure 92 shows the geometrical characteristics and the loading input.

For the solution, the vault was divided into 20 voussoirs and the thrust line was calculated in a step analysis; the results are shown in Figure 93. It is seen that the thrust at each springing is 67.68 kN and the vertical reaction is 123.0 kN.

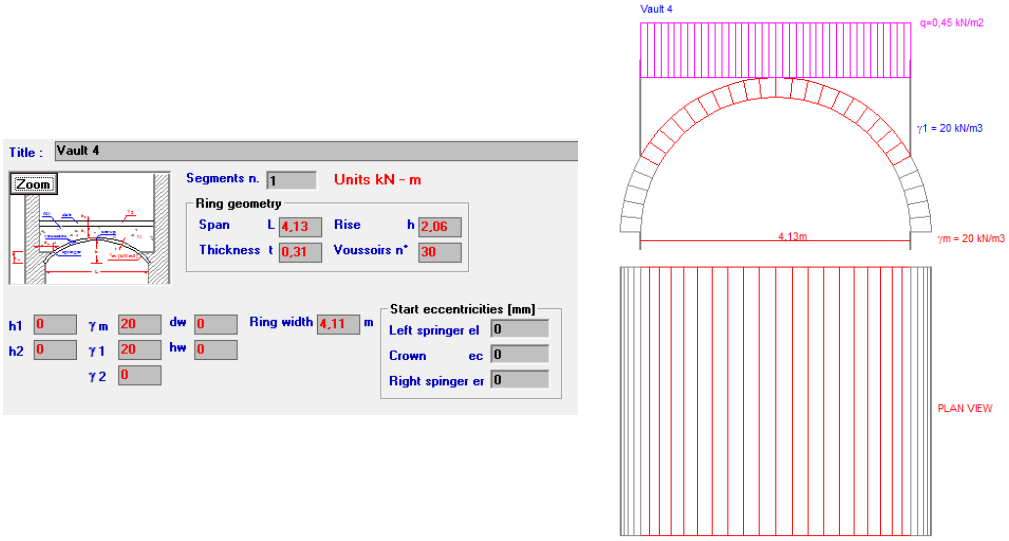

Figure 92. Geometry and loading input for analysis of vault 4 in software Arco

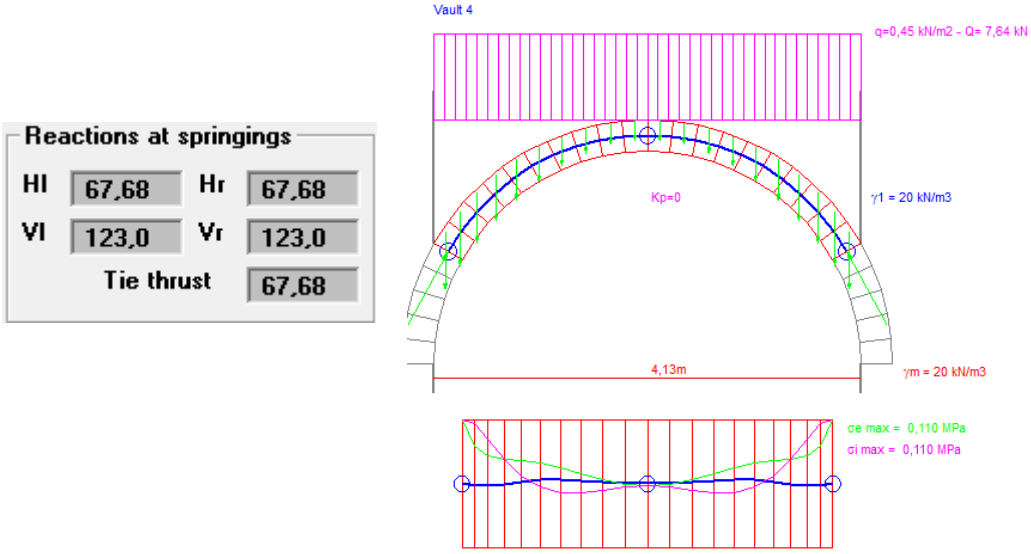

Figure 93. Thrust line of the vault 4 and reactions at springings

The initial analysis has considered the ties located under the vault whose tension state was calculated by means of the dynamic characterization test, explained in the section 4.2.4.

This test revealed that the tie N22 located under the vault is subjected to **32.7 KN,** since there are two ties at this level, the first analysis has been taken into account a tension $\mathbf{T_{va}}$**=65.4 KN.**

It is important to notice that the result of the tension is quite close to the thrust generated by the vault.

For the loading evaluation, the seismic load combination has been considered (sections 5.5 and section 7.3); the force diagram for mechanism 1 is shown in Figure 94 and the corresponding values are presented in Table 51.

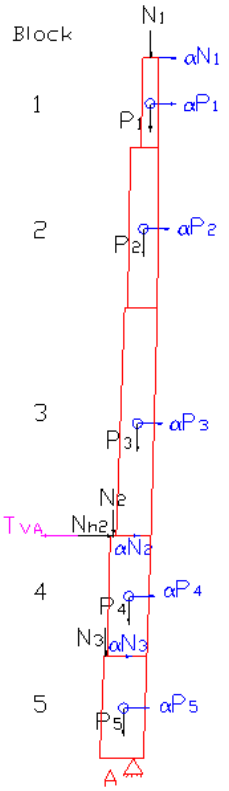

Figure 94. Force diagram for mechanism 1

Table 51. Forces acting in mechanism 1

Element	Load (kN)	
Block 1 (battlement)	P_1	149.83
Block 2 (with vaulted windows)	P_2	533.51
Block 3 (with one window)	P_3	1054.23
Block 4	P_4	682.27
Block 5	P_5	630.66
25% roof self-weight	N_1	21.23
Vertical resultant of vault 4	N_2	123.00
50% wooden platf.1 self-weight	N_3	9.8
Thrust of vault 4	N_{h2}	67.68
Ties under vaults	T_{va}	**65.4**

Considering zero tensile strength for the masonry, the hypothesized kinematism is given by a rotation of the whole wall around the hinge A (Figure 95). This hinge is determined by the point where the reacting section ends, whose amplitude (distance t_1) can be calculated by limiting the maximum stress in the most compressed edge to the value of compression strength σ_c (Ref. [16]). The distance t_1 is calculated with the following expression and the result is presented in Table 52.

$$t_1 = \frac{2}{3}\frac{\sum(P_i + N_i)}{\sigma_c * l} \qquad (41)$$

Where l is the effective wall length.

Table 52. Distance t_1 for mechanism 1

σ_c	0.94	Mpa
l	6,91	m
t_1	**0,33**	m

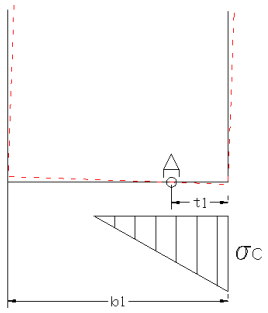

Figure 95. Representation of point of rotation A

The masonry wall is subjected to rotational moment $\mathbf{M_r}$ given by the action of the vault thrust and the seismic forces (relative to self-weight load). This rotational moment will tend to make rotate the macroelement around the hinge A at the base. This action is opposed by the action of a stabilizing moment M_s generated by the self-weight force of the wall itself and the external vertical loads. By imposing the conditions of equilibrium Mr=Ms, the coefficient that activates the mechanism α_0 is obtained by means of the following equations:

$$\boldsymbol{M_s = \sum(P_i\, x_{i,P} + N_i\, x_{i,N}) + \sum T_i\, y_{i,T}} \qquad (42)$$

$$\boldsymbol{M_r = \alpha_o \sum(P_i\, y_{i,P} + N_i\, y_{i,N}) + \sum N_{hi}\, y_{i,N}} \qquad (43)$$

$$\boldsymbol{M_s = M_r \;\rightarrow \alpha_o}$$

$$\boldsymbol{\alpha_o = \frac{\sum(P_i\, x_{i,P} + N_i\, x_{i,N}) + \sum T_i\, y_{i,T} - \sum N_{hi}\, y_{i,N}}{\sum(P_i\, y_{i,P} + N_i\, y_{i,N})}} \qquad (44)$$

The distances x_i and y_i correspond to the horizontal and vertical distance from the point of rotation to the point of application of the load.

Table 53 shows the parameters for calculation of the coefficient of activation α_o and the spectral acceleration a^*_0. It is seen that some distances x_i are negative because the point of application of those loads are to the right of the point of rotation A (Figure 94), therefore, these loads are not stabilizing the system.

Table 53. Parameters for calculation of α_o and a^*_0

Load (kN)		xi	yi	M_{si} (KN m)	M_{ri}(KN m)	$\delta_{x,i}$	$P_i*\delta x,i$	$Pi*\delta x,i^2$
P_1	149.83	-0.47	22.22	-70.84	3329.53	0.93	139.95	130.73
P_2	533.51	-0.24	17.98	-130.55	9593.37	0.76	403.25	304.80
P_3	1054.23	-0.13	11.38	-138.84	11995.00	0.48	504.20	241.14
P_4	682.27	0.15	5.52	104.73	3764.29	0.23	158.23	36.70
P_5	630.66	0.33	1.73	209.69	1089.40	0.07	45.79	3.32
N_1	21.23	-0.47	23.79	-10.04	505.16	1.00	21.23	21.23
N_2	123.00	0.68	7.56	83.85	930.09	0.32	39.10	12.43
N_3	9.8	0.93	3.47	9.17	34.06	0.15	1.43	0.21
N_{h2}	67.68	*0.68*	7.56		**511.78**			
T_{va}	**65.4**		**7.56**	**494.54**				

Following the equations presented in the methodology (section 7.3), the values of α_o and a^*_o were obtained and are shown below:

Multiplier that activate the mechanism	**α_o**	**0,001**	
Stabilizing moment	**M_{si}**	551.70	KN*m
Rotation moment	**M_{ri}**	551.70	KN*m
Equivalent mass	**M***	234.21	
Fraction of the mass participant in the kinemat.	**e***	0,717	
Confidence factor	**FC**	1.27	
Spectral acceleration for activation of mechanism	**a^*_0**	**0,01**	m/s^2
	a^*_0	**0,001**	g

The linear kinematic verification has been carried out for both DLS (Damage Limit State) and ULS (Ultimate Limit State) and the results values are shown in the following table:

Table 54. Linear kinematic verification mechanism 1

		DLS	ULS
Peak ground acceleration	**a_g (g)**	0,043	0,099
Soil factor	**S**	1,2	1,2
Structure factor	**q**	2,5	2
Height of the whole structure	**H (m)**	47,20	47,20
Distance from ground to barycenter of moving mass	**Z (m)**	**33.16**	**33.16**
Spectral acceleration for activation of mechanism	**a^*_0 (g)**	**0,001**	**0,001**
Limit value: a_g S/q (1+1,5 Z/H)	**(g)**	**0,042**	**0,122**
		NO VERIFIED	**NO VERIFIED**

The mechanism is not verified using linear analysis; therefore, non-linear kinematic analysis is required.

7.6.2 Non-Linear Kinematic Analysis

Next table shows the parameters to calculate the finite rotation θ that annuls the steadying moment M_S.

Table 55. Parameters to calculate θ

Load	β_i (degrees)	Ri (m)	F_i*R_i	$Fv_i*R_i*\cos(\beta+\theta)$	$Fh_i*R_i*\sin(\beta+\theta)$
P_1	*91.10*	22.23	3330.63	-71.60	-
P_2	*90.60*	17.98	9595.13	-122.54	-
P_3	*90.50*	11.38	11995.85	-132.27	-
P_4	88.41	5.52	3765.72	95.83	-
P_5	79.10	1.76	1109.39	207.27	-
N_1	*91.40*	23.77	504.76	-13.49	-
N_2	84.85	7.59	513.85	44.95	-
N_3	74.94	3.59	35.27	9.09	-
N_{h2}	**84.85**	**7.59**	**513.85**	**-**	**-511.88**
T_{va}	84.85	7.59	496.54		494.64
			Σ	0.00	

The results for non-linear kinematic analysis are shown below:

Steadying moment MS=0 →	**Ms**	**0.00**	KN*m
FINITE rotation θ that annuls the steadying moment M_S	**θ**	**0.002**	Rad.
		0.13	°
Control height	**H_k**	9.75	m
Displacement of the control point	**d_{k0}**	0.02	m
Virtual horizontal displacement of the point k	**$\delta_{x,k}$**	0.41	m
Equivalent spectral displacement corresponding to the displacement dk_0	**d^*_0**	0.022	m
Ultimate displacement capacity for SDF	**d^*_u**	0.0090	m
Displacement of equivalent SDF system (0.4 d^*_u)	**d^*_s**	0.0036	m
Spectral acceleration for activation of mechanism	**a^*_0**	0.0138	m/s^2
		0.0014	g
Spectral acceleration related for the displacement d^*_s	**a^*_s**	**0.0012**	g

Displacement demand of the earthquake Δd (from spectrum)

		DLS	ULS
Secant period	T_s (s)	3.5	3.5
First natural period of the structure (test)	T_{1t} (s)	0.64	0.64
First natural period of the structure (NTC)	T_{1NTC} (s)	0.90	0.90
Peak ground acceleration	a_g (g)	0.04	0.10
Soil factor	S	1.20	1.20
Height of the whole structure	H (m)	47.20	47.20
Distance from ground to barycenter of moving mass	Z (m)	33.16	33.16
	T_D (s)	1.77	2.00
	1,5 *T_1 (s)	1.35	1.35
Displacement demand of the earthquake	**Δ(Ts) (cm)**	11.00	28.54
Ultimate displacement capacity	**d^*_u (cm)**	0.90	0.90
		NO VERIFIED	NO VERIFIED

The mechanism is not verified, the displacement demand of the earthquake is much higher that the ultimate displacement capacity of the structure. The corresponding simplified capacity curve is presented in Figure 96. Extra tie-rods might be included in the analysis for the verification of the mechanism.

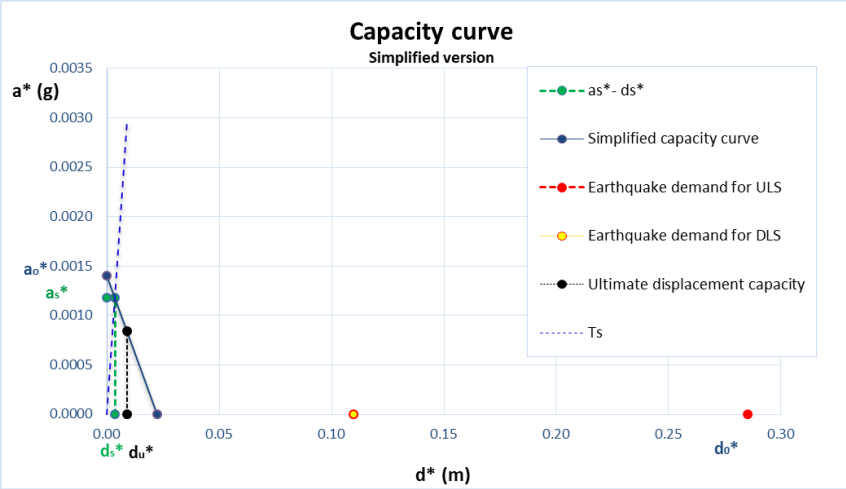

Figure 96. Simplified capacity curve for mechanism 1 (including two tie-rods under the vault)

7.6.3 Linear Kinematic Analysis considering extra Tie-Rods

The goal is to calculate the lowest number of ties necessary to make the mechanism verified. For that the analysis was carried out introducing the ties one by one until achieving the verification. The positions of

ties, that have been considered, are shown in Figure 97. As the ties have different cross section area, a conservative area was chosen, corresponding to Φ18 mm, A=254.5 mm^2 (see section 7.5).

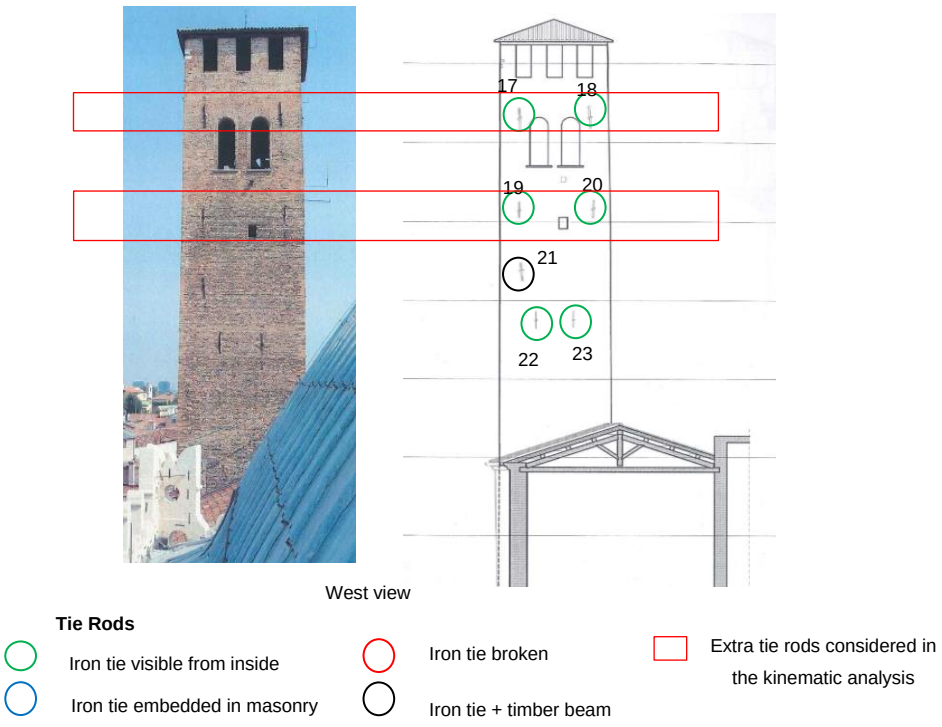

Figure 97. Distribution of tie rods in direction W-E to be considered in the analysis

Figure 98 shows the forces involved in the mechanism 1 considering the extra tie-rods whose tension capacity for each failure mechanism is presented in Table 56 (it was calculated following procedure shown in section 7.5). It is seen that the minimum tension capacity of the ties is the one obtained using the first failure mechanism (T1) equal to 45.8 kN.

On the other hand, it was found that the minimum number of ties for the structure to be verified is 3 distributed as it is shown in Table 56.

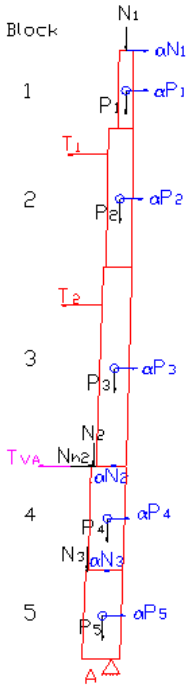

Figure 98. Forces involved in the mechanism 1 considering extra tie-rods

Table 56. Tension capacity of ties

	Tie 1 - T_1	**Tie 2- T_2**
Thickness wall- t (m)	0,98	1,17
Tension capacity - T1 (KN)	**45,80**	**45,80**
Tension capacity -T2 (KN)	148.65	198.81
Tension capacity -T3 (KN)	103.4	103.4
Quantity of ties	**2**	**1**

By imposing the conditions of equilibrium Mr=Ms by means of the same equations used in the previous analysis, the coefficient that activates the mechanism α_0 is obtained. Table 57 shows the parameters for calculation of the coefficient α_o and the spectral acceleration a^*_0 for activation of the mechanism:

Table 57. Parameters for calculation of α_o and a^*_o for mechanism 1considering extra tie rods

	Load (kN)	xi	yi	M_{si} (KN m)	M_{ri}(KN m)	$\delta_{x,i}$	$P_i*\delta x,i$	$Pi*\delta x,i^2$
P_1	149.83	-0.47	22.22	-70.84	3329.53	0.93	139.95	130.73
P_2	533.51	-0.24	17.98	-130.55	9593.37	0.76	403.25	304.80
P_3	1054.23	-0.13	11.38	-138.84	11995.00	0.48	504.20	241.14
P_4	682.27	0.15	5.52	104.73	3764.29	0.23	158.23	36.70
P_5	630.66	0.33	1.73	209.69	1089.40	0.07	45.79	3.32
N_1	21.23	-0.47	23.79	-10.04	505.16	1.00	21.23	21.23
N_2	123.00	0.68	7.56	83.85	930.09	0.32	39.10	12.43
N_3	9.8	0.93	3.47	9.17	34.06	0.15	1.43	0.21
N_{h2}	67.68	*0.68*	7.56		**511.78**			
T_1	**91.6**		**19.70**	**1804.69**				
T_2	**45.8**		**13.82**	**633.14**				
T_{va}	**65.4**		**7.56**	**494.54**				

Following the equations presented in the methodology (section 7.3), the values of α_o and a^*_o were obtained and are shown below:

Multiplier that activate the mechanism	**α_o**	**0.079**	
Stabilizing moment	**M_{si}**	2989.52	KN*m
Rotation moment	**M_{ri}**	2989.52	KN*m
Equivalent mass	**M***	234.21	
Fraction of the mass participant in the kinemat.	**e***	0.717	
Confidence factor	**FC**	1.270	
Spectral acceleration for activation of mechanism	**a^*_0**	**0.85**	m/s^2
	a^*_0	**0.087**	g

The linear kinematic verification has been carried out for both DLS (Damage Limit State) and ULS (Ultimate Limit State) and the results values are shown in the following table:

Table 58. Linear kinematic verification mechanism 1 (considering extra ties)

		DLS	ULS
Peak ground acceleration	**a_g (g)**	0.043	0.099
Soil factor	**S**	1.2	1.2
Structure factor	**q**	2.5	2
Height of the whole structure	**H (m)**	47.20	47.20
Distance from ground to barycenter of moving mass	**Z (m)**	**33.16**	**33.16**
Spectral acceleration for activation of mechanism	**a^*_0 (g)**	**0.0871**	**0.087**
Limit value: a_g S/q (1+1,5 Z/H)	**(g)**	**0.042**	**0.122**
		VERIFIED	**NO VERIFIED**

The mechanism is not verified for ULS; therefore, non-linear kinematic analysis is required.

7.6.4 Non-Linear Kinematic Analysis considering extra Tie-Rods

Table 59 shows the parameters to calculate the finite rotation θ that annuls the steadying moment M_S.

Table 59. Parameters to calculate θ for mechanism 1 (considering extra ties)

Load	β_i (degrees)	Ri (m)	F_i*R_i	$Fv_i*R_i*\cos(\beta+\theta)$	$Fh_i*R_i*\sin(\beta+\theta)$
P_1	*91.10*	22.23	3330.63	-334.17	-
P_2	*90.60*	17.98	9595.13	-879.37	-
P_3	*90.50*	11.38	11995.85	-1078.54	-
P_4	88.41	5.52	3765.72	-201.57	-
P_5	79.10	1.76	1109.39	120.61	-
N_1	*91.40*	23.77	504.76	-53.27	-

N_2	84.85	7.59	513.85	4.41	-	
N_3	74.94	3.59	35.27	6.37	-	
N_{h2}	**84.85**	**7.59**	**513.85**	**-**		**-513.83**
T_1	89.66	19.70	1804.99	-		1799.86
T_2	83.40	13.83	633.34	-		632.97
T_{va}	84.85	7.59	496.54			496.52
			∑		0.00	

The results of non-linear kinematic analysis are shown below:

Steadying moment MS=0 →	**Ms**	**0.00**	KN*m
FINITE rotation θ that annuls the steadying moment M_S	**θ**	**0.081** **4.66**	Rad. o
Control height	H_k	9.75	m
Displacement of the control point	d_{k0}	0.79	m
Virtual horizontal displacement of the point k	$\delta_{x,k}$	0.41	m
Equivalent spectral displacement corresponding to the displacement dk_0	d^*_0	0.792	m
Ultimate displacement capacity for SDF	d^*_u	0.3167	m
Displacement of equivalent SDF system (0.4 d^*_u)	d^*_s	0.1267	m
Spectral acceleration for activation of mechanism	a^*_0	0.8545 0.0871	m/s^2 g
Spectral acceleration related for the displacement d^*_s	a^*_s	**0.0732**	g

Displacement demand of the earthquake Δd (from spectrum):

		DLS	ULS
Secant period	**T_s (s)**	**2.6**	**2.6**
First natural period of the structure (test)	**T_{1t} (s)**	0.64	0.64
First natural period of the structure (NTC)	**T_{1NTC} (s)**	**0.90**	**0.90**
Peak ground acceleration	**a_g (g)**	0.04	0.10
Soil factor	**S**	1.20	1.20
Height of the whole structure	**H (m)**	47.20	47.20
Distance from ground to barycenter of moving mass	**Z (m)**	33.16	33.16
	T_D (s)	**1.77**	**2.00**
	1,5 *T_1 (s)	**1.35**	**1.35**
Displacement demand of the earthquake	**Δ(Ts) (cm)**	**11.00**	**28.54**
Ultimate displacement capacity	**d^*_u (cm)**	**31.67**	**31.67**
		VERIFIED	**VERIFIED**

The mechanism 1 including the 3 iron ties (plus 2 ties under vault) is verified with Non-Linear Kinematic Analysis for both DLS and ULS; the corresponding simplified capacity curve is presented in Figure 99. The ultimate displacement capacity of the structure is 31.67cm, while the displacement demanded by the earthquake is 11.00 cm for DLS and 28.54 cm for ULS.

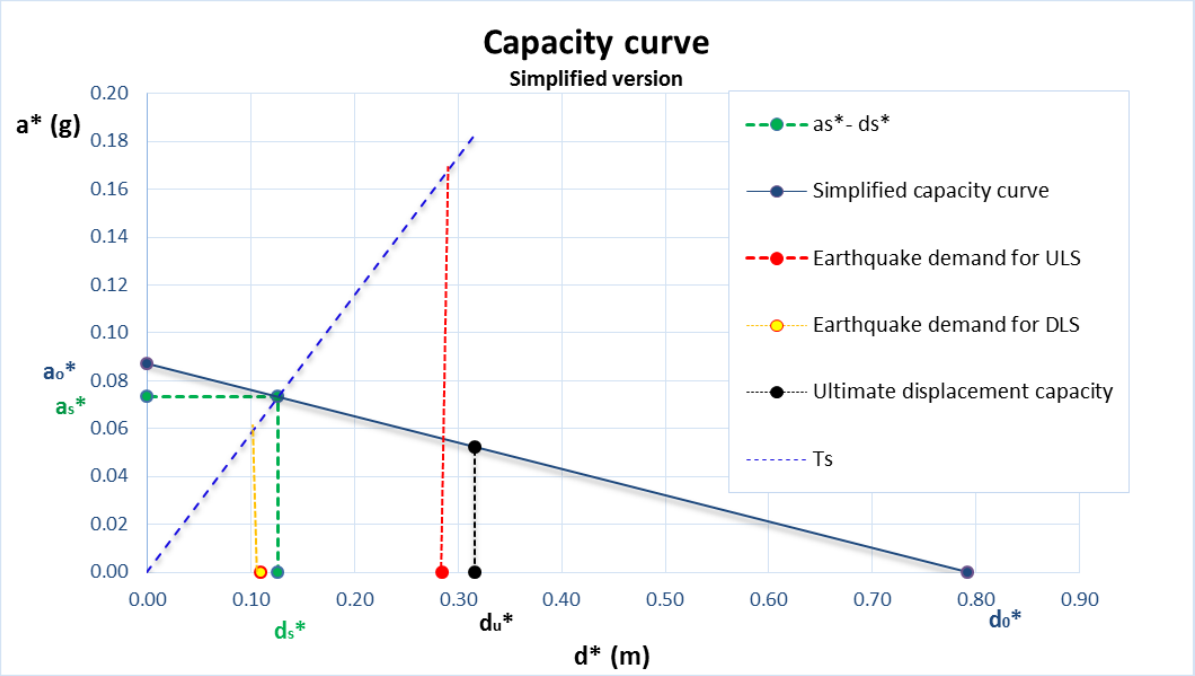

Figure 99. Simplified capacity curve for mechanism 1 (including 3 iron ties)

7.7 Mechanism 2 – Simple out of plane wall failure of the southern wall

7.7.1 Linear Kinematic Analysis

As same as the eastern wall, the southern wall was analyzed taking into account the self-weight of the bell and bell yoke, which are supported on northern and southern wall, and the thrust generated by the barrel vault 5 located under the belfry. The mechanism consists in the rotation of the upper part of the wall out of its plane from the level where it is constrained by the neighboring buildings. It takes into account the changes of geometry and thickness of wall, the openings such as vaulted windows and battlement (crenels), the effect of the roof (25% self-weight is applied at the top of this wall), the effect of the wooden platform 2 (50% of self-weight is considered), the half of self-weight of the bell and bell yoke and the effect of both the vertical reaction and the thrust made by the barrel vault 5(See Figure 100).

The macroelement has been divided in 6 blocks whose geometry is presented in Table 60.

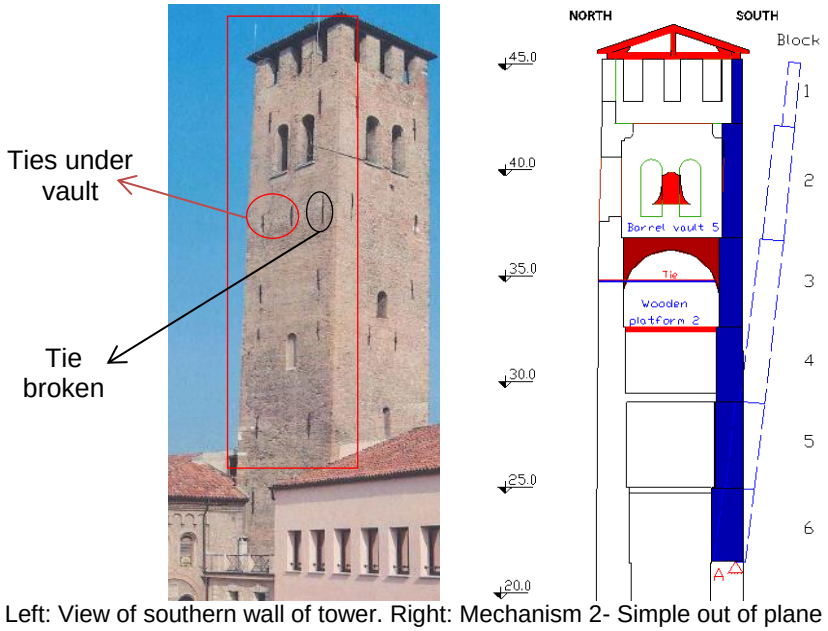

Figure 100. Left: View of southern wall of tower. Right: Mechanism 2- Simple out of plane southern wall failure

Table 60. Geometrical characteristics of blocks for mechanism 2

Block	b-Thickness (m)	h-Height (m)	Depth (m)	Cross Area (m^2)	V (m^3)
1 (battlement)	0,57	3,05	6,60	1,74	8,40
2 (with vaulted windows)	0,98	5,44	6,69	5,33	29,82
3	1,13	4,24	6,76	4,79	32,39
4	1,23	3,54	6,76	4,35	29,43
5	1,34	4,08	6,80	5,47	37,18
6	1,47	3,47	6,81	5,10	34,74

As same as the analysis for mechanism 1, the thrust generated by the vault 5 was determined using the software “Arco” (Civil Engineering Free Software - Programmi Gratuiti per Ingegneria Civile sviluppati con la collaborazione degli student da Piero Gelfi) which is an analysis tool for masonry arches and vaults based on the “safe theorem” of the plastic analysis method.

In addition to the self-weight of the vault, the imposed load has been considered taking into account the seismic load combination (sections 5.5 and section 7.3). Since the service load is 1.5 kN/m^2 and the factor ψ_{2j} is 0.3, the imposed load for the vault is 0.45 KN/m^2. Figure 101 shows the geometrical characteristics and the loading input.

For the solution the vault was divided into 20 voussoirs and the thrust line was calculated in a step anaylisis; the results are shown in Figure 102. It is seen that the thrust at each springing is 134.2 kN and the vertical reaction is 199.0 kN.

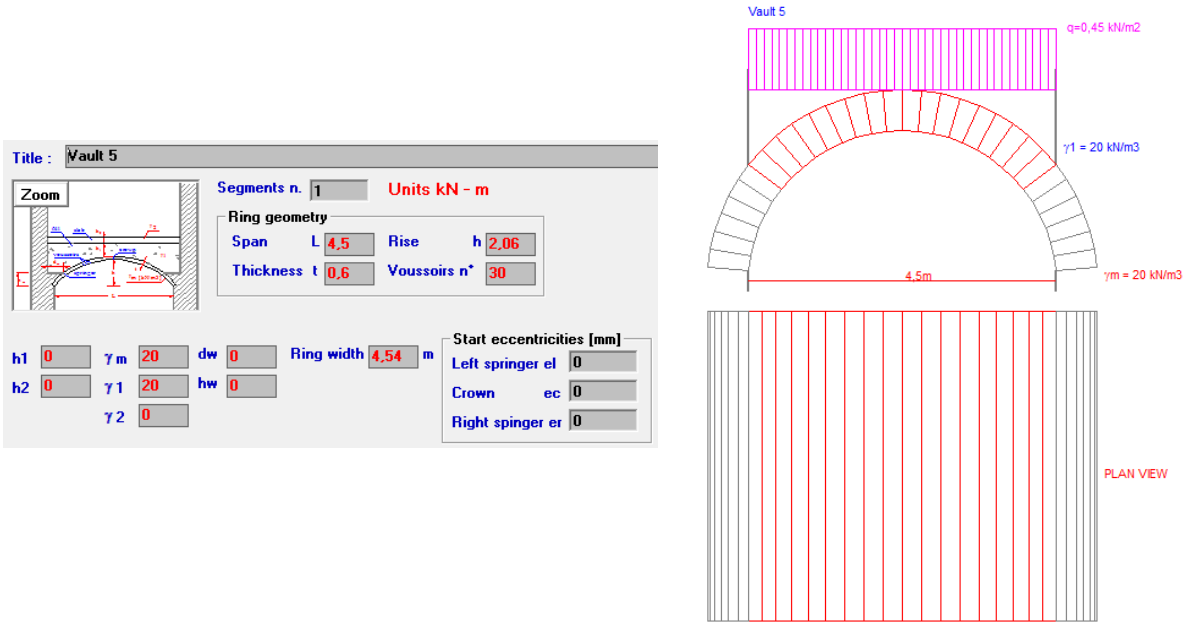

Figure 101. Geometry and loading input for analysis of vault 5 in software *Arco*

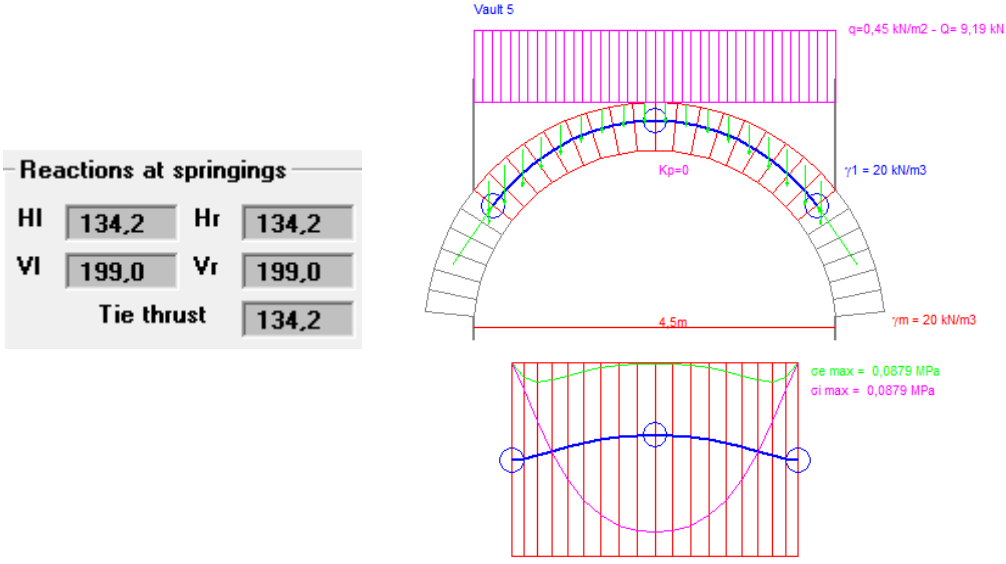

Figure 102. Thrust line of the vault 5 and reactions at springings

The initial analysis has considered the ties located under the vault whose tension state was calculated by means of the dynamic characterization test, explained in the section 4.2.4.

However, the test made on tie N13, located under the vault, was rejected because of the results were not reliable due to a very high deviation standard. Therefore, it was assumed that the ties under the vault are completely active working subjected to their tension capacity.

The tension bearing capacity (following criteria in section 7.5) of the ties located under the vault is shown in Table 61. It is seen that the minimum value is 45.8 kN corresponding to T1, therefore, this value has been used in the calculation.

As it is seen in Figure 100, there are three ties under the vault but one of them is broken, so just two were considered in the analysis.

Table 61. Tension capacity of ties under vault 5

	T_{VA}
Thickness wall- t (m)	1.13
Tension capacity - T1 (KN)	**45.80**
Tension capacity -T2 (KN)	187.67
Tension capacity -T3 (KN)	103.40
Quantity of ties	**2**

For the loading evaluation, the seismic load combination has been considered (sections 5.5 and section 7.3); the force diagram for mechanism 2 is shown in Figure 103 and the corresponding values are presented in Table 62.

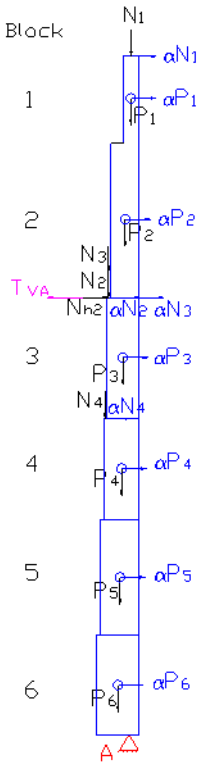

Figure 103. Force diagram for mechanism 2

Table 62. Forces acting in mechanism 2

Element	Load (kN)	
Block 1 (battlement)	P_1	151.13
Block 2 (with vaulted windows)	P_2	536.85
Block 3 (with one window)	P_3	582.99
Block 4	P_4	529.82
Block 5	P_5	669.19
Block 6	P_6	625.27
25% roof self-weight	N_1	21.23
Vertical resultant of vault 5	N_2	199.00
50% of bell and bell yoke self-weight	N_3	21.58
50% wooden platf.2 self-weight	N_4	10.5
Thrust of vault 5	N_{h2}	134.20
Ties under vault	T_{va}	**91.6**

The distance t_1, for location of point of rotation A, was calculated following the procedure presented for the mechanism 1; the result is presented in Table 63.

Table 63. Calculation of distance t_1 for mechanism 2

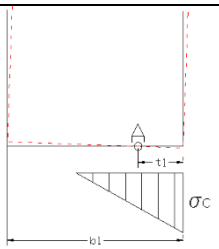

$$t_1 = \frac{2}{3}\frac{\sum(P_i + N_i)}{\sigma_c * l}$$

σ_c	0.94	Mpa
l	6.81	m
t_1	**0.35**	m

By imposing the conditions of equilibrium Mr=Ms, the coefficient that activates the mechanism α_0 is obtained by means of the following equations (already mentioned for mechanism 1). Table 64 shows the parameters for calculation of the coefficient of activation α_o and the spectral acceleration a^*_0.

$$M_s = \sum(P_i\, x_{i,P} + N_i\, x_{i,N}) + \sum T_i\, y_{i,T}$$

$$M_r = \alpha_o \sum(P_i\, y_{i,P} + N_i\, y_{i,N}) + \sum N_{hi}\, y_{i,N}$$

$$M_s = M_r \rightarrow \alpha_o$$

$$\alpha_o = \frac{\sum(P_i\, x_{i,P} + N_i\, x_{i,N}) + \sum T_i\, y_{i,T} - \sum N_{hi}\, y_{i,N}}{\sum(P_i\, y_{i,P} + N_i\, y_{i,N})}$$

Table 64. Parameters for calculation of α_o and a^*_0 for mechanism 2

Load (kN)		xi	yi	M_{si} (KN m)	M_{ri}(KN m)	$\delta_{x,i}$	P_i*δx,i	Pi*δx,i^2
P_1	151.13	-0.06	22.30	-9.62	3369.44	0.94	141.45	132.40
P_2	536.85	0.14	18.05	75.90	9690.12	0.76	406.81	308.26
P_3	582.99	0.22	13.21	126.14	7701.34	0.55	323.31	179.30
P_4	529.82	0.27	9.32	141.13	4937.91	0.39	207.30	81.11
P_5	669.19	0.32	5.51	215.06	3687.21	0.23	154.79	35.81
P_6	625.27	0.39	1.74	241.59	1084.84	0.07	45.54	3.32
N_1	21.23	-0.06	23.82	-1.35	505.79	1.00	21.23	21.23
N_2	199.00	0.72	15.31	143.68	3046.35	0.64	127.89	82.19
N_3	21.58	0.72	15.31	15.58	330.38	0.64	13.87	8.91
N_4	10.5	0.84	11.07	8.81	116.18	0.46	4.88	2.27
N_{h2}	134.20	*0.72*	**15.31**		**2054.37**			
T_{va}	**91.6**		**15.31**	**1402.38**				

Following the equations presented in the methodology (section 7.3), the values of α_o and a^*_o were obtained and are shown below:

Multiplier that activate the mechanism	**α_o**	**0.009**	
Stabilizing moment	**M_{si}**	2359.29	KN*m
Rotation moment	**M_{ri}**	2359.29	KN*m
Equivalent mass	**M***	249.72	
Fraction of the mass participant in the kinemat.	**e***	0.732	
Confidence factor	**FC**	1.270	
Spectral acceleration for activation of mechanism	**a^*_0**	**0.093**	m/s^2
	a^*_0	**0.010**	g

The linear kinematic verification has been carried out for both DLS (Damage Limit State) and ULS (Ultimate Limit State) and the results values are shown in the following table:

Table 65. Linear kinematic verification mechanism 2

		DLS	ULS
Peak ground acceleration	**a_g (g)**	0.043	0.099
Soil factor	**S**	1.2	1.2
Structure factor	**q**	2.5	2
Height of the whole structure	**H (m)**	47.20	47.20
Distance from ground to barycenter of moving mass	**Z (m)**	**33.68**	**33.68**
Spectral acceleration for activation of mechanism	**a^*_0 (g)**	**0.010**	**0.010**
Limit value: a_g S/q (1+1,5 Z/H)	**(g)**	**0.043**	**0.123**
		NO VERIFIED	**NO VERIFIED**

The mechanism is not verified; therefore, non-linear kinematic analysis is required.

7.7.2 Non-Linear Kinematic Analysis

The following table shows the parameters to calculate the finite rotation θ that annuls the steadying moment M_S.

Table 66. Parameters to calculate θ for mechanism 2

Element	β_i (degrees)	Ri (m)	F_i*R_i	$Fv_i*R_i*\cos(\beta+\theta)$	$Fh_i*R_i*\sin(\beta+\theta)$
P_1	90.17	22.30	3369.45	-33.91	-
P_2	89.56	18.05	9690.39	5.63	-
P_3	89.07	13.21	7702.33	70.35	-
P_4	88.38	9.32	4939.87	104.60	-
P_5	86.68	5.52	3693.37	187.72	-
P_6	77.51	1.78	1111.16	232.60	-
N_1	90.17	23.76	504.61	-5.08	-
N_2	87.30	15.33	2056.66	82.30	-
N_3	87.30	15.33	0.00	0.00	
N_4	85.66	11.10	116.51	7.99	-
N_{h2}	**87.3**	**15.33**	**2056.66**	**-**	**-2055.01**
T_{va}	87.30	15.33	1403.93	-	1402.81
			∑	0.00	

The results for non-linear kinematic analysis are shown below:

Steadying moment MS=0 →		**Ms**	**0.00**	KN*m
FINITE rotation θ that annuls the steadying moment M_S		**θ**	**0.007**	Rad.
			0.41	°
Control height		**H_k**	10.30	m
Displacement of the control point		**d_{k0}**	0.07	m
Virtual horizontal displacement of the point k		**$\delta_{x,k}$**	0.43	m
Equivalent spectral displacement corresponding to the displacement dk_0		**d^*_0**	0.073	m
Ultimate displacement capacity for SDF		**d^*_u**	0.0292	m
Displacement of equivalent SDF system (0.4 d^*_u)		**d^*_s**	0.0117	m
Spectral acceleration for activation of mechanism		**a^*_0**	0.0934	m/s^2
			0.01	g
Spectral acceleration related for the displacement d^*_s		**a^*_s**	**0.01**	g

Displacement demand of the earthquake Δd (from spectrum)

		DLS	ULS
Secant period	**T_s (s)**	**2.4**	**2.4**
First natural period of the structure (test)	**T_{1t} (s)**	0.64	0.64

First natural period of the structure (NTC)	**T_{1NTC} (s)**	**0.90**	**0.90**
Peak ground acceleration	**a_g (g)**	0.04	0.10
Soil factor	**S**	1.20	1.20
Height of the whole structure	**H (m)**	47.20	47.20
Distance from ground to barycenter of moving mass	**Z (m)**	33.68	33.68
	T_D (s)	**1.77**	**2.00**
	1,5 *T_1 (s)	**1.35**	**1.35**
Displacement demand of the earthquake	**Δ(Ts) (cm)**	**11.08**	**28.75**
Ultimate displacement capacity	**d^*_u (cm)**	**2.92**	**2.92**
		NO VERIFIED	**NO VERIFIED**

The mechanism is not verified, the displacement demand of the earthquake is much higher that the ultimate displacement capacity of the structure. The corresponding simplified capacity curve is presented in Figure 104. Extra tie-rods might be included in the analysis for the verification of the mechanism.

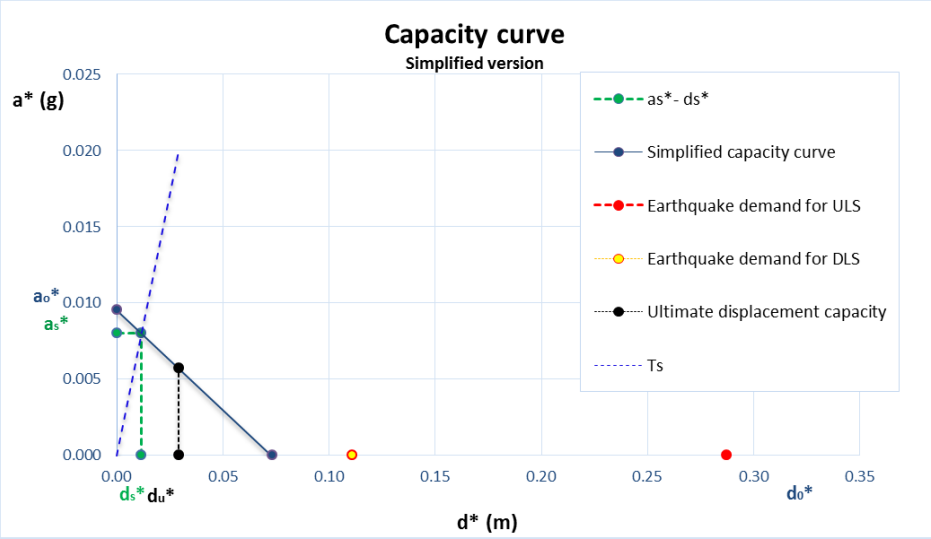

Figure 104. Simplified capacity curve for mechanism 2 (including two tie-rods under the vault)

7.7.3 Linear Kinematic Analysis considering extra Tie-Rods

The goal is to calculate the lowest number of ties necessary to make the mechanism verified. For that the analysis was carried out introducing the ties one by one until achieving the verification. The ties that have been considered are shown in Figure 105. As the ties have different cross section area, a conservative area was chosen, corresponding to Φ18 mm, A=254.5 mm^2 (see section 7.5).

Figure 106 shows the forces involved in the mechanism 2 considering the tie-rods; the tension capacity for each failure mechanism is presented in Table 67(calculated following procedure shown in section 7.5). It is seen that the minimum tension capacity of the ties is the one obtained using the first failure mechanism (T1) equal to 45.8 kN.

On the other hand, as well as the mechanism 1, it was found that the minimum number of ties for the structure to be verified is 3 distributed as it is shown in Table 67.

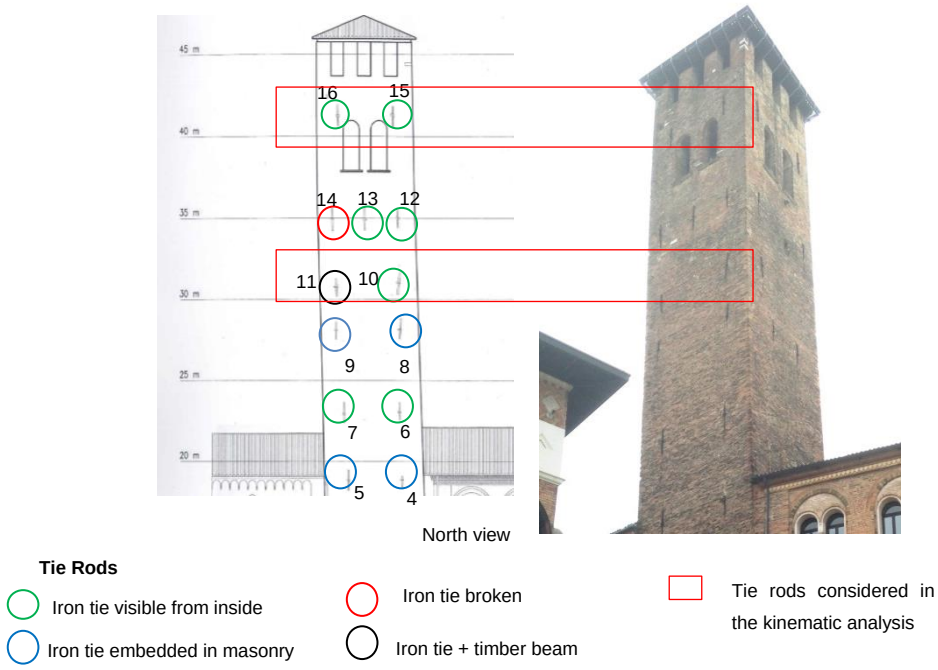

Figure 105. Distribution of tie rods in direction N-S to be considered in the analysis

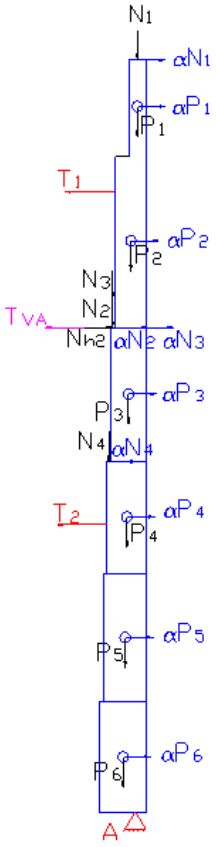

Figure 106. Forces involved in the mechanism 2 considering extra tie-rods

Table 67. Tension capacity of ties for mechanism 2

	Tie 1 - T_1	**Tie 2- T_2**
Thickness wall- t (m)	0.98	1.23
Tension capacity - T1 (KN)	**45.80**	**45.80**
Tension capacity -T2 (KN)	148.65	216.09
Tension capacity -T3 (KN)	103.40	103.40
Quantity of ties	**2**	**1**

By imposing the conditions of equilibrium Mr=Ms by means of the same equations used in the previous analysis, the coefficient that activates the mechanism α_0 is obtained.

Next table shows the parameters for calculation of the coefficient α_o and the spectral acceleration a^*_0 for activation of the mechanism:

Table 68. Parameters for calculation of α_o and a^*_o for mechanism 2 considering extra tie rods

Load (kN)		xi	yi	M_{si} (KN m)	M_{ri}(KN m)	$\delta_{x,i}$	$P_i*\delta x,i$	$Pi*\delta x,i^2$
P_1	151.13	-0.06	22.30	-9.62	3369.44	0.94	141.45	132.40
P_2	536.85	0.14	18.05	75.90	9690.12	0.76	406.81	308.26
P_3	582.99	0.22	13.21	126.14	7701.34	0.55	323.31	179.30
P_4	529.82	0.27	9.32	141.13	4937.91	0.39	207.30	81.11
P_5	669.19	0.32	5.51	215.06	3687.21	0.23	154.79	35.81
P_6	625.27	0.39	1.74	241.59	1084.84	0.07	45.54	3.32

N_1	21.23	-0.06	23.82	-1.35	505.79	1.00	21.23	21.23
N_2	199.00	0.72	15.31	143.68	3046.35	0.64	127.89	82.19
N_3	21.58	0.72	15.31	15.58	330.38	0.64	13.87	8.91
N_4	10.5	0.84	11.07	8.81	116.18	0.46	4.88	2.27
N_{h2}	134.20	*0.72*	**15.31**		**2054.37**			
T_1	**91.6**		**19.60**	**1795.12**				
T_{va}	**91.6**		**15.31**	**1402.38**				
T_2	**45.8**		**9.08**	**415.70**				

Following the equations presented in the methodology (section 7.3), the values of α_o and a^*_o were obtained and are shown below:

Multiplier that activate the mechanism	**α_o**	**0.073**	
Stabilizing moment	**M_{si}**	4570.11	KN*m
Rotation moment	**M_{ri}**	4570.11	KN*m
Equivalent mass	**M***	249.72	
Fraction of the mass participant in the kinemat.	**e***	0.732	
Confidence factor	**FC**	1.270	
Spectral acceleration for activation of mechanism	**a^*_0**	**0.770**	m/s^2
	a^*_0	**0.079**	g

The linear kinematic verification has been carried out for both DLS (Damage Limit State) and ULS (Ultimate Limit State) and the results values are shown in the following table:

Table 69. Linear kinematic verification mechanism 2 (considering extra ties)

		DLS	**ULS**
Peak ground acceleration	**a_g (g)**	0.043	0.099
Soil factor	**S**	1.2	1.2
Structure factor	**q**	2.5	2
Height of the whole structure	**H (m)**	47.20	47.20
Distance from ground to barycenter of moving mass	**Z (m)**	**33.68**	**33.68**
Spectral acceleration for activation of mechanism	**a^*_0 (g)**	**0.079**	**0.079**
Limit value: a_g S/q (1+1,5 Z/H)	**(g)**	**0.043**	**0.123**
		VERIFIED	**NO VERIFIED**

As same the mechanism 1, the mechanism 2 including 3 tie rods is not verified for ULS; therefore, non-linear kinematic analysis is required.

7.7.4 Non-Linear Kinematic Analysis considering extra Tie-Rods

The following table shows the parameters to calculate the finite rotation θ that annuls the steadying moment M_S.

Table 70. Parameters to calculate θ for mechanism 2 (considering extra ties)

Element	β_i (degrees)	Ri (m)	F_i*R_i	$Fv_i*R_i*\cos(\beta+\theta)$	$Fh_i*R_i*\sin(\beta+\theta)$
P_1	90.17	22.30	3369.45	-254.85	-
P_2	89.56	18.05	9690.39	-630.03	-
P_3	89.07	13.21	7702.33	-435.03	-
P_4	88.38	9.32	4939.87	-219.59	-
P_5	86.68	5.52	3693.37	-54.65	-
P_6	77.51	1.78	1111.16	160.83	-
N_1	90.17	23.76	504.61	-38.17	-
N_2	87.30	15.33	2056.66	-52.68	-
N_3	87.30	15.33	1403.93	-35.96	
N_4	85.66	11.10	116.51	0.35	-
N_{h2}	**87.3**	**15.33**	**2056.66**	**-**	**-2055.98**
T_1	88.09	19.61	1796.13	-	1794.73
T_{va}	87.30	15.33	1403.93	-	1403.47
T_2	84.40	9.12	417.69		417.56
			∑	0.00	

The results of non-linear kinematic analysis are shown below:

Steadying moment MS=0 →	**Ms**	**0.00**	KN*m	
FINITE rotation θ that annuls the steadying moment M_S	**θ**	**0.073**	Rad.	
		4.17	°	
Control height	H_k	10.30	m	
Displacement of the control point	d_{k0}	0.75	m	
Virtual horizontal displacement of the point k	$\delta_{x,k}$	0.43	m	
Equivalent spectral displacement corresponding to the displacement dk_0	d^*_0	0.748	m	
Ultimate displacement capacity for SDF	d^*_u	0.2993	m	
Displacement of equivalent SDF system (0.4 d^*_u)	d^*_s	0.1197	m	
Spectral acceleration for activation of mechanism	a^*_0	0.7704	m/s^2	
		0.08	g	

Spectral acceleration related for the displacement d*$_s$	**a*$_s$**	**0.07**	g

Displacement demand of the earthquake Δd (from spectrum)

		DLS	ULS
Secant period	**T_s (s)**	**2.7**	**2.7**
First natural period of the structure (test)	**T_{1t} (s)**	0.64	0.64
First natural period of the structure (NTC)	**T_{1NTC} (s)**	**0.90**	**0.90**
Peak ground acceleration	**a_g (g)**	0.04	0.10
Soil factor	**S**	1.20	1.20
Height of the whole structure	**H (m)**	47.20	47.20
Distance from ground to barycenter of moving mass	**Z (m)**	33.68	33.68
	T_D (s)	**1.77**	**2.00**
	1,5 *T_1 (s)	**1.35**	**1.35**
Displacement demand of the earthquake	**Δ(Ts) (cm)**	**11.08**	**28.75**
Ultimate displacement capacity	**d*$_u$ (cm)**	**29.93**	**29.93**
		VERIFIED	**VERIFIED**

The mechanism 2 including the 3 iron ties (plus 2 ties under vault) is verified with Non-Linear Kinematic Analysis for both DLS and ULS; the corresponding simplified capacity curve is presented in Figure 107. The ultimate displacement capacity of the structure is 29.93 cm while the displacement demanded by the earthquake is 11.08 cm for DLS and 28.75 cm for ULS.

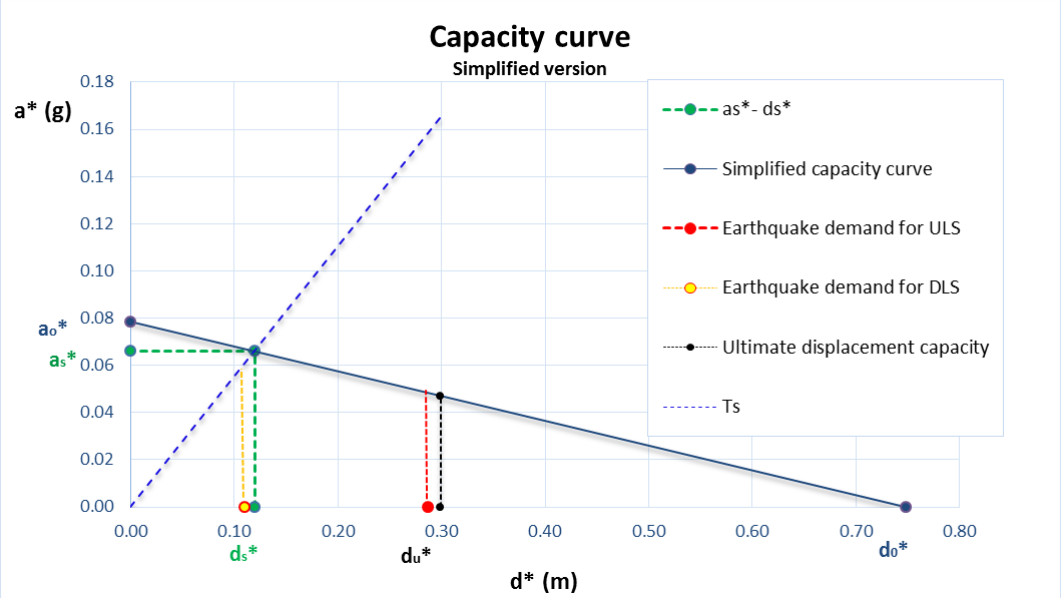

Figure 107. Simplified capacity curve for mechanism 2 (including 3 ties)

7.8 Mechanism 3 –Simple out of plane wall failure of belfry and battlement

7.8.1 Linear Kinematic Analysis

The mechanism consists in the rotation of the vulnerable slender wall, belonging to belfry and battlement, out of its plane (Figure 108). It takes into account the changes of geometry and thickness of wall, the openings such as vaulted windows and crenels and the effect of the roof (25% self-weight is applied at the top of this wall).

The macroelement has been divided in 2 blocks whose geometry is presented in Table 71.

Figure 108. Left: View of belfry and battlement from inside. Right: Mechanism 3- Simple out of plane failure of upper wall

Table 71. Geometrical characteristics of blocks for mechanism 3

Block	b-Thickness (m)	h-Height (m)	Depth (m)	Cross Area (m^2)	V (m^3)
1 (battlement)	0,57	3,05	6,6	1,74	8,40
2 (with vaulted windows)	0,98	5,44	6,69	5,33	29,82

For the loading evaluation, the seismic load combination has been considered (sections 5.5 and section 7.3); the force diagram for mechanism 2 is shown in Figure 109 and the corresponding values are presented in Table 72.

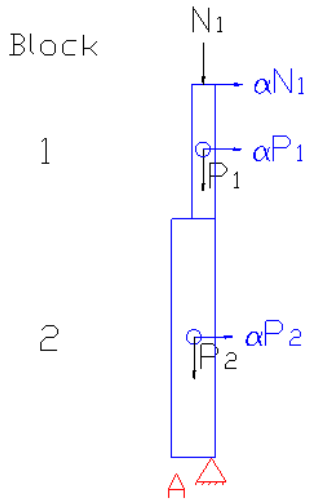

Figure 109. Force diagram for mechanism 3

Table 72. Forces acting in mechanism 3

Element	Load (kN)	
Block 1 (battlement)	P_1	151.13
Block 2 (with vaulted windows)	P_2	536.85
25% roof self-weight	N_1	21.23

The distance t_1, for location of point of rotation A, was calculated following the procedure presented for the mechanism 1; the result is presented in Table 73.

Table 73. Calculation of distance t_1 for mechanism 3

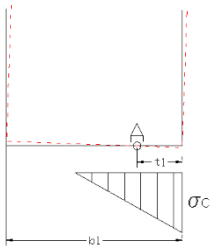

$$t_1 = \frac{2}{3}\frac{\sum(P_i + N_i)}{\sigma_c * l}$$

σ_c	0.94	Mpa
l	6.69	m
t_1	**0.075**	m

By imposing the conditions of equilibrium Mr=Ms, the coefficient that activates the mechanism α_0 is obtained by means of the following equations (already mentioned for mechanism 1):

$$\boldsymbol{M_s = \sum(P_i\, x_{i,P} + N_i\, x_{i,N}) + \sum T_i\, y_{i,T}}$$

$$\boldsymbol{M_r = \alpha_o \sum(P_i\, y_{i,P} + N_i\, y_{i,N}) + \sum N_{hi}\, y_{i,N}}$$

$$\boldsymbol{M_s = M_r \rightarrow \alpha_o}$$

$$\boldsymbol{\alpha_o = \frac{\sum(P_i\, x_{i,P} + N_i\, x_{i,N}) + \sum T_i\, y_{i,T} - \sum N_{hi}\, y_{i,N}}{\sum(P_i\, y_{i,P} + N_i\, y_{i,N})}}$$

The following table shows the parameters for calculation of the coefficient of activation α_o and the spectral acceleration a^*_0.

Table 74. Parameters for calculation of α_o and a^*_0 for mechanism 3

Load (kN)		xi	yi	M_{si} (KN m)	M_{ri}(KN m)	$\delta_{x,i}$	$P_i*\delta x,i$	$Pi*\delta x,i^2$
P_1	151.13	0.21	6.97	31.71	1052.62	0.82	123.98	101.71
P_2	536.85	0.41	2.72	222.69	1460.23	0.32	171.99	55.10
N_1	21.23	0.21	8.49	4.46	180.28	1.00	21.23	21.23

Following the equations presented in the methodology (section 7.3), the values of α_o and a^*_o were obtained and are shown below:

Multiplier that activate the mechanism	α_o	**0.096**	
Stabilizing moment	M_{si}	258.86	KN*m
Rotation moment	M_{ri}	258.86	KN*m
Equivalent mass	M*	57.61	
Fraction of the mass participant in the kinemat.	e*	0.797	
Confidence factor	FC	1.270	
Spectral acceleration for activation of mechanism	a^*_0	**0.93**	m/s^2
	a^*_0	**0.09**	g

The linear kinematic verification has been carried out for both DLS (Damage Limit State) and ULS (Ultimate Limit State) and the results values are shown in the following table:

Table 75. Linear kinematic verification mechanism 3

		DLS	ULS
Peak ground acceleration	a_g (g)	0.043	0.099
Soil factor	S	1.2	1.2
Structure factor	q	2.5	2
Height of the whole structure	H (m)	47.20	47.20
Distance from ground to barycenter of moving mass	Z (m)	**42.51**	**42.51**
Spectral acceleration for activation of mechanism	a^*_0 (g)	**0.09**	**0.09**
Limit value: a_g S/q (1+1,5 Z/H)	(g)	**0.05**	**0.14**
		VERIFIED	**NO VERIFIED**

The mechanism is not verified for ULS; therefore, non-linear kinematic analysis is required.

7.8.2 Non-Linear Kinematic Analysis

The following table shows the parameters to calculate the finite rotation θ that annuls the steadying moment M_S.

Table 76. Parameters to calculate θ for mechanism 3

Element	β_i (degrees)	Ri (m)	F_i*R_i	$Fv_i*R_i*\cos(\beta+\theta)$
P_1	88.44	6.99	1056.29	-66.84
P_2	81.76	2.77	1486.00	79.12
N_1	88.74	8.44	179.28	-12.28
			∑	0.00

The results for non-linear kinematic analysis are shown below:

Steadying moment MS=0 →	**Ms**	**0.00**	KN*m
FINITE rotation θ that annuls the steadying moment M_S	**θ**	**0.091** **5.19**	Rad. °
Control height	H_k	3.80	m
Displacement of the control point	d_{k0}	0.34	m
Virtual horizontal displacement of the point k	$\delta_{x,k}$	0.45	m
Equivalent spectral displacement corresponding to the displacement dk_0	d^*_0	0.343	m
Ultimate displacement capacity for SDF	d^*_u	0.1373	m
Displacement of equivalent SDF system (0.4 d^*_u)	d^*_s	0.0549	m
Spectral acceleration for activation of mechanism	a^*_0	0.9317 0.09	m/s^2 g
Spectral acceleration related for the displacement d^*_s	a^*_s	**0.08**	g

Displacement demand of the earthquake Δd (from spectrum)

		DLS	ULS
Secant period	T_s (s)	**1.7**	**1.7**
First natural period of the structure (test)	T_{1t} (s)	0.64	0.64
First natural period of the structure (NTC)	T_{1NTC} (s)	**0.90**	**0.90**
Peak ground acceleration	a_g (g)	0.043	0.099
Soil factor	S	1.20	1.20
Height of the whole structure	H (m)	47.20	47.20
Distance from ground to barycenter of moving mass	Z (m)	42.51	42.51

	T_D (s)	1.77	2.00
	1,5 *T_1 (s)	1.35	1.35
Displacement demand of the earthquake	Δ(Ts) (cm)	11.71	26.96
Ultimate displacement capacity	d^*_u (cm)	13.73	13.73
		VERIFIED	NO VERIFIED

The mechanism is not verified either for ULS, the displacement demand of the earthquake is almost the double of the ultimate displacement capacity of the structure. The corresponding simplified capacity curve is presented below. Extra tie-rods might be included in the analysis for the verification of the mechanism.

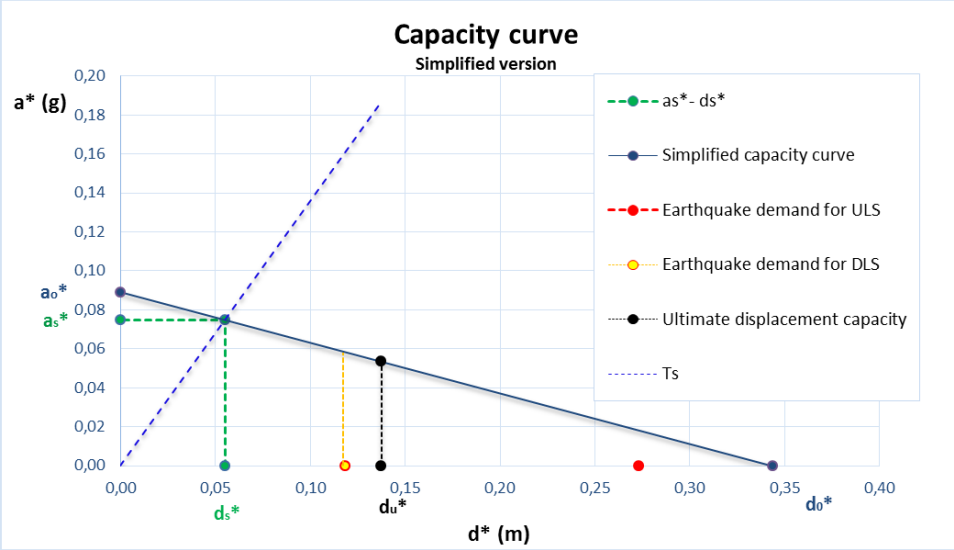

Figure 110. Simplified capacity curve for mechanism 3

7.8.3 Linear Kinematic Analysis considering extra Tie-Rods

The goal was to calculate the lowest number of ties necessary to make the mechanism verified. For that the analysis was carried out introducing the ties one by one until achieving the verification. The two ties that have been considered are shown in Figure 111.

Figure 112 shows the forces involved in the mechanism 3 considering the tie-rods whose tension capacity values for each failure mechanism is presented in Table 77. As same as for the first two mechanisms, it is seen that the minimum tension capacity of the ties is the one obtained using the first failure mechanism (T1) equal to 45.8 kN.

On the other hand, it was found that the minimum number of ties for the structure to be verified is 1.

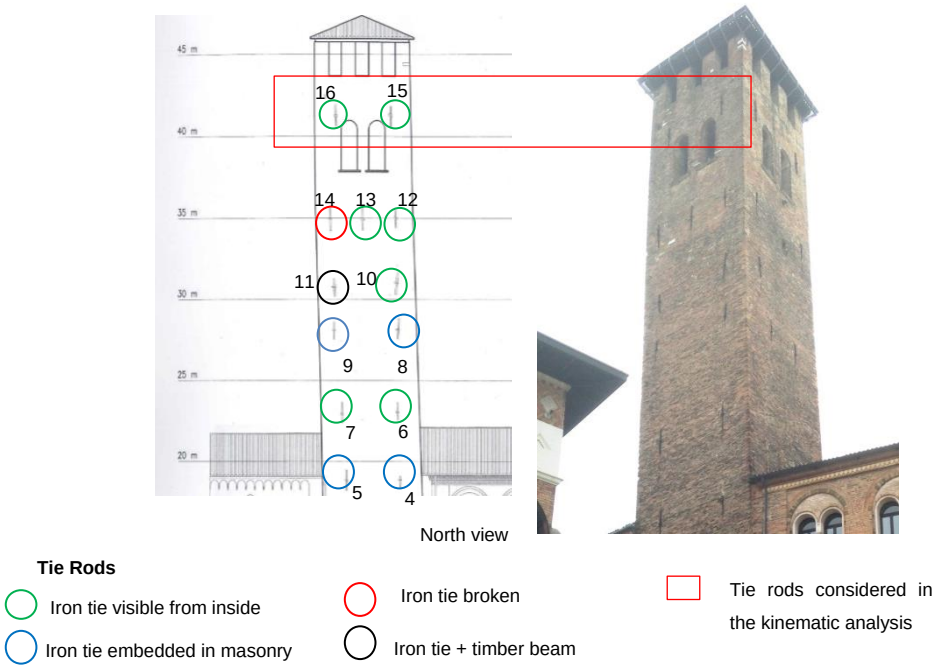

Figure 111. Distribution of tie rods in direction N-S to be considered in the analysis for mechanism 3

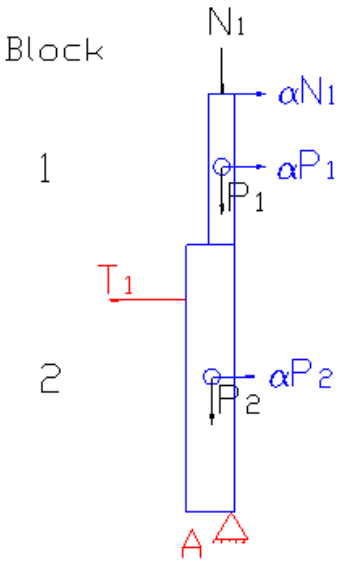

Figure 112. Forces involved in the mechanism 3 considering tie-rod

Table 77. Tension capacity of ties for mechanism 3

	Tie 1 - T_1
Thickness wall- t (m)	0.98
Tension capacity - T1 (KN)	**45.80**
Tension capacity -T2 (KN)	148.65
Tension capacity -T3 (KN)	103.40
Quantity of ties	**1**

By imposing the conditions of equilibrium Mr=Ms by means of the same equations used in the previous analysis, the coefficient that activates the mechanism α_0 is obtained. Next table shows the parameters for calculation of the coefficient α_o and the spectral acceleration a^*_0 for activation of the mechanism:

Table 78. Parameters for calculation of α_o and a^*_o for mechanism 3 considering tie rods

Load (kN)		xi	yi	M_{si} (KN m)	M_{ri}(KN m)	$\delta_{x,i}$	$P_i*\delta x,i$	$Pi*\delta x,i^2$
P_1	151.13	0.21	6.97	31.71	1052.62	0.82	123.98	101.71
P_2	536.85	0.41	2.72	222.69	1460.23	0.32	171.99	55.10
N_1	21.23	0.21	8.49	4.46	180.28	1.00	21.23	21.23
T_1	**45.8**		**4.29**	**196.38**				

Following the equations presented in the methodology (section 7.3), the values of α_o and a^*_o were obtained and are shown below:

Multiplier that activate the mechanism	**α_o**	**0.169**	
Stabilizing moment	**M_{si}**	455.23	KN*m
Rotation moment	**M_{ri}**	455.23	KN*m
Equivalent mass	**M***	57.61	
Fraction of the mass participant in the kinemat.	**e***	0.797	
Confidence factor	**FC**	1.270	
Spectral acceleration for activation of mechanism	**a^*_0**	**1.64**	m/s^2
	a^*_0	**0.17**	g

The linear kinematic verification has been carried out for both DLS (Damage Limit State) and ULS (Ultimate Limit State) and the results values are shown in the following table:

Table 79. Linear kinematic verification mechanism 3 considering ties

		DLS	**ULS**
Peak ground acceleration	**a_g (g)**	0.043	0.099
Soil factor	**S**	1.2	1.2
Structure factor	**q**	2.5	2
Height of the whole structure	**H (m)**	47.20	47.20
Distance from ground to barycenter of moving mass	**Z (m)**	**42.51**	**42.51**
Spectral acceleration for activation of mechanism	**a^*_0 (g)**	**0.17**	**0.17**
Limit value: a_g S/q (1+1,5 Z/H)	**(g)**	**0.05**	**0.14**
		VERIFIED	**VERIFIED**

The mechanism 3 including 1 tie rod is verified for both DLS and ULS; therefore, non-linear kinematic analysis is not required.

7.9 Mechanism 4 – Global overturning of the tower above the level of adjacent buildings

7.9.1 Linear Kinematic Analysis

The three first mechanisms already presented consisted in simple out of plane wall failure taking into account poor connection between walls, however it is important also to analyze the structure as one macroelement and consider its possible rotation under action of an earthquake.

The mechanism consists in the overturning from west to east of the whole upper part of the tower from the level constrained by neighboring buildings (Figure 113). It takes into account all the structural elements such as walls, vaults, wooden platforms and roof, as well as the bell and bell yoke.

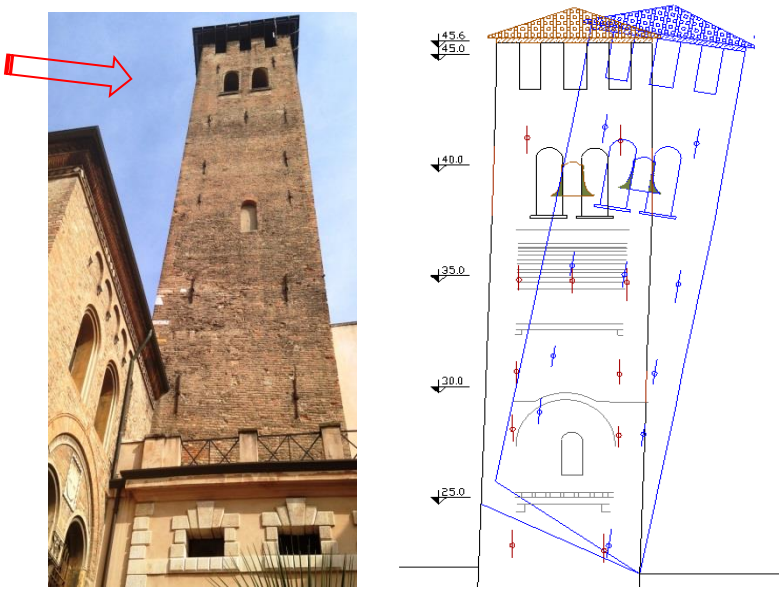

Figure 113. Left: South façade of tower. Right: Mechanism 4- Global overturning of the tower above the level of neighboring buildings

As it is seen in Figure 114, the macroelement has been divided in 6 blocks (A, B, C, D, E, F), considering also the wooden platforms and vaults. For the loading evaluation, the seismic load combination has been considered (sections 5.5 and section 7.3) and the corresponding values are presented in Table 80.

The center of rotation is the lowest extreme of the macroelement corresponding to the level of the roof of the next building. The distances x_i and y_i from the center of rotation to the barycenter of each element is presented in Table 80.

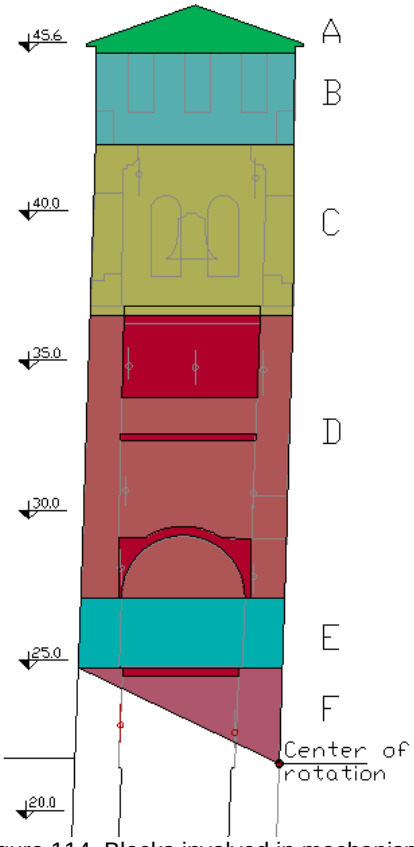

Figure 114. Blocks involved in mechanism 4

Table 80. Forces acting in mechanism 4

Block	xi	yi	Pi (kN)
A - roof	2.81	24.27	84.94
B - battlement	2.80	22.19	484.83
C (+bell+yoke)	2.87	17.81	1942.99
D	3.08	10.25	4386.05
Vault 5 (barrel)	2.95	13.74	*392.55*
Wooden platf.2	3.04	10.91	*20.99*
Vault 4 (barrel)	3.02	7.10	*203.96*
E	3.26	4.37	1258.47
Wooden platf.1	3.29	3.05	*19.64*
F	2.20	2.14	933.24

By imposing the conditions of equilibrium Mr=Ms, the coefficient that activates the mechanism α_0 is obtained by means of the following equation (already mentioned for mechanism 1):

$$\boldsymbol{M_s = \sum (P_i\, x_{i,P})}$$

$$\boldsymbol{M_r = \alpha_o \sum (P_i\, y_{i,P})}$$

$$\boldsymbol{M_s = M_r \rightarrow \alpha_o}$$

$$\boldsymbol{\alpha_o = \frac{\sum (P_i \cdot x_{i,P})}{\sum (P_i \cdot y_{i,P})}}$$

The following table shows the parameters for calculation of the coefficient of activation α_o and the spectral acceleration a^*_0.

Table 81. Parameters for calculation of α_o and a^*_0 for mechanism 4

Block	xi	yi	Pi (kN)	$P_i * x_i$ (KN m)	$P_i * y_i$ (KN m)	$\delta_{x,i}$	$P_i * \delta x,i$	$Pi * \delta x,i^2$
A - roof	2.81	24.27	84.94	238.69	2061.59	**1.00**	84.94	84.94
B - battlement	2.80	22.19	484.83	1359.43	10759.06	0.91	443.26	405.26
C (+bell+yoke)	2.87	17.81	1942.99	5580.65	34604.20	0.73	1425.66	1046.07
D	3.08	10.25	4386.05	13492.81	44937.29	0.42	1851.37	781.47
Vault 5 (barrel)	2.95	13.74	*392.55*	1157.44	5393.86	0.57	222.22	125.80
Wooden platf.2	3.04	10.91	*20.99*	63.77	228.92	0.45	9.43	4.24
Vault 4 (barrel)	3.02	7.10	*203.96*	615.87	1447.90	0.29	59.65	17.45
E	3.26	4.37	1258.47	4101.22	5497.87	0.18	226.51	40.77
Wooden platf.1	3.29	3.05	*19.64*	64.55	59.98	0.13	2.47	0.31
F	2.20	2.14	933.24	2055.26	1996.28	0.09	82.24	7.25

Following the equations presented in the methodology (section 7.3), the values of α_o and a^*_o were obtained and are shown below:

Stabilizing moment (vertical force)	$\sum P_i * x_i$	28729.69	KN*m
Rotation moment (horizontal forces)	$\sum P_i * y_i$	106986.97	KN*m
Multiplier that activate the mechanism	α_o	**0.269**	
Equivalent mass	**M***	787.92	
Fraction of the mass participant in the kinemat.	**e***	0.79	
Confidence factor	**FC**	1.270	
Spectral acceleration for activation of mechanism	a^*_0	**2.61**	m/sec^2
	a^*_0	**0.27**	g

The linear kinematic verification has been carried out for both DLS (Damage Limit State) and ULS (Ultimate Limit State) and the results values are shown in the following table:

Table 82. Linear kinematic verification mechanism 4

		DLS	ULS
Peak ground acceleration	a_g (g)	0.043	0.099
Soil factor	**S**	1.2	1.2
Structure factor	**q**	**2.5**	**2**
Height of the whole structure	**H (m)**	47.20	47.20
Distance from ground to barycenter of moving mass	**Z (m)**	**33.93**	**33.93**
Spectral acceleration for activation of mechanism	a^*_0 **(g)**	**0.27**	**0.27**
Limit value: a_g S/q (1+1,5 Z/H)	**(g)**	**0.04**	**0.12**
		VERIFIED	**VERIFIED**

The mechanism is verified for both DLS and ULS; non-linear kinematic analysis is not required.

7.10 Mechanism 5 – Rigid rotation in-plane of belfry pillars

7.10.1 Linear Kinematic Analysis

The mechanism consists in rotation in-plane of the belfry pillars from west to east (Figure 115), taking into account the self-weight of walls, roof, bell and bell yoke.

As it is seen in Figure 115, the bell yoke is supported by means of 4 beams fixed to northern and southern walls; it has been assumed that 60% of the self-weight is transferred by the lower beams and 40% by the upper beams.

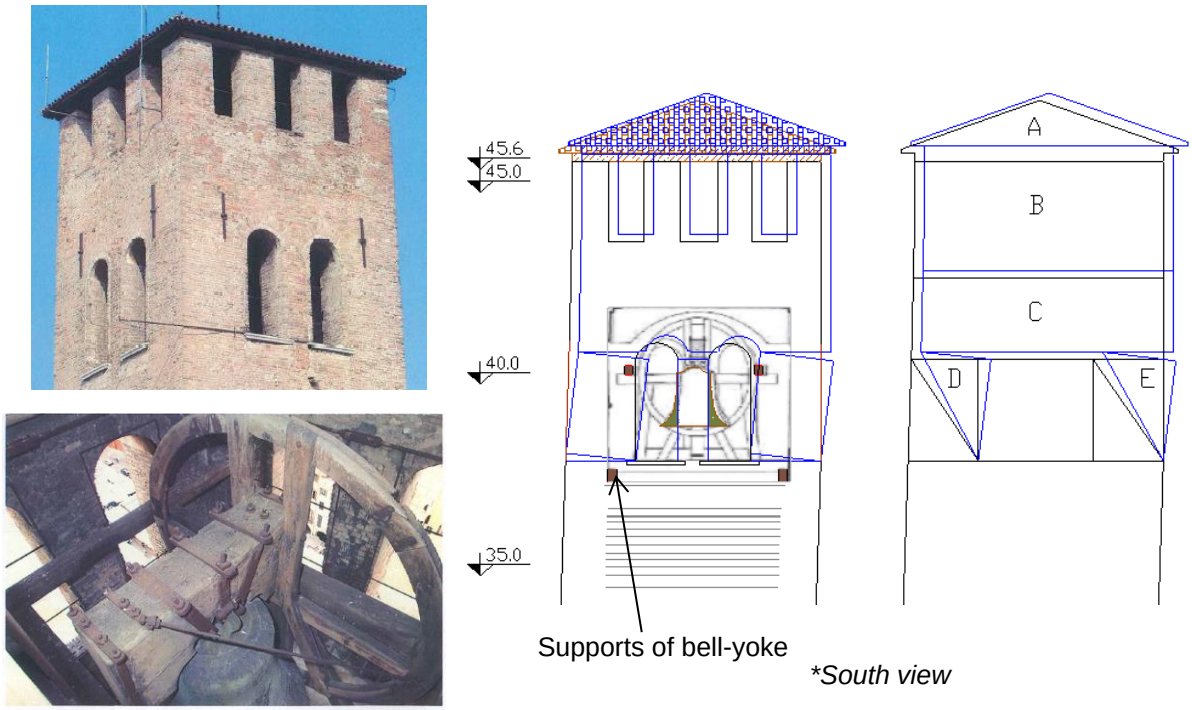

Figure 115. Left: View of belfry from outside and inside. Right: Mechanism 5- Rigid rotation in-plane of belfry pillars from west to east

The macroelement has been divided in 5 blocks (A, B, C, D, E). Since, one of the upper bell yoke beams is located inside the block D, 20% of self-weight of the bell and bell yoke has been applied in that point (load D'). For the loading evaluation, the seismic load combination has been considered (sections 5.5 and section 7.3) and the corresponding values are presented in Table 83.

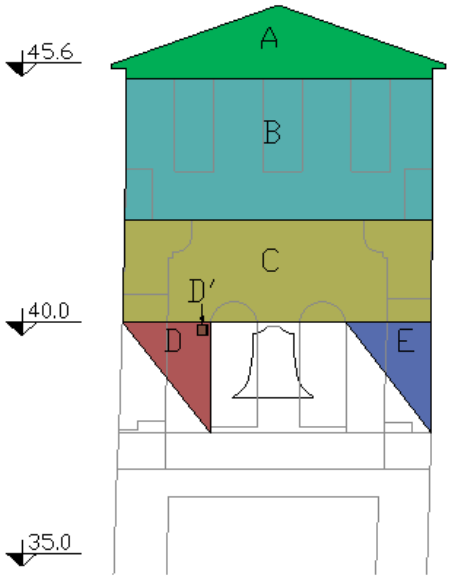

Figure 116. Blocks involved in mechanism 5

Table 83. Forces acting on mechanism 5

Load	W (kN)
A - roof	84.94
B - Battlement	484.83
C	1039.78
D	130.33
D' (20% (bell+yoke))	8,63
E	173.53

It is required to determinate the equivalent load from blocks A, B and C acting on pillars D and E; it is possible by assuming the system as a simple supported beam as it is presented in Figure 117.

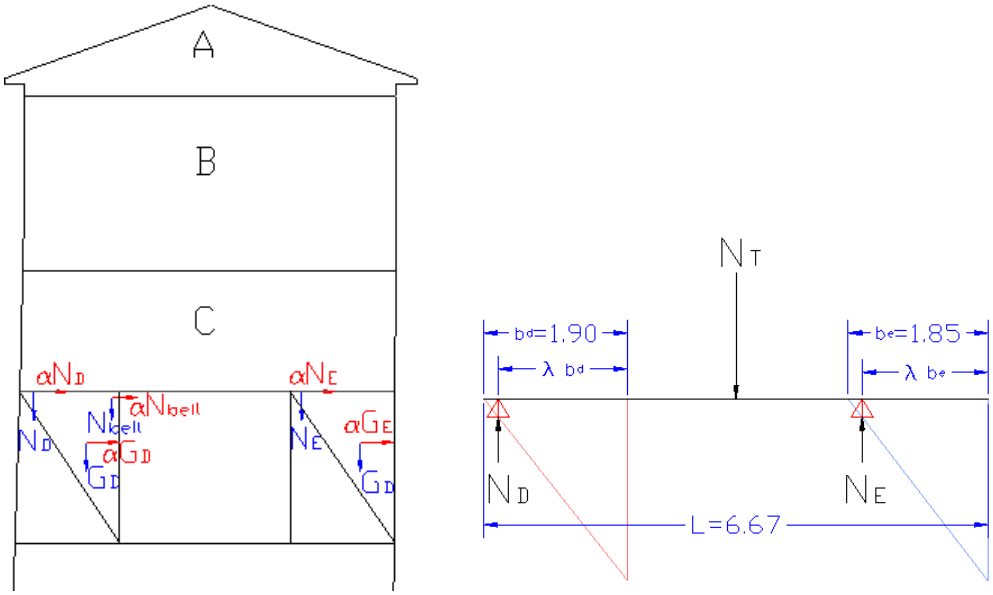

Figure 117.Left: Force diagram of mechanism 5.
Right: Determination of N_D and N_E as reactions of a simple supported beam

The force N_D is applied in the contact zone (to λ times b) and not in the edge of the panel; λ has been assumed as 0.9. On the other hand, by equalizing sum of moment from point E to cero, the load N_D can be obtained using the following equations, the results are shown in Table 84:

$$\sum M_E = 0 = N_T \left[\frac{L}{2} - \lambda b_e\right] - N_D\left[L - [\lambda\, b_e + (1-\lambda) b_D]\right] \quad (45)$$

$$N_D = \frac{N_T\left[\frac{L}{2} - \lambda b_e\right]}{L - [\lambda\, b_e + (1-\lambda) b_D]} \quad (46)$$

Table 84. Load on pillar D and pillar E

Length	**L**	6.67	m
Loads A+B+C	**N_T**	**1609.55**	kN
Proportion from border	**λ**	0.9	
Height of pillars	**h**	2.40	m
Width of pillar D	**b_d**	1.90	m
Width of pillar E	**b_e**	1.85	m
Load on pillar D	**N_d**	**558.24**	kN
Load on pillar E	**N_e**	**1051.30**	kN

By imposing the conditions of equilibrium Mr=Ms, the coefficient that activates the mechanism α_0 is obtained by means of the following equation (already mentioned for mechanism 1):

$$\boldsymbol{M_s} = \sum (\boldsymbol{P_i}\, \boldsymbol{x_{i,P}})$$

$$\boldsymbol{M_r} = \boldsymbol{\alpha_o} \sum (\boldsymbol{P_i}\, \boldsymbol{y_{i,P}})$$

$$\boldsymbol{\alpha_o} = \frac{\sum (\boldsymbol{P_i} \cdot \boldsymbol{x_{i,P}})}{\sum (\boldsymbol{P_i} \cdot \boldsymbol{y_{i,P}})}$$

The following table shows the parameters for calculation of the coefficient of activation α_o.

Table 85. Parameters for calculation of α_o for mechanism 5

	Center of rotation on pillar D			**Center of rotation on pillar E**	
	N_d	**N_{bell}**	**G_d**	**N_e**	**G_e**
Load (KN)	558.24	8.63	130.33	1051.30	173.53
x_i	1.71	0.18	0.63	1.665	0.62
y_i	2.40	2.22	1.6	2.40	1.6

Table 86 shows the coefficient of activation of the mechanism α_o for both pillars, it is seen that the α_o value for the rotation of pillar E is slightly lower, therefore this mechanism has been considered for calculation of spectral acceleration a^*_0.

Table 86. Coefficient α_o for rotation mechanism of both pillars

		Pillar D	Pillar E
Stabilizing moment (vertical force)	$\sum P_i * x_i$ *(KN*m)*	1038.69	1857.43
Rotation moment (horizontal forces)	$\sum P_i * y_i$ *(KN*m)*	1567.47	2800.77
Multiplier that activate the mechanism	α_o	0.66303	**0.66296**

Following the equations presented in the methodology (section 7.3), the value of the spectral acceleration a^*_0 has been obtained and is shown below:

Virtual displacement at N_E	δ_{xN}	1	m
Virtual displacement at G_E	δ_{xG}	2/3	m
Gravity	**g**	9.81	m/sec^2
Equivalent mass	**M***	123.02	
Fraction of the mass participant in the kinemat.	**e***	0.99	
Confidence factor	**FC**	1.270	
Spectral acceleration for activation of mechanism	a^*_0	**5.20**	m/sec^2
	a^*_0	**0.53**	g

The linear kinematic verification has been carried out for both DLS (Damage Limit State) and ULS (Ultimate Limit State) and the results values are shown Table 87.

Table 87. Linear kinematic verification mechanism 5

		DLS	ULS
Peak ground acceleration	a_g (g)	0.04	0.10
Soil factor	S	1.20	1.20
Structure factor	q	2.50	2.00
Height of the whole structure	H (m)	47.20	47.20
Distance from ground to barycenter of moving mass	**Z (m)**	**43.05**	**43.05**
Spectral acceleration for activation of mechanism	**a^*_0 (g)**	**0.53**	**0.53**
Limit value: a_g S/q (1+1,5 Z/H)	**(g)**	**0.05**	**0.14**
		VERIFIED	**VERIFIED**

The mechanism is verified for both DLS and ULS; non-linear kinematic analysis is not required.

7.11 Conclusions

The main objective of this work was to implement a methodology for seismic assessment where the Tower Anziani could be analyzed in two ways: locally and globally, taking into account the inspection and testing campaign performed.

- On one hand, local assessment was carried out by means of Kinematic Limit Analysis considering 5 possible collapse mechanisms which arise from the careful observation of this kind of masonry structures after earthquakes and the current state of the tower. Table 108 shows results summary.

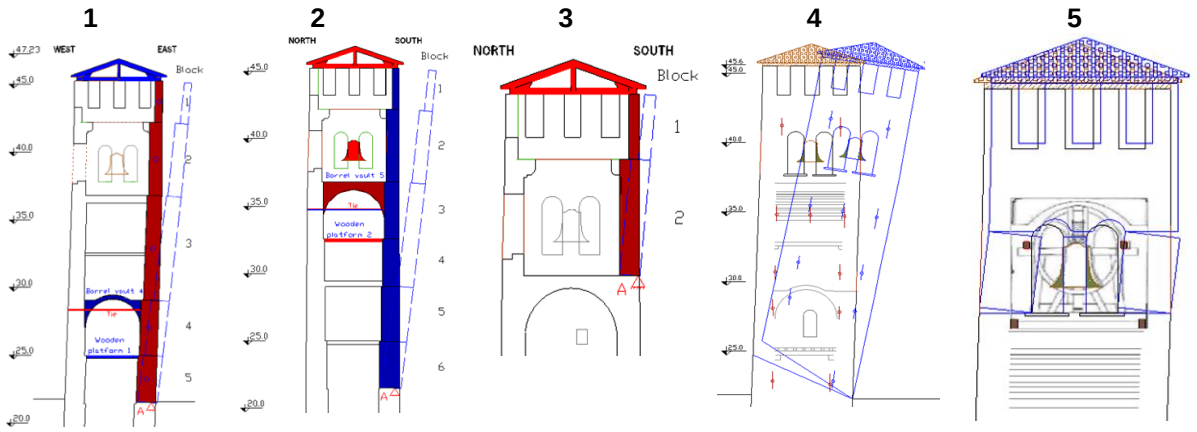

Figure 118. Analyzed collapse mechanisms

Table 88. Summary of kinematic analysis

Mech.	Type of mechanism	Element involved	Ties Required		Linear Analysis	Non-linear Analysis
			Under vaults	Extra		
1	Simple out of plane wall failure	Leaned eastern wall	**2**	**3**	No verified	**Verified**
2	Simple out of plane wall failure	Southern wall	**2**	**3**	No verified	**Verified**
3	Simple out of plane wall failure	Belfry and battlement	-	**1**	**Verified**	-
4	Global overturning	Tower above adjacent walls	-	-	**Verified**	-
5	Rigid rotation in-plane	Belfry pillars	-	-	**Verified**	-

It was found that all mechanisms type simple out of plane wall failure are verified only when the specified number of rod ties are included. Therefore, the assurance that those tie-rods are correctly set up, with geometrical and mechanical characteristics specified in this document, is paramount.

8 DYNAMIC MODAL ANALYSIS

In order to assess globally the structure, Dynamic Modal Analysis or also called Response Spectrum Analysis by means of Finite Element Method has been used. The reasons of this analysis choice for this case study have been explained in section 6.1 and 6.3.

According to Guidelines for Evaluation and Mitigation of Seismic Risk to Cultural Heritage, Dynamic Modal Analysis can be used with great confidence in easily modelled, flexible structures, for example, towers, bell towers and other structures which develop primarily along vertical lines, for which the contribution of superior modes may be important.

In addition, considering the minor geometric and constructive complexity of the Tower Anzini compared to other often historic buildings such as religions buildings, villas or masonry bridges, triumphal arches, etc, most of the factors regarding to the vulnerability of the tower, can be accurately studied using linear models since the redistribution of forces in such as isostatic structure is always conservative. This allows the use of dynamic analysis, in particular modal types, for understanding the aspects regarding to amplification of motion due to vulnerability factors (Ref. [23]).

On the other hand, the first and second natural period of vibration of the tower are known from the Dynamic Characterization Test (section 4.1.2) which are essential information for calibrating the FEM model for Dynamic Modal Analysis.

8.1 Overview

Linear Dynamic Modal Analysis allows determining the peak response of a structure subjected to an earthquake directly from either the response or design spectrum. For SDOF systems, the peak response can be calculated directly from the response spectrum (knowing the natural frequency) without doing a modal analysis, but for MDOF systems, the response must be calculated for the most significant modes of vibration. In fact, the global response of the structure depends on the coupling of the response for those modes of vibration.

The general analysis procedure, proposed in *§.7.3.3.1 NTC 08,* consists in the determination of the vibration modes of the structure, followed by the calculation of the effect of the seismic action (spectral acceleration) from the design response spectrum for each vibration mode, and finally the combination of the response for all the significant modes.

Not all the vibration modes must be taken into account, but also just the ones with significant mass participation. According to NTC, it is appropriated to take into consideration all modes with an individual participation mass higher than 5%, having for all considered modes a total mass participation higher than 85%.

For a detailed explanation of Linear Dynamic Modal Analysis, the method can be divided into the following steps proposed by *Chopra, 2007*:

1. Define the structural properties such as mass matrix **m** and stiffness matrix **k**

2. Determine the natural frequencies ω_n (natural periods $Tn=2\pi/\omega_n$) and natural modes Φ_n of vibration

3. Compute the peak response in the *n*th mode by the following steps to be repeated for all modes, n=1,2,3…N.

   a) Corresponding to natural frequency ω_n and damping ratio ξ, determine the deformation spectrum ordinate D_n and the pseudo acceleration A_n, from the earthquake response spectrum or the design spectrum

   b) Calculates the modal displacement magnitudes.

   c) Compute the story forces – shear and overturning moment - and element forces – bending moments and shears- by static analysis of the structure subjected to lateral forces. According to NTC, the verification is performed by means of bending moment and shear forces compared with the resistance of the material.

4. Calculate maximum responses using either CQC method (Complete Quadratic Combination) if the natural frequencies are closely spaced or SRSS method (Square Root of the Sum of the Squares) if the natural frequencies are well separated.

The next sections show a mathematical description of the method as same as it is presented by *Chopra, 2007, Ref* [25*]*.

8.1.1 Natural frequencies and modes of vibration

Solving the eigenvalue problem, the natural frequencies and modes of a system are obtained. It can be easily explained analyzing the free vibration of an undamped linear MDOF system, which is governed by the next equation:

$$\boldsymbol{m}\ddot{u} + \boldsymbol{k}\boldsymbol{u} = 0 \qquad (47)$$

This equation represents N homogenous differential equations that are coupled through the mass matrix **m** and the stiffness matrix **k**, N represents the number of degree of freedom.

The relative displacement for one of the modes is described mathematically by:

$$\boldsymbol{u}(t) = q_n(t)\Phi_n \qquad (48)$$

Where the deflected shape Φ_n does not vary with the time. The time variation of the displacement can be described by the simple harmonic function:

$$q_n(t) = A_n \cos \omega_n t + B_n \sin \omega_n t \qquad (49)$$

Where A_n and B_n are constants of integration. Combining equations (48) y (49):

$$\boldsymbol{u}(t) = \Phi_n(A_n \cos \omega_n t + B_n \sin \omega_n t) \qquad (50)$$

Where the natural frequency ω_n and natural mode Φ_n are unknown.

Combining equations (47) and (50) gives:

$$[-\omega_n^2 \boldsymbol{m}\, \Phi_n + \boldsymbol{k}\, \Phi_n] q_n(t) = 0 \qquad (51)$$

This equation is satisfied in two ways. The first is the trivial solution when $q_n(t)=0$ which bring $u(t)=0$ and there is no motion of the system. The second one is when the frequencies ω_n and modes Φ_n satisfy the next expression:

$$\boldsymbol{k}\, \Phi_n = \omega_n^2 \boldsymbol{m}\, \Phi_n \qquad (52)$$

This algebraic equation is called the matrix eigenvalue problem, and it is a very useful condition to determine the scalar ω_n^2 and vector Φ_n in function of the stiffness matrix **k** and mass matrix **m**.

The formal solution for the previous equation is:

$$[\boldsymbol{k} - \omega_n^2 \boldsymbol{m}\,]\Phi_n = 0 \qquad (53)$$

This represents a set of N homogeneous equations for the N elements. The non-trivial is given by:

$$\boldsymbol{det}\,[\boldsymbol{k} - \omega_n^2 \boldsymbol{m}\,] = 0 \qquad (54)$$

Equation (54) is known as characteristic equation or frequency equation which has N real and positive roots for ω_n^2 because **m** and **k** are symmetric and positive definite.

Summarizing, a vibrating system with N degrees of freedom has N natural vibration frequencies ω_n, arranged in sequence from smallest to largest; corresponding natural periods T_n, and natural modes Φ_n, which depend just on the mass and stiffness properties of the structure *(Chopra, 2007)*.

8.1.2 Modal and spectral matrices

The N eigenvalues and N natural modes can be assembled into matrices. If the natural mode Φ_n corresponding to the natural frequency ω_n have elements Φ_{jn}, where j is the number of degrees of freedom, the N eigenvectors can be represented in a single square matrix where each column represents a natural mode (*Chopra, 2007*):

$$\Phi = [\phi_{jn}] = \begin{bmatrix} \phi_{11} & \phi_{12} & \cdots & \phi_{1N} \\ \phi_{21} & \phi_{22} & \cdots & \phi_{2N} \\ \vdots & \vdots & \ddots & \vdots \\ \phi_{N1} & \phi_{N2} & \cdots & \phi_{NN} \end{bmatrix}$$

The matrix Φ is also called modal matrix for the eigenvalue problem. The N eigenvalues ω_n^2 can be assembled into a diagonal matrix Ω^2, which is known as the spectral matrix of the eigenvalue problem:

$$\Omega^2 = \begin{bmatrix} \omega_1^2 & & & \\ & \omega_2^2 & & \\ & & \ddots & \\ & & & \omega_N^2 \end{bmatrix}$$

Each eigenvalue and eigenvector satisfies equation (55), which can be expressed in a matrix form as equation (56):

$$\boldsymbol{k}\,\Phi_n = \boldsymbol{m}\,\Phi_n\;\omega_n^2 \qquad (55)$$

$$\boldsymbol{k}\,\boldsymbol{\Phi} = \boldsymbol{m}\,\boldsymbol{\Phi}\,\boldsymbol{\Omega^2} \qquad (56)$$

Equation (56) provides a global presentation of the equations relating to all eigenvalues and eigenvectors of a system.

The FEM software, such as Strauss 7 (the one which will be used), solves equation (56) to get the natural frequencies and modes of vibration. Calculating and assembles the element stiffness and mass matrices to form the global stiffness and mass matrices.

On the other hand, the natural modes corresponding to different natural frequencies satisfy the next Orthogonality conditions:

$$\Phi_n^T \boldsymbol{k} \Phi_m = 0 \qquad \Phi_n^T \boldsymbol{m} \Phi_m = 0 \qquad (57)$$

The meaning of the modal orthogonality is that the work done by the *n*th mode inertia forces in going through the *m*th mode displacements is zero. Also, the work done by the equivalent static forces associated with displacements in the *n*th mode going through the *m*th mode displacements is zero (Chopra, 2007).

8.1.3 Modal Analysis

Dynamic modal analysis computes the peak response of a structure during an earthquake directly from the earthquake response or design spectrum, without the need for accelerograms (response history analysis).

Chopra, 2007, presents a complete explanation and mathematical background of Dynamic Modal Analysis and Earthquake Analysis of Linear Systems, which is not showed in this document. However a general description of the method is presented below.

8.1.3.1 General equation of motion

It is well known that only the relative motion *u* produces elastic and damping forces ($ku, c\dot{u}$). On the other hand, the inertia force is related to both the ground acceleration and the acceleration of the mass ($m(\ddot{u}_g + \ddot{u})$).

Considering dynamic equilibrium, the differential equation governing the response of an MDF system subjected to an earthquake ground motion is:

$$\boldsymbol{m}\ddot{u} + \boldsymbol{c}\dot{\boldsymbol{u}} + \boldsymbol{k}\boldsymbol{u} = P_{eff}(t) \qquad (58)$$

Where P_{eff} is the effective earthquake forces defined as:

$$P_{eff}(t) = -\boldsymbol{m}\boldsymbol{I}\ddot{u}_g(t) \qquad (59)$$

Where I represents the influence vector, which is composed by "1" and "0", and relates the DOFs of the motion with the DOFs of the structure. It represents the displacement of the masses resulting from static application of a unit ground displacement.

The damping matrix c would not be needed in modal analysis of earthquake response; instead modal damping ratios are sufficient.

The solution procedure of equation (58) is not presented in this document but can be easily found in any book of Dynamics of Structures.

8.1.3.2 The modal mass M_n

The modal mass for each mode of vibration is calculated as follows:

$$M_n = \Phi_n^T \boldsymbol{m} \Phi_n \qquad (60)$$

8.1.3.3 Modal earthquake excitation factor L_n

The modal earthquake excitation factor is defined by the following equation:

$$L_n = \Phi_n^T \boldsymbol{m}\, \boldsymbol{I} \qquad (61)$$

8.1.3.4 Modal participation factor Γ_n

The modal participation factor for *n*th mode is obtained in function of the modal mass M_n and the modal earthquake excitation factor L_n:

$$\Gamma_n = \frac{L_n}{M_n} \qquad (62)$$

The modal participation factor is independent of how the modes are normalized.

8.1.3.5 Effective modal mass M_n^{eff} (participation mass)

The effective modal mass for each mode can be calculated as follows:

$$M_n^{eff} = \frac{L_n^2}{M_n} \qquad (63)$$

The sum of the effective modal masses for all the N modes should be equal to the total mass of the system so the following condition must be verified.

$$\sum_{n=1}^{N} M_n^{eff} = M_{structure} \qquad (64)$$

The percentage of participation mass for each mode is obtained dividing the effective *n*th modal mass by the total mass of the structure, and multiplying by 100.

It is important to notice that, within the modal analysis, the contribution of all modes must be included in the calculations to obtain the exact value of the response. However, when dealing with a various number of degrees of freedom and modes, relative few modes provide sufficiently accurate results.

According to *§.7.3.3.1 NTC 08,* it is appropriated to take into consideration all modes with an individual participation mass higher than 5%, having a total mass participation higher than 85% for all considered modes.

8.1.3.6 Modal response

The equation of motion (58) can be rewritten of a multi degree of freedom system (MDOF) as:

$$\ddot{D}_n(t) + 2\xi_n\omega_n\dot{D}(t) + {\omega_n}^2 D_n(t) = -\ddot{u}_g(t) \qquad (65)$$

In time history analysis, the previous equation is solved for D_n using a numerical time-stepping method such as Newmark.

The time variation of the displacement is defined by:

$$q_n(t) = \Gamma_n D_n(t) \qquad (66)$$

The contribution of the *n*th mode to the nodal displacement u(t) is:

$$u_n(t) = \phi_n q_n(t) \qquad (67)$$

Finally, combining equations (66) and (67), the displacement can be expressed as:

$$\boldsymbol{u}_n(t) = \phi_n \Gamma_n D_n(t) \qquad (68)$$

Where:

n is n_{th} vibration mode, Γ_n is the modal participation factor for each mode and Φ_n is the mode shape

8.1.4 Response Spectrum Analysis Procedure

Spectral acceleration for all modes is available from the response design spectrum (section 5.4) by using the corresponding frequency value. Then, the (pseudo) spectral displacement is defined by dividing the spectral acceleration by the respective squared frequency:

$$S_{d,n} = \frac{S_{a,n}}{{\omega_n}^2} \qquad (69)$$

To get the contribution of the *n*th mode to the displacement, the equation (68) can be expressed as:

$$u_{jn} = S_{d,n}\, \Gamma_n\, \phi_{jn} \qquad (70)$$

Where:

S_{an}: Spectral acceleration for each mode (as a function of natural periods and damping ratio)

$\omega_{n:}$ natural frequencies

Γ_n: modal participation factor for each mode

Φ: mode shape

j_{th}: degree of freedom

n_{th}: mode of vibration

The maximum modal lateral forces, at various levels, are given by:

$$V_{jn,max} = \Gamma_n\, S_{a,n} \phi_{jn}\, m_j \qquad (71)$$

The base shear is given by:

$$V_{bn,max} = \sum_{j=1}^{N} V_{jn,max} = M_n^{eff} S_{a,n} = \frac{L_n^2}{M_n}\, S_{a,n} \qquad (72)$$

The overturning moment can be obtained as a function of the height vector of the analyzed points and the corresponding lateral forces vector:

$$M_{bn} = h_j\, V_{jn,max} \qquad (73)$$

8.1.5 Modal combination rules

The combination of the responses, calculated at different modes, can be performed using either CQC method (Complete Quadratic Combination) if the natural frequencies are closely spaced or SRSS method (Square Root of the Sum of the Squares) if the natural frequencies are well separated.

According to §.7.3.3.1 NTC 08 , if each oscillation period T_i differed from the others less than 10%, CQC method might be applied. If each oscillation periods T_i are well distinct from the others (more than 10%), SRSS method might be applied. The equations for both methods are shown below:

$$CQC \rightarrow E = \sqrt{\sum_i \sum_j \rho_{ij} E_i E_j} \qquad (74)$$

$$SRSS \rightarrow E = \sqrt{\sum_i E_i^2} \qquad (75)$$

Where E is the global value of the action (*u, T, M*), E_i is the value at *i*th mode of the action and ρ_{ij} is a correlation coefficient between mode *i* and *j* which is defined in *§.7.3.3.1 NTC 08.*

As it will be explain further, the chosen combination rule for this work was SRSS since the difference between natural periods was higher than 10%.

8.1.6 Safety verifications (NTC 2008)

According to Guidelines for Evaluation and Mitigation of Seismic Risk to Cultural Heritage (Ref. [23]) and NTC 2008, the safety verifications for linear dynamic analysis must be done by comparing both the calculated acting moment M_a with the ultimate resistance moment M_u and the acting shear force V_a with the shear resistance V_t, assuming that the masonry is not resistant to traction.

The verification should be performed according to the two main directions of inertia of the section at different heights, because of the impossibility of identification of critical sections in advance due to different thickness of masonry walls and weaknesses generated by openings.

8.1.6.1 Bending Moment verification

The bending moment verification must satisfy:

$$M_u > M_a$$

Where M_u is the ultimate resistance moment and M_a is the acting moment.

Following NTC 2008 (*§7.8.2.2.1)* the ultimate resistance moment is defined by the next equation:

$$M_u = \left(l^2 t \sigma_0 / 2\right)\left(1 - \sigma_0 / 0{,}85 f_d\right) \qquad (76)$$

Where: l is the length of masonry wall

t is the masonry wall pressed thickness

σ_0 is normal stress of wall, referred to section total area (if it is subjected to tension M_u=0)

f_{dm} is design compressive strength for the masonry (section 6.7.3)

8.1.6.2 Shear verification

Shear verification must satisfy:

$$V_t > V_a$$

Where V_t is the shear resistance moment and V_a is the acting shear force.

Following *Circolare 2009* (*§C8.7.1.5)* the shear resistance is defined by the following expression:

$$V_t = l \cdot t \frac{1{,}5\tau_{0d}}{b} \sqrt{1 + \frac{\sigma_0}{1{,}5\tau_{0d}}} = l \cdot t \frac{f_{td}}{b} \sqrt{1 + \frac{\sigma_0}{f_{td}}} \qquad (77)$$

Where l is the length of masonry wall

t is the masonry wall thickness

σ_0 is normal stress of wall, referred to section total area

f_{td} is tension strength of masonry wall

τ_{0d} id the design shear strength of masonry wall (section 6.7.4)

b is a coefficient that depend on masonry wall slenderness. It is possible to assume $b = h/l$, but it must be less than 1.5 and higher than 1.

8.2 Modeling - Preprocessing

Dynamic Modal Analysis was carried out by means of Finite Element Method using the software *Strand 7* (also called *Straus 7*).

8.2.1 FEM

Finite Element Method is a numerical analysis technique for obtaining approximate solutions to many engineering problems in the field of continuum mechanics. The mathematical background of the method is not presented in this document but can be easily found in books.

In general terms, the method gives a numerical technique for modeling the whole structure as an assemblage of discrete parts or finite elements connected each other at specified points or nodes.

Essentially, the FEM woks following the next steps (Huebner, 1982):

1. Discretize the continuum, 2. Select interpolation functions or shape functions, 3. Find the element properties, 4. Assemble the element properties to obtain the system equations, 5. Solve the system of equations.

The body can be discretized in finite elements with a variety of element shapes such as triangles and quadrilaterals for 2D domains, or hexahedral and tetrahedral for 3D domains, considering that different element shapes may be employed in the same solution region.

The next step is to assign nodes to each element and then choose the type of interpolation function (shape function) to represent the variation of the field variable over the element. Usually, polynomials are selected as interpolation functions for the field variable because they are easy to integrate and

differentiate. The degree of the polynomial depends of the number of nodes assigned to the element, the nature and number of unknowns at each node, and certain continuity requirements imposed at the nodes along the element boundaries (Huebner, 1982).

Finite element method solves problems that concerns kinematic equations (strain in terms of displacements and shape functions), constitutive equations (stress in function of strain) and equilibrium equations (equilibrium of forces), generally by means of the virtual work principle. It can be performed either for lineal elasticity considering linear relationship between the components of stress and strain or nonlinearity considering a nonlinear function such as plastic or viscous-plastic.

8.2.2 Description of model

The modeling was carried out by means of the FEM software *Strand 7,* using bidimensional plate elements, with a mesh composed by triangular and quadrilateral elements, with 3 and 4 nodes respectively. These elements are suitable for modelling general 3D structures made from relatively slender components such as walls. Plate elements in *Strand7* may be either thin or thick. Thick plates consider the effects of shear deformation.

Plane elements have only two degrees of freedom per node corresponding to the translation in their plane; they transmit stress only along their plane. They do not transfer any stiffness to the other degrees of freedom.

At first a 3D model was elaborated in Autocad based on the plans elaborated during the geometrical survey; then, it was exported to Strand 7.

The Tower elements taken into account in the model were:

1. Brick masonry walls

2. Brick masonry vaults

3. Wooden platforms

4. Roof

5. Bell and bell yoke

All of those elements has been depicted in section 2.3, chapter 3, and the corresponding loading is presented in section 5.1. Some other factors considered in the model were:

*Tower’s tilt

*The openings in walls, vaults and wooden platforms.

*The constraint by the adjacent buildings

For defining the model the 11 levels of the tower were taking into account considering the different thickness of the walls. The geometrical characteristics, including the plate thickness, are presented in Table 89.

At the lower part of the tower, the four walls have different thickness (being the eastern one thicker due to the buttress), while in the upper part, the thickness of the different walls is more constant.

Table 89. Geometry of model

Section	Element	Length	Thickness		Height	Elevation	
			Real	For model			
		(m)	(m)	(m)	(m)	From (m)	To (m)
Level 1 *Ground floor*	Eastern wall	7.12	4.39	4.39	4.82	0	4.82
	Western wall	7.12	2.40	2.40			
	Northern wall	10.3	1.88	1.88			
	Southern wall	10.3	2.45	*2.40*			
	Vault 1 (barrel)		*0.54*	*0.54*			
Level 2	Eastern wall	7.1	3.34	3.34	4.52	4.82	9.34
	Western wall	7.1	2.21	2.21			
	Northern wall	8.51	1.84	1.75			
	Southern wall	8.51	1.65				
	Vault 2 (cross)		*0.46*	*0.46*			
Level 3	Eastern wall	7.13	2.90	2.90	3.9	9.34	13.24
	Western wall	7.13	2.06	2.06			
	Northern wall	8.24	1.78	1.76			
	Southern wall	8.24	1.73				
	Vault 3 (cross)		*0.31*	*0.31*			
Level 4 Entrance	Eastern wall	7.05	2.34	2.34	3.91	13.24	17.15
	Western wall	7.05	1.98	1.84			
	Northern wall	7.60	1.83				
	Southern wall	7.60	1.72				
Level 5	Eastern wall	7.00	1.62	1.65	4.61	17.15	21.76
	Western wall	7.00	1.66				
	Northern wall	7.41	1.65				
	Southern wall	7.41	1.67				
Level 6	Eastern wall	6.86	1.51	1.51	3.55	21.76	25.31
	Western wall	6.86	1.51				
	Northern wall	6.85	1.51				
	Southern wall	6.85	1.49				
	Wooden platf.1			*0.1*			

Level 7	Eastern wall	6.83	1.33	1.35	4.15	25.31	29.46
	Western wall	6.83	1.36				
	Northern wall	6.62	1.34				
	Southern wall	6.62	1.36				
	Vault 4 (barrel)		*0.31*	*0.31*			
Level 8	Eastern wall	6.80	1.17	1.20	3.44	29.46	32.9
	Western wall	6.80	1.18				
	Northern wall	6.79	1.21				
	Southern wall	6.79	1.24				
	Wooden platf.2			*0.1*			
Level 9	Eastern wall	6.78	1.14	1.14	3.95	32.9	36.85
	Western wall	6.78	1.14				
	Northern wall	6.79	1.13				
	Southern wall	6.79	1.13				
	Vault 5 (barrel)		*0.60*	*0.60*			
Level 10 Belfry	Eastern wall	6.72	0.98	0.98	5.7	36.85	42.55
	Western wall	6.72	0.99				
	Northern wall	6.78	0.98				
	Southern wall	6.78	0.98				
Level 11- Top Battlement	Eastern wall	6.61	0.57	0.57	3.05	42.55	45.6
	Western wall	6.61	0.57				
	Northern wall	6.63	0.57				
	Southern wall	6.63	0.57				
	Roof			0.1	1.63	45.6	47.23

The properties of the elements and the loading are defined according to the parameters and values defined in previous chapters of the document (chapter 5 and section 6.7). However, the elastic modulus for the brick masonry, calculated according to NTC 2008, equal to 1500 MPa has been used just as a starting value for the FEM model; the real value will be obtained by means of the calibration of the model since the first and second frequencies are known. The passion's ratio has been taken as 0.2. The specific weight of the masonry is 18 kN/m^3.

The whole model is shown in Figure 119, including the walls, vaults, wooden platforms and roof. The mesh is composed by 8891 plate elements and 8415 nodes. The mesh is composed by quadrilateral and triangular elements of different dimension; the average is 0.45 x 0.45 m.

North view (Figure 119) shows clearly the tilt of the tower.

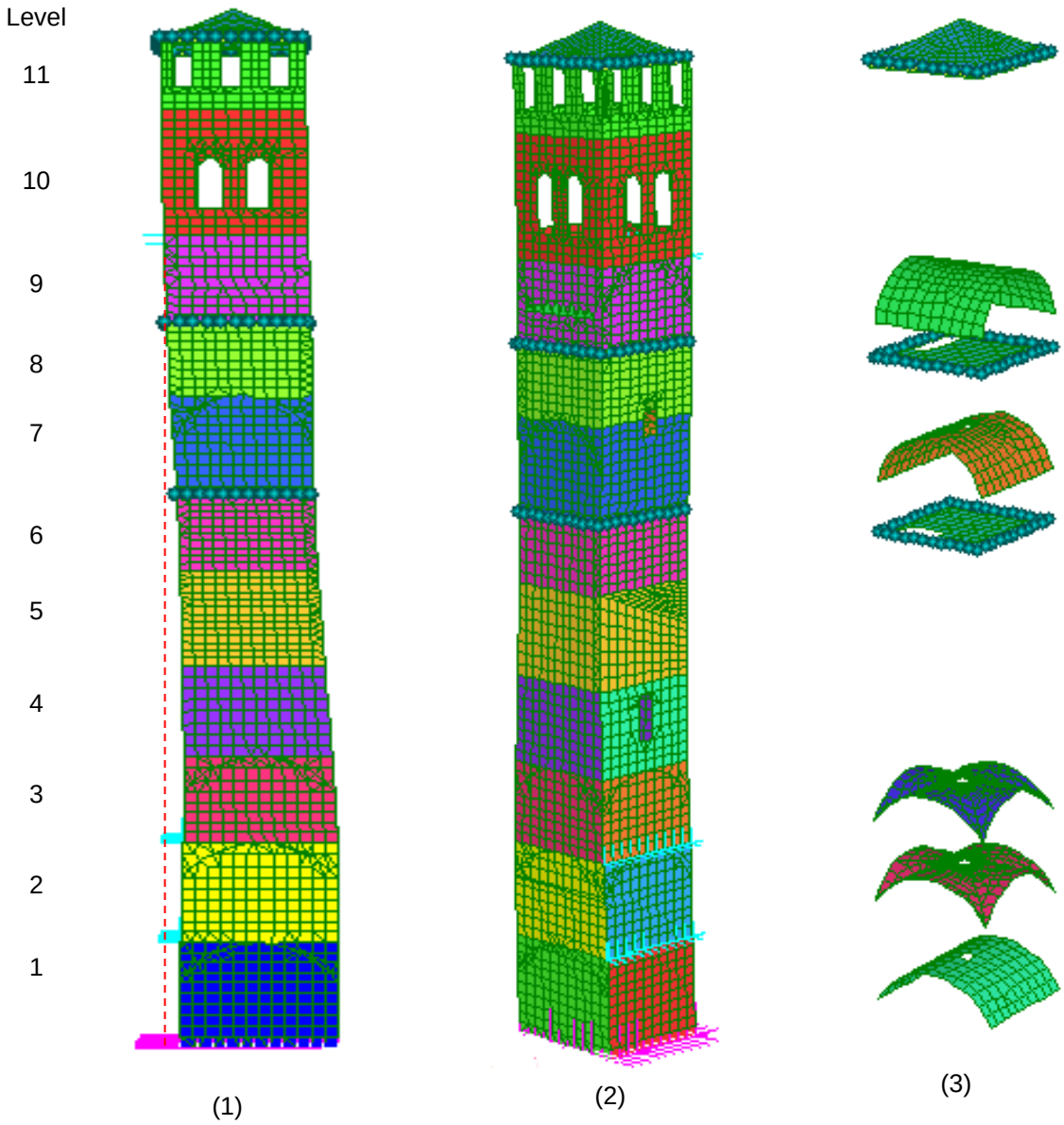

Figure 119. *Strand7* model of Tower Anziani. (1) North view. (2) View south-east. (3) Vaults, platforms and roof

The boundary conditions of the system are defined by the assumptions that the base is fixed and the restrictions given by the walls of the adjacent buildings (Figure 120 and Figure 121).

The adjacent walls were modelled, according to the geometrical survey, in order to simulate the displacements restrictions that they cause to the tower. These restrictions could have been modelled with rigid constraints in nodes but they would make the tower much stiffer and the natural frequencies of vibration would change considerably from the reality. The material density for these walls was assumed to be very low (almost cero) and the modulus of elasticity was changed several times in the model calibration until reaching the correct dynamic properties (it is explained further on).

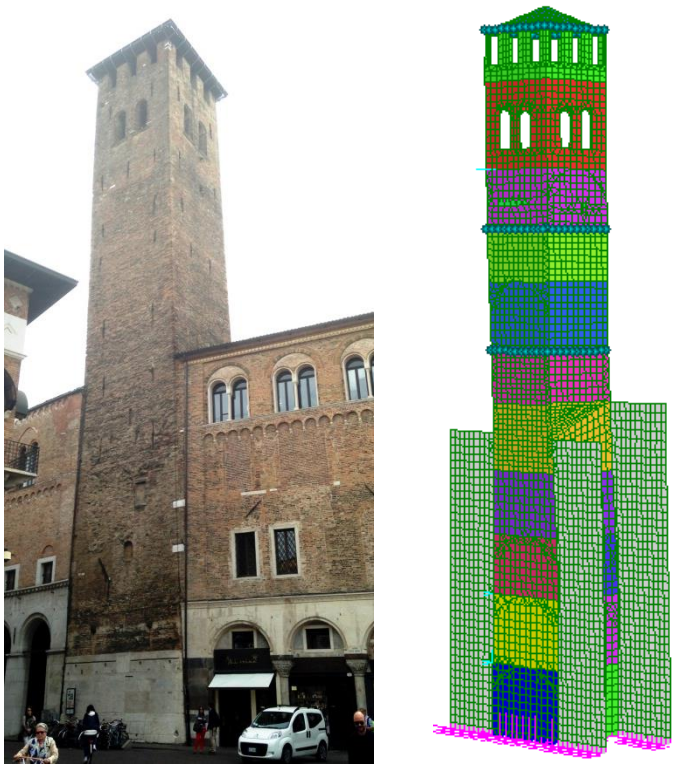

Figure 120. North-west view of the tower and *Strand7* model showing adjacent walls

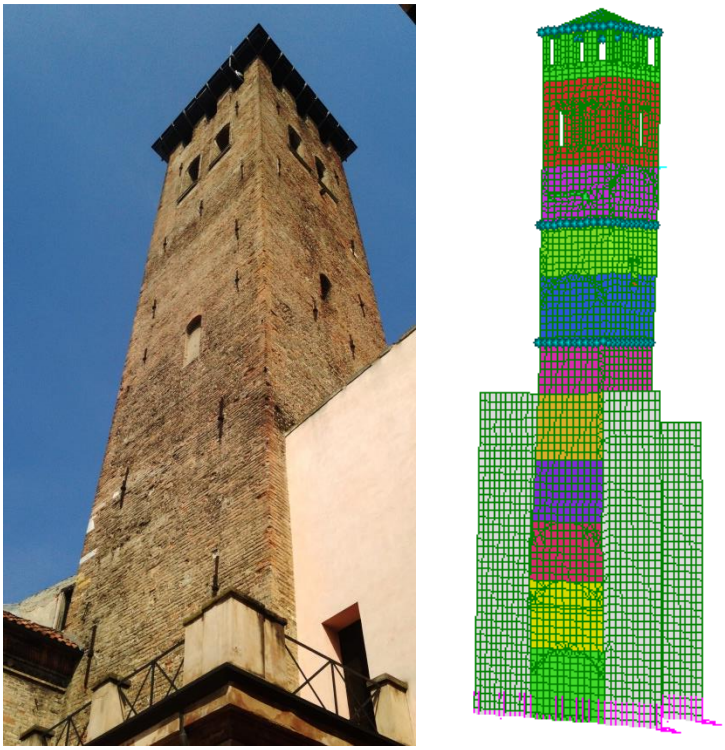

Figure 121. South-east view the tower and *Strand7* model showing adjacent walls

The tower is composed by 2 cross vaults and 3 barrel vaults (Figure 119). All of them have different thickness and they are made of the brick masonry as well. They were modelled using quadrilateral elements with 4 nodes with an average dimension of 0.45x0.45 m. Vaults located at the lower part of the tower are shown in the following figure.

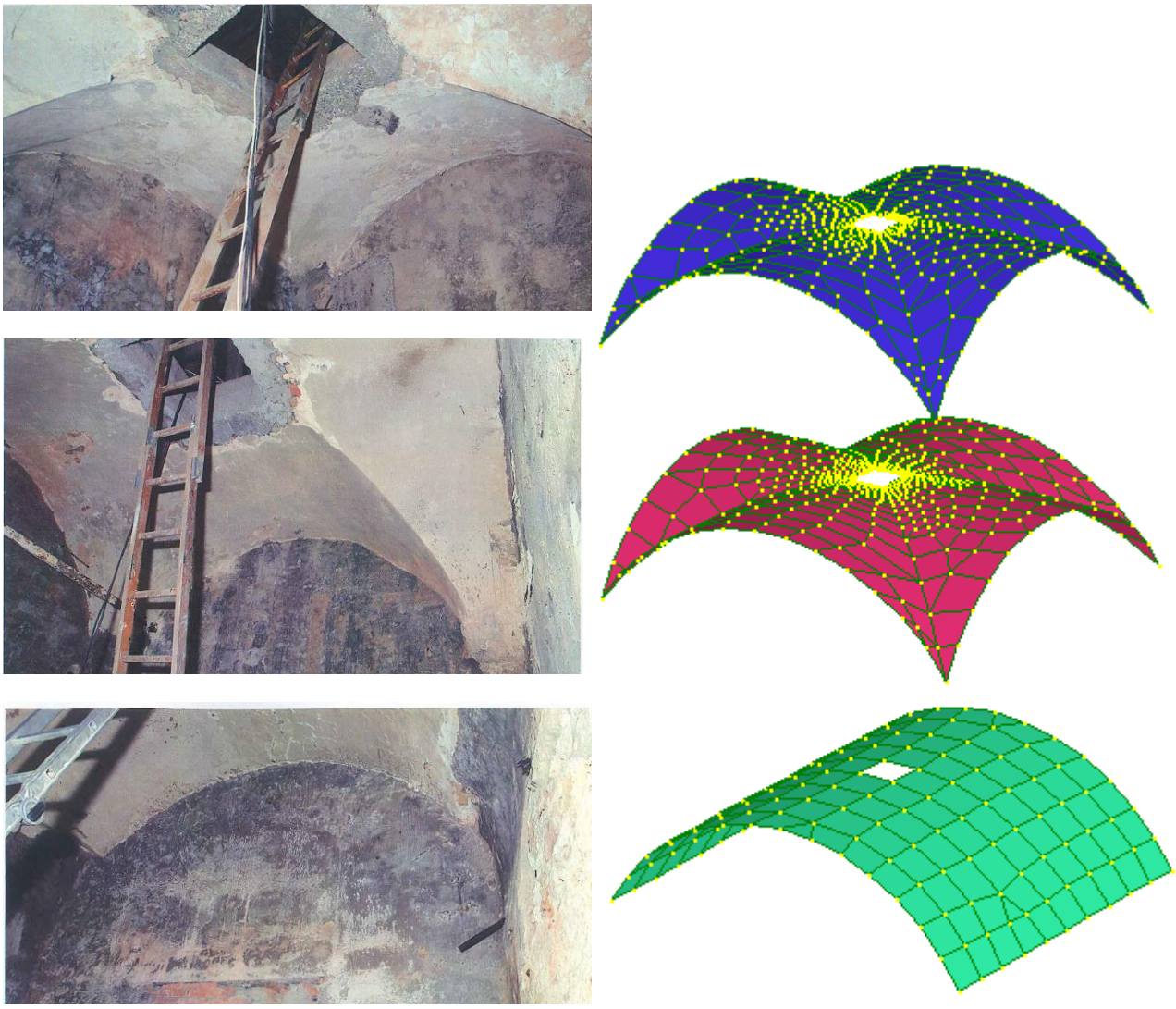

Figure 122. Image of vaults at lower part of the tower and *Strand7* modeling

Wooden platforms and the roof were modelled with structural translational masses acting in three directions x, y, and z (Figure 123 and Figure 124).

The loading determination for those elements is presented in sections 5.1.1 and 5.1.2.

Considering that the self-weight of wooden platform 1 is transferred mainly to eastern and western walls the 80% of the total mass was distributed in the connection nodes located at those walls and the 20% in the connection nodes at northern and southern walls. For the case of the platform 2, the 80% of the total mass was distributed in connection nodes at northern and southern walls and the 20% in the other walls.

The total self-weight of the roof was distributed equally as structural masses in the connection nodes, since it is assumed that each wall receives a quarter of the roof load.

The plate elements of those components were defined with the corresponding timber properties (larch timber) but with almost zero density in order to consider deformation but no extra load.

Wooden platform 2

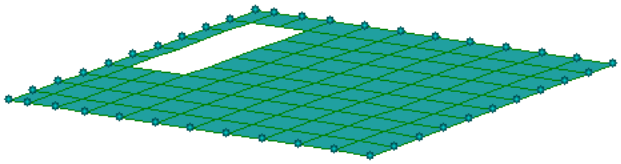

Wooden platform 1

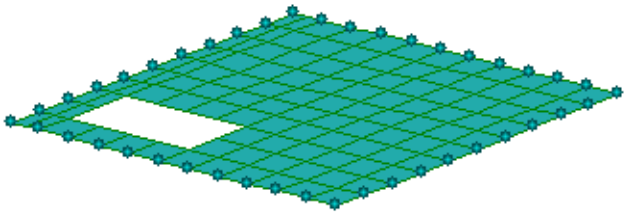

Figure 124. *Strand7* wooden platforms modeling

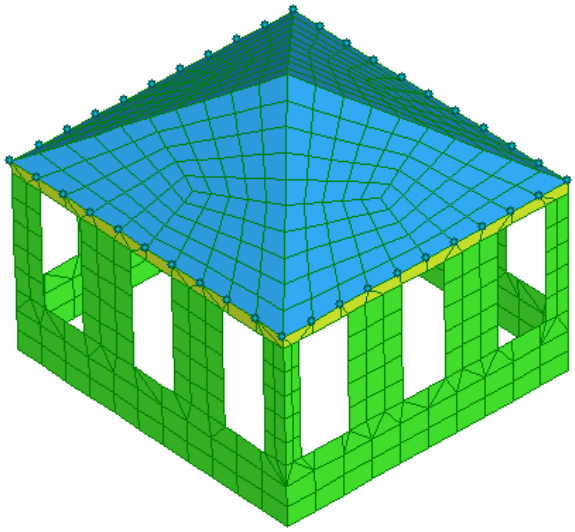

Figure 123. *Strand7* roof modeling

Considering that the bell yoke is supported just on northern and southern wall. The bell and bell yoke were modelled using rigid links from northern and southern wall joined together in a master node in the barycenter of the section. A translational mass acting in the three directions x, y, and z was set up in the master node (Figure 125 - Figure 128).

Arrangement and characteristics of bell and bell tower are presented in sections 2.3.1 and 5.1.3.

Table 90 shows all the elements modelled as structural mass acting in directions x, y and z.

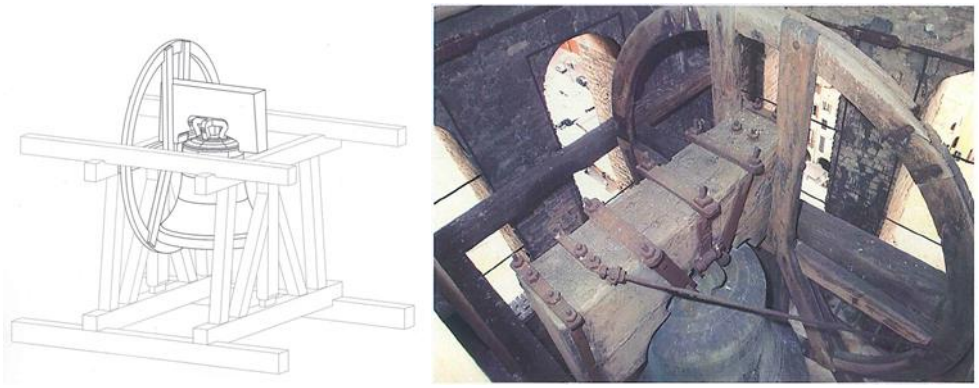

Figure 125. Arrangement of bell and bell yoke

Figure 126. Detail of bell yoke

Figure 128. Detail of yoke connection to northern wall

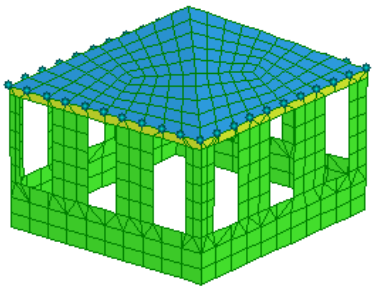

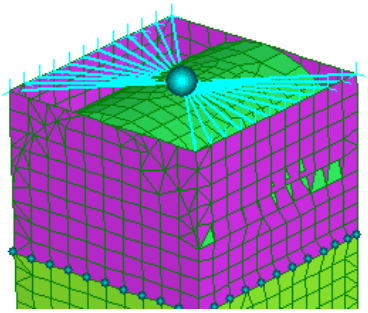

Figure 127. *Strand7* model of bell and bell yoke

Table 90. Elements modeled as structural mass

Element	Load (kN)	Mass (Kg)
Roof	84.94	8658.08
Wooden platform 1	13.73	1399.61
Wooden platform 2	13.32	1357.38
Bell	35.32	3600.00
Bell yoke	7.85	800.00

Wind action is described in section 5.3. Wind is acting in west-east direction; therefore a positive pressure is generated on western wall and negative pressure (suction) on eastern wall. This action was modeled as surface pressure assigned normal to the plate surface.

The northern and southern walls are subjected to a tangential action, it was modelled as surface pressure assigned tangential to the plate surface (Figure 129).

Snow action, described in section 5.2, was modeled as surface pressure assigned normal to the plate surfaces belonging to the roof.

Both wind and snow actions will be used for a static analysis previous to dynamic one.

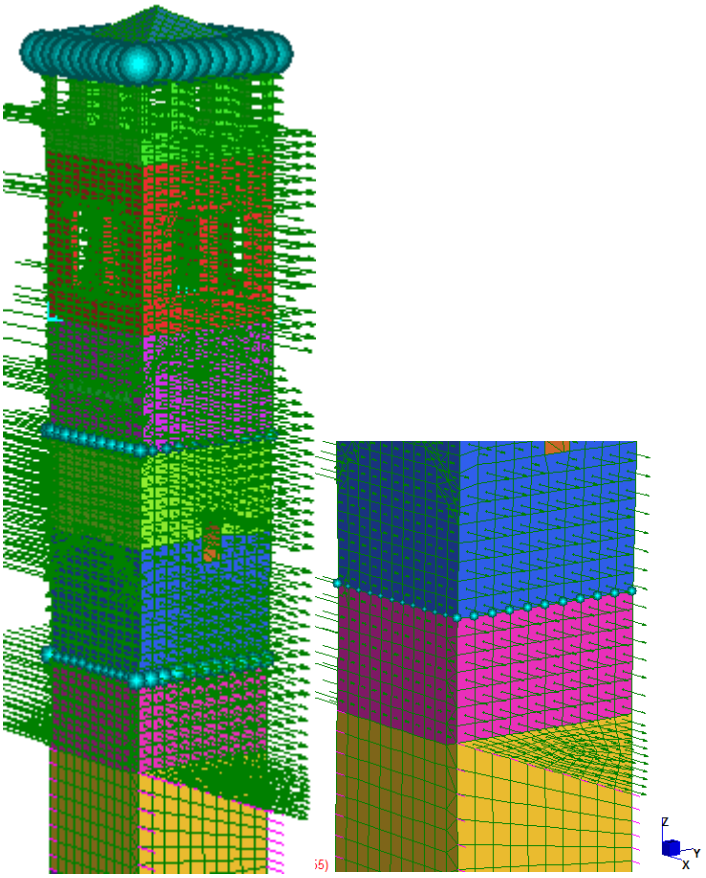

Figure 129. Wind action (direction west-east)

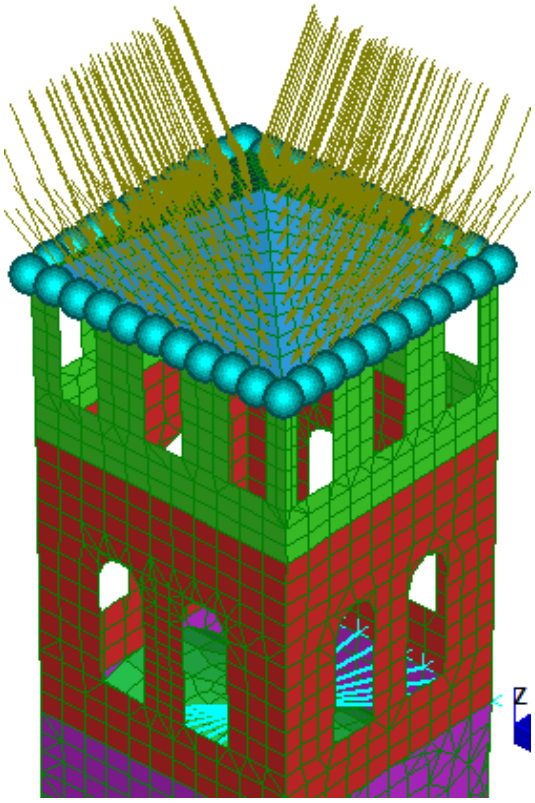

Figure 130. Snow action

8.3 Results – Post-processing

8.3.1 Calibration of Model and Natural Frequency Analysis

Strand7 Natural Frequency Solver calculates the natural frequencies corresponding to the vibration modes of an undamped structure. The natural frequency analysis problem is formulated as the following eigenvalue problem (explained in section 8.1.1):

$$\boldsymbol{k}\,\Phi_n = \omega_n^2\,\boldsymbol{m}\,\Phi_n \qquad (78)$$

Where **k** is the global stiffness matrix, **m** is the global mass matrix, Φ is the vibration mode vector and ω is the natural frequency.

The software calculates and assembles the element stiffness and mass matrices to form the global stiffness and mass matrices. Constraints are assembled in this process. It solves the eigenvalue problem to get frequencies and the corresponding mode shapes using the Sub-Space Iteration Method.

8.3.1.1 Calibration

The model was calibrated taking into account the knowledge about the first and second natural frequencies obtained in the dynamic characterization test (section 4.1.2) as well as the vertical reaction at the base due to self-weight (section 5.1).

Natural frequencies, corresponding periods and direction of mode vibration, obtained experimentally, are shown in Table 91. On the other hand the self-weight of the entire structure is 28286.7 kN.

Table 91. Natural frequencies obtained experimentally

N	Direction	Natural frequency (Hz)	Natural period (s)
1st	North-South	**1.59**	0.63
2nd	East-West	**1.90**	0.53

The model was run several times until getting an acceptable error between experimental and modeled natural frequencies as well as between the real and the modeled vertical reaction on the walls at the base of the tower.

The error between frequencies has been calculated by means of the following equation:

$$\boldsymbol{e} = \frac{\boldsymbol{f_m - f_s}}{\boldsymbol{f_s}} * \boldsymbol{100} \qquad (79)$$

Where f_m is the frequency obtained in the model and f_s is the frequency obtained experimentally

The error corresponding to vertical reaction at base has been calculated by means of the following equation:

$$e = \frac{R_m - R_s}{R_s} * 100 \qquad (80)$$

Where R_m is the reaction obtained in the model and R_s is the total-self weight of the tower.

For getting convergence in the calibration, the modulus of elasticity from both brick masonry and the adjacent walls were slightly changed in each running. The starting value of modulus of elasticity for brick masonry was the value recommended by NTC 2008 (section 6.7.1).

Table 92 shows the most representative steps in the calibration. It is seen that the stiffness of both brick masonry and adjacent walls influence in the reaction at base of the tower and the natural frequencies.

At first, rigid constrains were set up on the corresponding nodes to restrict west-east displacement instead of adjacent walls, for that case, the error regarding to the reaction at the base was almost cero but the error regarding to natural frequencies was quite high (over 50%). The participation mass in x direction (west-east) resulted to be very low (37.3%).

Table 92. Calibration of model

Modulus of Elasticity (Mpa)		Reaction at base		1st frequency		2nd frequency		Mass Participation (%)	
Brick masonry	Boundary cond. /Adjacent wall	R_m (kN)	Error (%)	ω_1 (Hz)	Error (%)	ω_2 (Hz)	Error (%)	Dir X	Dir Y
1500	Rigid constr. in X	28301.8	**0.1**	0.77	***51.7***	1.71	***10.2***	37.3	91.5
4000	Rigid constr. in X	28366.0	**0.3**	1.25	***21.2***	2.78	***46.5***	37.3	91.4
1500	15000	4868.0	**82.8**	1.59	***0.0***	1.90	***0.3***	77.8	86.8
1500	1500	17948.7	36.5	0.98	*38.3*	1.45	*23.8*	87.9	91.4
4000	3500	18767.3	33.7	1.56	*1.5*	2.31	*21.5*	88.0	91.3
3500	3000	18887.1	33.2	1.45	*8.5*	2.15	*13.2*	88.1	91.2
4000	3000	19643.5	30.6	1.52	*4.1*	2.24	*17.9*	88.3	91.5
4500	3000	20279.9	28.3	1.59	*0.3*	2.33	*22.7*	88.4	91.2
3500	2000	21034.7	25.6	1.37	*13.4*	2.00	*5.3*	88.7	91.2
4000	2000	21699.1	23.3	1.44	*9.0*	2.09	*9.8*	88.9	91.2
4500	2000	22221.8	21.4	1.51	*4.8*	2.17	*14.0*	89.0	91.5
5000	2000	24190.4	14.5	1.53	*3.4*	2.01	*6.0*	89.4	91.5
5500	2000	24468.9	13.5	1.59	*0.5*	2.08	*9.6*	89.5	91.1
5500	1000	25962.3	8.2	1.53	*3.8*	1.91	*0.7*	90.2	91.3
6000	1000	26094.7	7.7	1.59	*0.1*	1.98	*4.4*	90.2	91.3
6000	**750**	**29105.9**	**2.9**	**1.57**	***1.0***	**1.94**	***1.9***	***90.4***	***91.3***

In contrast, using very stiff adjacent walls (E=15000 MPa), the error in natural frequencies was almost cero but the error in the vertical reaction was too high (82.8 %).

After many combination attempts, an acceptable error for all parameters was obtained (less than 3%), using for that a modulus of elasticity for brick masonry of 6000 MPa and 750 MPa for adjacent walls.

It is important to bring out that the modulus of elasticity used in the structural analysis of Tower Anziani, performed in 2005 (Ref. [9]), was also 6000 MPa. That report said that this value was obtained by means of a Flat Jack Test, but unfortunately results of that test were not available nowadays, therefore that value was not taken into account previously in this document, however it matches with the model calibration.

8.3.1.2 Natural Frequencies of Vibration

Once the model was calibrated, the natural frequencies for the first 30 modes of vibration were calculated. As it was mentioned previously, according to *§.7.3.3.1 NTC 08,* it is appropriated to take into consideration all modes with an individual participation mass higher than 5%, having a total mass participation higher than 85% for all considered modes.

Table 93 shows each frequency with the corresponding modal mass and mass participation in direction x (west-east) and Y (north-south). The total mass participation is over 90% in each direction, however just 10 frequencies were chosen (green color) for having mass participation higher than 5%, except two frequencies that are lower but their contribution is important compared with the others neglected. All the neglected values are in red.

Table 93. First 30 natural frequencies with mass participation

Mode	Frequency (Hz)	Modal Mass (Engineering)	PF-X (%)	PF-Y (%)
1	1.57	398200	0.00	48.31
2	1.94	358900	45.38	0.00
3	6.52	243700	0.00	22.01
4	7.09	243900	23.44	0.00
5	7.91	610800	0.00	0.06
6	12.90	800500	0.12	0.01
7	13.53	141100	0.00	9.24
8	14.62	145100	8.86	0.00
9	18.27	267800	0.00	0.00
10	20.66	100800	0.00	4.95
11	22.54	111100	5.52	0.00
12	24.97	157900	0.00	0.00
13	26.58	177700	0.00	0.02
14	28.22	35440	0.00	0.01

15	28.89	38690	0.00	2.78
16	31.06	33330	2.33	0.00
17	31.29	308100	0.31	0.00
18	32.33	846000	0.00	0.01
19	33.01	22250	0.00	1.01
20	34.93	20190	1.20	0.00
21	35.41	8208	0.05	0.00
22	36.44	166500	0.00	0.00
23	39.62	138600	0.01	0.52
24	39.76	94650	0.01	0.98
25	42.05	47380	1.10	0.00
26	42.52	48140	0.00	1.37
27	44.71	50040	0.00	0.01
28	45.74	59310	1.98	0.00
29	46.13	2490	0.02	0.00
30	46.48	50020	0.01	0.00
----	----------	----------	--------	----------
TOTAL MASS PARTICIPATION FACTORS			90.4	91.3

It was figured out that all the representative modes involve just flexion of the tower in both directions (X and Y), torsion modes were not representative. The final natural frequencies that primarily influence in the dynamic response of the tower and corresponding mass participation are shown in the following table.

Table 94. Representative natural frequencies of Tower Anziani

Direction	Mode	Frequency (Hz)	Period (s)	Mass Participation (%)	Total mass Participation (%)
Y North-South	1	1.57	0.64	48.31	87.29
	3	6.52	0.15	22.01	
	7	13.53	0.07	9.24	
	10	20.66	0.05	4.95	
	15	28.89	0.03	2.78	
X West-East	2	1.94	0.52	45.38	85.53
	4	7.09	0.14	23.44	
	8	14.62	0.07	8.86	
	11	22.54	0.04	5.52	
	16	31.06	0.03	2.33	

The following images show the first 4 vibration modes from FEM model:

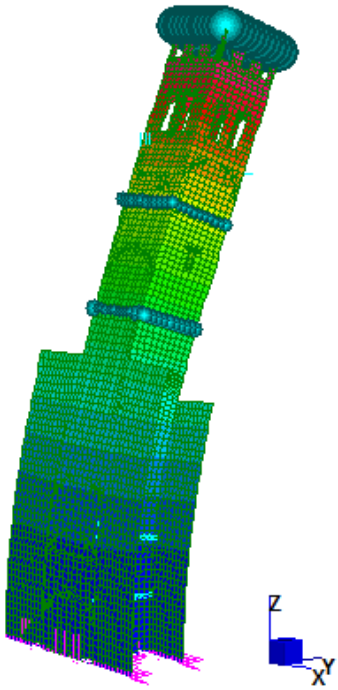

Figure 131. Vibration mode 1 in Y direction (f=1.57 Hz)

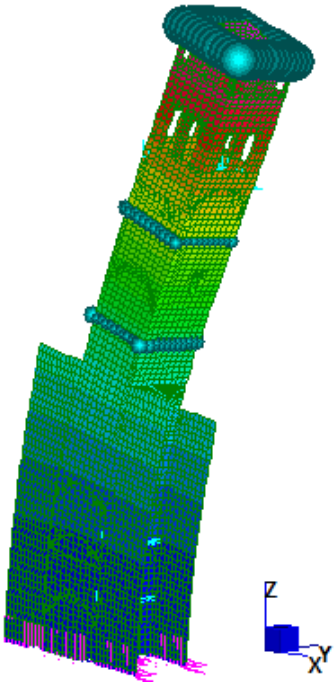

Figure 132. Vibration mode 2 in X direction (f=1.94 Hz)

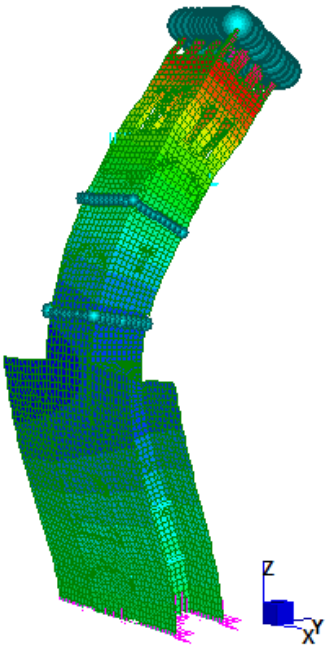

Figure 133. Vibration mode 3 in Y direction (f=6.52 Hz)

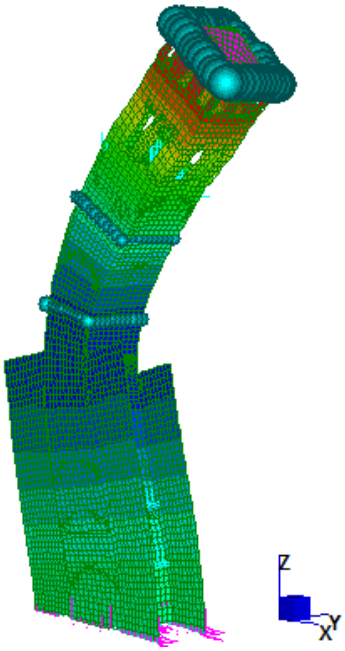

Figure 134. Vibration mode 4 in X direction (f=7.09 Hz)

8.3.2 Static Analysis of the Structure subjected to Permanent and Imposed Loads

Before modal analysis, a linear static analysis was carried out to check the static behavior of the tower taking into the fundamental load combinations which are in function of self-weight, wind and snow actions.

The linear static solution is obtained assuming that the structure's behavior is linear and the loading is static. The solver calculates and assembles element stiffness matrices, equivalent element force vectors and external nodal force vectors. Constraints are also assembled in this process. At the end of this assembly procedure, the following linear system of equilibrium equations is formed:

$$\boldsymbol{k}\ d = P \qquad (81)$$

Where k is the global stiffness matrix, d is the unknown nodal displacement vector and P is the global nodal load vector.

The software solves the equations of equilibrium for the unknown nodal displacements and calculates element strains, stresses, stress resultants and strain energy densities as requested.

8.3.2.1 Load combinations

The description of the actions on the structure and load combinations is presented in Chapter 5. For static analysis, three different load types have been considered, self-weight of structural elements (G_1), self-weight of bell and bell yoke (G_2), wind (Q_1) and snow (Q_2). In that way, the fundamental combination can be expressed as:

$$\boldsymbol{\gamma_{G1} G_1 + \gamma_{G2} G_2 + \gamma_{Q1} Q_{k1} + \gamma_{Q2} \psi_{02} Q_{k2}} \qquad (82)$$

Self-weight of the bell was modelled as a point load on the same node where the mass was applied for modal analysis.

The load coefficients are shown in Table 42. Four load combinations (scenarios) were considered, two of them including the imposed loads and load coefficients and the others two considering just the self-weight with no load coefficients.

Table 95. Load combinations for static analysis

1	Unfavorable G_1 - unfavorable G_2 – Wind dominant	$\boldsymbol{1.3\ G_1 + 1.5\ G_2 + 1.5\ Q_1 + 0.75\ Q_2}$
2	Unfavorable G_1 - unfavorable G_2 – Snow dominant	$\boldsymbol{1.3\ G_1 + 1.5\ G_2 + 1.5\ Q_2 + 0.9\ Q_1}$
3	Considering the self-weight of structural elements, bell and bell yoke (with no load coefficients)	$\boldsymbol{1\ G_1 + 1 G_2}$
4	Considering just the self-weight of structural elements (no bell self-weight and no load coefficients)	$\boldsymbol{1\ G_1 + 0\ G_2}$

8.3.2.2 Static analysis of the structure subjected to wind action

Before going through the load combinations, the analysis was performed just for the wind action, to see how it does affect the tower. Figure 135 shows the contour plot of vertical stress due just to wind action, since the wind is acting in direction west-east, it produces slight tension stress on western wall and compression stress on eastern wall (adjacent wall have been hidden).

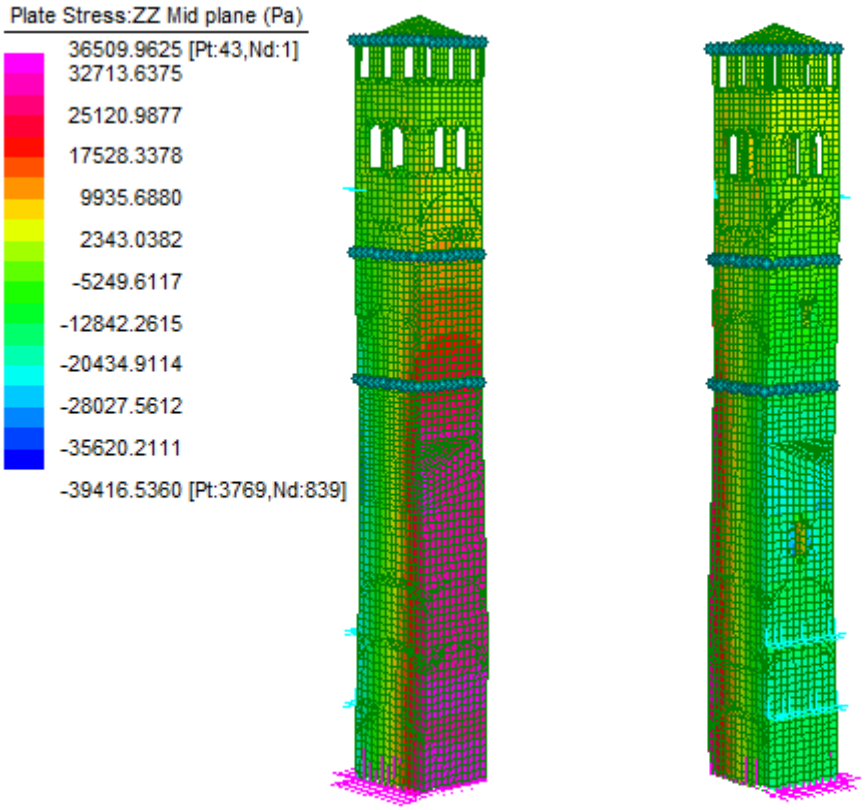

Figure 135. Contour plot of vertical stress due to wind action. (1) View North- West. (2) View South-East

The maximum stress state is produced around the level where the tower is constrained by the adjacent walls. However, the level of tension stress is very low (Table 96), and surely it will be insignificant when the self-weight and other actions come into the analysis.

Table 96. Results of static analysis under wind action

Max stress at level +21.8 m - western wall	**$\sigma_{zz,+21.8}$ (MPa)**	**0.0365**	Tension
Max stress at level +21.8 m - eastern wall (tilted side)	**$\sigma_{zz,+21.8}$ (MPa)**	**-0.0394**	Compression

8.3.2.3 Stress state of the tower subjected to load combinations

Figure 136 shows the contour plot of vertical stress of the tower for load combination 1 which is the one that presents the highest level of stress (it is subjected just to compression stress).

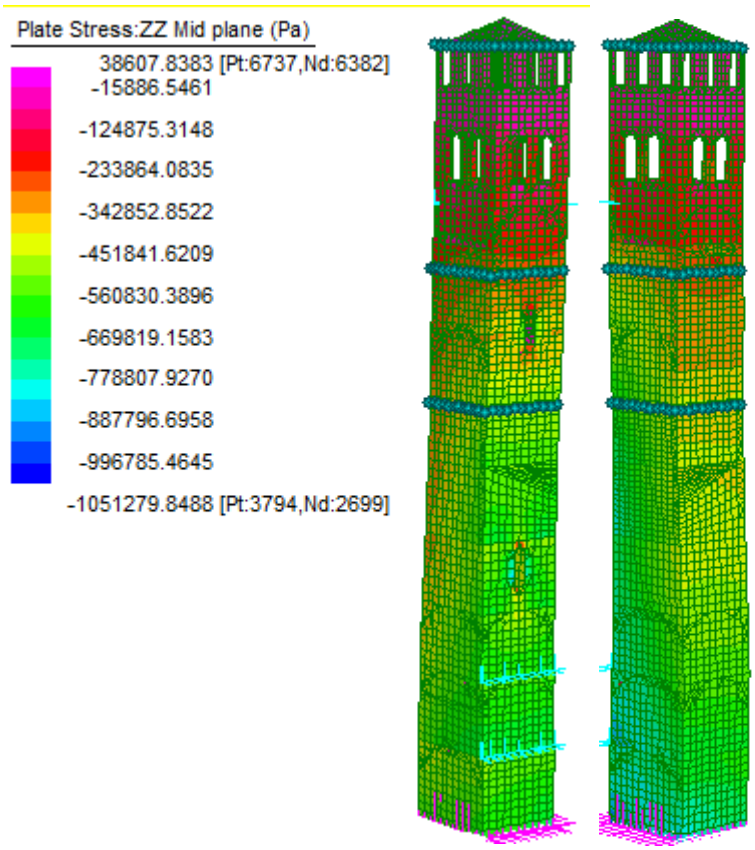

Figure 136. Contour plot of vertical stress for load combination 1. Left: South-East view. Right: North-West view

Eastern wall is subjected to higher stress state than others due to tower's tilt toward the east. However, the stress distribution at the base is almost uniform on all the walls for all load combinations, what means that there is no significant acting moment.

Figure 137 shows the distribution of vertical stress at the base on eastern wall for all 4 load combinations; it is seen that the stress distribution for combinations 1 and 2 (affected by load coefficients) are almost the same having a maximum stress value around -0.71 MPa. Stress distribution for combinations 3 and 4 (not affected by load coefficients) are also almost the same with a stress value around -0.55 MPa, so the static effect of the bell is not significant.

Figure 138 shows the node vertical reaction at the base on each wall for load combination 3, it is seen that the distribution is almost uniform and it is clear that reaction on eastern wall is higher than on the other walls.

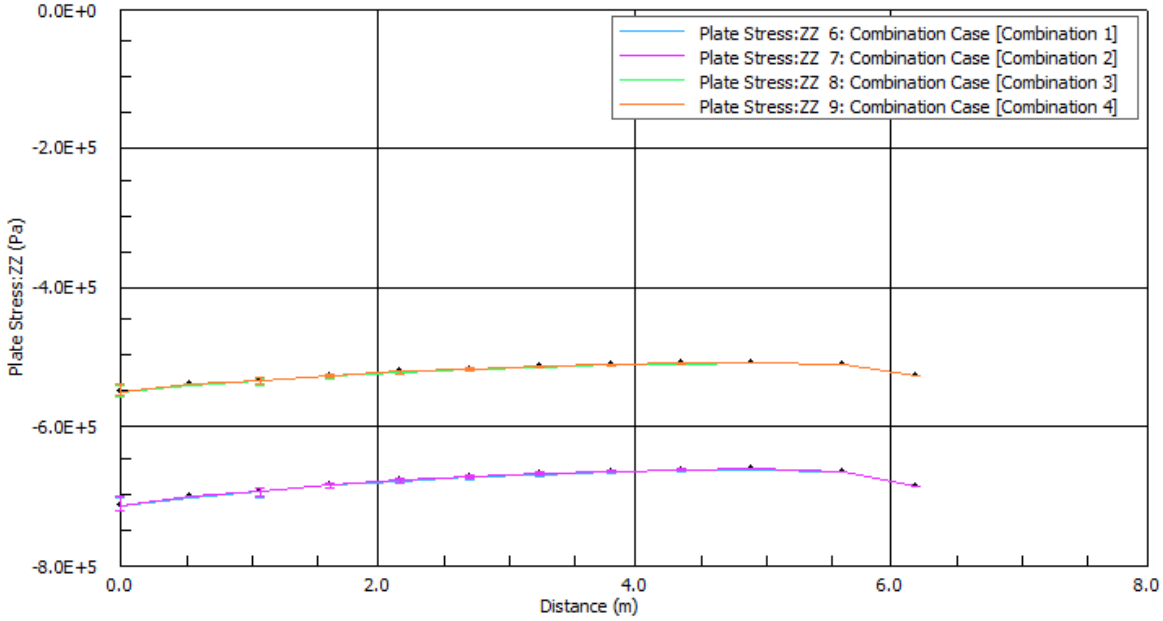

Figure 137. Distribution of stress at the base (eastern wall)

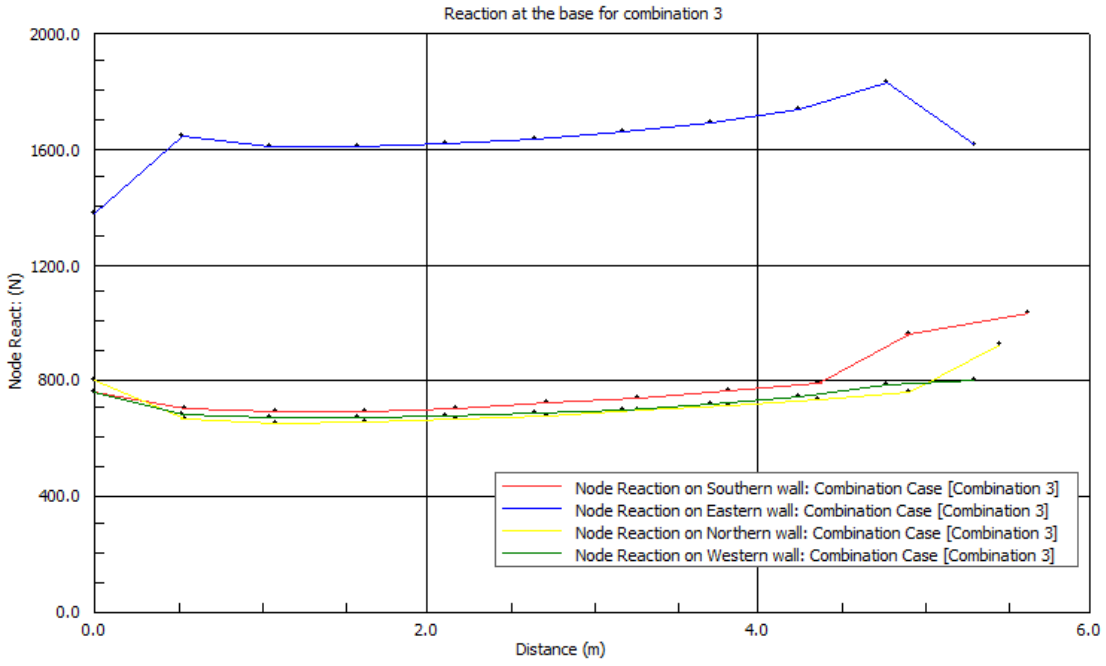

Figure 138. Vertical node reaction on each wall at the base of the tower (combination 3)

Table 97 shows reactions and the stress state at critical points for all the load combinations, the maximum compression stress is 0.713 MPa at the base of the tower, it corresponds to the load combination 1. The design compression strength of the tower is 0.94 MPa (section 6.7.3); therefore, the compression stress is less than 75% of the compression strength.

Table 97. Results of static analysis for each load combination

Load combination		**Comb. 1**	Comb. 2	**Comb. 3**	Comb. 4
Reaction at base	**N (KN)**	**39270.8**	39206.1	**29105.9**	29062.7
Maximum stress at base - eastern wall	**$\sigma_{zz,base}$ (MPa)**	**-0.713**	-0.712	**-0.555**	-0.554
Stress at level +21.8 m - eastern wall (tilted side)	**$\sigma_{zz,+21.8}$ (MPa)**	**-0.569**	-0.566	**-0.405**	-0.403
Stress at level +21.8 m - western wall	**$\sigma_{zz,+21.8}$ (MPa)**	**-0.341**	-0.340	**-0.291**	-0.290

8.3.2.4 Displacement at top

The deformed shape and contour plot of both vertical and horizontal displacement for combination 1 is presented below.

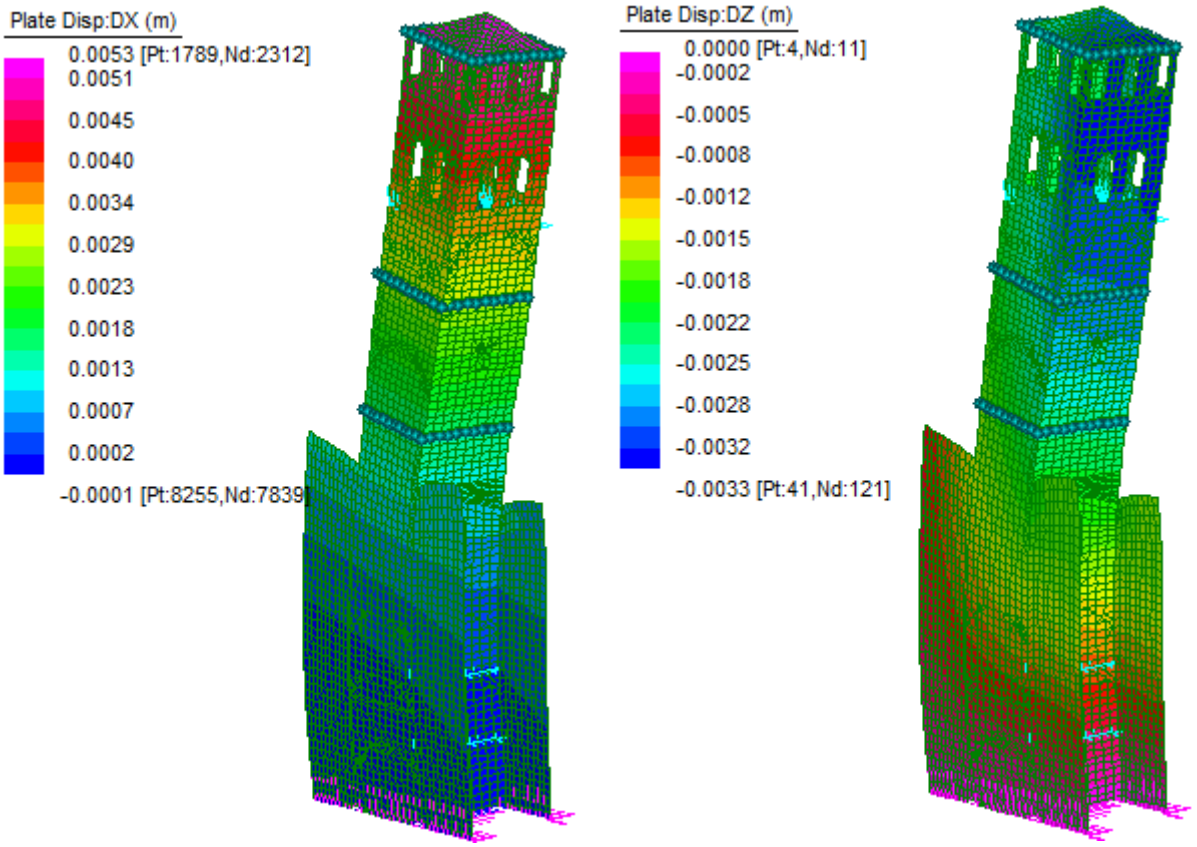

Figure 139. Deformed shape and contour plot of displacement for load combination 1(south-east view). Left: Horizontal displacement. Right: Vertical displacement

Table 98 shows the displacement at top in all directions for the 4 load combinations. The maximum displacement is 5.0 mm and it occurs in direction west-east for combinations 1 and 2.

Table 98. Displacement at top

Displacement at top (mm)				
Direction	**Comb. 1**	**Comb. 2**	**Comb. 3**	**Comb. 4**
Displacement W-E (DX)	5.0	5.0	1.9	1.9
Displacement S-N (DY)	0.6	0.6	0.5	0.5
Vertical displacement (DZ)	-3.3	-3.3	2.3	2.3

8.3.3 Modal Spectral Analysis

The spectral modal analysis determines the response of a structure subjected to a dynamic loading defined as a response or design spectrum. For each representative natural frequency, the modal response of the structure is calculated.

The base excitation spectrum is applied as a translational excitation at the base, equally at all fixed degrees of freedom. The spectrum simulates a random dynamic loading applied to the structure.

The description of generation of the design spectrum based on NTC-2008 is presented in section 5.4 (seismic action). Table 99 shows the parameters of the design spectrum and Figure 140 shows the design spectrum for ULS which was introduced to *Strauss7.*

The action of the earthquake was applied in two horizontal directions X (west-east) and Y (north-south) using the following spectral cases:

Main direction of motion: X	**Main direction of motion: Y**
$X + 0.3Y$	$0.3\,X + Y$
$X - 0.3Y$	$-0.3\,X + Y$
$-X + 0.3Y$	$0.3\,X - Y$
$-X - 0.3Y$	$-0.3\,X - Y$

Table 99. Parameters for calculation of design spectrum based on NTC-2008

Parameters to calculate the seismic action (NTC-2008)

Location	
Region:	Veneto
Province:	Padova
Municipality:	Padova
Nominal life (V_N)	50 years
Class of use:	III

Seismic Hazard Parameters

		Damage Limit State (DLS)	**Ultimate Limit State (ULS)**
T_R	years	75	**712**
a_g	**(g)**	0.043	0.099
T_c*	**(s)**	0.279	0.342
F_o		2.534	2.597

Soil Type and Topographic Condition

		Damage Limit State (DLS)	**Ultimate Limit State (ULS)**
S		1.2	1.2
T_B	**(s)**	0.132	0.155
T_c	**(s)**	0.396	0.466
T_D	**(s)**	1.773	1.995

Subsoil category	B
Topographic condition	T1
Structure factor q	3.6

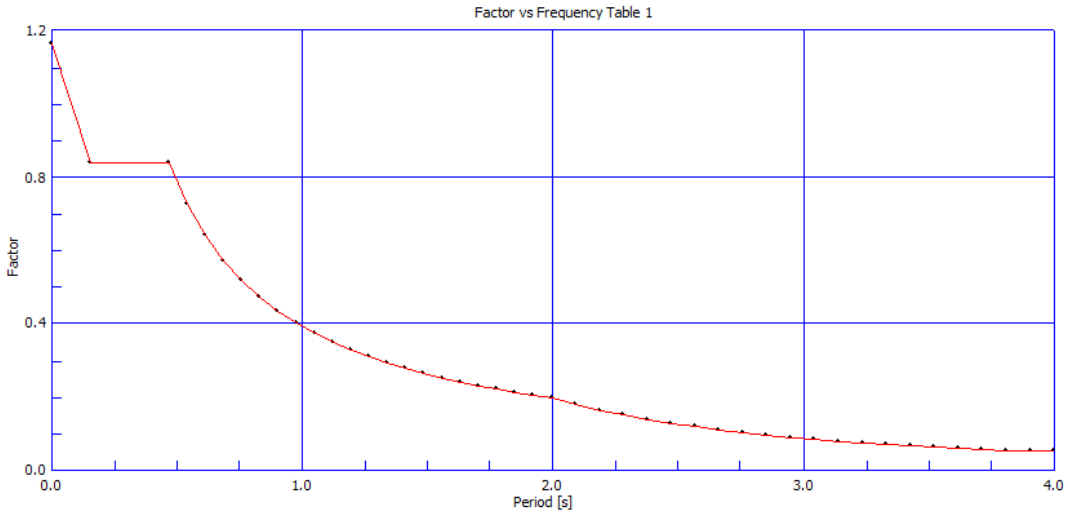

Figure 140. Design spectrum for ULS affected by structure factor q (units in m/s^2)

The representative natural frequencies of the tower used in the modal analysis are shown in Table 94. The modal responses have been combined using SRSS method (square root of the sum of the squares) since the difference between natural periods resulted to be higher than 10%.

The maximum response of the structure subjected mainly to motion in direction X (west-east) was obtained with the spectral case X+0.3Y, while for motion in direction Y (north-south), the maximum response corresponded to spectral case 0.3X+Y. Anyway, the responses for all cases, corresponding to the same main motion direction, were very close each other.

Total mass participation for motion in direction X (west-east) was 85.7% and for motion in direction Y (north-south) was 87.2%:

Table 100. Modal results of spectral case X+0.3Y

EXCITATION FACTORS FOR CASE 1: "x+0.3y"

Mode	Spectral Value	Excitation	Amplitude	Participation (%)
1	6.153896E-01	3.566636E+02	2.258934E+00	3.797
2	7.599767E-01	1.183354E+03	6.079988E+00	41.802
3	8.418599E-01	2.401175E+02	1.204384E-01	1.721
4	8.674481E-01	8.507553E+02	3.722141E-01	21.606
7	1.007689E+00	1.632521E+02	2.277203E-02	0.796
8	1.019254E+00	5.215650E+02	6.297081E-02	8.121
10	1.060969E+00	1.146888E+02	7.220335E-03	0.393
11	1.069372E+00	4.126552E+02	2.201016E-02	5.083
15	1.089746E+00	8.540390E+01	2.824553E-03	0.218
16	1.094804E+00	2.689615E+02	7.729169E-03	2.159

TOTAL MASS PARTICIPATION: 85.696%

Table 101. Modal results of spectral case 0.3X+Y

EXCITATION FACTORS FOR CASE 5: "0.3x+1y"

Mode	Spectral Value	Excitation	Amplitude	Participation (%)
1	6.153896E-01	1.215853E+03	7.700626E+00	44.129
2	7.599767E-01	3.624776E+02	1.862384E+00	3.922
3	8.418599E-01	8.204426E+02	4.115184E-01	20.094
4	8.674481E-01	2.614063E+02	1.143679E-01	2.040
7	1.007689E+00	5.339713E+02	7.448360E-02	8.511
8	1.019254E+00	1.553120E+02	1.875149E-02	0.720
10	1.060969E+00	3.893490E+02	2.451181E-02	4.525
11	1.069372E+00	1.260346E+02	6.722422E-03	0.474
15	1.089746E+00	2.913702E+02	9.636452E-03	2.534
16	1.094804E+00	8.466148E+01	2.432924E-03	0.214

TOTAL MASS PARTICIPATION: 87.165%

The final response of the structure was obtained using the seismic combination, presented in section 5.5, combining permanent, imposed and seismic loads.

The following figures show the deformed shapes of the tower and contour plot of displacements for both motion directions (considering SRSS envelope and seismic combination).

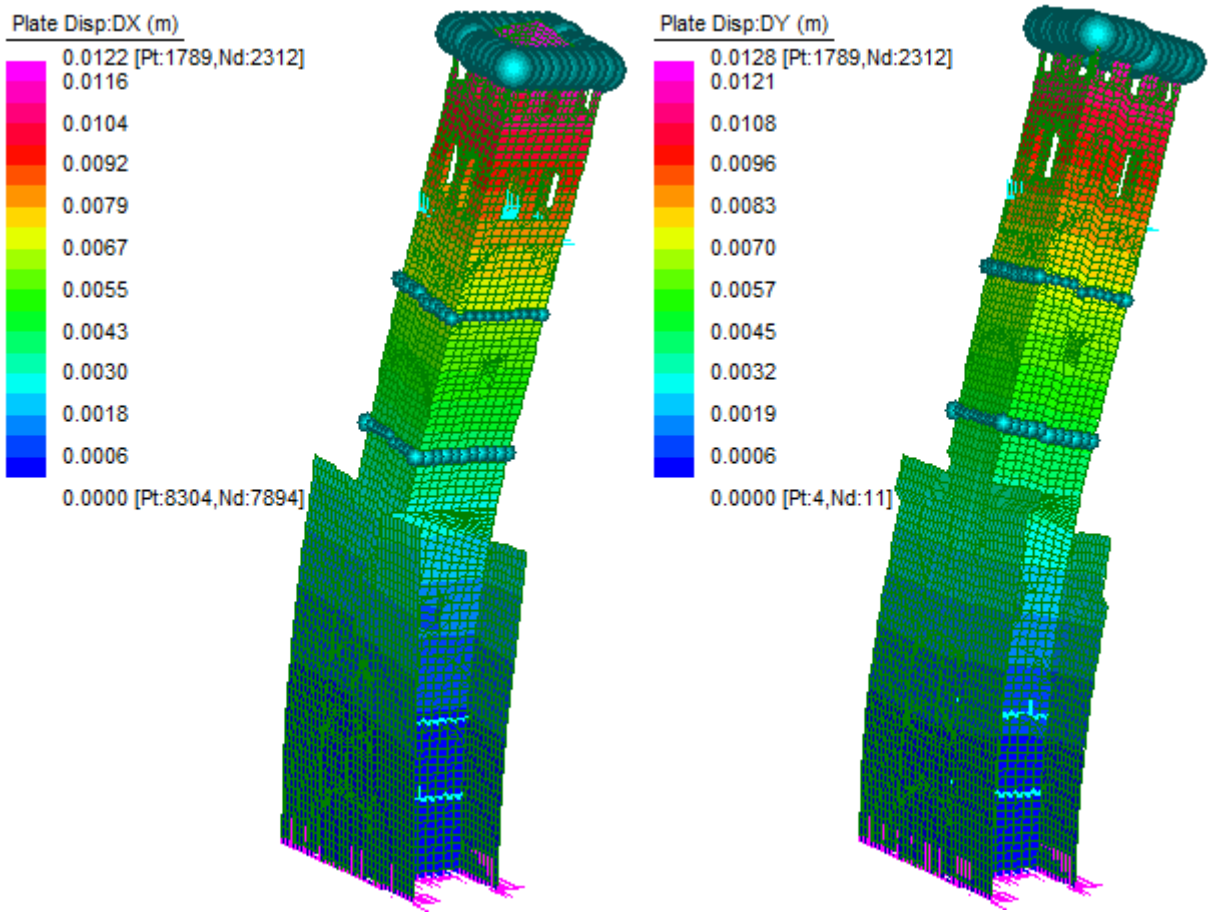

Figure 141. Deformed shape and contour plot of horizontal displacement (south-east view)
Left: Displacement W-E for motion direction in X. Right: Displacement N-S for motion in direction in Y.

The maximum displacements at top for both static and dynamic analysis are shown in the table below, maximum displacement occurs in N-S direction, corresponding to 12.8 mm.

Table 102. Displacement at top of the tower

Displacement at top (mm)		
Direction	**Static Analysis (under permanent load)**	**Dynamic Analysis**
Displacement W-E (DX)	1.9	12.2
Displacement N-S (DY)	0.5	12.8

Next figures show vertical stress distribution of the tower subjected to ground motion in both directions:

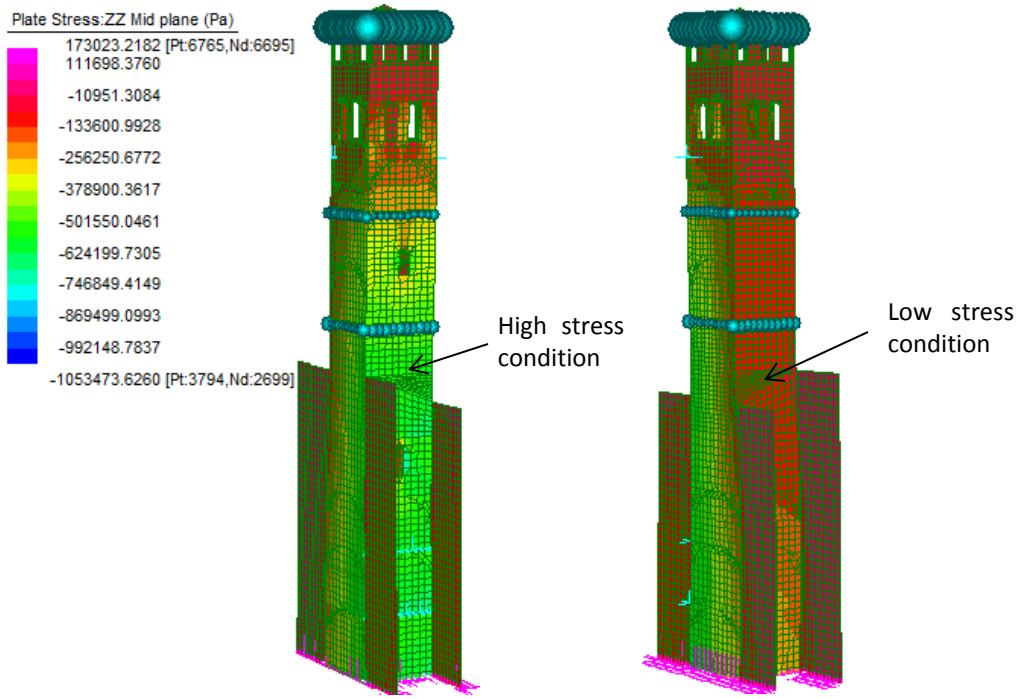

Figure 142. Contour plot of vertical stress for ground motion direction X (west-east)
Left: South-east view. Right: North-west view

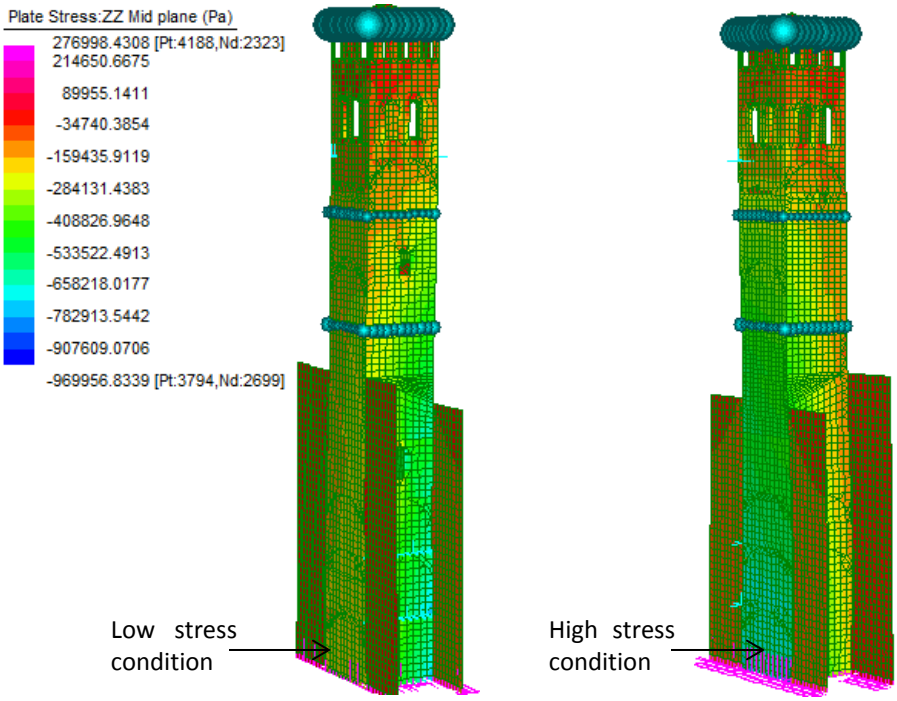

Figure 143. Contour plot of vertical stress for ground motion direction Y (north-south)
Left: South-east view. Right: North-west view

It is seen that when the earthquake acts in west-east direction, the eastern wall (tilted side) is subjected to high level of stress around the upper part of the adjacent wall, while the western wall is subjected to low stress. In the same way, when the earthquake acts in north-south direction, the northern wall is subjected to high level of stress at the base, while the southern wall is undergone to low stress state.

This fact causes a slope in the stress distribution on walls which are parallel to the ground motion which can cause important bending moment. This phenomenon is showed clearly in the following stress distribution plots of some sections (notice that maximum compression stress is slightly lower than 85% of compression strength):

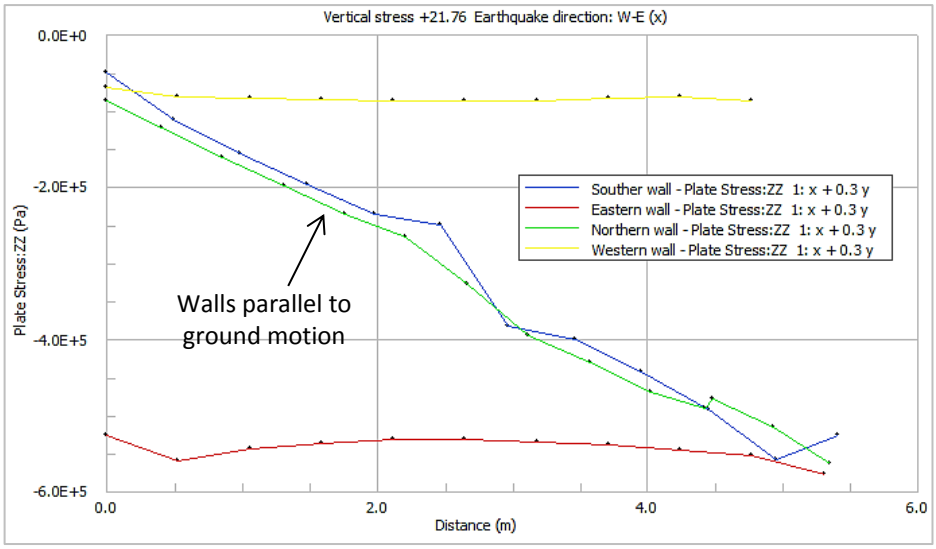

Figure 144. Vertical stress distribution for all walls at level +21.76 m – Motion direction: west-east (X)

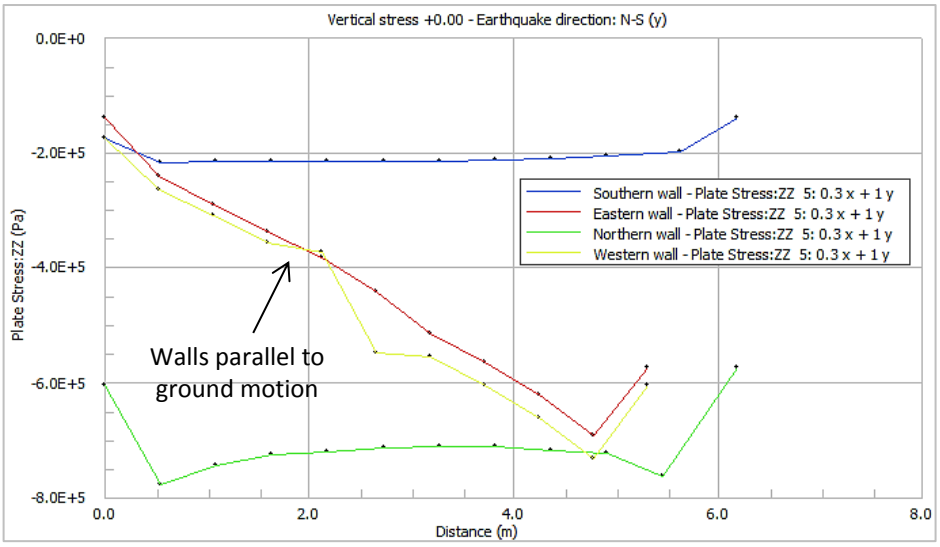

Figure 145. Vertical stress distribution for all walls at level +0.00 m – Motion direction: north-south (Y)

Shear stress distribution depends as well on the direction of ground motion; just the walls located parallel to the ground motion are subjected to shear stress, the walls located perpendicular to the ground motion resist almost cero (Figure 146). The shear stress distribution is almost parabolic.

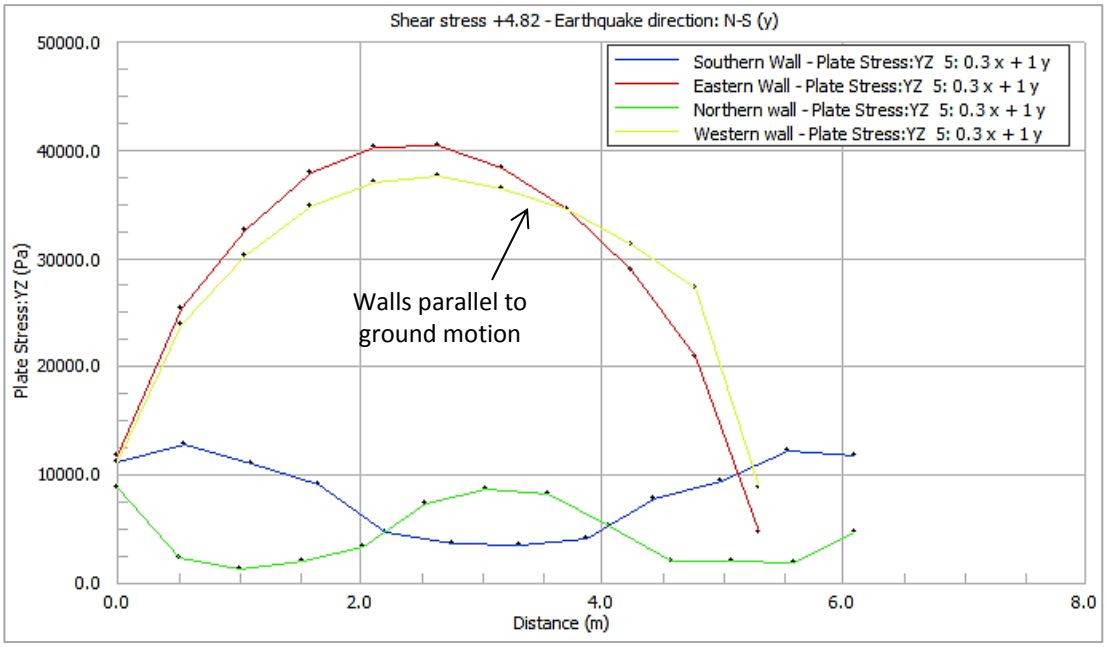

Figure 146. Shear stress distribution YZ for all walls at level +4.82 m – Motion direction: north-south (Y)

Since safety verifications must be done for both moment and shear at different height levels, the distribution of vertical stress (σ_{zz}) and shear stress ($\sigma_{yz,xz}$) pear each wall and each motion direction were obtained for all the 11 levels of the tower; the corresponding graphs are presented in APPENDIX 5.

Once the stress distribution on each wall has been determined, normal forces, bending moments and shear forces can be obtained by means of the following expression:

Normal force acting on each section is given by:

$$\boldsymbol{N = \int \sigma_{zz}\, dA = b \int_0^l \sigma_{zz}(x)\ dx} \qquad (83)$$

Shear force acting on each section is given by:

$$\boldsymbol{V_a = \int \sigma_{yz,xy}\, dA = b \int_0^l \sigma_{yz,xy}(x)\ dx} \qquad (84)$$

The acting moment on each section is given by:

$$\boldsymbol{M_a = b \int_0^l \sigma_{zz}(x)\ x\, dx} \qquad (85)$$

Where b is the thickness of the wall. The integral of the stress distribution function has been determined as the area under the corresponding curves (obtained with *Strand7*).

Figure 147 and Figure 148 show the distribution of axial force on all four walls through the tower height. The maximum and minimum axial force are developed when the wall is perpendicular to the motion direction, for example for northern wall, the minimum axial force occurs in motion direction W-E, while the maximum force occurs in motion direction N-S. Regardless to the direction of the earthquake, the eastern wall is subjected to higher axial force.

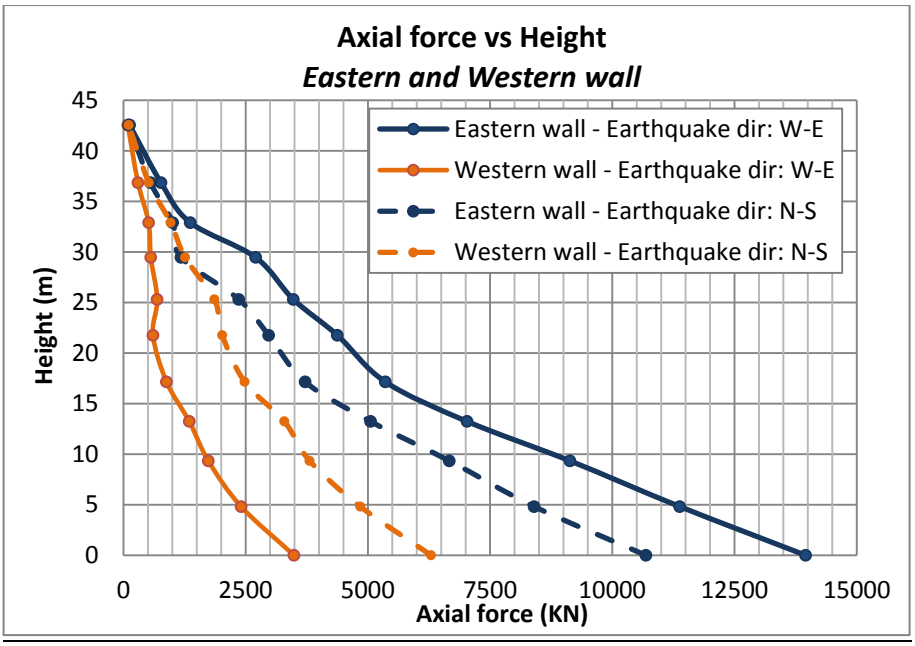

Figure 147. Axial force distribution on eastern and western wall through tower height

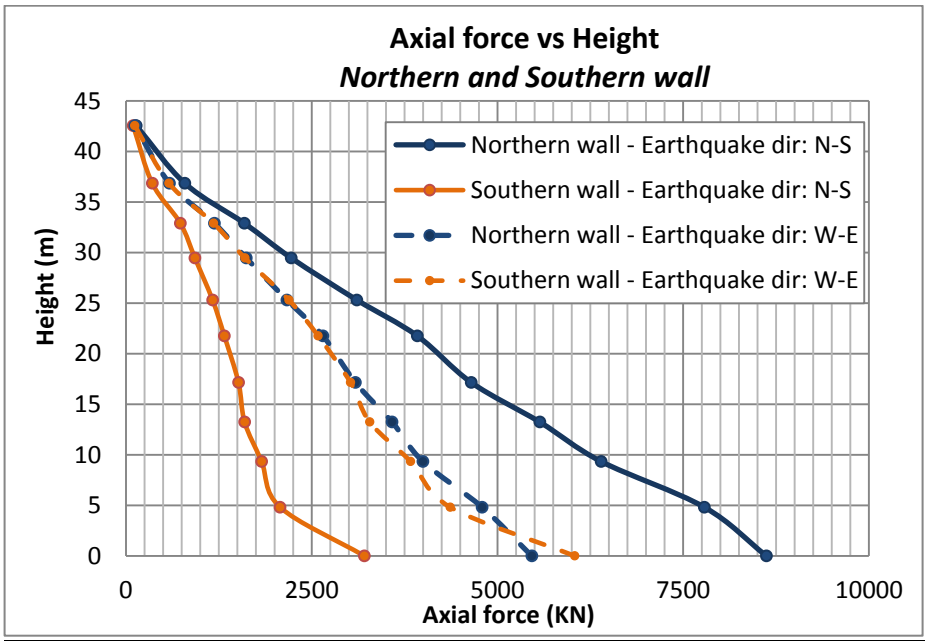

Figure 148. Axial force distribution on northern and southern wall through tower height

Figure 149 and Figure 150show the bending moment distribution on all four walls through height of the tower. It is clear that the maximum bending moment is produced when the motion direction is parallel to the wall, in fact when the motion direction is perpendicular to the wall, the moment is very low (sometimes almost cero).

Maximum moment is developed at the base of the tower and it decreases through height; however on lower part of northern and southern wall, moment tends to be constant due to the adjacent wall constraint.

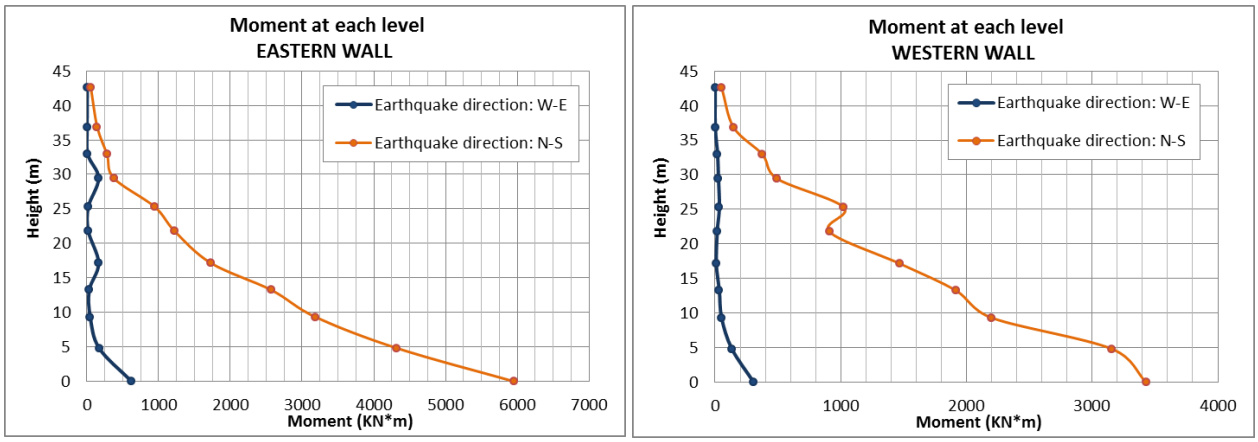

Figure 149. Bending moment through height for both motion directions. Left: Eastern wall. Right: Western wall

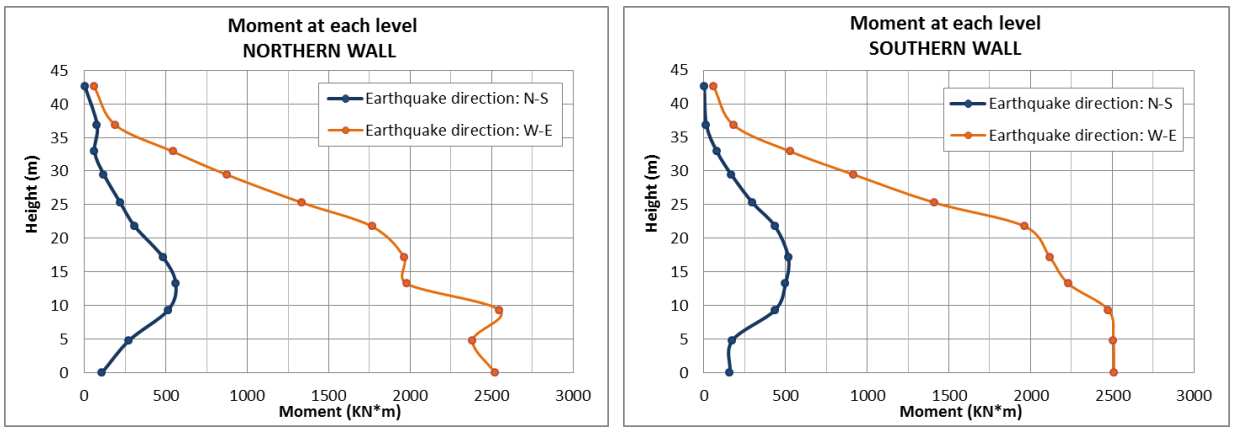

Figure 150. Bending moment through height for both motion directions. Left: Northern wall. Right: Southern wall

Figure 151 shows the shear force distribution through the tower height considering both motion directions, the distribution for northern and southern walls is very close each other, the same happen with eastern and western walls.

It is important to notice that for northern and southern walls, the maximum shear force does not occur at the base and it seems to be strongly affected by the adjacent wall. The maximum shear corresponds to 550 kN at the base.

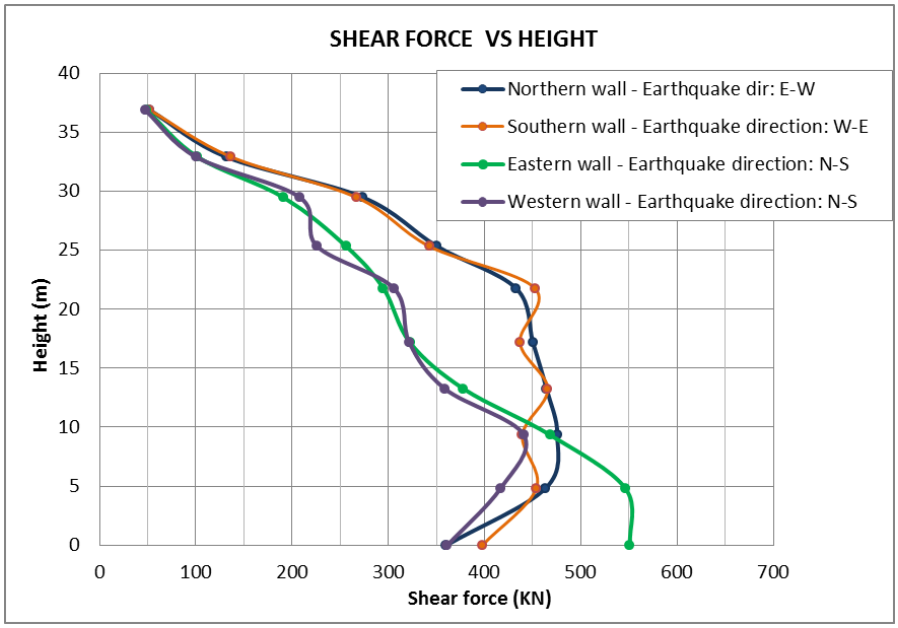

Figure 151. Shear force distribution through tower height

8.4 Safety Verifications

Procedure for safety verifications has been explained in section 8.1.6; it must be done for bending moment and shear force at different heights by comparing the calculated acting agent with the ultimate resistance capacity of the masonry assuming that it is not resistant to traction.

Table 103 shows the bending moment verification for each wall at different levels and for both motion directions. The tower is almost totally verified except for 3 sections: eastern wall at levels +0.00 m and +4.82 m and western wall at level +0.00, both of them for ground motion direction N-S, presenting safety factors of 0.9, 0.6 and 0.7 respectively.

Table 104 shows the shear verification for each wall at different levels and also for both motion directions. It is seen that the tower is totally verified presenting an average safety factor of 3.4.

Table 103. Safety verification by bending moment

Level	Wall	Thickness (m)	Effective Length (m)	Direction of earthquake	Max σ_{zz} (MPa)	Min σ_{zz} (MPa)	Area under σ_{zz} (MPa*m)	N (KN)	M_a (KN*m)	M_u (KN*m)	VERIFICATION	SF
0.00	East	4.39	5.24	x (E-W)	-0.71	-0.57	3.18	13955.59	622.20	4929.34	VERIFIED	7.9
4.82	East	3.34	5.26	x (E-W)	-0.66	-0.63	3.41	11379.11	169.96	5315.63	VERIFIED	31.3
9.34	East	2.90	5.35	x (E-W)	-0.62	-0.58	3.15	9133.06	45.54	5658.75	VERIFIED	124.2
13.24	East	2.34	5.22	x (E-W)	-0.60	-0.41	3.00	7027.61	32.09	4721.84	VERIFIED	147.1
17.15	East	1.62	5.35	x (E-W)	-0.68	-0.50	3.31	5356.37	162.38	2353.13	VERIFIED	14.5
21.76	East	1.51	5.35	x (E-W)	-0.59	-0.53	2.90	4376.30	18.75	3311.79	VERIFIED	176.6
25.31	East	1.33	5.49	x (E-W)	-0.51	-0.48	2.61	3474.39	18.84	3685.26	VERIFIED	195.6
29.46	East	1.17	5.59	x (E-W)	-0.45	-0.41	2.31	2703.90	162.32	3584.64	VERIFIED	22.1
32.90	East	1.14	5.65	x (E-W)	-0.27	-0.24	1.20	1366.83	11.32	3234.08	VERIFIED	285.8
36.85	East	0.98	5.74	x (E-W)	-0.18	-0.11	0.78	767.10	2.47	2220.50	VERIFIED	900.2
42.55	East	0.57	6.04	x (E-W)	-0.05	-0.03	0.22	124.74	3.91	445.31	VERIFIED	114.0
0.00	North	1.88	5.91	x (E-W)	-0.71	-0.32	2.91	5461.71	2521.59	2685.31	VERIFIED	1.1
4.82	North	1.84	5.17	x (E-W)	-0.66	-0.20	2.60	4792.61	2383.56	2831.12	VERIFIED	1.2
9.34	North	1.78	5.34	x (E-W)	-0.62	-0.15	2.24	3995.74	2548.90	3460.33	VERIFIED	1.4
13.24	North	1.83	5.26	x (E-W)	-0.60	-0.12	1.96	3581.62	1979.86	3749.53	VERIFIED	1.9
17.15	North	1.65	5.79	x (E-W)	-0.58	-0.09	1.87	3087.94	1962.63	4364.62	VERIFIED	2.2
21.76	North	1.51	5.34	x (E-W)	-0.56	-0.09	1.76	2650.51	1766.00	3578.84	VERIFIED	2.0
25.31	North	1.34	5.29	x (E-W)	-0.51	-0.10	1.62	2166.70	1334.26	3461.91	VERIFIED	2.6
29.46	North	1.21	5.62	x (E-W)	-0.35	-0.10	1.34	1618.19	874.40	3760.48	VERIFIED	4.3
32.90	North	1.13	5.65	x (E-W)	-0.27	-0.09	1.05	1189.63	542.81	3205.71	VERIFIED	5.9
36.85	North	0.98	5.8	x (E-W)	-0.22	-0.08	0.60	585.70	188.38	2627.34	VERIFIED	13.9
42.55	North	0.57	6.06	x (E-W)	-0.05	-0.01	0.21	119.95	57.88	535.57	VERIFIED	9.3
0.00	South	2.45	5.91	x (E-W)	-0.64	-0.26	2.47	6039.71	2510.83	5493.05	VERIFIED	2.2
4.82	South	1.65	5.17	x (E-W)	-0.66	-0.18	2.65	4364.33	2507.65	2536.89	VERIFIED	1.0
9.34	South	1.73	5.34	x (E-W)	-0.62	-0.14	2.21	3830.52	2477.50	3462.64	VERIFIED	1.4
13.24	South	1.72	5.26	x (E-W)	-0.59	-0.12	1.91	3280.60	2232.81	3625.53	VERIFIED	1.6

17.15	South	1.67	5.79	x (E-W)	-0.56	-0.09	1.81	3022.95	2119.43	4703.40	VERIFIED	2.2
21.76	South	1.49	5.34	x (E-W)	-0.59	-0.06	1.74	2586.17	1966.20	3255.72	VERIFIED	1.7
25.31	South	1.36	5.29	x (E-W)	-0.51	-0.09	1.61	2192.71	1411.88	3498.82	VERIFIED	2.5
29.46	South	1.24	5.62	x (E-W)	-0.36	-0.09	1.29	1600.59	919.06	3873.29	VERIFIED	4.2
32.90	South	1.13	5.65	x (E-W)	-0.26	-0.09	1.04	1178.90	530.29	3170.53	VERIFIED	6.0
36.85	South	0.98	5.8	x (E-W)	-0.22	-0.08	0.59	579.13	181.03	2622.62	VERIFIED	14.5
42.55	South	0.57	6.06	x (E-W)	-0.06	-0.01	0.21	118.68	59.56	574.39	VERIFIED	9.6
0.00	West	2.40	5.24	x (E-W)	-0.32	-0.26	1.45	3487.94	307.90	6301.58	VERIFIED	20.5
4.82	West	2.21	5.26	x (E-W)	-0.21	-0.18	1.09	2406.38	133.74	4784.37	VERIFIED	35.8
9.34	West	2.06	5.35	x (E-W)	-0.16	-0.14	0.84	1735.95	51.41	3842.50	VERIFIED	74.7
13.24	West	1.98	5.22	x (E-W)	-0.13	-0.12	0.68	1347.21	33.59	2970.79	VERIFIED	88.4
17.15	West	1.66	5.35	x (E-W)	-0.10	-0.09	0.53	880.13	9.73	2155.58	VERIFIED	221.6
21.76	West	1.51	5.35	x (E-W)	-0.09	-0.07	0.40	603.39	16.87	1673.25	VERIFIED	99.2
25.31	West	1.36	5.49	x (E-W)	-0.10	-0.09	0.51	690.28	33.96	1787.75	VERIFIED	52.6
29.46	West	1.18	5.59	x (E-W)	-0.10	-0.09	0.47	558.47	27.04	1574.60	VERIFIED	58.2
32.90	West	1.14	5.65	x (E-W)	-0.09	-0.07	0.45	514.81	20.14	1501.66	VERIFIED	74.5
36.85	West	0.99	5.74	x (E-W)	-0.08	-0.04	0.30	297.32	1.73	1181.17	VERIFIED	681.4
42.55	West	0.57	6.04	x (E-W)	-0.04	-0.02	0.16	88.59	0.81	374.79	VERIFIED	461.1
0.00	East	4.39	5.24	y (N-S)	-0.69	-0.20	2.43	10689.00	5955.95	5649.61	NO VERIFIED	0.9
4.82	East	3.34	5.26	y (N-S)	-0.74	-0.22	2.52	8401.29	4322.53	2502.35	NO VERIFIED	0.6
9.34	East	2.90	5.35	y (N-S)	-0.68	-0.22	2.30	6666.20	3187.90	4333.27	VERIFIED	1.4
13.24	East	2.34	5.22	y (N-S)	-0.63	-0.22	2.16	5054.31	2572.31	4316.55	VERIFIED	1.7
17.15	East	1.62	5.35	y (N-S)	-0.62	-0.24	2.29	3716.24	1730.00	3165.65	VERIFIED	1.8
21.76	East	1.51	5.35	y (N-S)	-0.55	-0.22	1.97	2970.64	1224.11	3693.64	VERIFIED	3.0
25.31	East	1.33	5.49	y (N-S)	-0.48	-0.20	1.77	2358.21	944.44	3822.46	VERIFIED	4.0
29.46	East	1.17	5.59	y (N-S)	-0.30	-0.16	1.01	1177.18	374.01	3413.40	VERIFIED	9.1
32.90	East	1.14	5.65	y (N-S)	-0.25	-0.13	0.88	1008.13	279.76	3147.74	VERIFIED	11.3
36.85	East	0.98	5.74	y (N-S)	-0.15	-0.08	0.57	554.20	143.15	2016.81	VERIFIED	14.1
42.55	East	0.57	6.04	y (N-S)	-0.05	-0.01	0.18	105.32	54.03	500.91	VERIFIED	9.3

0.00	North	1.88	5.91	y (N-S)	-0.75	-0.71	4.58	8619.61	105.78	1400.04	VERIFIED	13.2
4.82	North	1.84	5.17	y (N-S)	-0.74	-0.66	4.23	7784.38	272.62	1331.77	VERIFIED	4.9
9.34	North	1.78	5.34	y (N-S)	-0.68	-0.55	3.59	6394.87	512.32	2649.80	VERIFIED	5.2
13.24	North	1.83	5.26	y (N-S)	-0.63	-0.49	3.04	5569.63	559.84	3427.70	VERIFIED	6.1
17.15	North	1.65	5.79	y (N-S)	-0.57	-0.45	2.82	4647.20	482.83	4564.58	VERIFIED	9.5
21.76	North	1.51	5.34	y (N-S)	-0.54	-0.44	2.60	3920.99	308.62	3782.98	VERIFIED	12.3
25.31	North	1.34	5.29	y (N-S)	-0.48	-0.41	2.32	3107.51	218.59	3575.72	VERIFIED	16.4
29.46	North	1.21	5.62	y (N-S)	-0.34	-0.31	1.84	2224.37	118.36	3731.47	VERIFIED	31.5
32.90	North	1.13	5.65	y (N-S)	-0.26	-0.23	1.41	1593.08	60.83	3142.85	VERIFIED	51.7
36.85	North	0.98	5.8	y (N-S)	-0.17	-0.12	0.81	792.38	76.46	2200.08	VERIFIED	28.8
42.55	North	0.57	6.06	y (N-S)	-0.07	-0.03	0.24	137.84	2.05	628.25	VERIFIED	307.1
0.00	South	2.45	5.91	y (N-S)	-0.22	-0.20	1.31	3208.56	159.78	6866.96	VERIFIED	43.0
4.82	South	1.65	5.17	y (N-S)	-0.22	-0.16	1.26	2073.68	173.75	3498.08	VERIFIED	20.1
9.34	South	1.73	5.34	y (N-S)	-0.22	-0.13	1.06	1825.21	435.19	3930.94	VERIFIED	9.0
13.24	South	1.72	5.26	y (N-S)	-0.22	-0.11	0.93	1596.40	499.09	3837.96	VERIFIED	7.7
17.15	South	1.67	5.79	y (N-S)	-0.22	-0.10	0.91	1514.32	517.14	4479.19	VERIFIED	8.7
21.76	South	1.49	5.34	y (N-S)	-0.22	-0.10	0.89	1323.90	436.52	3402.29	VERIFIED	7.8
25.31	South	1.36	5.29	y (N-S)	-0.20	-0.11	0.86	1165.73	296.99	2856.79	VERIFIED	9.6
29.46	South	1.24	5.62	y (N-S)	-0.15	-0.10	0.75	928.02	168.40	2399.21	VERIFIED	14.2
32.90	South	1.13	5.65	y (N-S)	-0.13	-0.10	0.65	731.96	79.55	1945.68	VERIFIED	24.5
36.85	South	0.98	5.8	y (N-S)	-0.08	-0.05	0.36	354.01	15.00	1237.69	VERIFIED	82.5
42.55	South	0.57	6.06	y (N-S)	-0.04	-0.03	0.17	96.56	1.55	362.53	VERIFIED	233.3
0.00	West	2.40	5.24	y (N-S)	-0.74	-0.22	2.62	6292.07	2709.00	1777.93	NO VERIFIED	0.7
4.82	West	2.21	5.26	y (N-S)	-0.66	-0.16	2.19	4845.46	3157.53	3452.31	VERIFIED	1.1
9.34	West	2.06	5.35	y (N-S)	-0.55	-0.13	1.85	3809.14	2199.66	5008.68	VERIFIED	2.3
13.24	West	1.98	5.22	y (N-S)	-0.49	-0.11	1.66	3290.17	1919.11	5085.56	VERIFIED	2.6
17.15	West	1.66	5.35	y (N-S)	-0.45	-0.10	1.49	2480.61	1471.49	4667.00	VERIFIED	3.2
21.76	West	1.51	5.35	y (N-S)	-0.44	-0.12	1.34	2022.02	909.58	4275.16	VERIFIED	4.7
25.31	West	1.36	5.49	y (N-S)	-0.42	-0.11	1.37	1860.71	1023.30	4087.24	VERIFIED	4.0

29.46	West	1.18	5.59	y (N-S)	-0.31	-0.10	1.07	1260.66	491.20	3483.61	VERIFIED	7.1
32.90	West	1.14	5.65	y (N-S)	-0.23	-0.10	0.85	964.50	378.71	2970.91	VERIFIED	7.8
36.85	West	0.99	5.74	y (N-S)	-0.15	-0.06	0.52	518.55	147.46	2030.63	VERIFIED	13.8
42.55	West	0.57	6.04	y (N-S)	-0.05	-0.01	0.19	107.86	52.99	497.18	VERIFIED	9.4

Table 104. Shear verification

Level	Wall	Thickness (m)	Effective Length (m)	Height (m)	b=h/l	Direction of earthquake	Max σ_{zz} (Mpa)	Min σ_{zz} (Mpa)	Max $\sigma_{zx,zy}$ (Mpa)	Area under $\sigma_{zx,zy}$ (Mpa*m)	V_a (KN)	V_t (KN*m)	VERIFICATION	SF
0.0.	North	1.84	5.17	4.82	1	x (E-W)	-0.66	-0.20	0.05	0.20	360.47	1505.27	VERIFIED	4.2
4.82	North	1.78	5.34	4.52	1	x (E-W)	-0.62	-0.15	0.08	0.26	463.34	1465.80	VERIFIED	3.2
9.34	North	1.83	5.26	3.9	1	x (E-W)	-0.60	-0.12	0.07	0.26	475.57	1459.53	VERIFIED	3.1
13.24	North	1.65	5.79	3.91	1	x (E-W)	-0.58	-0.09	0.07	0.28	464.40	1425.62	VERIFIED	3.1
17.15	North	1.51	5.34	4.61	1	x (E-W)	-0.56	-0.09	0.07	0.30	450.32	1184.23	VERIFIED	2.6
21.76	North	1.34	5.29	3.55	1	x (E-W)	-0.51	-0.10	0.07	0.32	432.83	993.25	VERIFIED	2.3
25.31	North	1.21	5.62	4.15	1	x (E-W)	-0.35	-0.10	0.06	0.29	350.88	802.57	VERIFIED	2.3
29.46	North	1.13	5.65	3.44	1	x (E-W)	-0.27	-0.09	0.05	0.24	274.00	666.67	VERIFIED	2.4
32.90	North	0.98	5.8	3.95	1	x (E-W)	-0.22	-0.08	0.03	0.13	131.86	545.58	VERIFIED	4.1
36.85	North	0.57	6.06	5.7	1	x (E-W)	-0.05	-0.01	0.03	0.09	52.61	197.65	VERIFIED	3.8
0.0.	South	1.65	5.17	4.82	1	x (E-W)	-0.66	-0.18	0.05	0.24	397.82	1349.96	VERIFIED	3.4
4.82	South	1.73	5.34	4.52	1	x (E-W)	-0.62	-0.14	0.07	0.26	453.78	1416.75	VERIFIED	3.1
9.34	South	1.72	5.26	3.9	1	x (E-W)	-0.59	-0.12	0.07	0.26	439.28	1362.57	VERIFIED	3.1
13.24	South	1.67	5.79	3.91	1	x (E-W)	-0.56	-0.09	0.06	0.28	465.58	1414.82	VERIFIED	3.0
17.15	South	1.49	5.34	4.61	1	x (E-W)	-0.59	-0.06	0.06	0.29	436.79	1196.59	VERIFIED	2.7
21.76	South	1.36	5.29	3.55	1	x (E-W)	-0.51	-0.09	0.08	0.33	452.48	1010.64	VERIFIED	2.2
25.31	South	1.24	5.62	4.15	1	x (E-W)	-0.36	-0.09	0.06	0.28	343.04	832.04	VERIFIED	2.4
29.46	South	1.13	5.65	3.44	1	x (E-W)	-0.26	-0.09	0.05	0.24	267.33	660.31	VERIFIED	2.5
32.90	South	0.98	5.8	3.95	1	x (E-W)	-0.22	-0.08	0.03	0.14	136.89	544.91	VERIFIED	4.0
36.85	South	0.57	6.06	5.7	1	x (E-W)	-0.06	-0.01	0.03	0.09	52.68	202.30	VERIFIED	3.8

0.0.	East	3.34	5.26	4.82	1	y (N-S)	-0.74	-0.22	0.04	0.17	551.23	2937.47	VERIFIED	5.3
4.82	East	2.9	5.35	4.52	1	y (N-S)	-0.68	-0.22	0.05	0.19	546.19	2483.08	VERIFIED	4.5
9.34	East	2.34	5.22	3.9	1	y (N-S)	-0.63	-0.22	0.09	0.20	468.02	1886.04	VERIFIED	4.0
13.24	East	1.62	5.35	3.91	1	y (N-S)	-0.62	-0.24	0.09	0.23	378.27	1336.18	VERIFIED	3.5
17.15	East	1.51	5.35	4.61	1	y (N-S)	-0.55	-0.22	0.05	0.21	322.69	1174.63	VERIFIED	3.6
21.76	East	1.33	5.49	3.55	1	y (N-S)	-0.48	-0.20	0.05	0.22	294.99	999.49	VERIFIED	3.4
25.31	East	1.17	5.59	4.15	1	y (N-S)	-0.30	-0.16	0.06	0.22	256.37	716.63	VERIFIED	2.8
29.46	East	1.14	5.65	3.44	1	y (N-S)	-0.25	-0.13	0.04	0.17	191.37	657.30	VERIFIED	3.4
32.90	East	0.98	5.74	3.95	1	y (N-S)	-0.15	-0.08	0.03	0.10	101.84	466.44	VERIFIED	4.6
36.85	East	0.57	6.04	5.7	1	y (N-S)	-0.05	-0.01	0.03	0.09	49.12	193.22	VERIFIED	3.9
0.0.	West	2.21	5.26	4.82	1	y (N-S)	-0.66	-0.16	0.04	0.16	361.45	1843.89	VERIFIED	5.1
4.82	West	2.06	5.35	4.52	1	y (N-S)	-0.55	-0.13	0.05	0.20	416.72	1606.13	VERIFIED	3.9
9.34	West	1.98	5.22	3.9	1	y (N-S)	-0.49	-0.11	0.05	0.22	440.77	1427.95	VERIFIED	3.2
13.24	West	1.66	5.35	3.91	1	y (N-S)	-0.45	-0.10	0.05	0.22	358.85	1175.74	VERIFIED	3.3
17.15	West	1.51	5.35	4.61	1	y (N-S)	-0.44	-0.12	0.06	0.21	321.88	1056.00	VERIFIED	3.3
21.76	West	1.36	5.49	3.55	1	y (N-S)	-0.42	-0.11	0.05	0.22	305.93	952.06	VERIFIED	3.1
25.31	West	1.18	5.59	4.15	1	y (N-S)	-0.31	-0.10	0.04	0.19	226.24	732.57	VERIFIED	3.2
29.46	West	1.14	5.65	3.44	1	y (N-S)	-0.23	-0.10	0.05	0.18	208.32	628.85	VERIFIED	3.0
32.90	West	0.99	5.74	3.95	1	y (N-S)	-0.15	-0.06	0.03	0.10	100.26	470.36	VERIFIED	4.7
36.85	West	0.57	6.04	5.7	1	y (N-S)	-0.05	-0.01	0.03	0.08	47.66	192.77	VERIFIED	4.0

8.5 Influence of Bell in Modal Analysis

In order to see how the bell does affect the dynamic response of the structure, the model was executed again removing the bell (modelled previously with a translational mass and rigid links). Natural frequencies obtained are shown in Table 105; it is seen that the same modes present representative mass participation and the frequencies are very similar each other.

Table 105. Natural frequencies and Mass participation including and no including the bell

Direction	Mode	Including Bell		With No Bell	
		Frequency (Hz)	Mass Particip. (%)	Frequency (Hz)	Mass Particip. (%)
Y North-South	1	1.569	48.31	1.572	48.23
	3	6.520	22.01	6.497	21.92
	7	13.530	9.24	13.450	9.34
	10	20.660	4.95	20.630	4.97
	15	28.890	2.78	28.580	2.53
X West-East	2	1.936	45.38	1.941	45.31
	4	7.087	23.44	7.080	23.41
	8	14.620	8.86	14.590	8.89
	11	22.540	5.52	22.530	5.56
	16	31.060	2.33	31.050	2.29

Table 106 shows the displacement at the top for both cases, the displacement just varies 0.1 mm for motion direction N-S.

Table 106. Displacement at top

Direction	INCLUDING BELL	NO BELL
Displacement W-E (DX)	12.2 mm	12.2 mm
Displacement N-S (DY)	12.8 mm	12.7 mm

Since the bell self-weight is 3.6 ton and the entire structure self-weight is 2879 ton, the bell does not affect considerably the dynamic response of the structure. Figure 152 shows vertical stress distribution of all walls at base of the tower for both cases, it is seen that the stress state remains almost the same (excluding some nodes in the corners which are out of tendency). In conclusion, the bell might not be an important element that affects the global vulnerability of the tower.

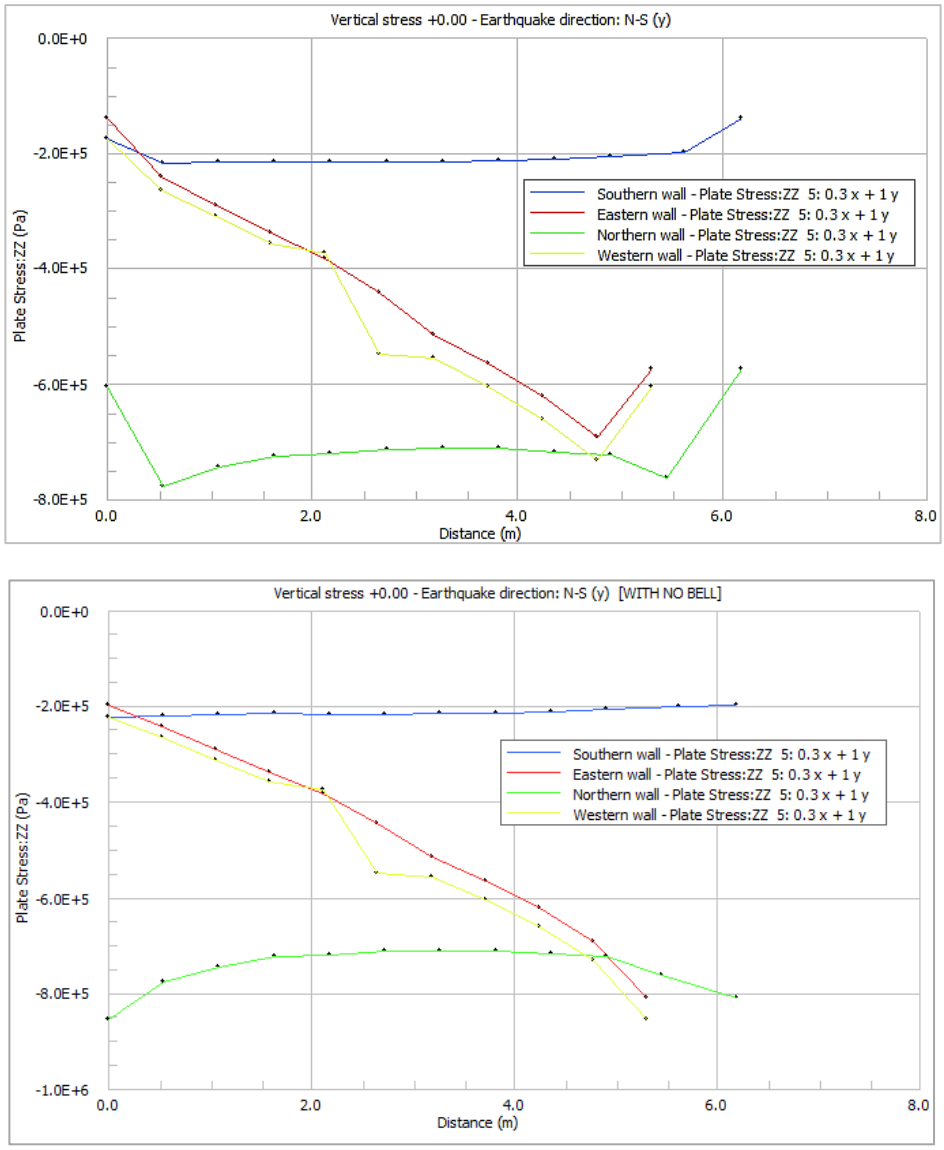

Figure 152. Vertical stress distribution at level +0.00 m for motion direction N-S
Above: Including Bell. Below: With No Bell

8.6 Conclusions

Global assessment was performed considering the seismic safety of the entire tower composed by several structural elements well connected each other. For this approach, Dynamic Modal Analysis by means of FEM was chosen following recommendations from literature about accurate seismic analysis on this kind of historical constructions.

It is important to remark that the model was calibrated by means of the known natural frequencies of vibration obtained in previous tests.

The safety verifications were made for bending moment and shear force for all walls at different heights. Table 109 shows the moment verification safety factors summary for each wall in the most critical earthquake direction.

Table 107. Safe factors for bending moment verification

Wall	Direction of earthquake	Maximum SF	Minimum SF	Average SF
North	x (E-W)	13.9	1.1	4.2
South	x (E-W)	20.5	1.0	5.6
East	y (N-S)	14.1	**0.6**	5.2
West	y (N-S)	13.8	**0.7**	5.1

In fact, safety factor average values are bigger than 1 in all analysis conditions; just three sections presented values between 0.6 and 0.9 which might be considered as satisfactory safety factors since mechanical properties of the brick masonry were assumed to be low and were affected by reduction factors. Additionally, the tower is completely verified for shear presenting an average safety factor of 3.4.

In summary, the tower is verified globally and it does not need urged structural intervention. Non-linear static analysis may be carried out but it usually provides higher values of safety factors because of consideration of material plasticity and possibility to cracking so it is not required.

Tower Anziani, as an historical masonry building, is much more vulnerable to local collapse mechanisms than to global ways of collapse. Therefore, Kinematic Limit Analysis is paramount for seismic assessment of all types of historic masonry structures before doing a complex global analysis.

Additionally, the bell might not be an important element that affects the global vulnerability of the tower, since it does not affect considerably the dynamic modal response of the tower, for this specific case.

9 CONCLUSIONS AND INTERVENTION PROPOSALS

The main objective of this work was to implement a methodology for seismic assessment where the Tower Anziani could be analyzed in two ways: locally and globally, taking into account the inspection and testing campaign performed.

- On one hand, local assessment was carried out by means of Kinematic Limit Analysis considering 5 possible collapse mechanisms which arise from the careful observation of this kind of masonry structures after earthquakes and the current state of the tower. Table 108 shows results summary.

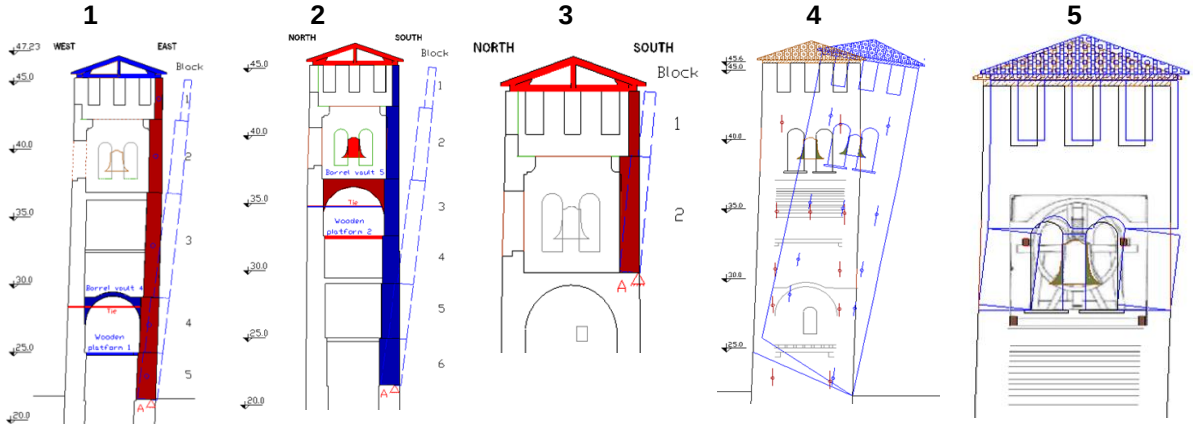

Figure 153. Analyzed collapse mechanisms

Table 108. Summary of kinematic analysis

Mech.	Type of mechanism	Element involved	Ties Required		Linear Analysis	Non-linear Analysis
			Under vaults	Extra		
1	Simple out of plane wall failure	Leaned eastern wall	**2**	**3**	No verified	**Verified**
2	Simple out of plane wall failure	Southern wall	**2**	**3**	No verified	**Verified**
3	Simple out of plane wall failure	Belfry and battlement	-	**1**	**Verified**	-
4	Global overturning	Tower above adjacent walls	-	-	**Verified**	-
5	Rigid rotation in-plane	Belfry pillars	-	-	**Verified**	-

It was found that all mechanisms type simple out of plane wall failure are verified only when the specified number of rod ties are included. Therefore, the assurance that those tie-rods are correctly set up, with geometrical and mechanical characteristics specified in this document, is paramount.

Intervention Proposal: The required tie-rods to make the elements stable are placed in the tower since 13th C (it is the only wall clamping technique used); however, during the inspection, it was found that most of them are affected by corrosion, so a deep study about the corrosion level is required.

When corrosion has affected the required effective cross area of a tie, it must be replaced by a new one with at least the geometrical and mechanical characteristics specified in the calculations on this document.

If ties do not need to be replaced, a protection intervention against rust might be performed. This intervention usually includes cleaning of the surface, application of a rust remover, cleaning again and application of a rust blocker.

- On the other hand, a global assessment was performed considering the seismic safety of the entire tower composed by several structural elements well connected each other. For this approach, Dynamic Modal Analysis by means of FEM was chosen following recommendations from literature about accurate seismic analysis on this kind of historical constructions.

  It is important to remark that the model was calibrated by means of the known natural frequencies of vibration obtained in previous tests.

  The safety verifications were made for bending moment and shear force for all walls at different heights. Table 109 shows the moment verification safety factors summary for each wall in the most critical earthquake direction.

Table 109. Safe factors for bending moment verification

Wall	Direction of earthquake	Maximum SF	Minimum SF	Average SF
North	x (E-W)	13.9	1.1	4.2
South	x (E-W)	20.5	1.0	5.6
East	y (N-S)	14.1	*0.6*	5.2
West	y (N-S)	13.8	*0.7*	5.1

In fact, safety factor average values are bigger than 1 in all analysis conditions; just three sections presented values between 0.6 and 0.9 which might be considered as satisfactory safety factors since mechanical properties of the brick masonry were assumed to be low and were affected by reduction factors. Additionally, the tower is completely verified for shear presenting an average safety factor of 3.4.

In summary, the tower is verified globally and it does not need urged structural intervention. Non-linear static analysis may be carried out but it usually provides higher values of safety factors because of consideration of material plasticity and possibility to cracking so it is not required.

- Tower Anziani as an historical masonry building is much more vulnerable to local collapse mechanisms than to global ways of collapse. Therefore, Kinematic Limit Analysis is paramount for seismic assessment of all types of historic masonry structures before doing a complex global analysis.

  It is important to mention that this type of analysis is widely used in Italy and some countries in Europe, but it is not widely implemented in many countries such as Colombia or Mexico where its use could be very useful for anlisisng cultural heritage. Therefore, publishing works about this methodology is essential for transmitting the knowledge.

- It was figured out that dynamic characterization test on tie-rods, under either environmental or forced vibration, is a quite useful tool to determine the natural frequencies and then the tension state.

  The results presented clearly evidence that the ties set up in 20th century are subjected to very low tension (almost inactive); in contrast, the original ties, installed during the construction of the tower, are active and subjected to important tension level.

  Although the ties from 20th C might work in a passive way and it is recommended to keep them, perhaps they will not behave adequately in presence of an earthquake because of unsatisfactory transmission of stress to the wall due to absence of anchor plates.

  On the other hand, since this type of test can't be performed on ties located very close to the walls or on those embedded into the masonry. It is highly recommended to verify the tension state on those ties utilizing other type of tests, for example by using electronic or fiber optic sensors.

- The bell might not be an important element that affects the global vulnerability of the tower, since it does not affect considerably the dynamic modal response of the tower, for this specific case.

- It was found that the mechanical properties values for masonry recommended by NTC2008 are quite conservative (much lower than real values); therefore, it is highly recommended to perform tests to get those values especially for compression strength and modulus of elasticity. Flat-jack test, a minor destructive technique, can be a good choice for this purpose.

- According to the static analysis, wind and snow actions do not affect significantly the behavior of the structure, producing very low stress.

- Tests made on timber ties (13th C) showed that they are affected from low to high decay level.

Intervention Proposal: Although those ties were not considered neither local nor global analysis, it is recommended to replace them by either normal tie-rods or replace just the timber element if the iron connectors are in good condition.

- According to inspection and testing campaign, the quality of the brick masonry is good; however, extensive biological colonization by pigeons and dropping deposits were found on the upper part of the tower.

  Intervention Proposal: Installation of protection nets on all openings, including windows and crenels from battlement, to prevent the entry of birds.

Additional recommendations

Once intervention proposals are carried out (especially tie-rod interventions), a rehabilitation project could be executed in order to open the tower to public who might be quite interested to visit it for many reasons including that Tower Anziani is an icon of the city, it is located on a strategic point of the city center of Padua, it is one of the highest structures nearby offering a beautiful view from the top, bells are not common structures to see closely, etc.

However, this rehabilitation project would have to include redesign of timber stairs and wooden platforms, adequacy of vaults to access to next levels, design of security measures for visitors, required installation systems, etc.

10 REFERENCES

[1] Brunelli, Bruno. Vicende della Torre degli Anziani, Stamperia Penada, Padua, 1940.

[2] Metralab servizi per l'ingegneria. Estratto del Rapporto Tecnico di Torre degli Anziani (Georadar test). Padua, September, 2004

[3] Metralab servizi per l'ingegneria. Caratterizzazione Dinamica di Torre degli Anziani (prova con energizzatore). Padua, September, 2004

[4] Studi e Diagnostica per i Beni Culturali. Caratterizzazione e studio petrografico dl 2 campioni di malta e laterizio prelevati dal campanile "Torre degli Anziani" a padova. Padua, November, 2005

[5] Briseghella, Lamberto. Relazione generale Comune di Padova la Torre degli Anziani (Genral report). Padua, October, 2005.

[6] NTC- NORME TECNICHE CONSTRUZIONI DM 14-01-08. Republic of Italy, 2008.

[7] EUROCODE en.1991. Part 1-3: Snow loads. Part 1-4: Wind actions.

[8] CIRCOLARE 2-02-09. Ministero delle Infrastrutture e dei Trasporti. Circolare del Ministero delle Infrastrutture e dei Trasporti n.617 del 2/2/09. Istruzioni per l'applicazione delle «Nuove norme tecniche per le costruzioni» di cui al decreto ministeriale, February 2nd, 2009.

[9] Briseghella, Lamberto. Relazione di Calcolo Comune di Padova la Torre degli Anziani. Padua, October, 2005.

[10] http://esse1.mi.ingv.it/

[11] Bento, R., Falcao, S., Rodrigues, F. Non-linear Static Procedures in Performance Based Seismic Design. 13th World Conference on Earthquake Engineering. Vancouver, B.C., Canada. 2004.

[12] Naeim, F., Bhatia, H., Lobo, R.M. Performance Based Seismic Engineering, chapter 15. Los Angeles, California. 2004.

[13] Fasciolo N.509. Comune Di Padova. Archivio Categoria IX, Classe 11, 1939.

[14] Bresciani Alvarez, G., Briseghella, L., Il Palazzo della Ragione in Padova 11, 1990.

[15] Briseghella, Lamberto. Elaborati Grafici,Comune di Padova la Torre degli Anziani. Padua, October, 2005.

[16] SAHC Lectures. SA3. Seismic Behavoir and Structural Dynamics. Erasmus Mundus Masters in Structural Analysis of Monuments and Historical Constructions. 2014

[17] Milano, L., Mannella, A., Morisi, C., Martinelli, A. Schede Illustrative dei Principali Meccanismi di Collasso Locali Negli Edifici Esistenti in Muratura e dei Relativi Modelli Cinematici di Analisi. Allegato alle Linee Guida per la Riparazione e il Rafforzamento di elementi strutturali, Tamponature e Partizioni. Italy, 2009.

[18] Milano, L., G. Bettiol, F. da Porto, C. Modena. Esempio di calcolo su rafforzamento locale di edifici in muratura con tiranti. Allegato alle Linee Guida per la Riparazione e il Rafforzamento di elementi strutturali, Tamponature e Partizioni. Italy, 2010.

[19] Binda, L., Saisi, A. Knowledge of the Building, on Site Investigation and Connected Problems. Politecnico di Milano. Milan, Italy, 2009.

[20] Gonzalez, C. Methodology for the analysis of vulnerability and seismic assessment, applied in the case of San Fermo Maggiore (Verona, It.). Master's Thesis of Structural Analysis of Monuments and Historical Constructions Program - SAHC. University of Padua. Italy, 2013.

[21] Relazione Geologico-Tecnica Palazzo della Regione. Comune Di Padova. Settore Edilizia Monumentale. Relazione n.7024 bis. TECNO IN sri. Pozzuoli, July, 1998.

[22] Juarez, B., Rodríguez, R. Mecanica de Suelos, Tomo I Fundamentos de la Mecanica de Suelos. Editorial Limusa. Mexico, 1963.

[23] Ministry for Cultural Heritage and Activities- General direction of architectural heritage and landscape. Guidelines for Evaluation and Mitigation of Seismic Risk to Cultural Heritage. Gangemi Editore. Italy, 2005.

[24] Binda, L., Drdácký, M,. Kasal, B. In-situ Evaluation & Non-destructive Testing of Historic Wood and Masonry Structures. ITAM. ARCCHIP. Prague, Czech Republic, 2007.

[25] Chopra, A.K., Dynamics of structures – Theory and applications to earthquake engineering, Pearson Prentice Hall, 2007.

[26] Huebner, K. The Finite Element Method for Engineers. Second edition. John Wiley & Sons. US, 1982.

[27] Candigliota E., Carpani, B., Inmordino, F., Poggianti, A. Damage to religious buildings due to the Pianura Padana Emiliana earthquake. EAI – Energia, Ambiente e Innovazione. Italy, 2012.

[28] http://www.strand7.com

11 APPENDIX

APPENDIX 1.Drawings elaborated in 2005. Ref [5].

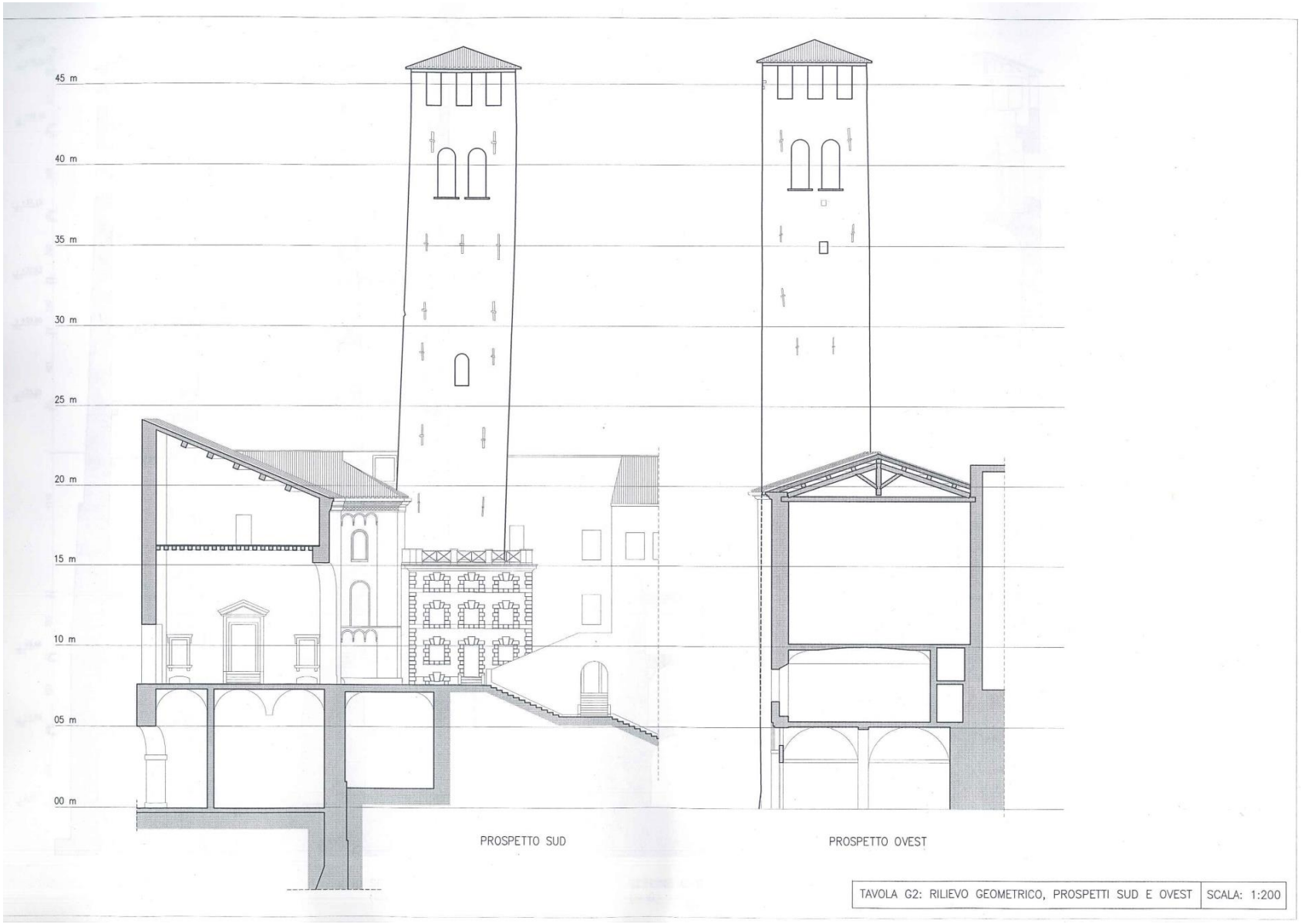
45 m
40 m
35 m
30 m
25 m
20 m
15 m
10 m
05 m
00 m
PROSPETTO SUD
PROSPETTO OVEST
TAVOLA G2: RILIEVO GEOMETRICO, PROSPETTI SUD E OVEST
SCALA: 1:200

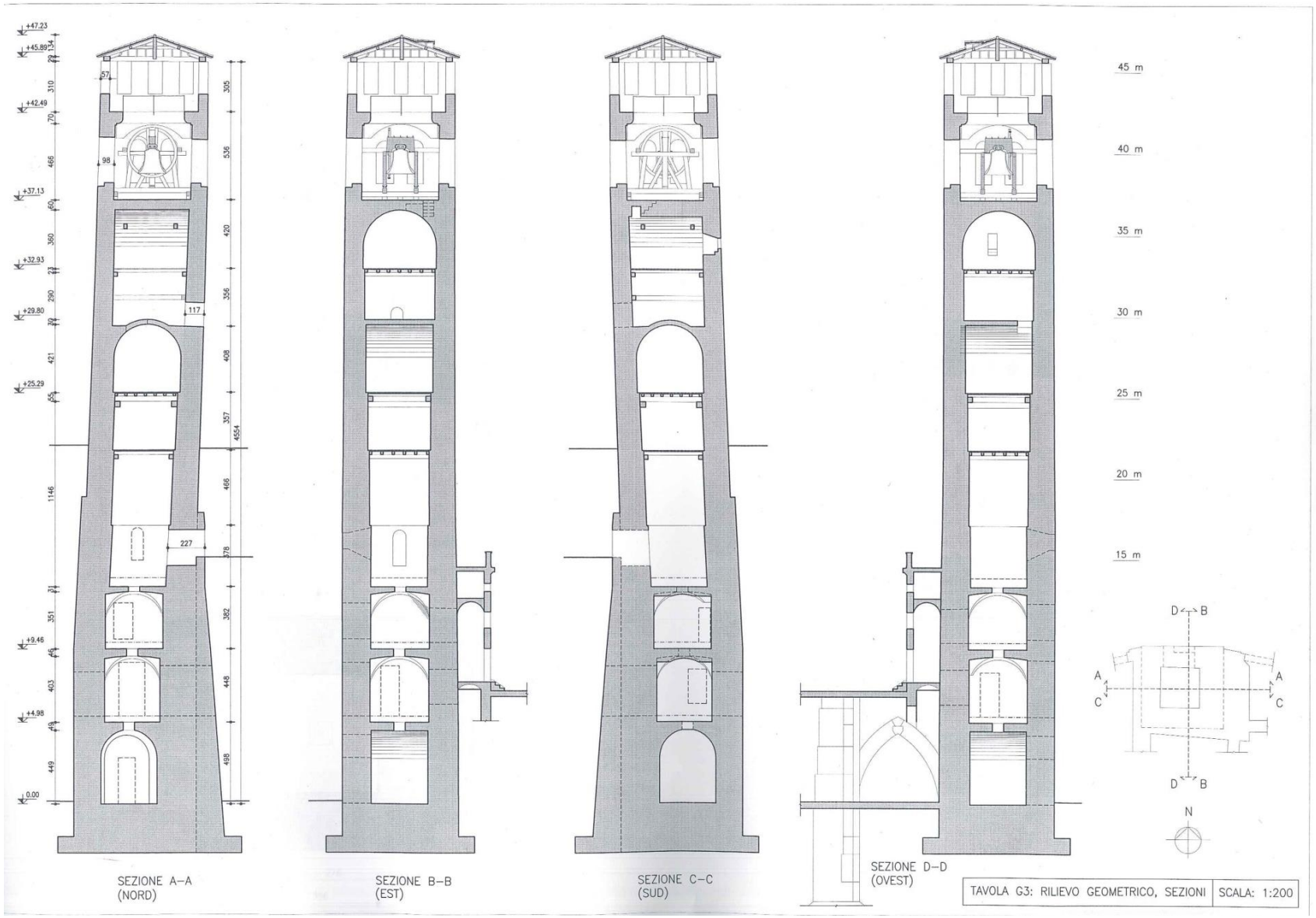
+47.23
+45.89
+42.49
+37.13
+32.93
+29.80
+25.29
+9.46
+4.98
0.00
45 m
40 m
35 m
30 m
25 m
20 m
15 m
SEZIONE A–A
(NORD)
SEZIONE B–B
(EST)
SEZIONE C–C
(SUD)
SEZIONE D–D
(OVEST)
TAVOLA G3: RILIEVO GEOMETRICO, SEZIONI
SCALA: 1:200
N


N
LIVELLO 01 (quota +1.00 m)
729
193
95
183
259
346
188
355
346
75
165
351
213
226
LIVELLO 02 (quota +6.00 m)
717
298
113
306
134
221
338
187
80
165
93
54
130
173
118
72
363
115
95
152
362
40
111
196
347
LIVELLO 03 (quota +10.00 m)
705
206
358
171
119
228
60
417
51
121
186
178
362
362
173
9
71
276
356
LIVELLO 04 (quota +15.50 m)
703
337
21
345
174
137
73
140
179
57
183
350
172
139
80
130
349
90
347
185
58
622
TERRAZZA
TAVOLA G4: RILIEVO GEOMETRICO, PIANTE
SCALA: 1:100

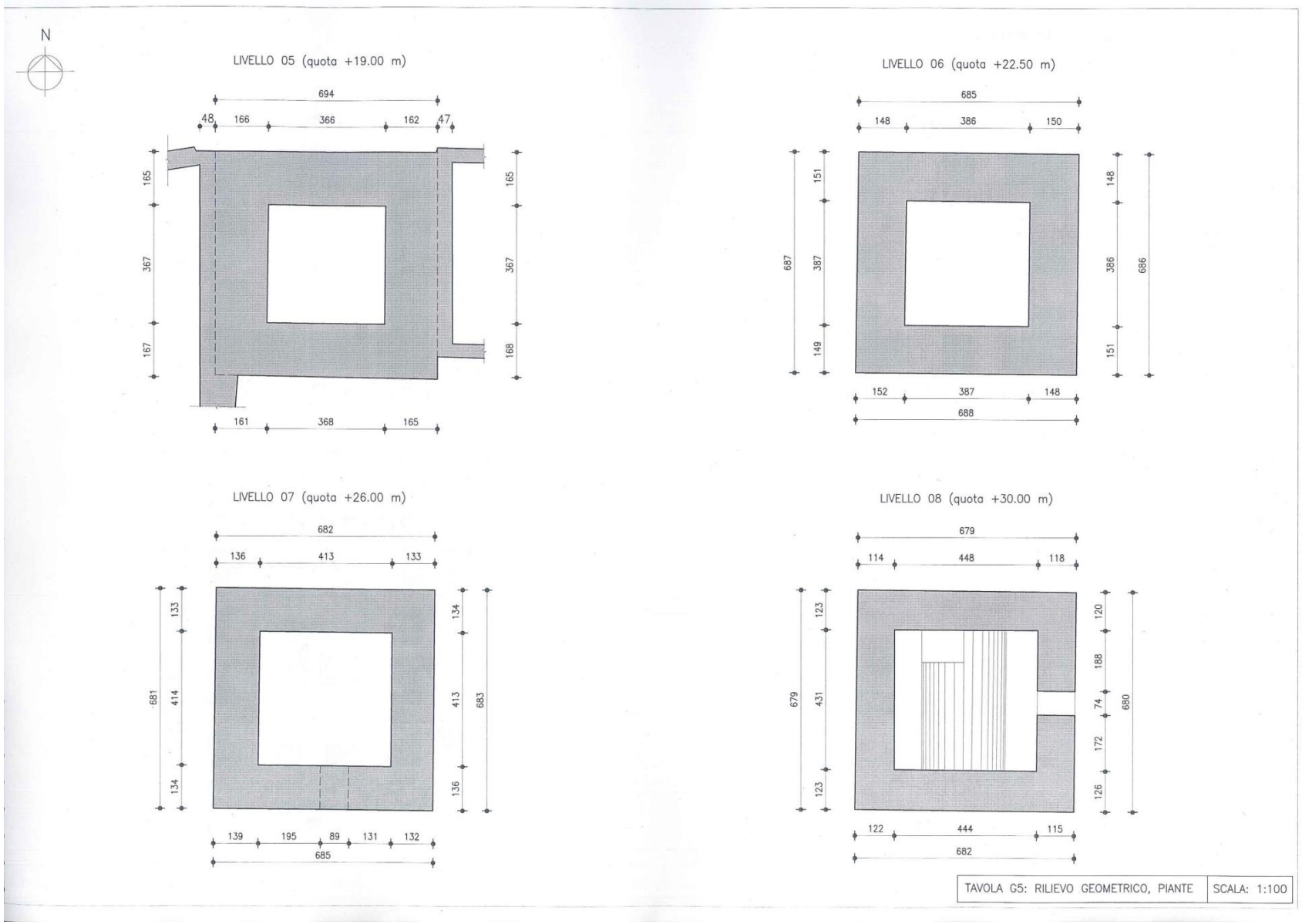
N
LIVELLO 05 (quota +19.00 m)
694
48
166
366
162
47
165
367
167
165
367
168
161
368
165
LIVELLO 06 (quota +22.50 m)
685
148
386
150
687
151
387
149
148
386
151
686
152
387
148
688
LIVELLO 07 (quota +26.00 m)
682
136
413
133
681
133
414
134
134
413
136
683
139
195
89
131
132
685
LIVELLO 08 (quota +30.00 m)
679
114
448
118
679
123
431
123
120
188
74
172
126
680
122
444
115
682
TAVOLA G5: RILIEVO GEOMETRICO, PIANTE
SCALA: 1:100

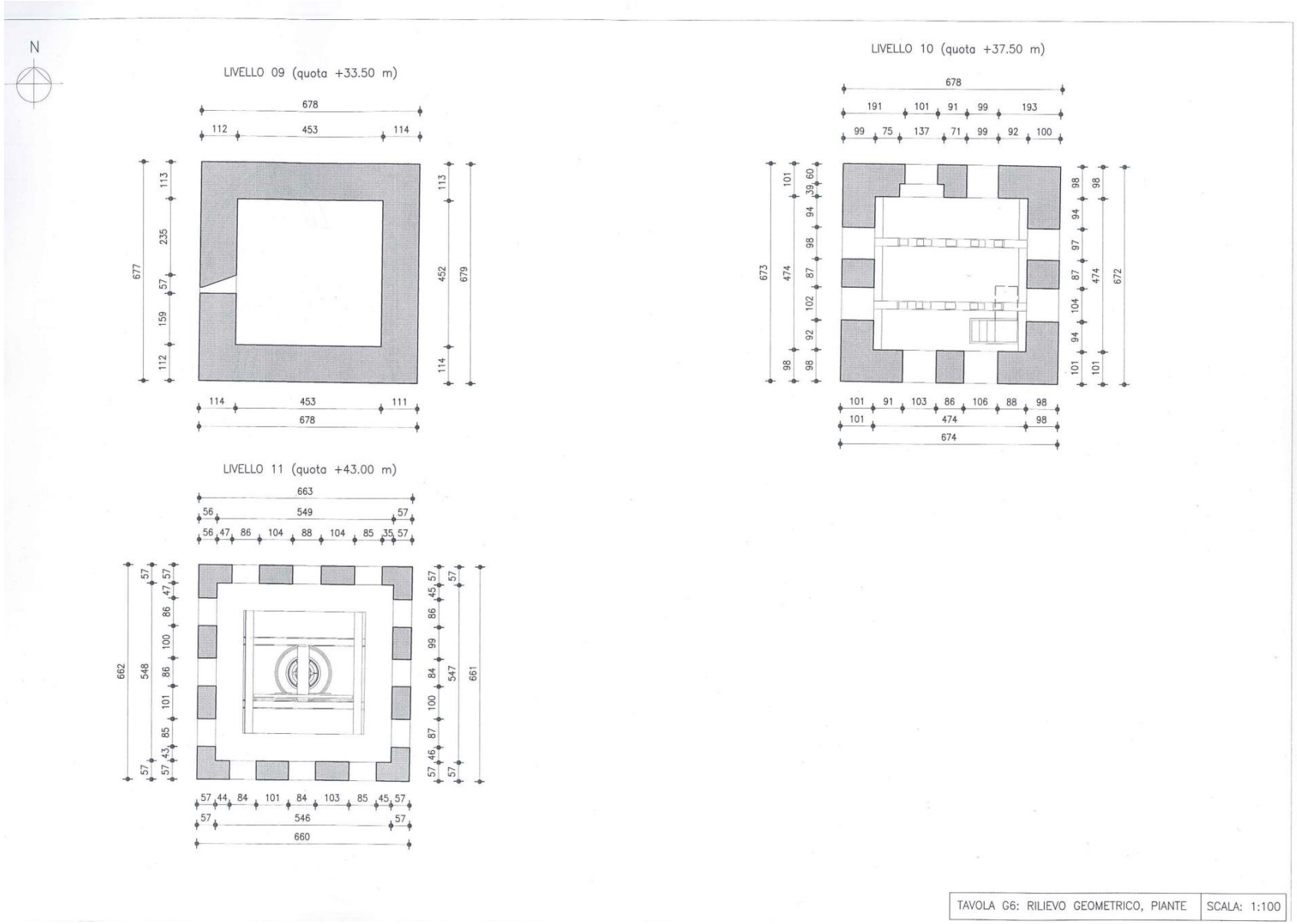
N
LIVELLO 09 (quota +33.50 m)
678
112
453
114
677
113
235
57
159
112
452
679
114
453
111
678
LIVELLO 10 (quota +37.50 m)
678
191
101
91
99
193
99
75
137
71
99
92
100
673
101
60
39
94
474
98
87
102
92
98
672
98
94
97
87
474
104
94
101
101
101
91
103
86
106
88
98
101
474
98
674
LIVELLO 11 (quota +43.00 m)
663
56
549
57
56
47
86
104
88
104
85
35
57
662
57
57
47
86
100
86
101
85
43
57
548
661
57
57
45
86
99
84
100
87
46
57
547
57
57
44
84
101
84
103
85
45
57
546
660
TAVOLA G6: RILIEVO GEOMETRICO, PIANTE
SCALA: 1:100

APPENDIX 2.Photographic survey from outside, 2005. Ref [5].

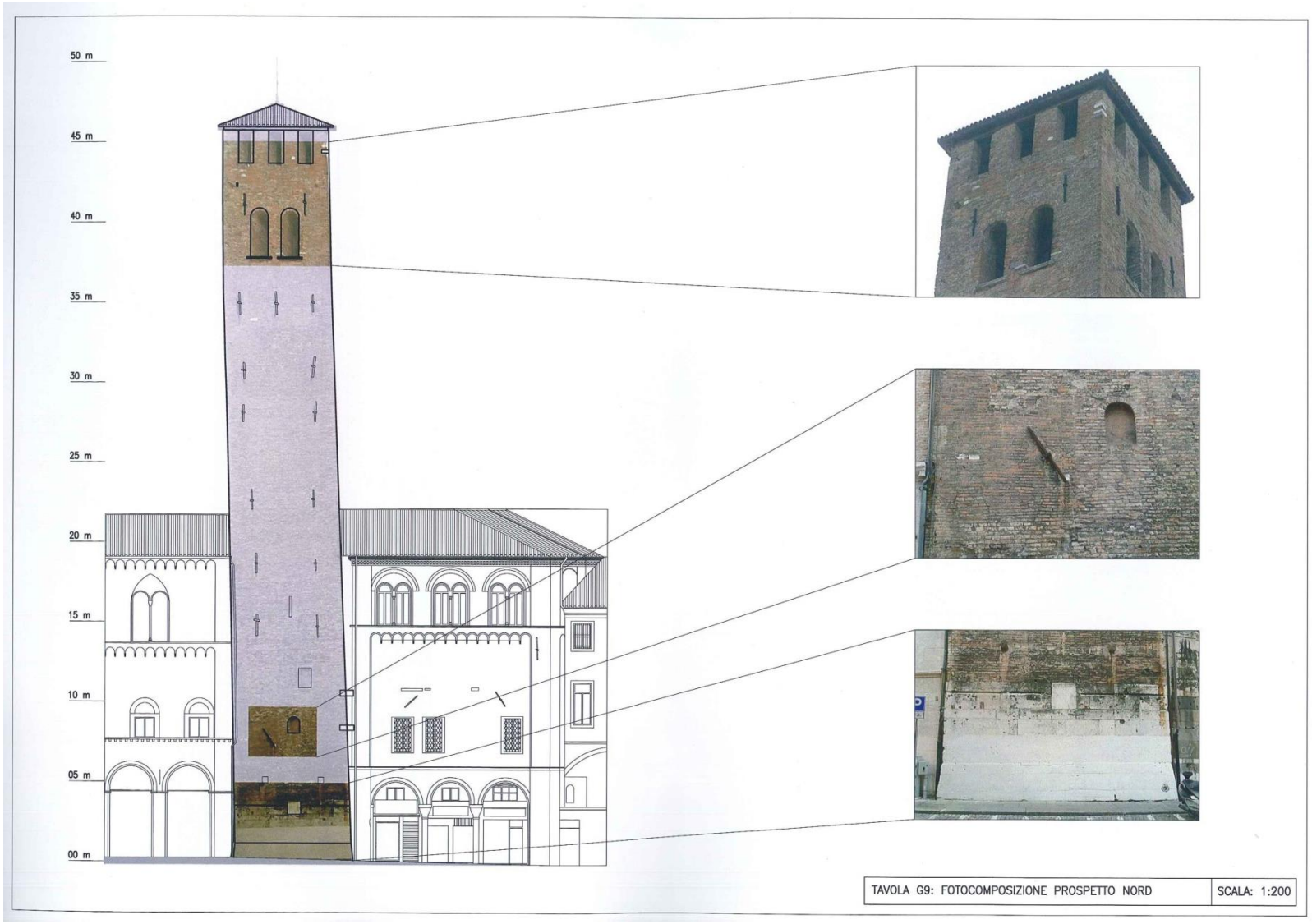

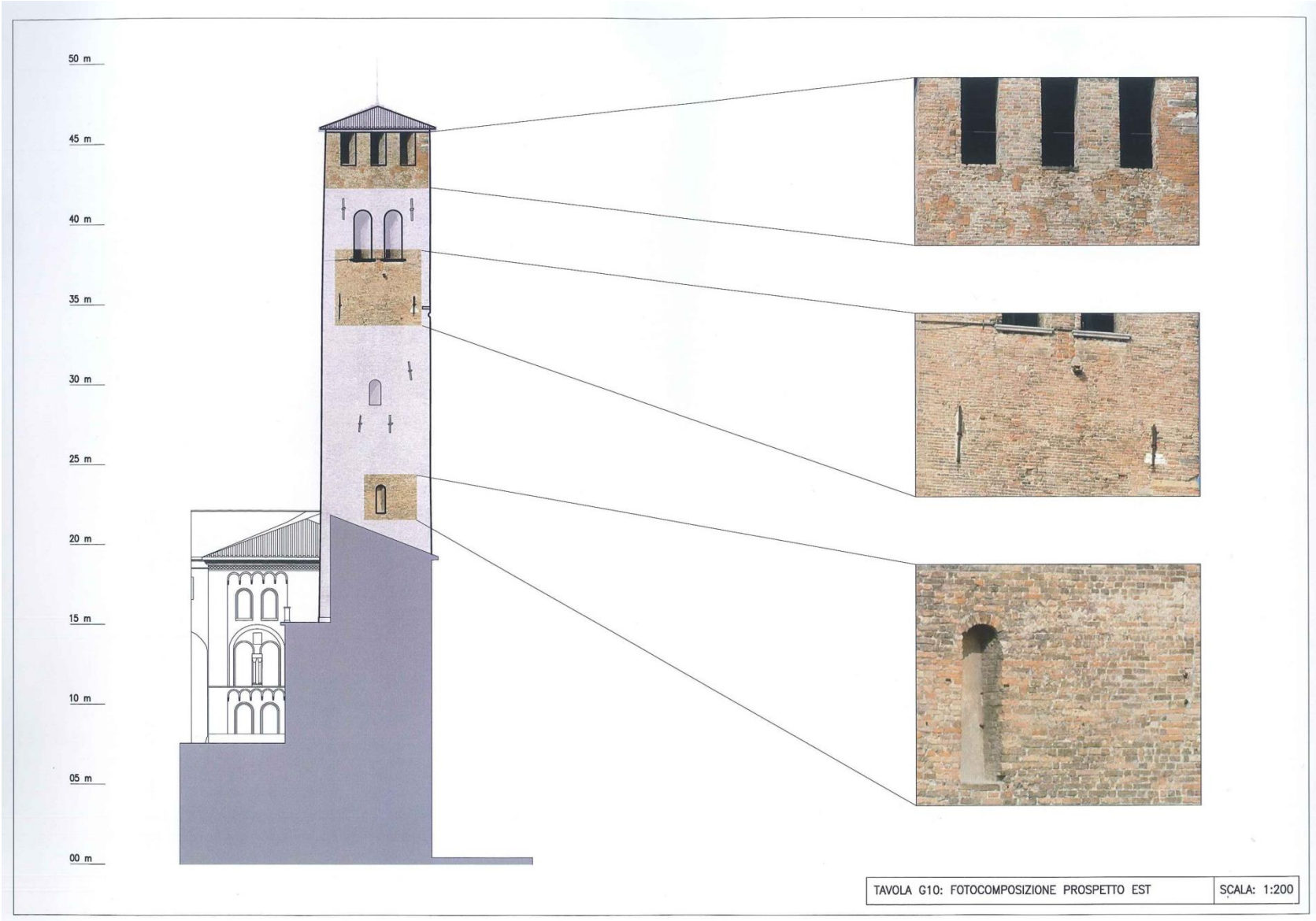
50 m
45 m
40 m
35 m
30 m
25 m
20 m
15 m
10 m
05 m
00 m
TAVOLA G10: FOTOCOMPOSIZIONE PROSPETTO EST
SCALA: 1:200

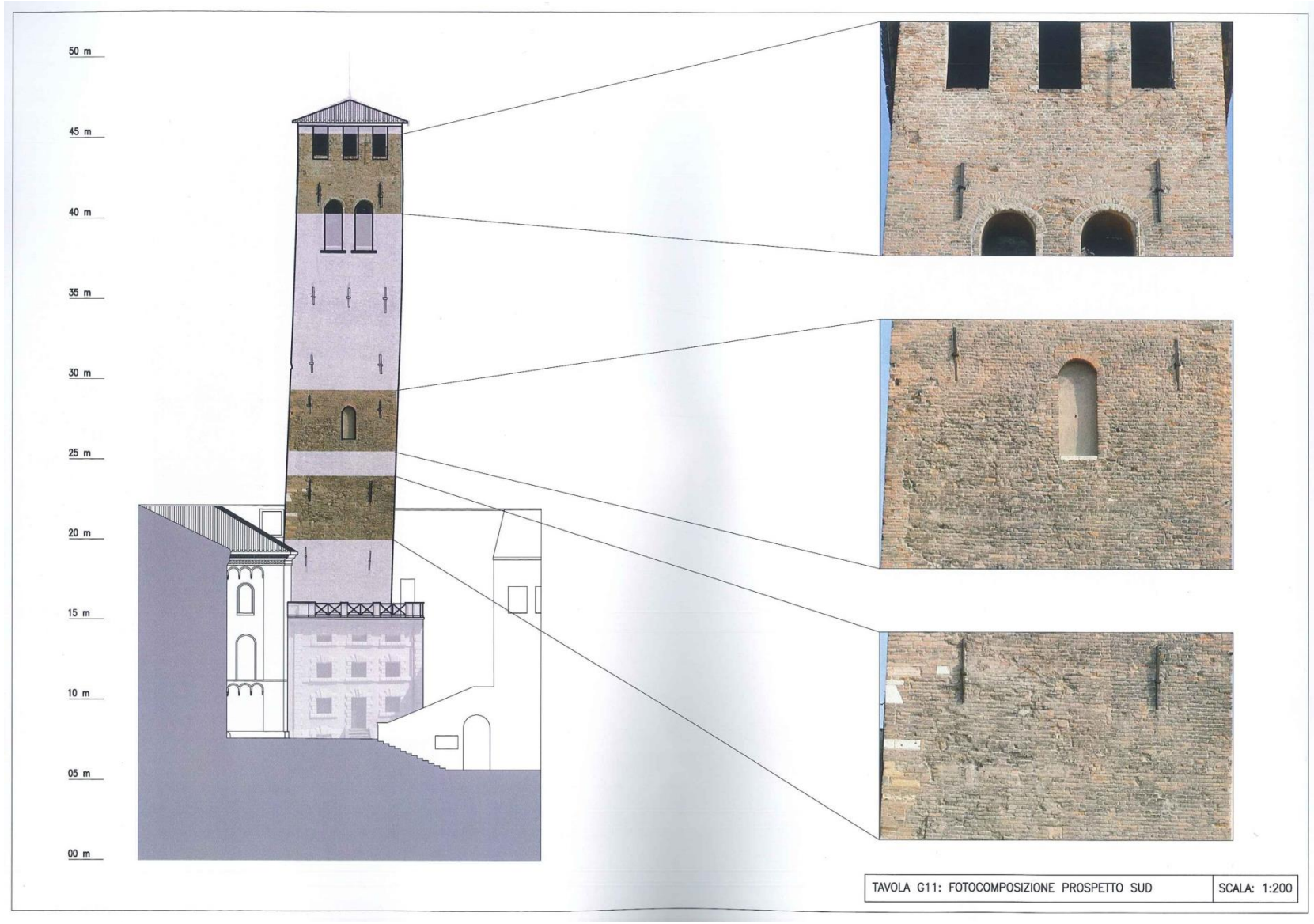
50 m
45 m
40 m
35 m
30 m
25 m
20 m
15 m
10 m
05 m
00 m
TAVOLA G11: FOTOCOMPOSIZIONE PROSPETTO SUD
SCALA: 1:200

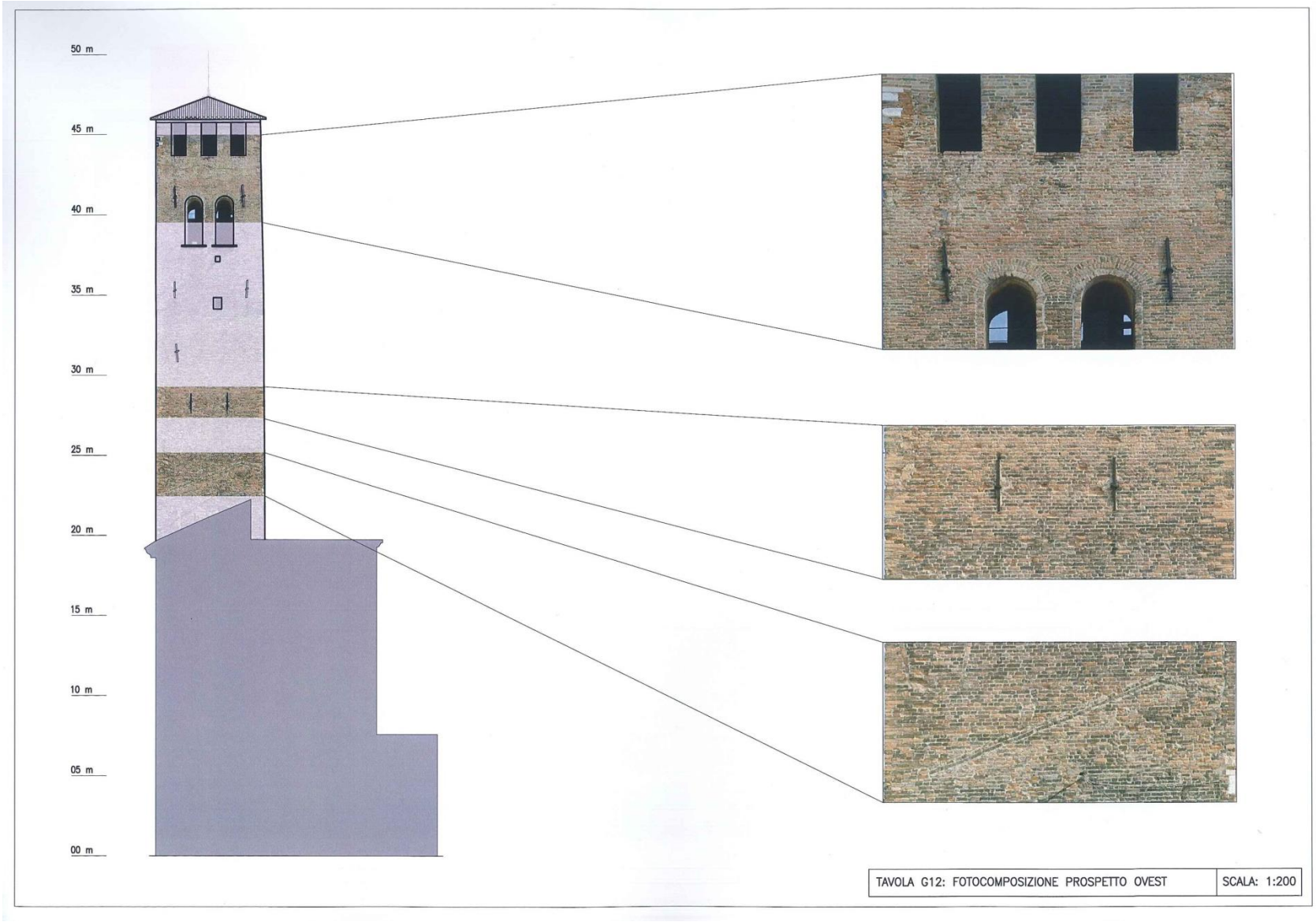
50 m
45 m
40 m
35 m
30 m
25 m
20 m
15 m
10 m
05 m
00 m
TAVOLA G12: FOTOCOMPOSIZIONE PROSPETTO OVEST
SCALA: 1:200

APPENDIX 3. Dynamic characterization (previous studies)

TEST N3

Sparo parete EST (file prova numero 3)

Segnale acquisito

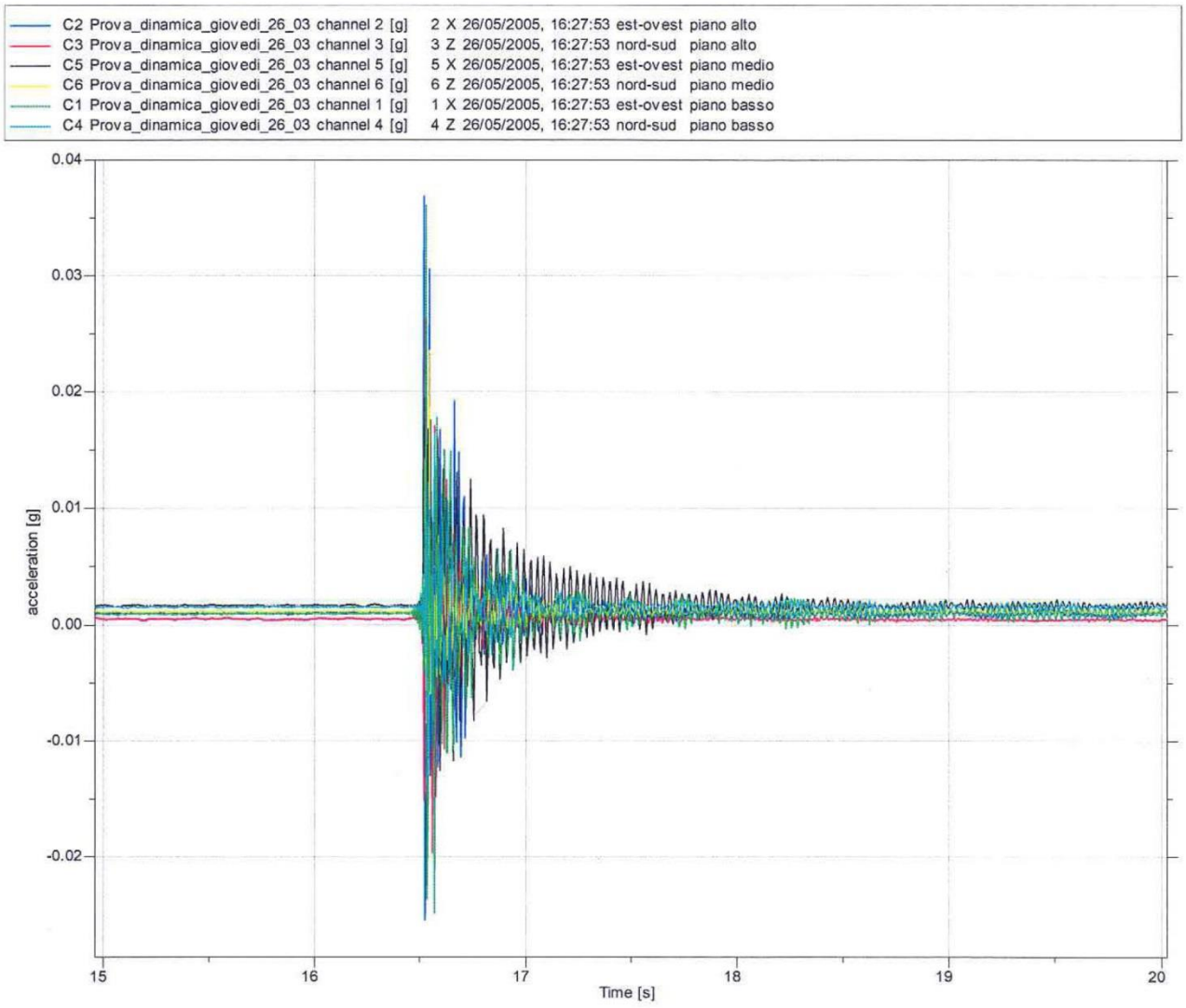

Particolare del segnale

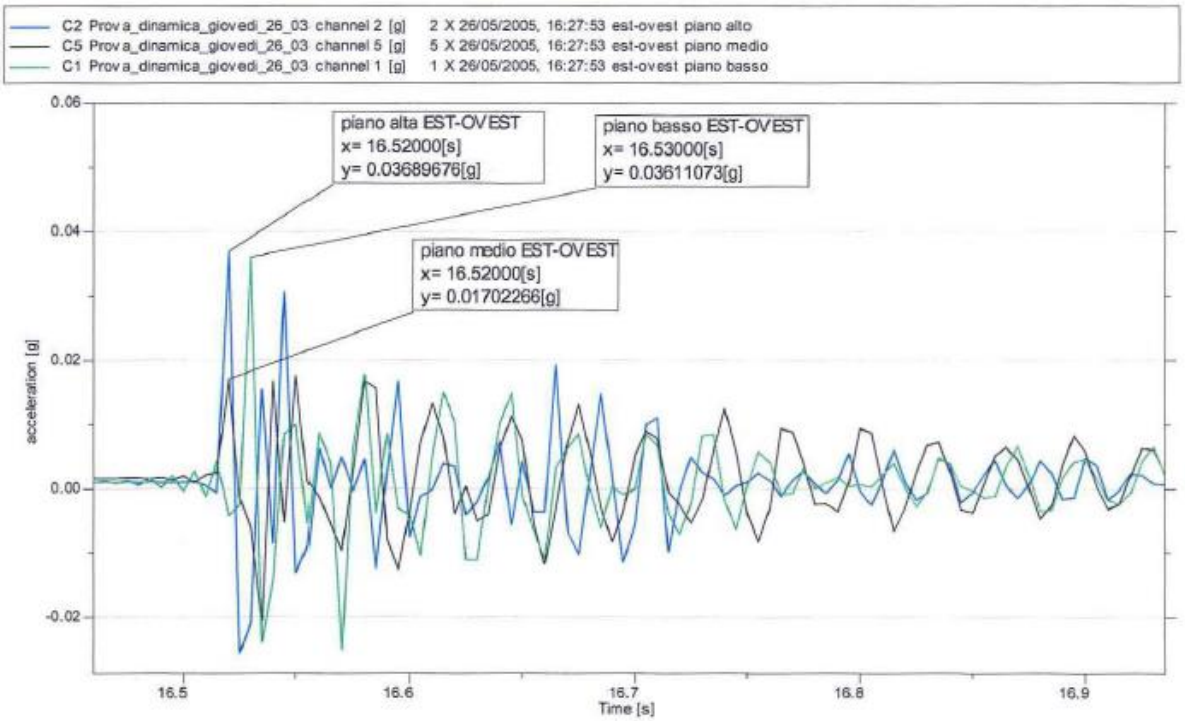

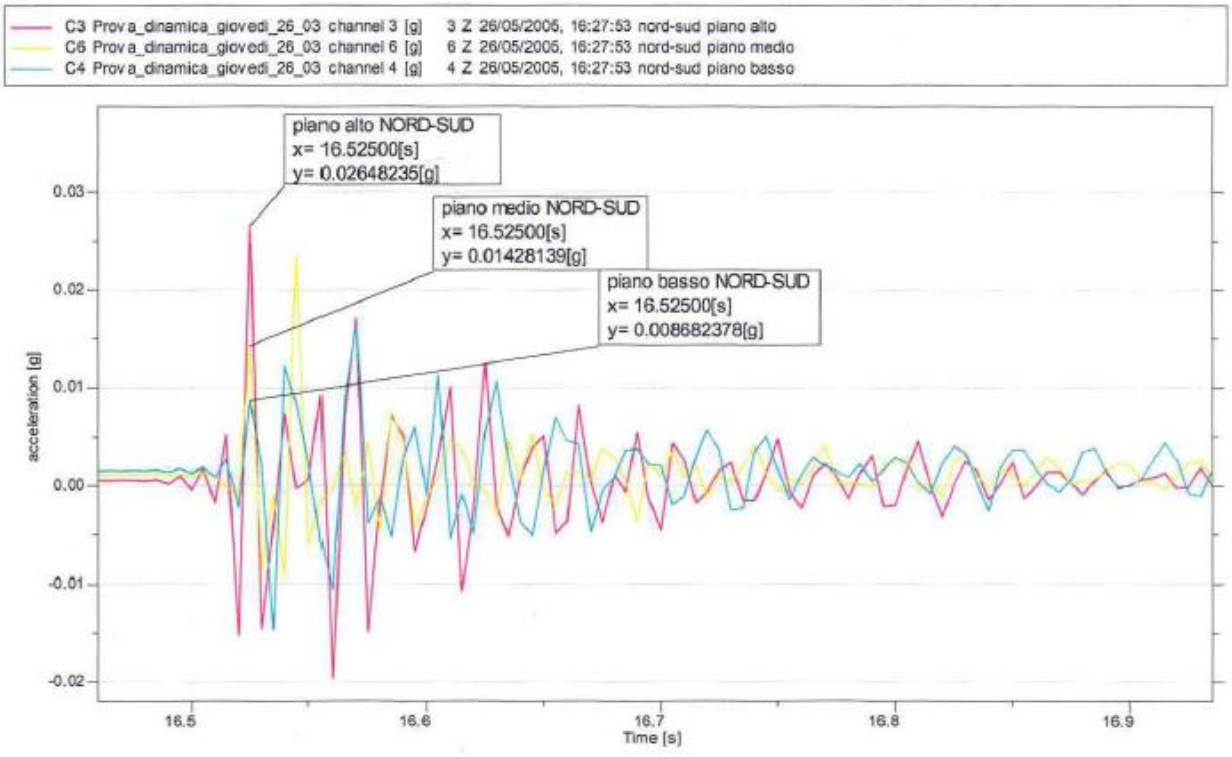

Impulso forza

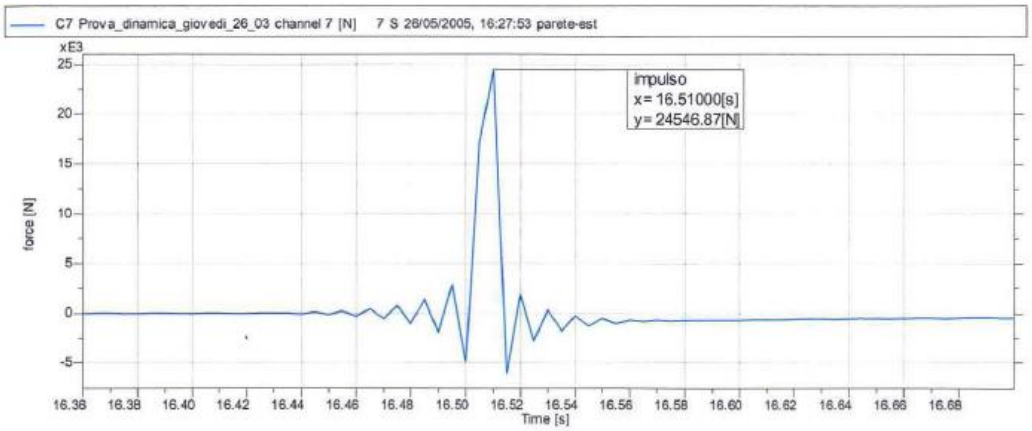

FFT del segnale

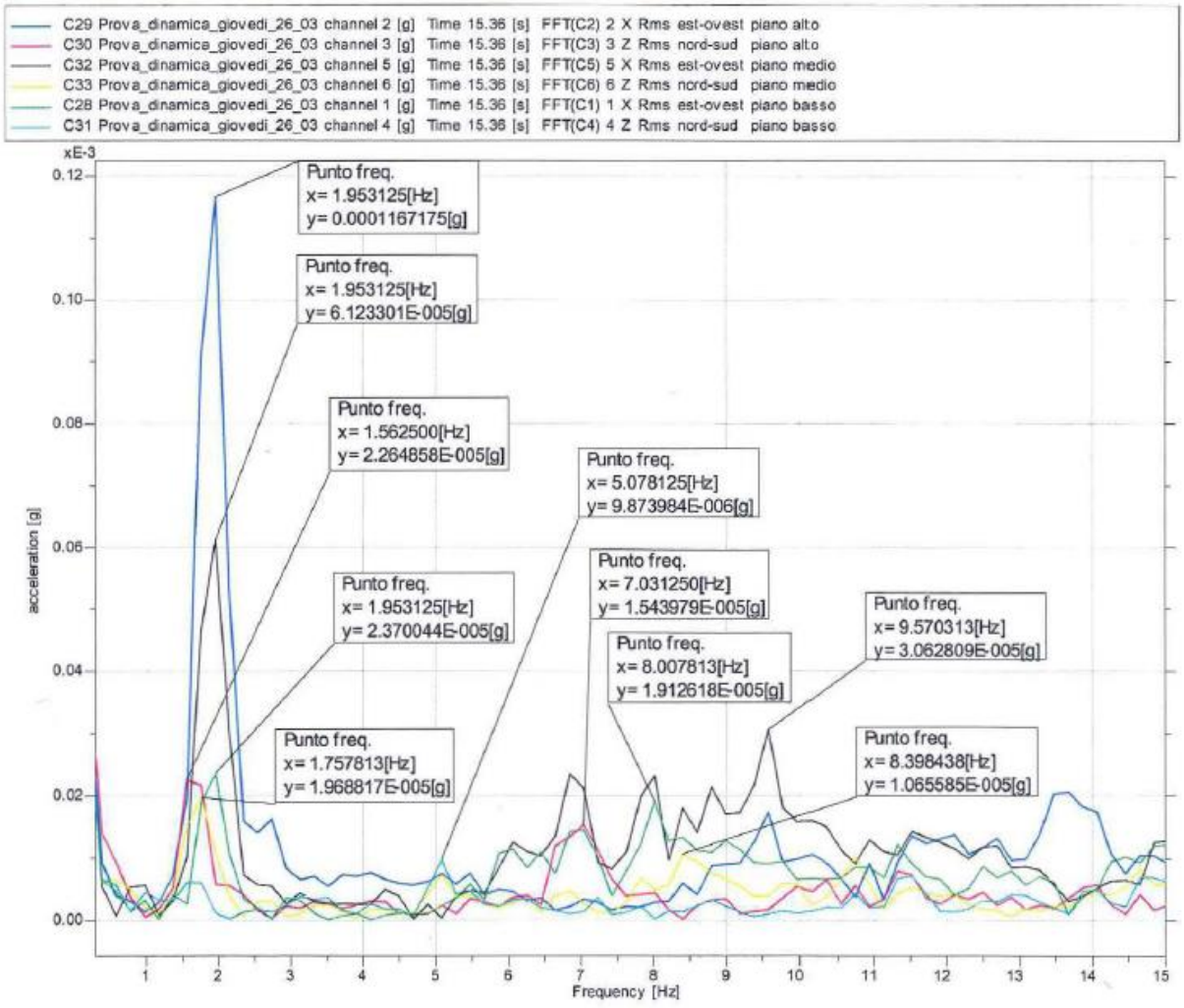

Test N4

Sparo parete EST (file prova numero 4)

Segnale acquisito

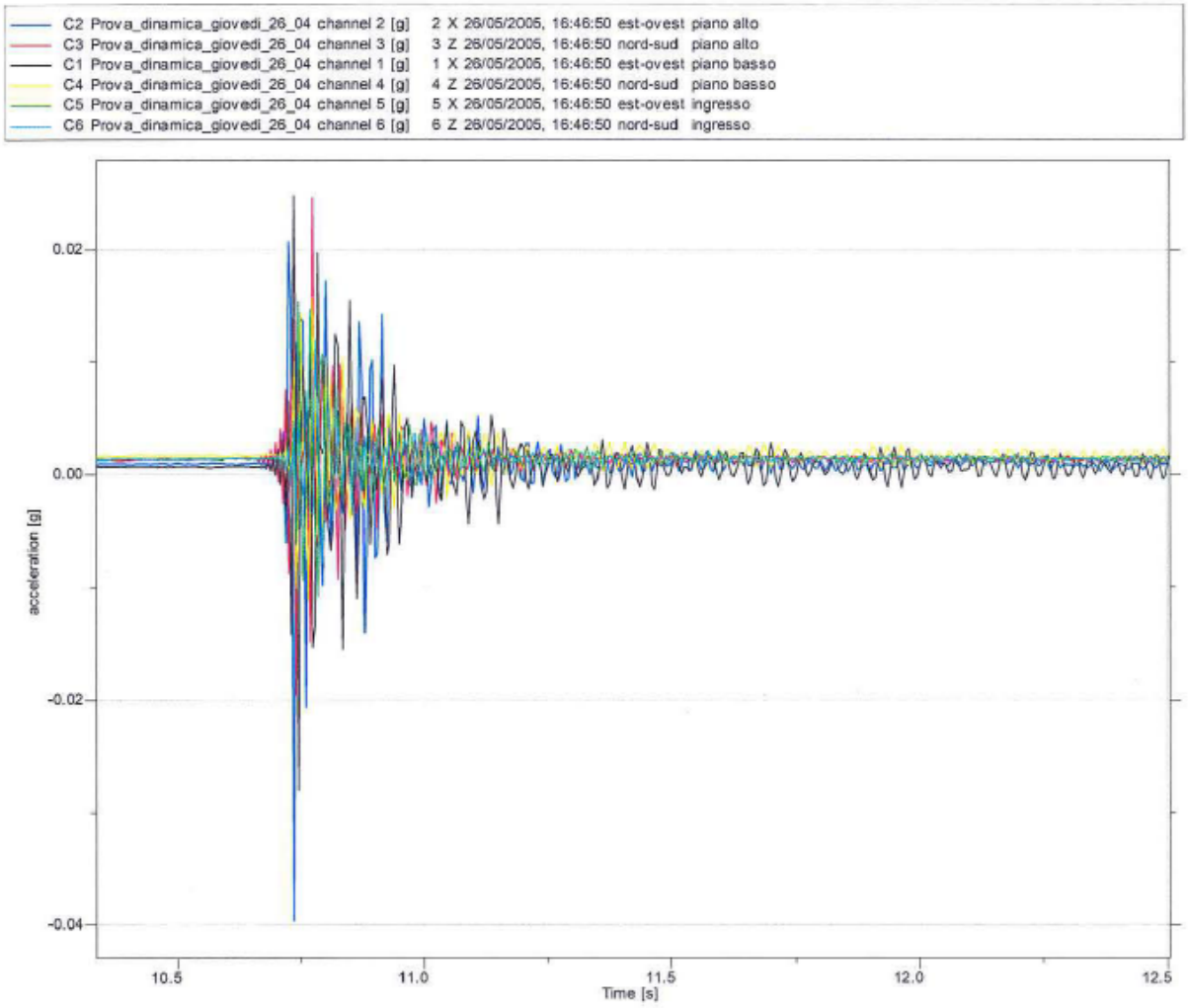

Particolare del segnale

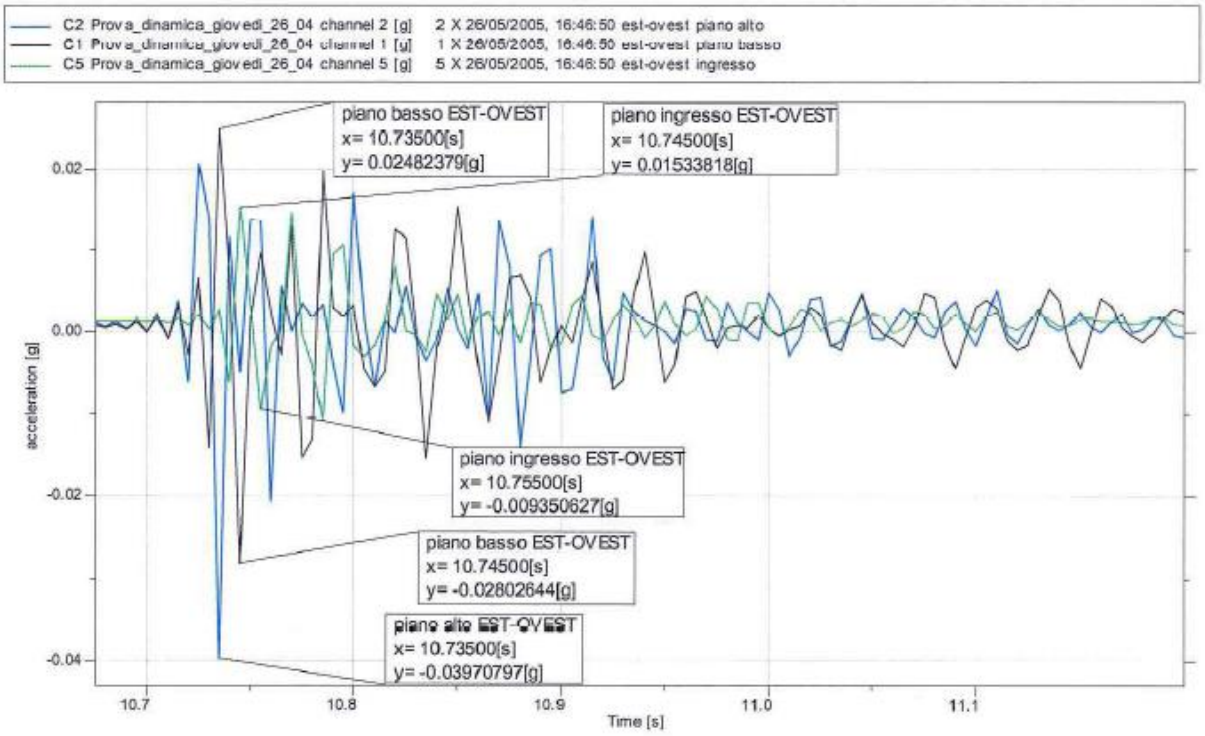

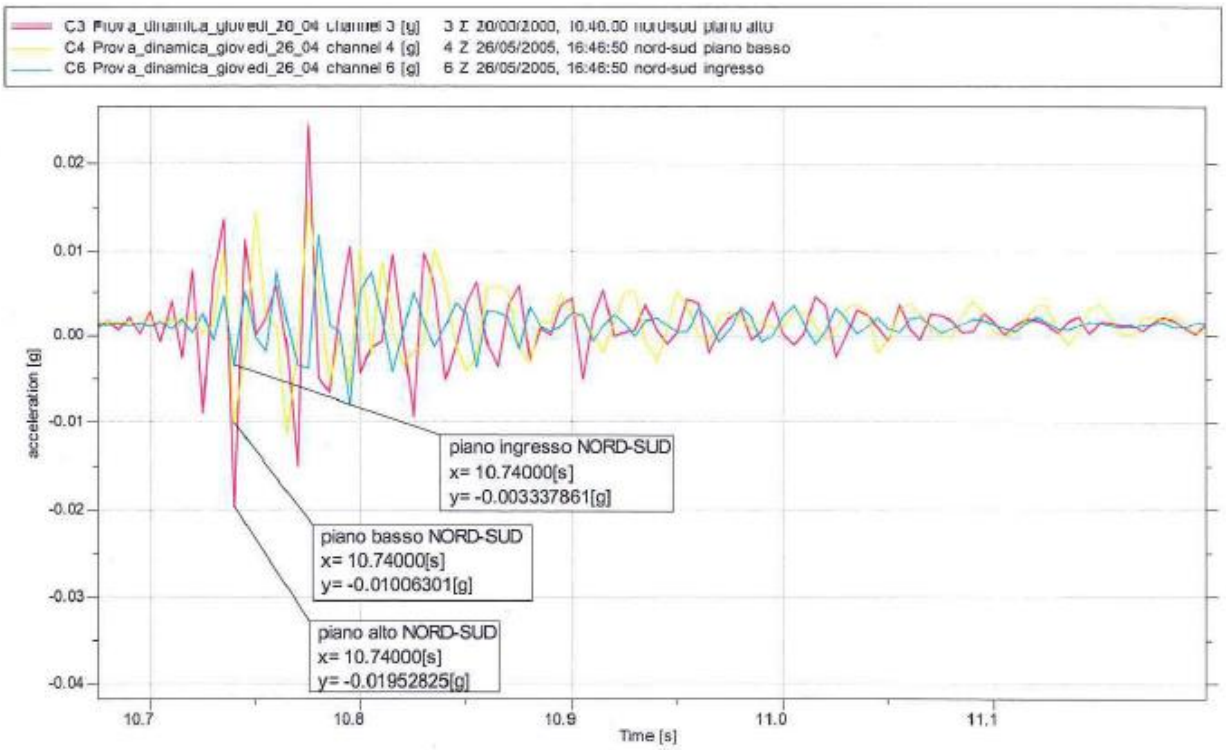

Impulso forza

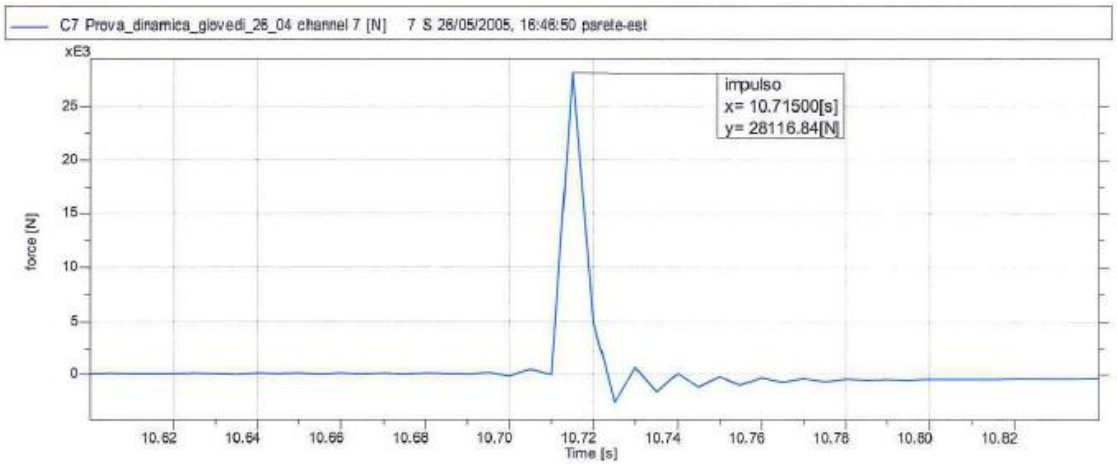

FFT del segnale

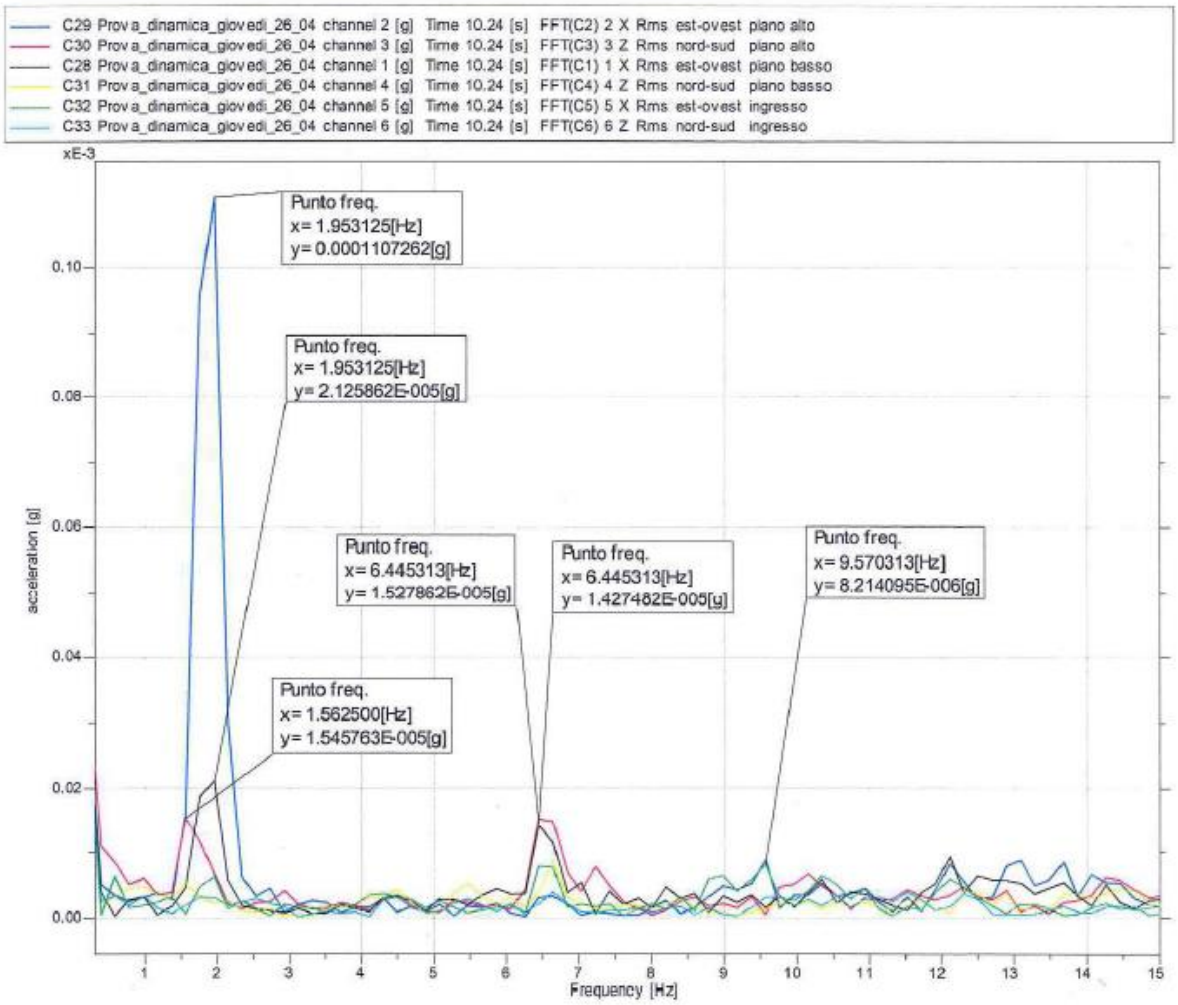

TEST N5

Sparo parete NORD (file prova numero 5)

Segnale acquisito

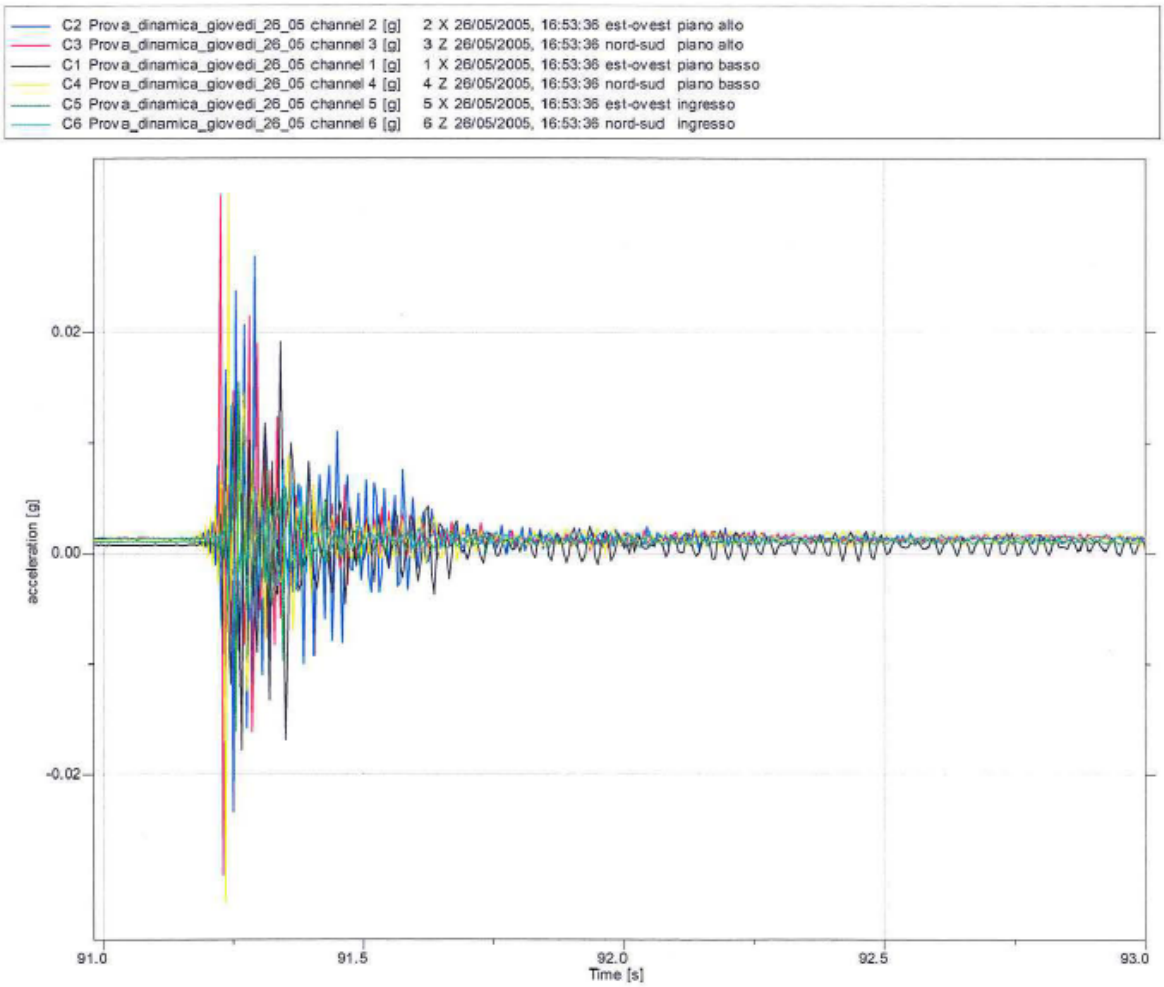

Particolare del segnale

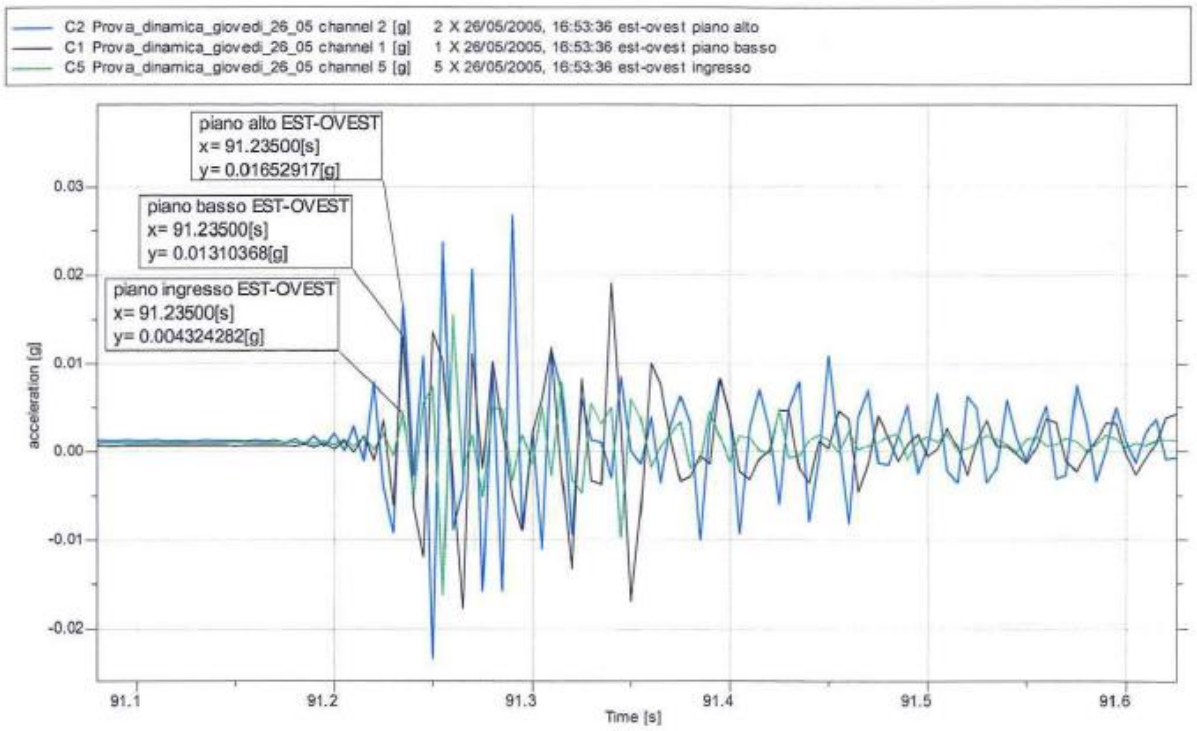

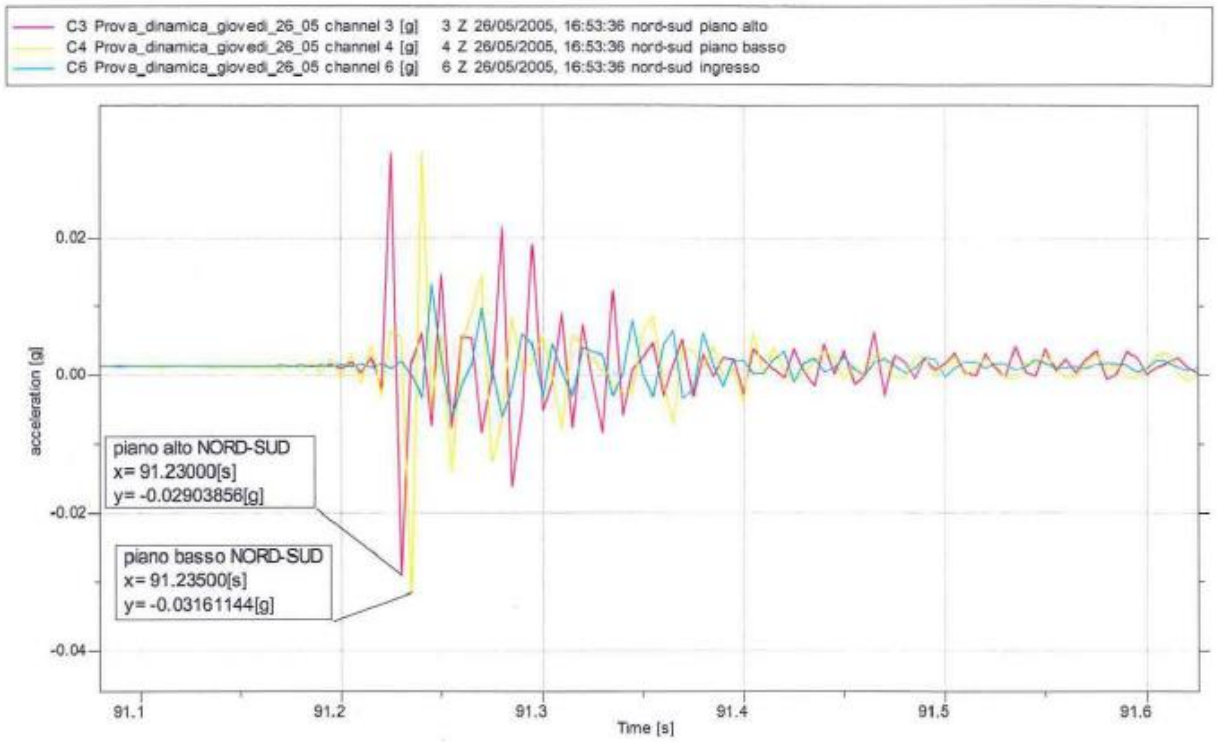

Impulso forza

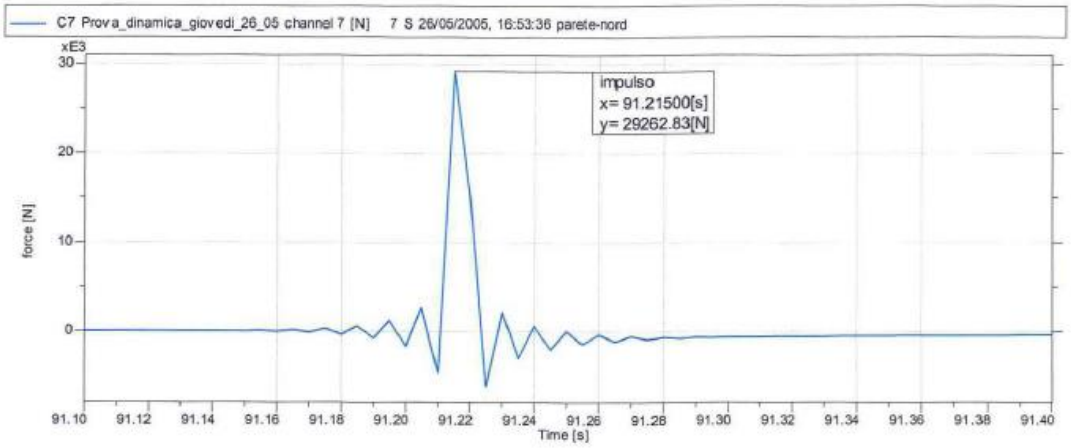

FFT del segnale

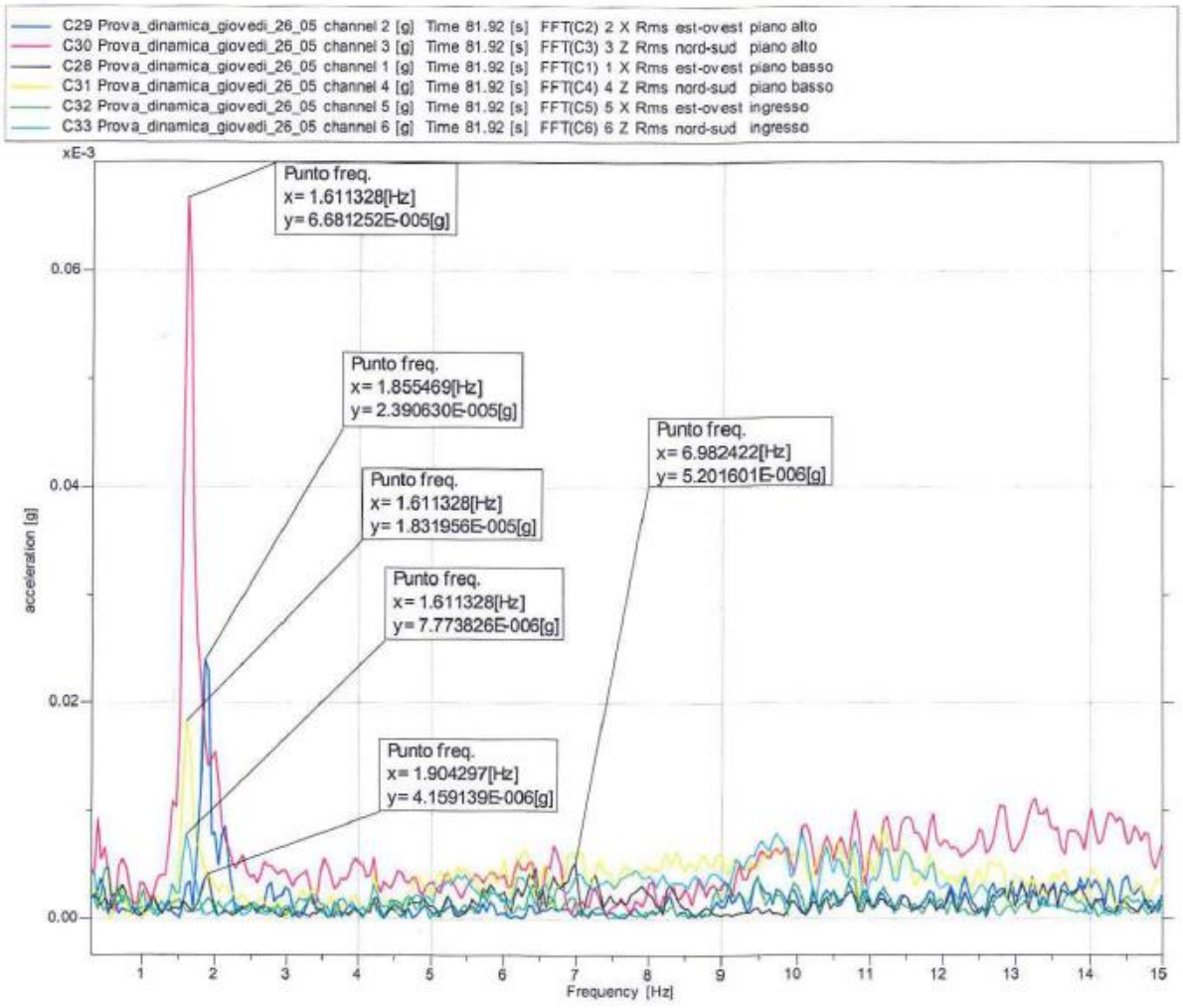

TEST N6

Sparo parete NORD (file prova numero 6)

Segnale acquisito

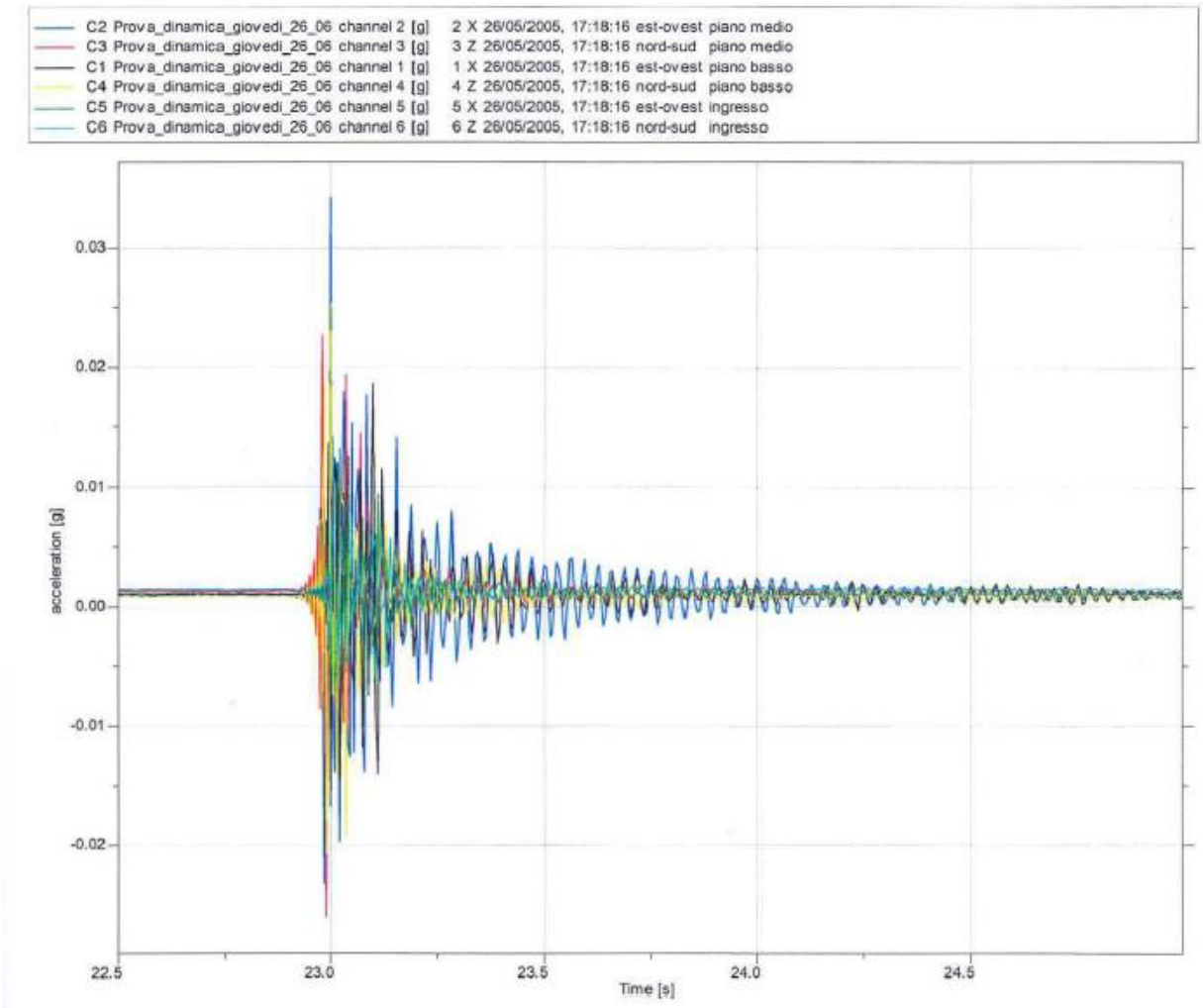

Particolare del segnale

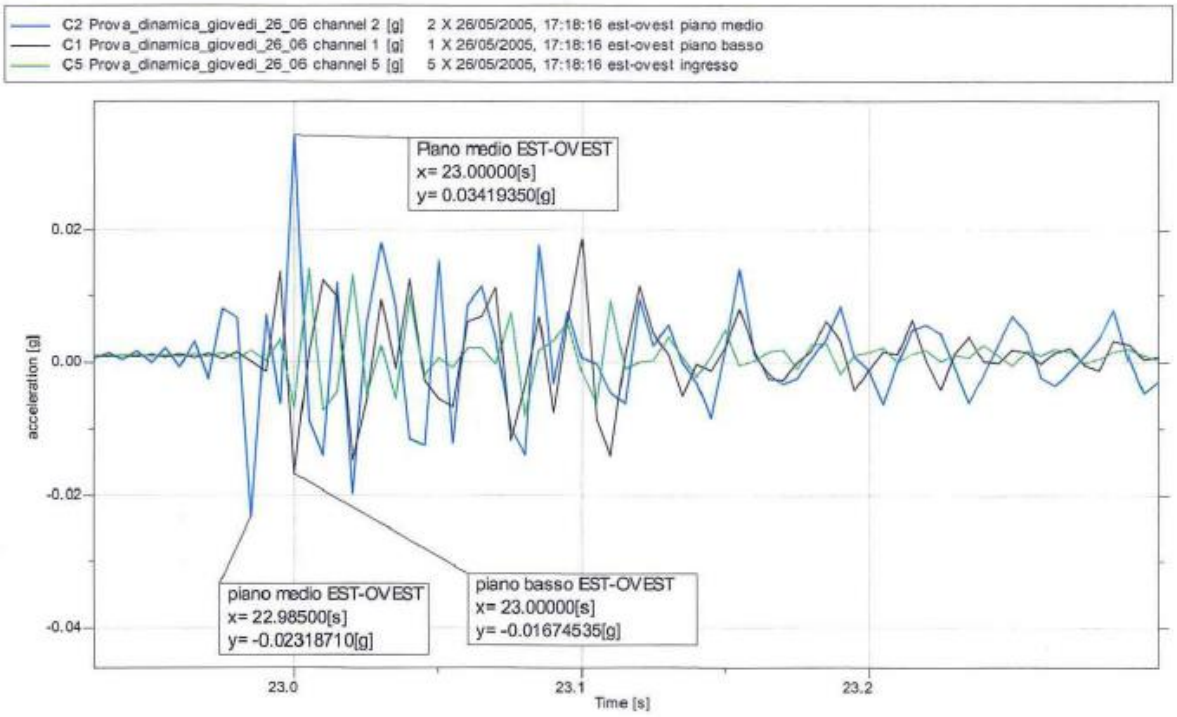

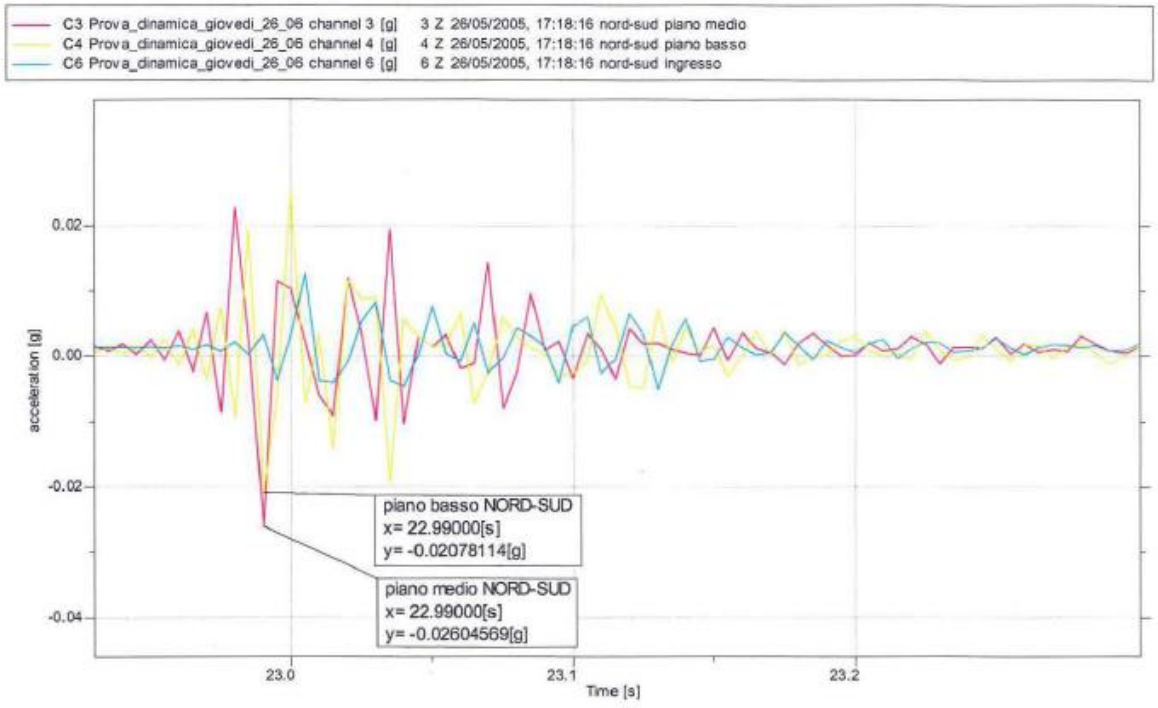

Impulso forza

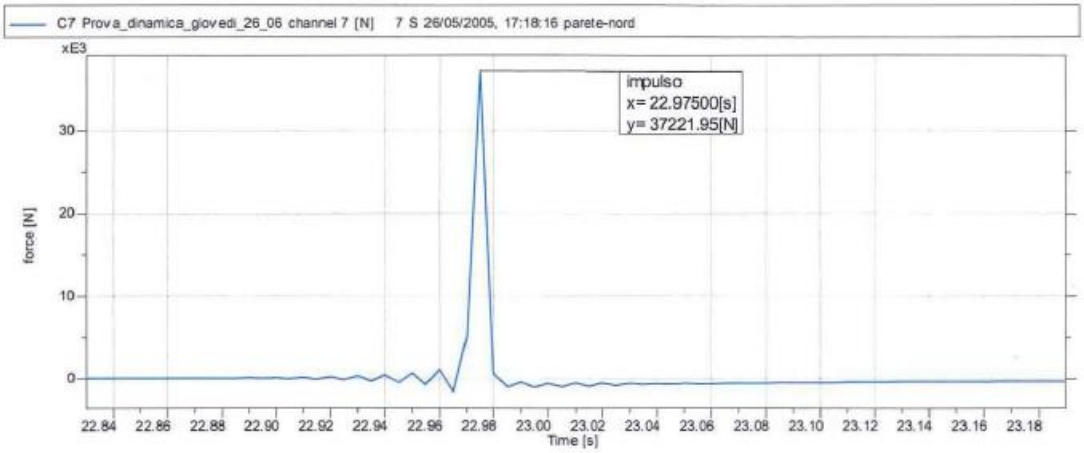

FFT del segnale

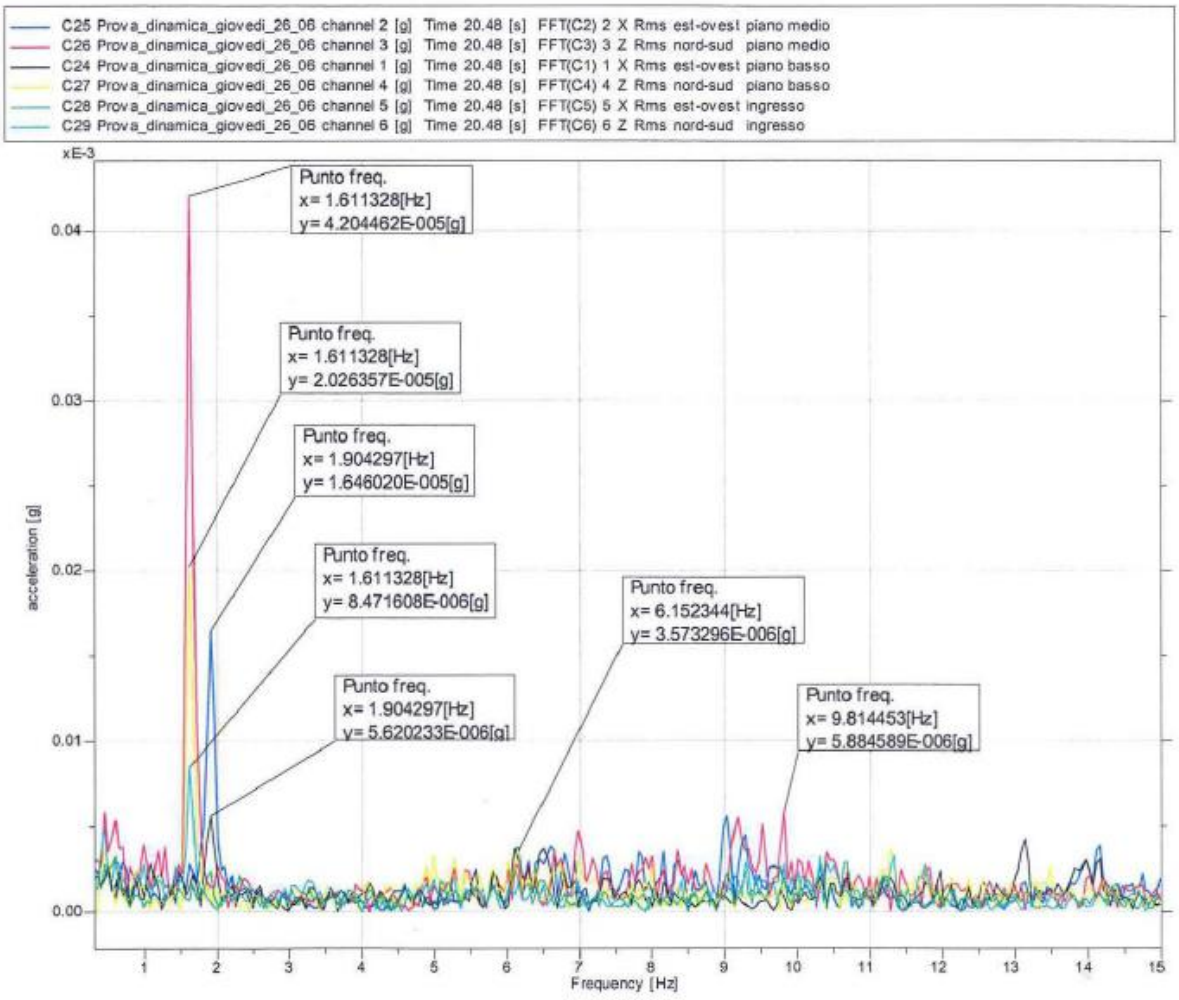

APPENDIX 4. Dynamic characterization of ties

TEST 1- Tie N29.

Response under environmental vibration in time domain (above) and FFT (below) - Measurement 2

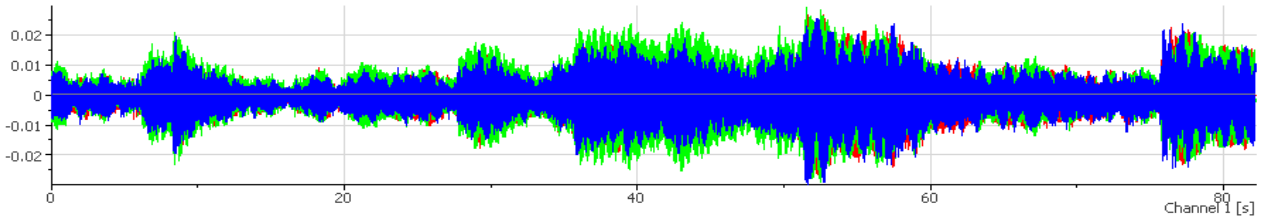

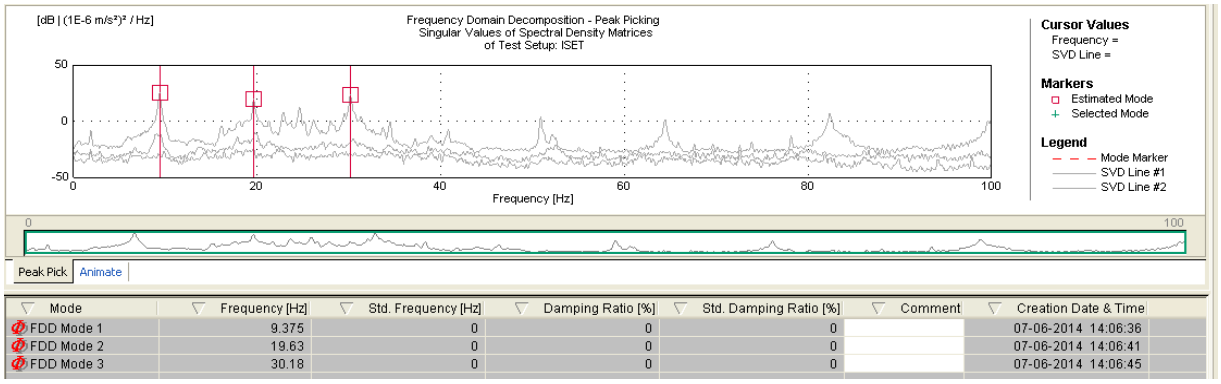

Mode	Frequency [Hz]	Std. Frequency [Hz]	Damping Ratio [%]	Std. Damping Ratio [%]	Comment	Creation Date & Time
FDD Mode 1	9.375	0	0	0		07-06-2014 14:06:36
FDD Mode 2	19.63	0	0	0		07-06-2014 14:06:41
FDD Mode 3	30.18	0	0	0		07-06-2014 14:06:45

Response under forced vibration in time domain (above) and FFT (below) - Measurement 2

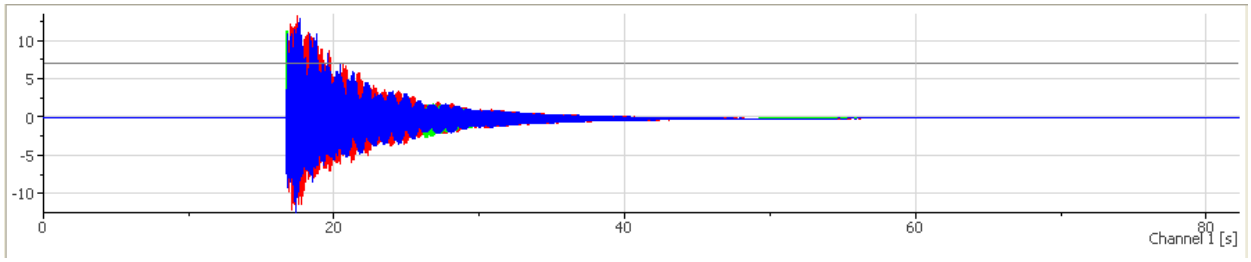

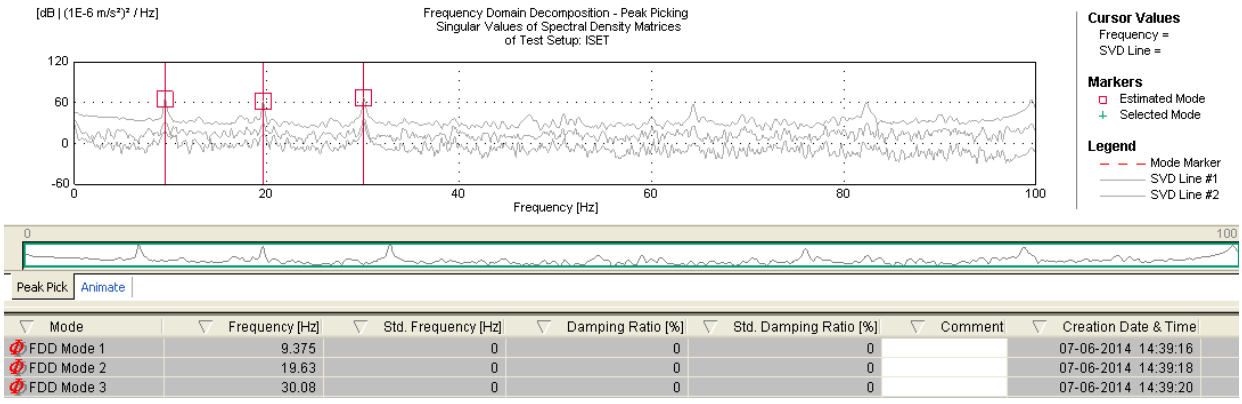

Mode	Frequency [Hz]	Std. Frequency [Hz]	Damping Ratio [%]	Std. Damping Ratio [%]	Comment	Creation Date & Time
FDD Mode 1	9.375	0	0	0		07-06-2014 14:39:16
FDD Mode 2	19.63	0	0	0		07-06-2014 14:39:18
FDD Mode 3	30.08	0	0	0		07-06-2014 14:39:20

Natural frequencies for T1 – Tie N29

T1		Natural frequencies (Hz)		
	Measurement	**I**	**II**	**III**
Environmental vibration	1	9.375	19.630	30.180
	2	9.375	19.630	30.180
	3	9.375	19.630	30.180
	Average	**9.375**	**19.630**	**30.180**
Forced Vibration	1	9.405	19.610	30.110
	2	9.375	19.630	30.080
	3	9.399	19.600	30.100
	Average	**9.393**	**19.613**	**30.097**

TEST 2- Tie N22.

Response under environmental vibration in time domain (above) and FFT (below) - Measurement 3

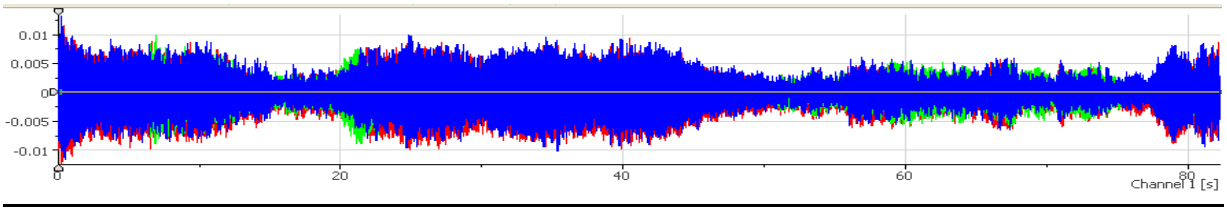

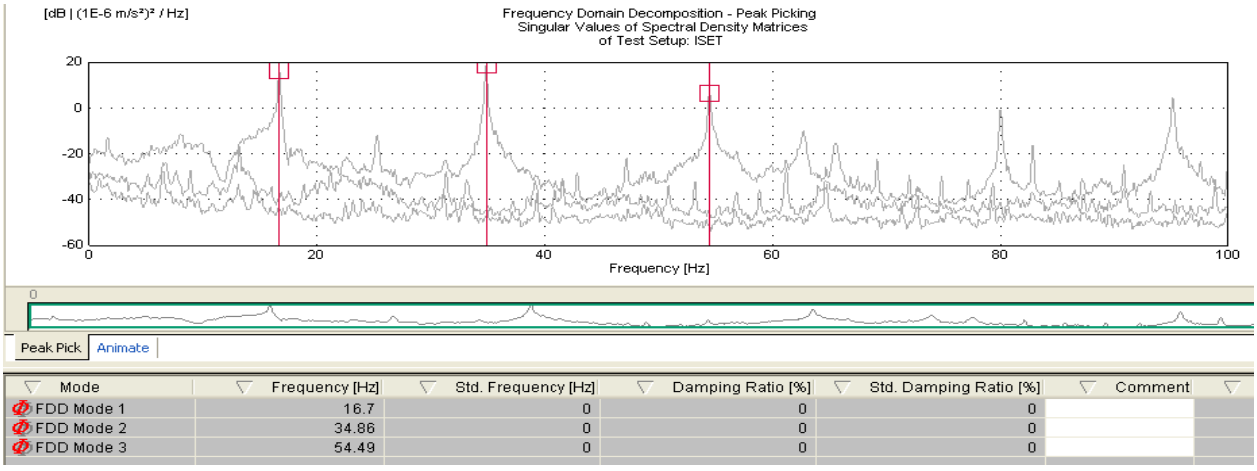

Mode	Frequency [Hz]	Std. Frequency [Hz]	Damping Ratio [%]	Std. Damping Ratio [%]	Comment
FDD Mode 1	16.7	0	0	0	
FDD Mode 2	34.86	0	0	0	
FDD Mode 3	54.49	0	0	0	

Response under forced vibration in time domain (above) and FFT (below) - Measurement 2

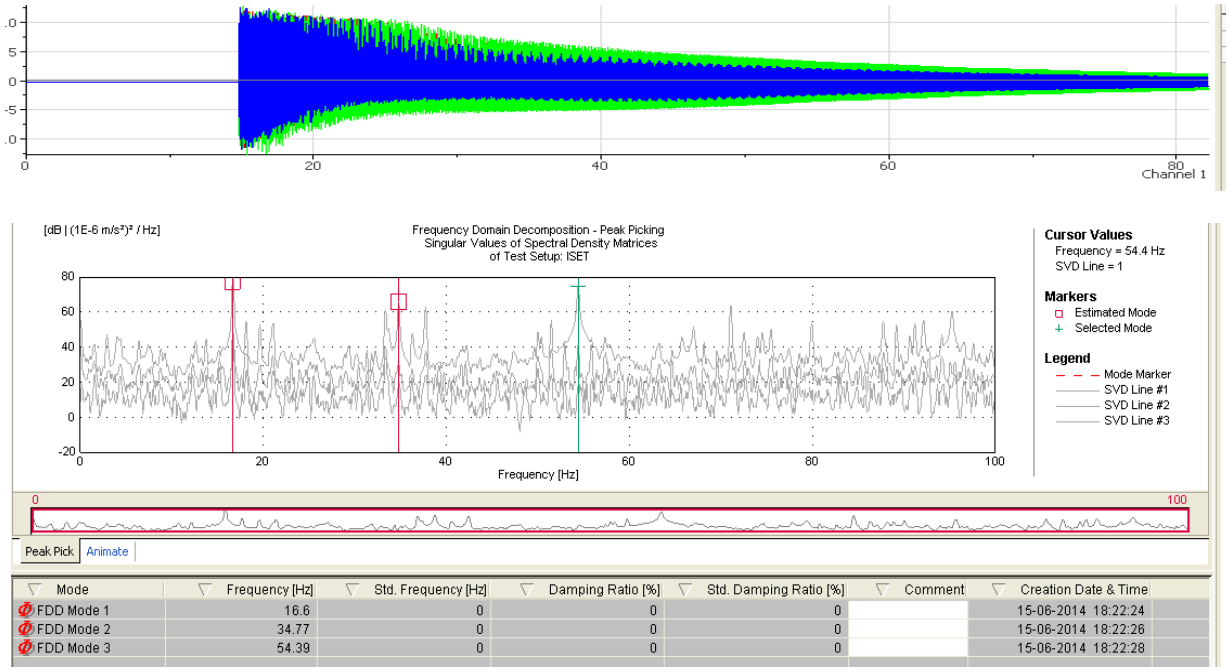

Natural frequencies for T2– Tie N22

TIE 2

		Natural frequencies (Hz)		
	Measurement	**I**	**II**	**III**
Environmental vibration	1	16.70	34.86	54.39
	2	16.70	34.86	54.49
	3	16.70	34.86	54.49
	Average	**16.70**	**34.86**	**54.46**
Forced Vibration	1	16.70	34.77	54.39
	2	16.70	34.77	54.39
	3	16.60	34.77	54.39
	Average			
		16.67	**34.77**	**54.39**

TEST 3- Tie N32.

Response under environmental vibration in frequency domain (FFT) - Measurement 1

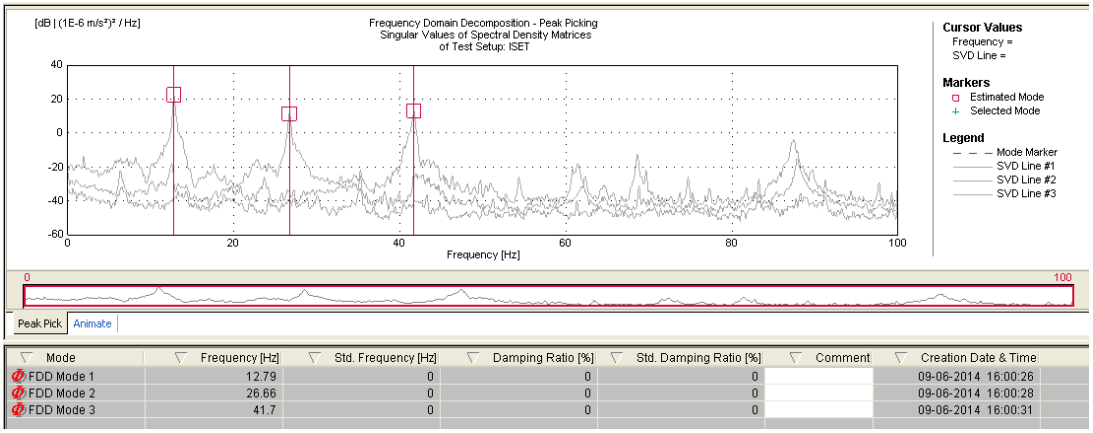

Mode	Frequency [Hz]	Std. Frequency [Hz]	Damping Ratio [%]	Std. Damping Ratio [%]	Comment	Creation Date & Time
FDD Mode 1	12.79	0	0	0		09-06-2014 16:00:26
FDD Mode 2	26.66	0	0	0		09-06-2014 16:00:28
FDD Mode 3	41.7	0	0	0		09-06-2014 16:00:31

Response under forced vibration in frequency domain (FFT) - Measurement 1

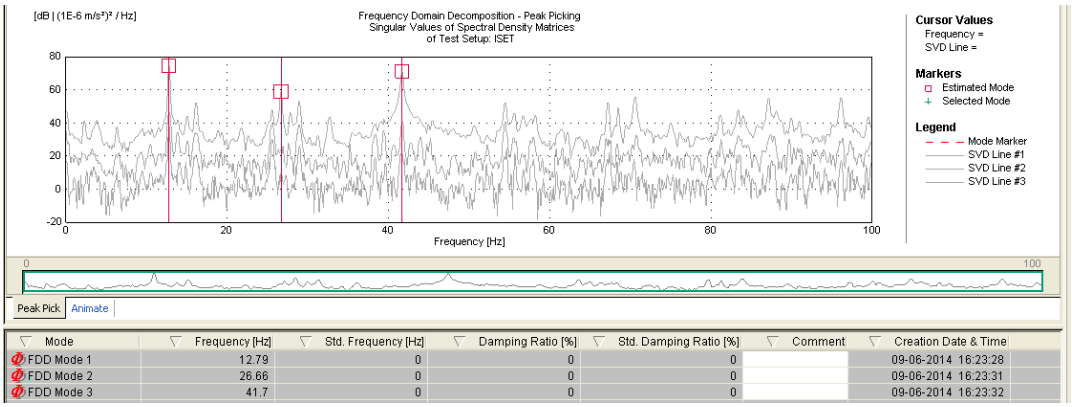

Mode	Frequency [Hz]	Std. Frequency [Hz]	Damping Ratio [%]	Std. Damping Ratio [%]	Comment	Creation Date & Time
FDD Mode 1	12.79	0	0	0		09-06-2014 16:23:28
FDD Mode 2	26.66	0	0	0		09-06-2014 16:23:31
FDD Mode 3	41.7	0	0	0		09-06-2014 16:23:32

Natural frequencies for T3– Tie N32

TIE 3

		Natural frequencies (Hz)		
	Measurement	**I**	**II**	**III**
Environmental vibration	1	12.790	26.660	41.700
	2	12.790	26.760	41.700
	3	12.790	26.760	41.700
	Average	**12.790**	**26.727**	**41.700**
Forced Vibration	1	12.790	26.660	41.700
	2	12.790	26.660	41.700
	3	12.790	26.660	41.700
		12.790	**26.660**	**41.700**

TEST 4- Tie N13.

Response under environmental vibration in frequency domain (FFT) - Measurement 2

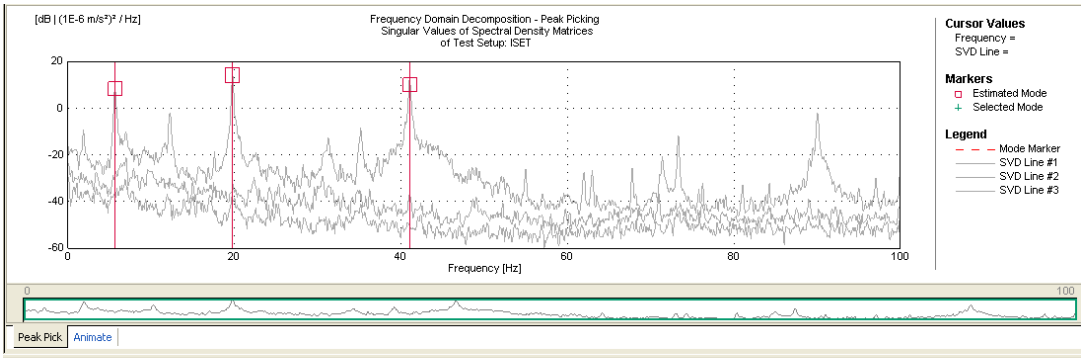

Mode	Frequency [Hz]	Std. Frequency [Hz]	Damping Ratio [%]	Std. Damping Ratio [%]	Comment	Creation Date & Time
FDD Mode 1	5.664	0	0	0		09-06-2014 17:03:15
FDD Mode 2	19.73	0	0	0		09-06-2014 17:03:18
FDD Mode 3	41.11	0	0	0		09-06-2014 17:03:21

Response under forced vibration in frequency domain (FFT) - Measurement 2

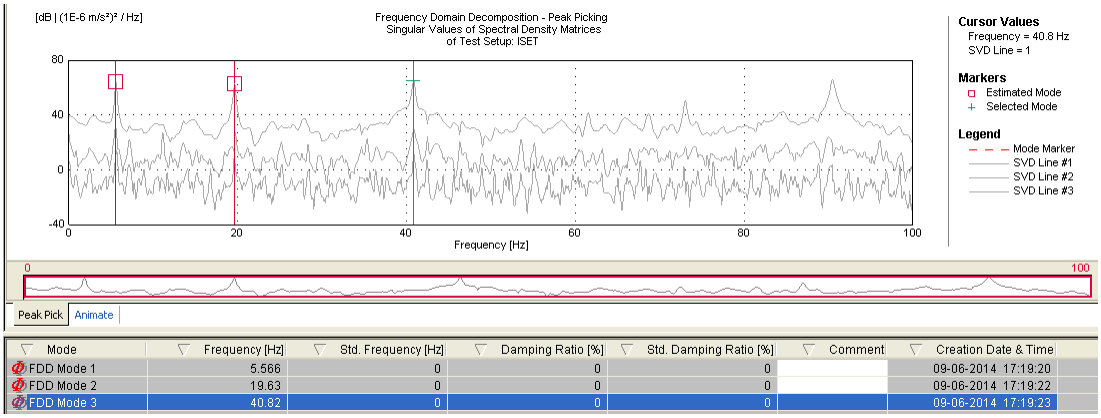

Mode	Frequency [Hz]	Std. Frequency [Hz]	Damping Ratio [%]	Std. Damping Ratio [%]	Comment	Creation Date & Time
FDD Mode 1	5.566	0	0	0		09-06-2014 17:19:20
FDD Mode 2	19.63	0	0	0		09-06-2014 17:19:22
FDD Mode 3	40.82	0	0	0		09-06-2014 17:19:23

Natural frequencies for T3– Tie N32

TIE 4

		Natural frequencies (Hz)		
	Measurement	**I**	**II**	**III**
Environmental vibration	1	5.566	19.730	41.020
	2	5.664	19.730	41.110
	3	5.664	19.730	41.020
	Average	**5.631**	**19.730**	**41.050**
Forced Vibration	1	5.566	19.630	40.920
	2	5.566	19.630	40.820
	3	5.566	19.630	40.820
	Average	**5.570**	**19.630**	**40.850**

APPENDIX 5. Stress distribution on different walls at different levels

1. Level +0.00 m

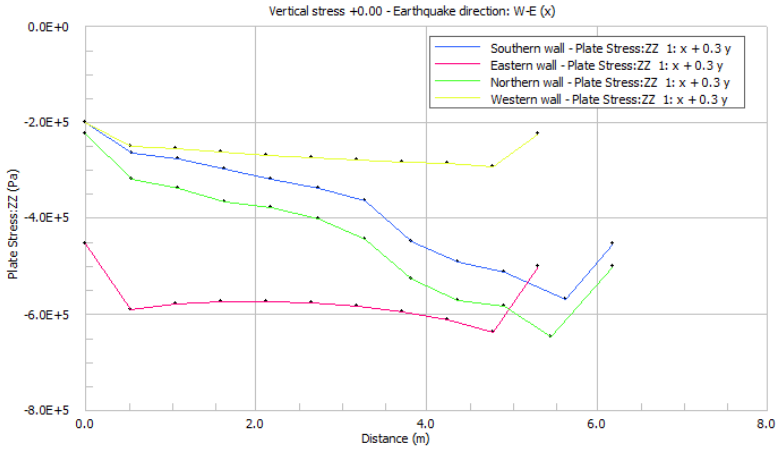

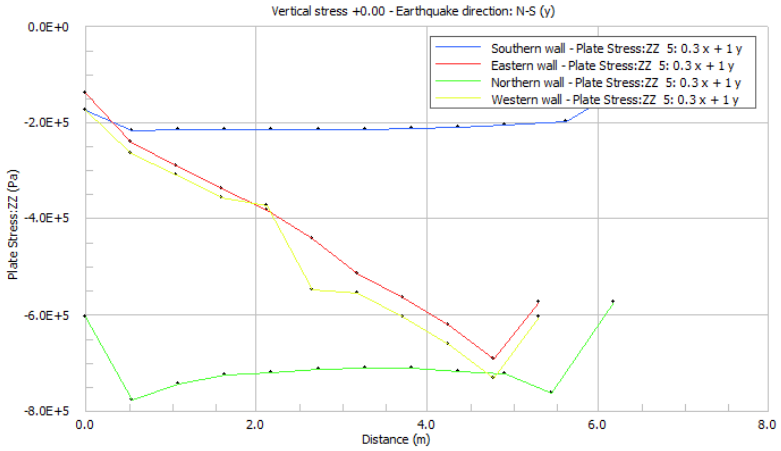

2. Level +4.82 m

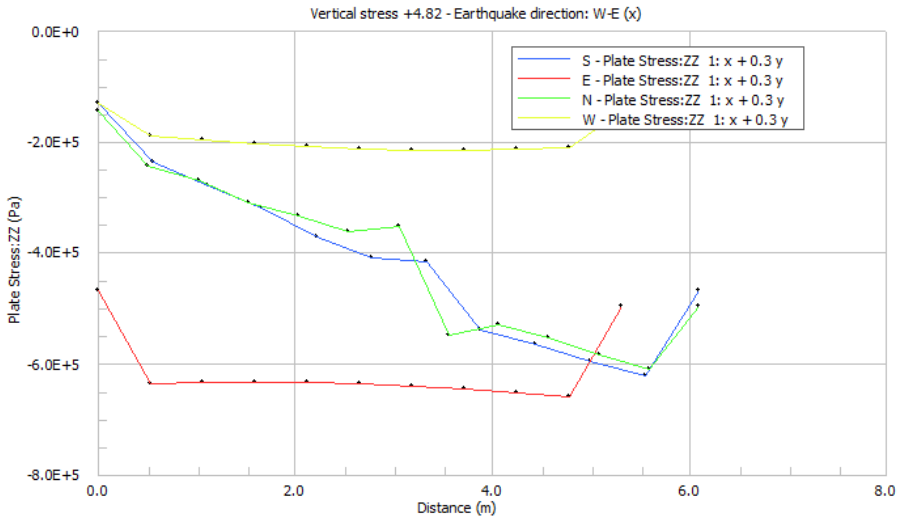

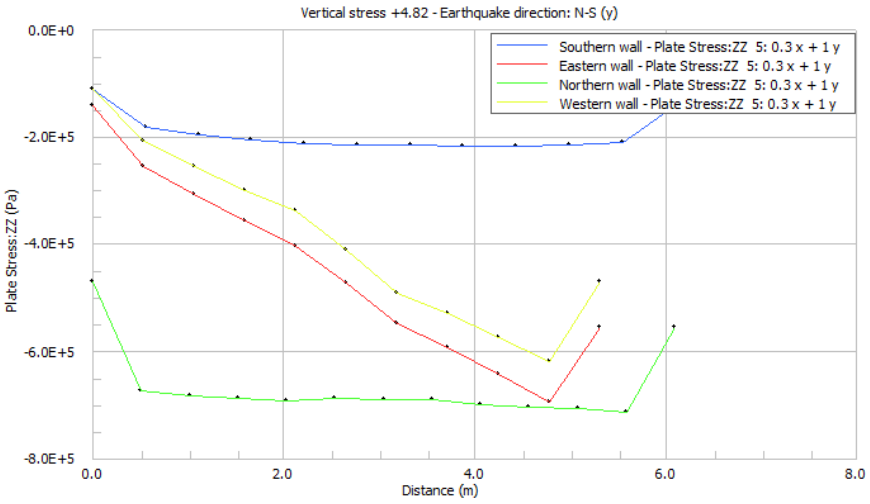
Vertical stress +4.82 - Earthquake direction: N-S (y)
Southern wall - Plate Stress:ZZ 5: 0.3 x + 1 y
Eastern wall - Plate Stress:ZZ 5: 0.3 x + 1 y
Northern wall - Plate Stress:ZZ 5: 0.3 x + 1 y
Western wall - Plate Stress:ZZ 5: 0.3 x + 1 y
Plate Stress:ZZ (Pa)
0.0E+0
-2.0E+5
-4.0E+5
-6.0E+5
-8.0E+5
0.0
2.0
4.0
6.0
8.0
Distance (m)

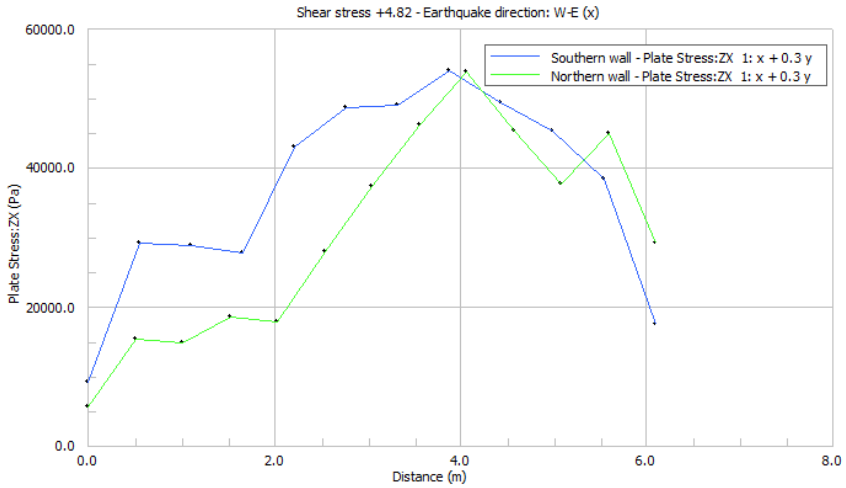
Shear stress +4.82 - Earthquake direction: W-E (x)
Southern wall - Plate Stress:ZX 1: x + 0.3 y
Northern wall - Plate Stress:ZX 1: x + 0.3 y
Plate Stress:ZX (Pa)
60000.0
40000.0
20000.0
0.0
0.0
2.0
4.0
6.0
8.0
Distance (m)

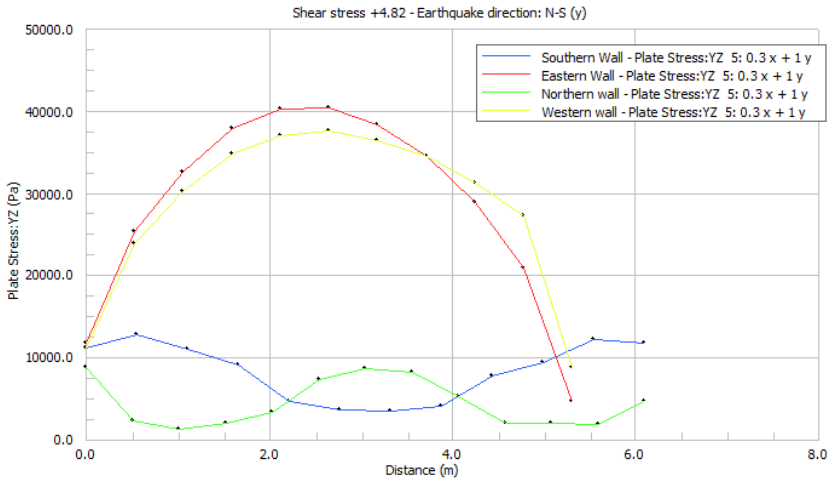
Shear stress +4.82 - Earthquake direction: N-S (y)
Southern Wall - Plate Stress:YZ 5: 0.3 x + 1 y
Eastern Wall - Plate Stress:YZ 5: 0.3 x + 1 y
Northern wall - Plate Stress:YZ 5: 0.3 x + 1 y
Western wall - Plate Stress:YZ 5: 0.3 x + 1 y
Plate Stress:YZ (Pa)
50000.0
40000.0
30000.0
20000.0
10000.0
0.0
0.0
2.0
4.0
6.0
8.0
Distance (m)

3. Level +9.34 m

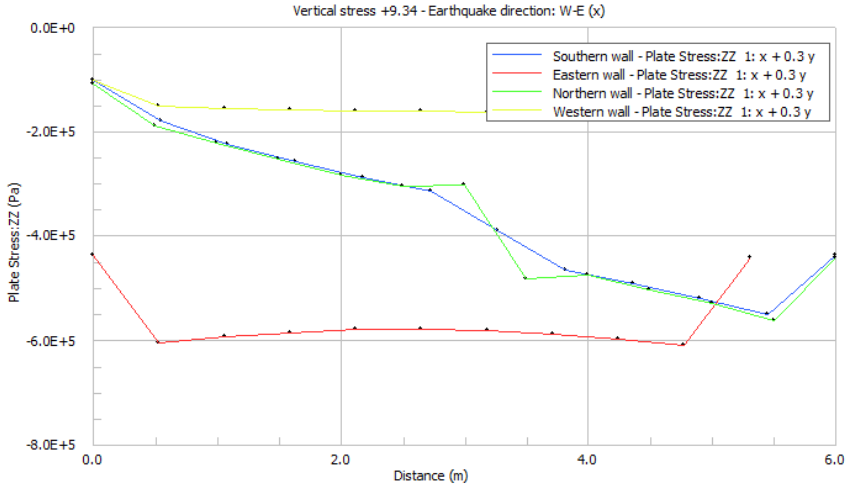
Vertical stress +9.34 - Earthquake direction: W-E (x)
Southern wall - Plate Stress:ZZ 1: x + 0.3 y
Eastern wall - Plate Stress:ZZ 1: x + 0.3 y
Northern wall - Plate Stress:ZZ 1: x + 0.3 y
Western wall - Plate Stress:ZZ 1: x + 0.3 y
Plate Stress:ZZ (Pa)
0.0E+0
-2.0E+5
-4.0E+5
-6.0E+5
-8.0E+5
0.0
2.0
4.0
6.0
Distance (m)

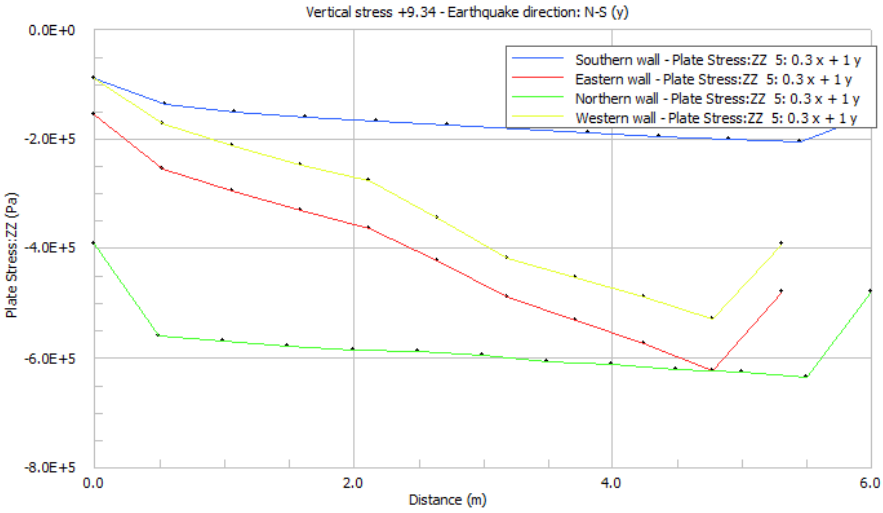
Vertical stress +9.34 - Earthquake direction: N-S (y)
Southern wall - Plate Stress:ZZ 5: 0.3 x + 1 y
Eastern wall - Plate Stress:ZZ 5: 0.3 x + 1 y
Northern wall - Plate Stress:ZZ 5: 0.3 x + 1 y
Western wall - Plate Stress:ZZ 5: 0.3 x + 1 y
Plate Stress:ZZ (Pa)
0.0E+0
-2.0E+5
-4.0E+5
-6.0E+5
-8.0E+5
0.0
2.0
4.0
6.0
Distance (m)

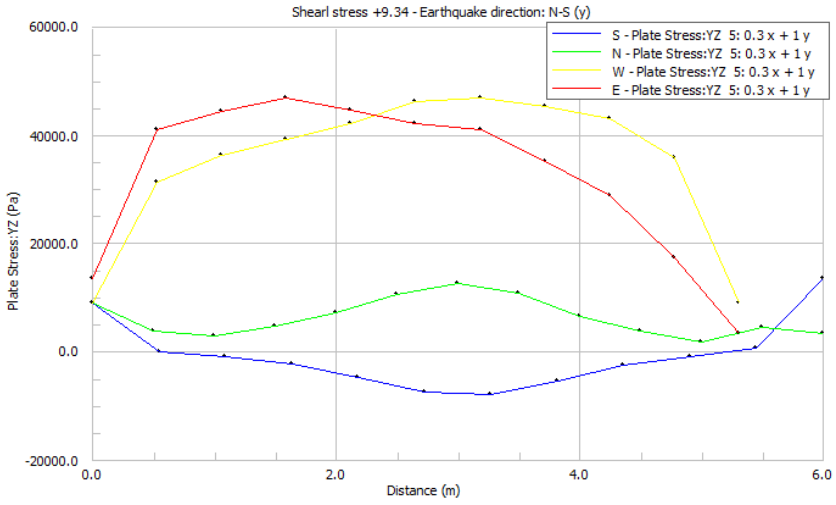
Shearl stress +9.34 - Earthquake direction: N-S (y)
S - Plate Stress:YZ 5: 0.3 x + 1 y
N - Plate Stress:YZ 5: 0.3 x + 1 y
W - Plate Stress:YZ 5: 0.3 x + 1 y
E - Plate Stress:YZ 5: 0.3 x + 1 y
Plate Stress:YZ (Pa)
60000.0
40000.0
20000.0
0.0
-20000.0
0.0
2.0
4.0
6.0
Distance (m)

4. Level +13.24 m

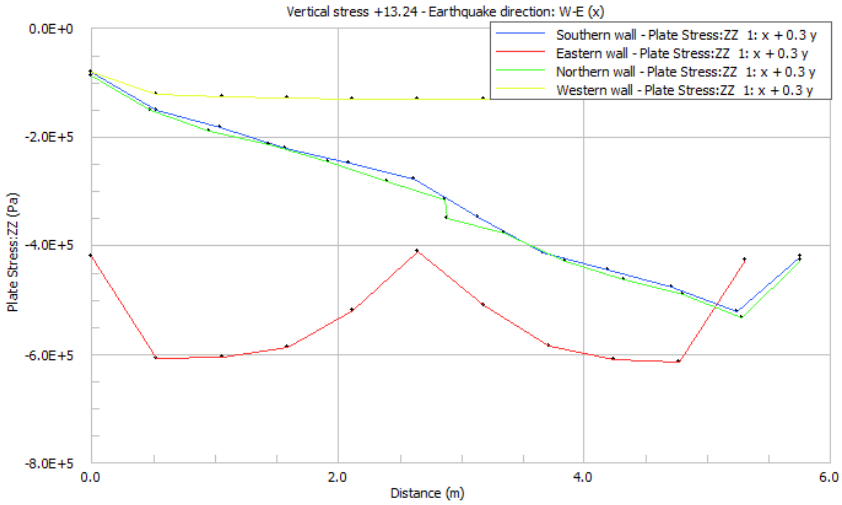

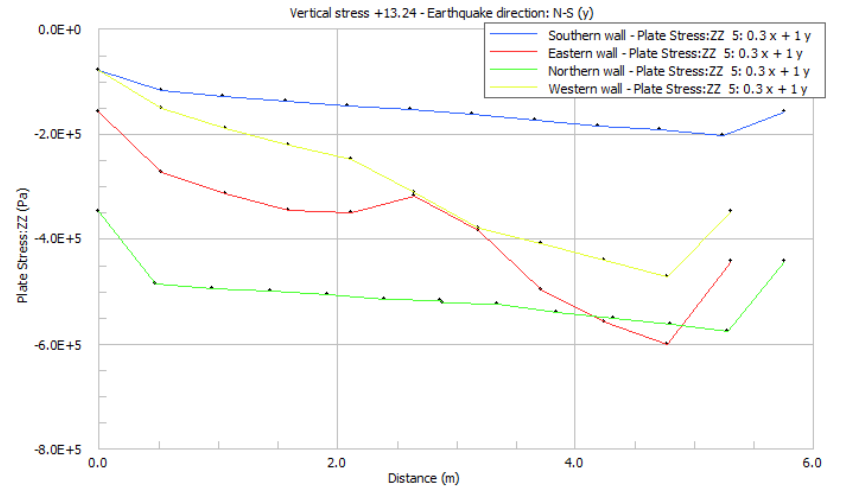

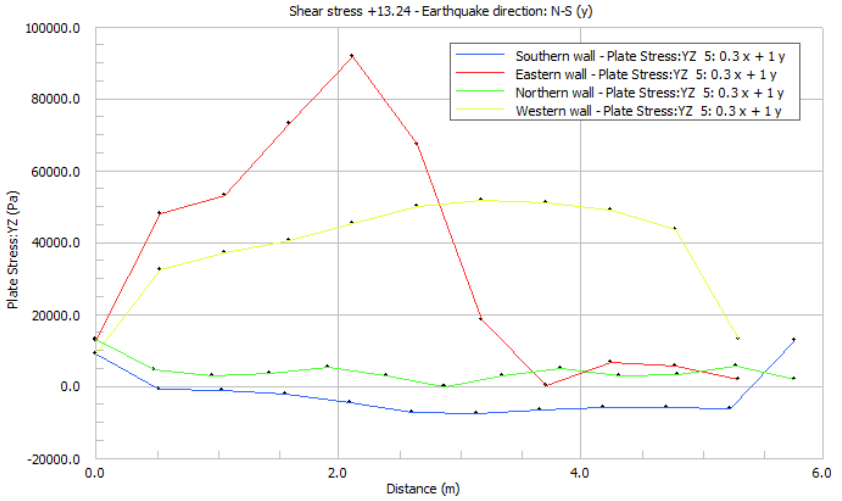

5. Level +17.15 m

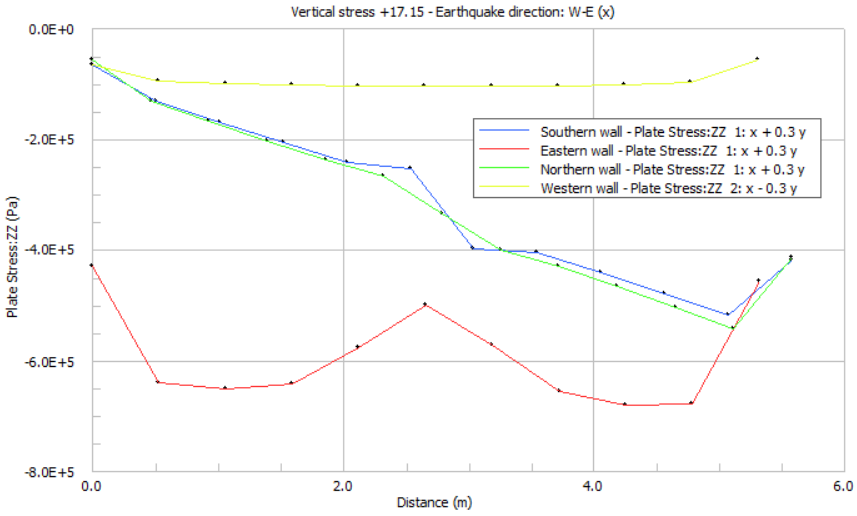

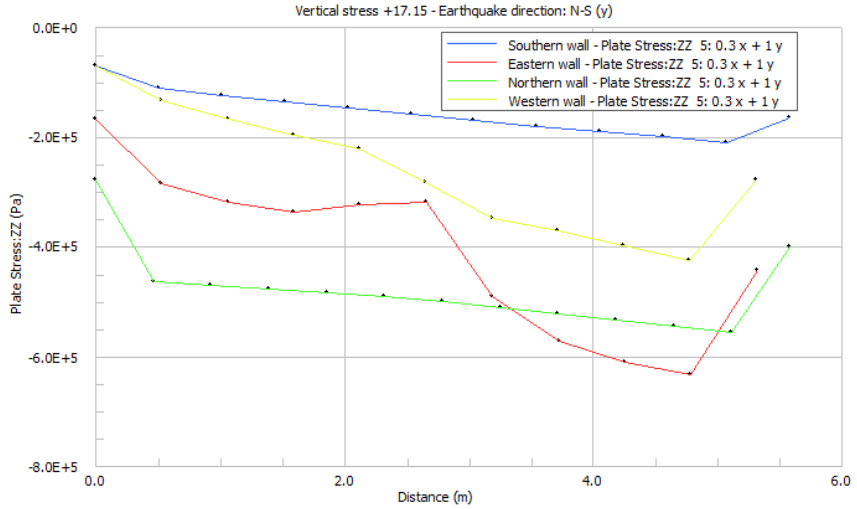

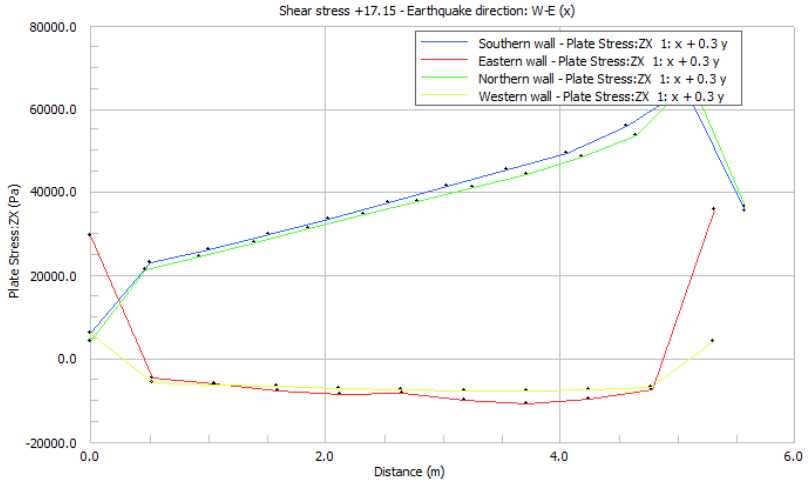

6. Level +21.76 m

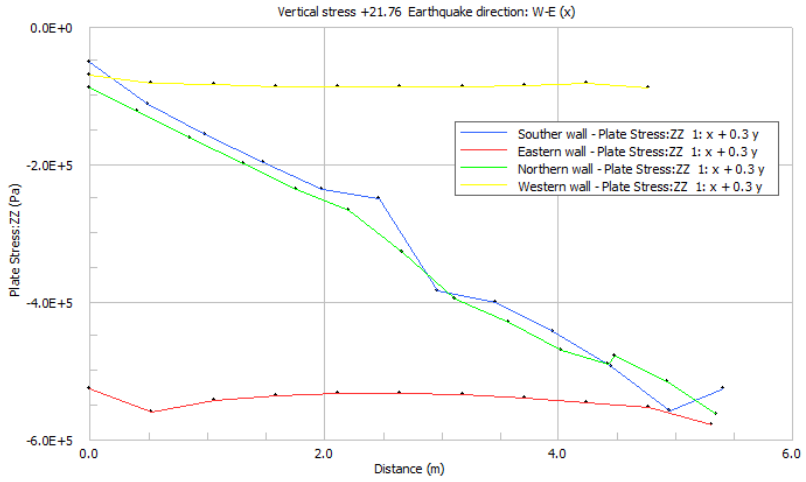

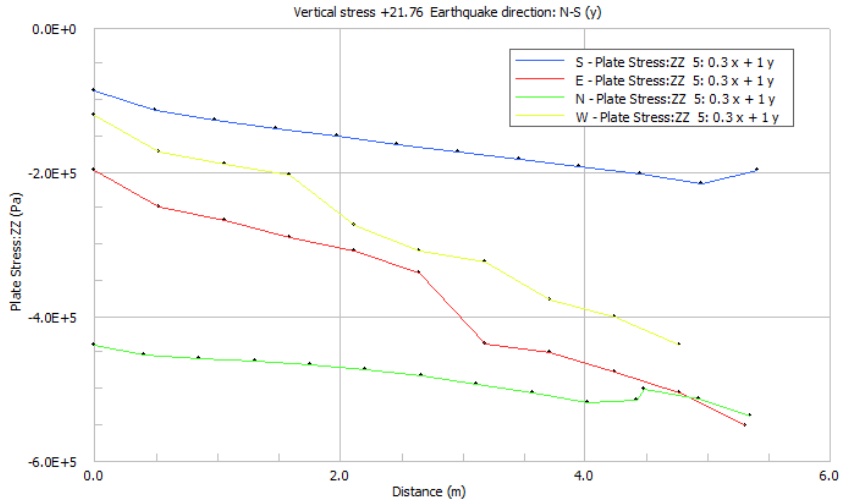

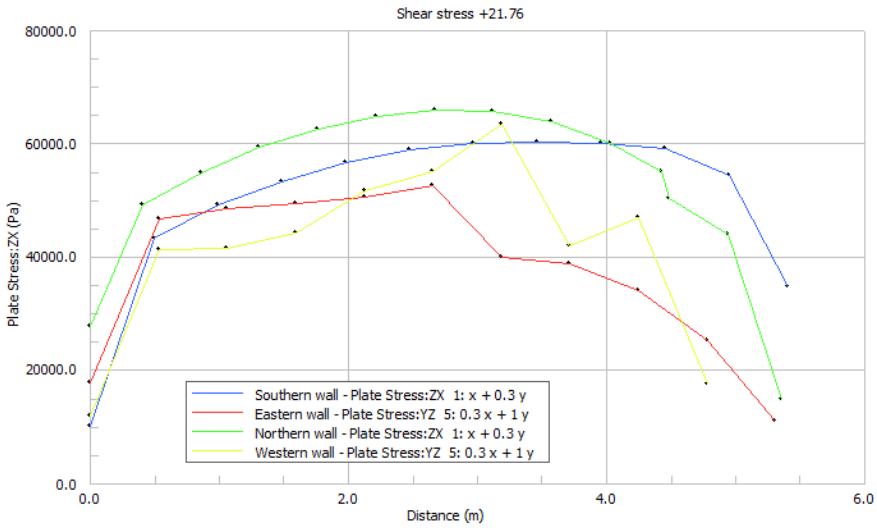

7. Level +25.31 m

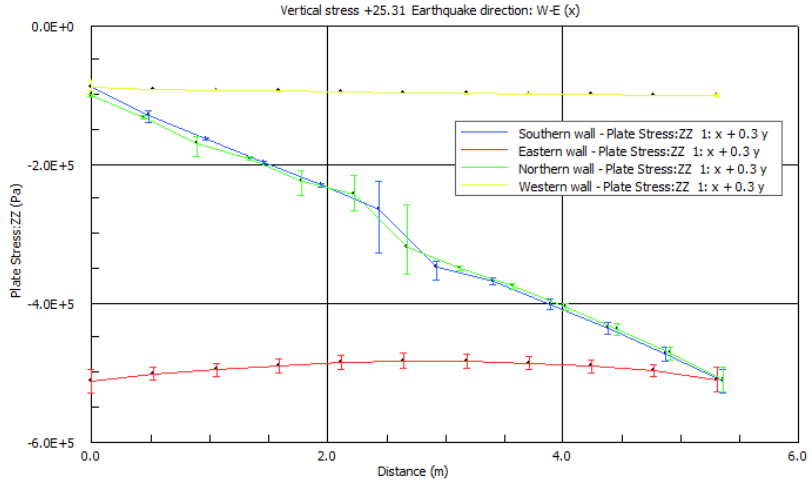

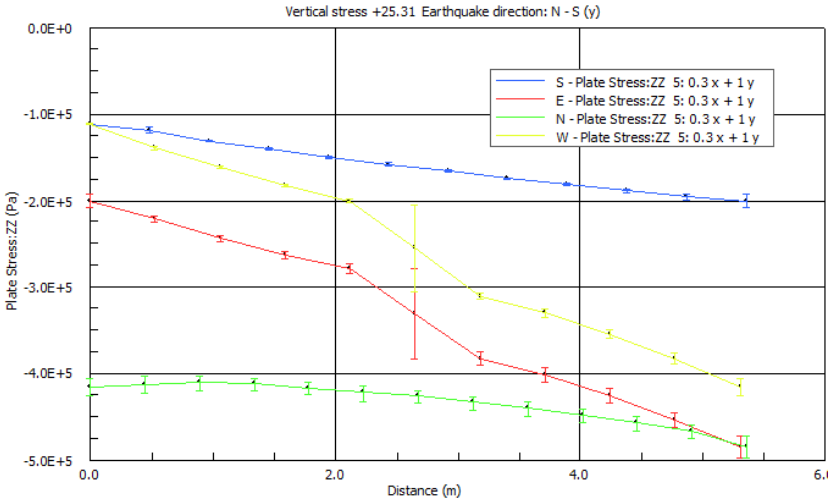

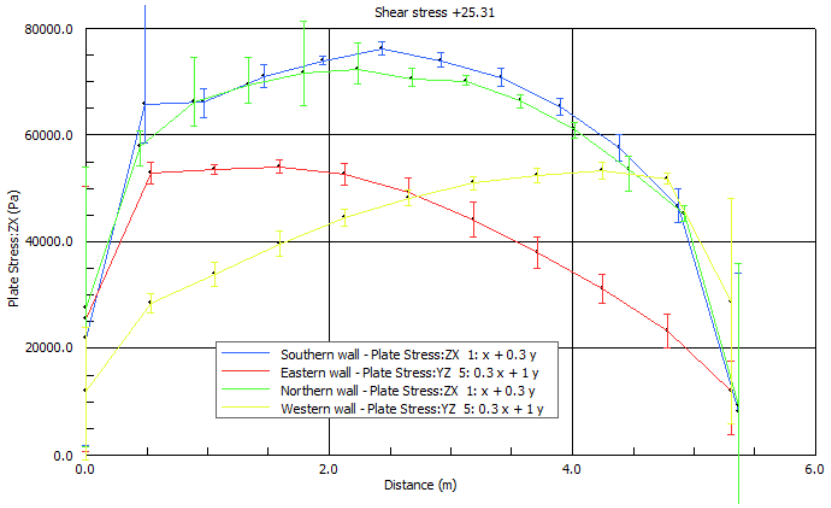

8. Level +29.46 m

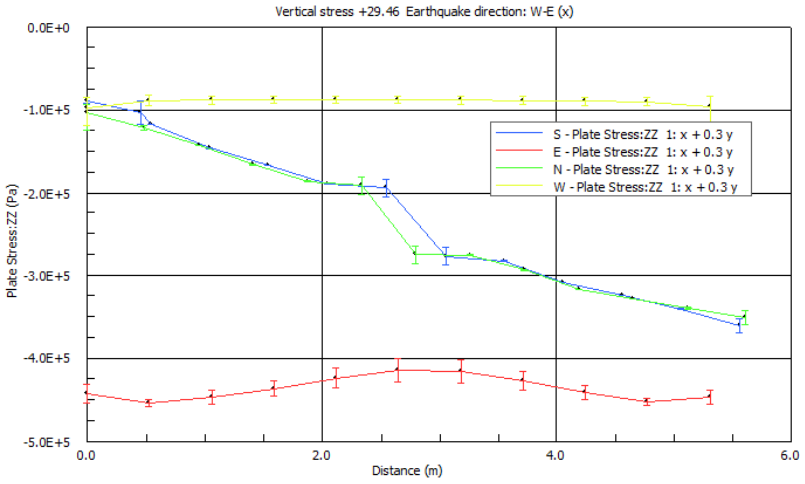

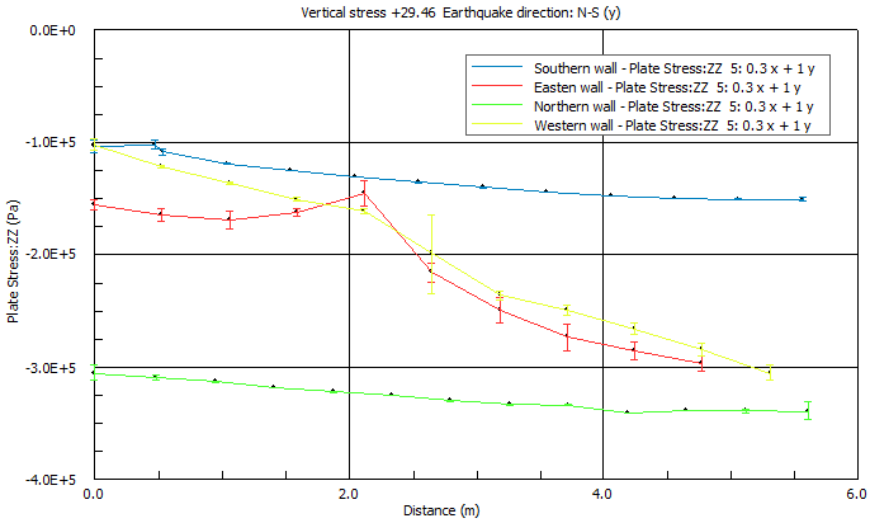

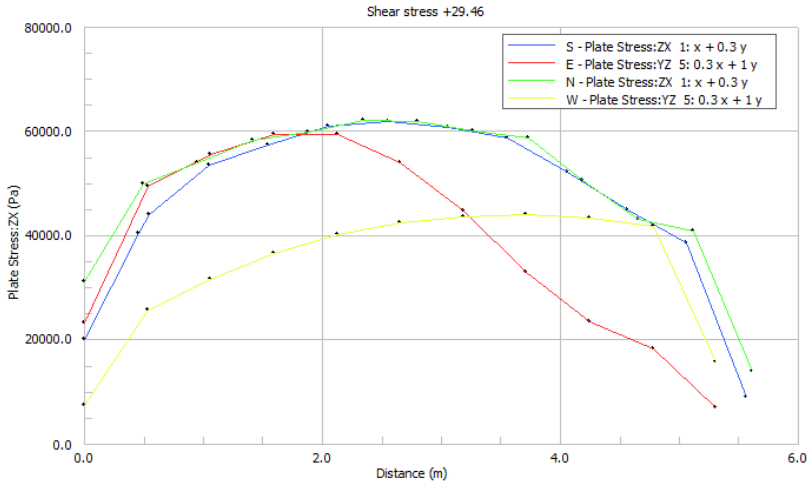

9. Level +32.9 m

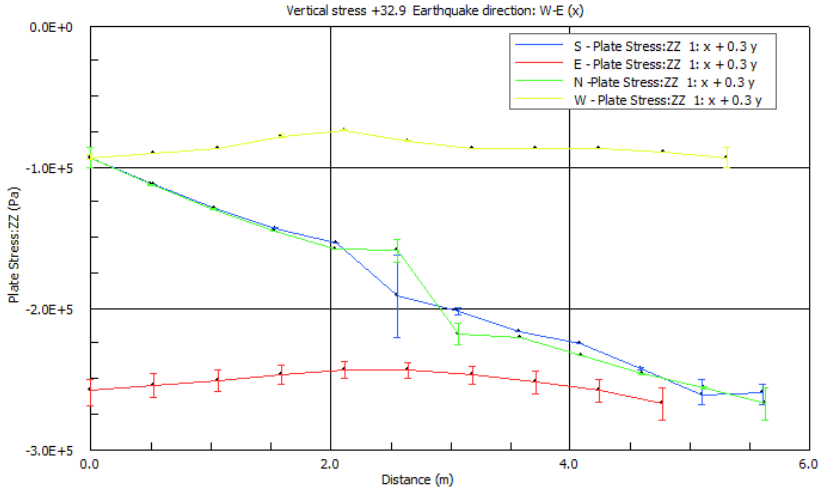
Vertical stress +32.9 Earthquake direction: W-E (x)
S - Plate Stress:ZZ 1: x + 0.3 y
E - Plate Stress:ZZ 1: x + 0.3 y
N -Plate Stress:ZZ 1: x + 0.3 y
W - Plate Stress:ZZ 1: x + 0.3 y
0.0E+0
-1.0E+5
-2.0E+5
-3.0E+5
Plate Stress:ZZ (Pa)
0.0
2.0
4.0
6.0
Distance (m)

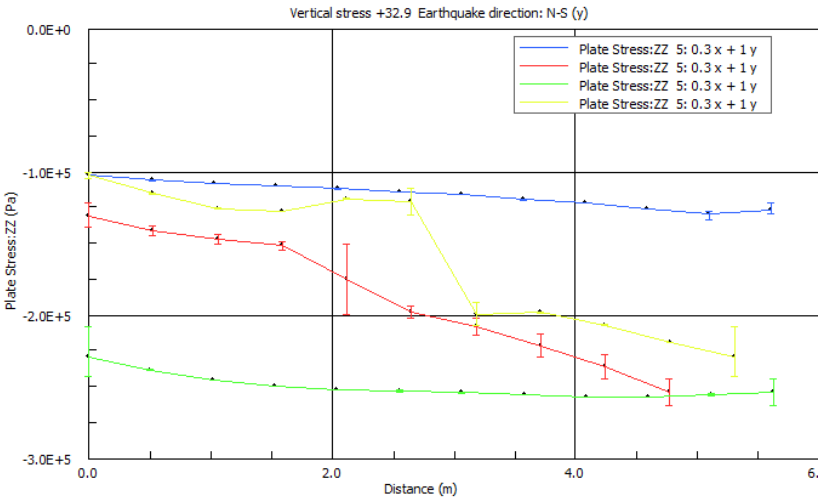
Vertical stress +32.9 Earthquake direction: N-S (y)
Plate Stress:ZZ 5: 0.3 x + 1 y
Plate Stress:ZZ 5: 0.3 x + 1 y
Plate Stress:ZZ 5: 0.3 x + 1 y
Plate Stress:ZZ 5: 0.3 x + 1 y
0.0E+0
-1.0E+5
-2.0E+5
-3.0E+5
Plate Stress:ZZ (Pa)
0.0
2.0
4.0
Distance (m)

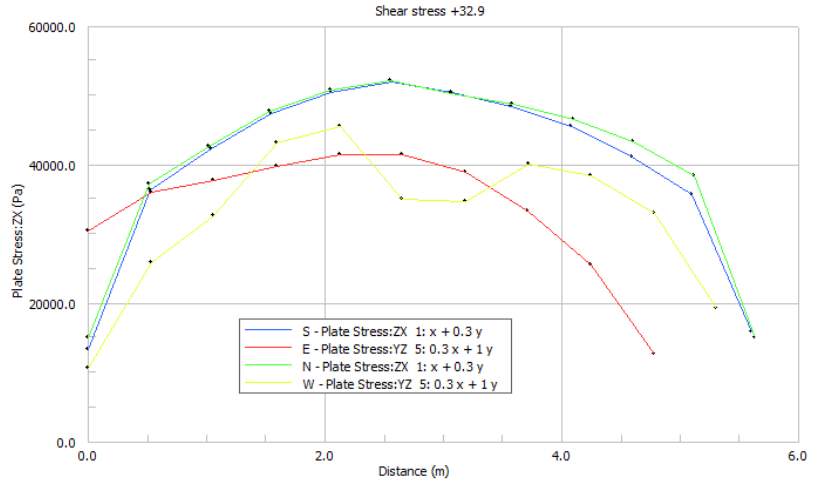
Shear stress +32.9
60000.0
40000.0
20000.0
0.0
Plate Stress:ZX (Pa)
S - Plate Stress:ZX 1: x + 0.3 y
E - Plate Stress:YZ 5: 0.3 x + 1 y
N - Plate Stress:ZX 1: x + 0.3 y
W - Plate Stress:YZ 5: 0.3 x + 1 y
0.0
2.0
4.0
6.0
Distance (m)

10. Level +36.85 m

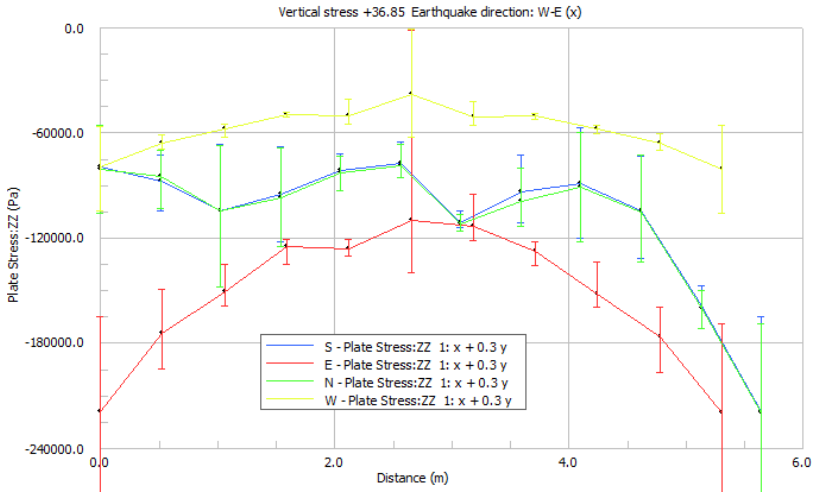

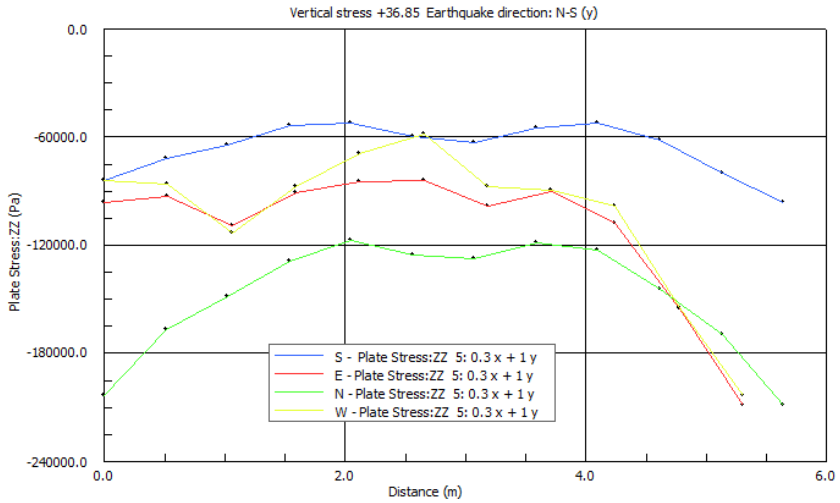

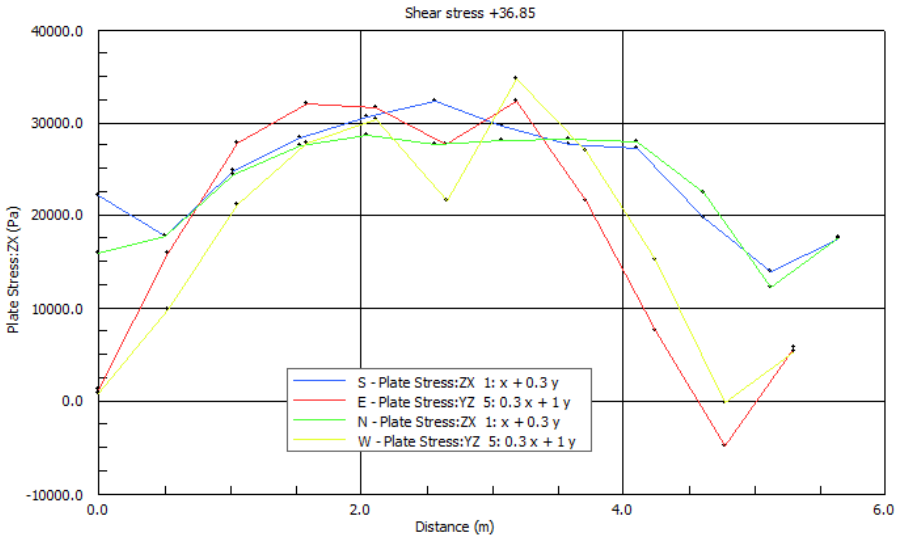

11. Level +42.55 m